



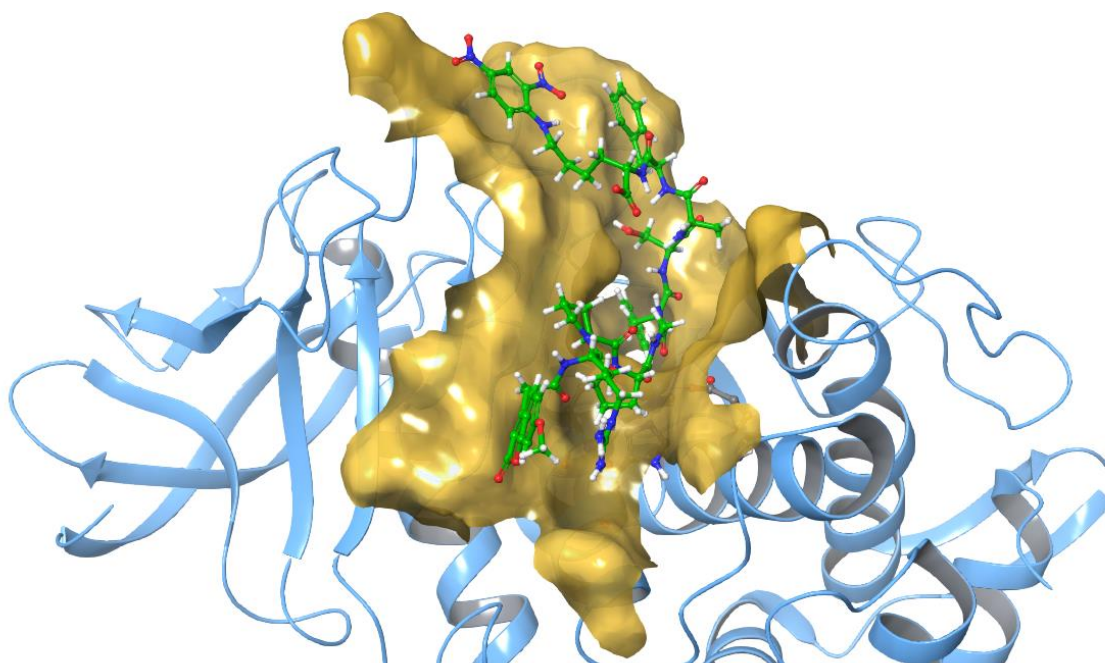
UiT The Arctic University of Norway

Faculty of Health Sciences
Department of Medical Biology

Zinc binding and chelating compounds as inhibitors of bacterial metalloproteases and human matrix metalloproteases

Fatema Amatur Rahman

A dissertation for the degree of Philosophiae Doctor (PhD), August 2023



HELSE · · · · · NORD

BioCat
Norwegian Graduate School
in Biocatalysis

The cover image highlights the structure of the active site cleft of Pseudolysin (PLN) with the substrate Mca-Arg-Pro-Pro-Gly-Phe-Ser-Ala-Phe-Lys(Dnp)-OH (ES005).

Zinc binding and chelating compounds as inhibitors of bacterial metalloproteases and human matrix metalloproteases

By

Fatema Amatur Rahman



A dissertation for the degree of Philosophiae Doctor

Tromsø, August 2023

Molecular Pharmacology and Toxicology Research group

Department of Medical Biology

Faculty of Health Sciences

UiT-The Arctic University of Norway

Table of Contents

ACKNOWLEDGEMENTS	I
LIST OF PAPERS	III
ABBREVIATIONS	V
ABSTRACT	VII
1. INTRODUCTION	1
1.1. THE MULTIDRUG RESISTANCE PROBLEM	1
<i>1.1.1. Multi-drug resistant bacteria and their virulence factors</i>	2
<i>1.1.2. Inhibition of bacterial virulence as a new strategy against bacterial infections</i>	3
1.2 CLASSIFICATION OF PROTEASES.....	4
<i>1.2.1 Metalloproteases</i>	5
1.3 CATALYTIC SITE NOMENCLATURE AND SPECIFICITY OF THE STUDIED PROTEASES	6
1.4 THERMOLYSIN, PSEUDOLYSIN AND AUREOLYSIN.....	9
<i>1.4.1 The maturation process</i>	9
<i>1.4.2 Three-dimensional structure</i>	11
1.4.2.1 Thermolysin	11
1.4.2.2 Pseudolysin	11
1.4.2.3 Aureolysin	12
1.5 HUMAN MATRIX METALLOPROTEASES	13
<i>1.5.1 Matrix Metalloprotease-9</i>	14
<i>1.5.2 Matrix Metalloprotease-14</i>	16
1.6. CATALYTIC MECHANISM OF METALLOPROTEASES	16
1.7 INHIBITORS OF ZINC METALLOPROTEASES	17
2. AIMS OF THE STUDY	23

3. EXPERIMENTAL SUMMARY	25
4. SUMMARY OF RESULTS	27
5. DISCUSSION	29
5.1. ANTIVIRULENCE STRATEGY AT THE DAWN OF THE POST-ANTIBIOTIC ERA	29
5.2. PUTATIVE CONSEQUENCES OF OFF-TARGET EFFECTS ON HUMAN MATRIX METALLOPROTEASES	30
5.3. PROMISING COMPOUNDS AS A SCAFFOLD FOR FUTURE LEAD COMPOUNDS.....	32
5.4. PUTATIVE METHODOLOGICAL LIMITATIONS.....	35
6. CONCLUSION	37
7. FUTURE PERSPECTIVES	37
8. REFERENCES	39

Paper I

Paper II

Paper III

Acknowledgements

First and foremost, all praises, thanks, and gratitude be to my Allah, the Almighty and the Most Merciful, for His showers of blessings and guidance throughout my journey of research and its successful completion.

My gratefulness and acknowledgement must go to The Arctic University of Norway (UiT) for allowing me to carry out this research study. I am thankful to Helse Nord (project number HNF1514-20) for providing the project costs for this study and the PhD school Biocat for supporting all the travel costs for several courses I have taken from other than Tromsø Universities.

I would like to acknowledge and give my warmest thanks to my supervisor Professor Ingebrigt Sylte and co-supervisor, Professor emeritus Jan-Olof Winberg (Joffe). Thank you so much for your excellent supervision and guidance throughout all the stages of this project. You both were always available and welcoming for me regardless of any situation and must deserve to be the best mentors in my academic arena.

Further, I would like to address my outermost appreciation to Assoc. Prof. Kurt Kristiansen and Imin Wushur, PhD, for assisting me in the molecular modelling computer lab.

My acknowledgement must also go to the very cordial, strong, friendly, confidant and of course, beautiful lady Linn Samira Mari Evenseth, PhD. She has always been a great support for me since I met her as a colleague. Thanks a lot, Linn, especially for helping me to understand the molecular modelling course.

I must be very grateful to another serious, sincere and beautiful colleague Clizia Russotto who provided me with strong help and mental support throughout all the difficulties during this study period.

I would like to express my immense love and gratitude for my two beloved sons, Saifan Bhuiyan and Saihan Bhuiyan, for their patience and cooperation during the entire period of this

research work. I am very thankful to my husband for his enormous cooperation and consideration during writing this thesis.

Last but not least, I would like to express my appreciation to other friends and family members who were directly or indirectly inspired me to continue this journey. Their prayer to Almighty Allah for me was a great help in this successful completion.

Zajakallahu Khairan ("May Allah reward you [with] goodness")

Fatema Amatur Rahman

Tromsø, August 2023

List of Papers

Paper I

Fatema Rahman, Tra-Mi Nguyen, Olayiwola A. Adekoya, Cristina Campestre, Paolo Tortorella, Ingebrigt Sylte & Jan-Olof Winberg. Inhibition of bacterial and human zinc metalloproteases by bisphosphonate- and catechol-containing compounds. *Journal of Enzyme Inhibition and Medicinal Chemistry* **2021**, 36:1, 819-830, DOI: 10.1080/14756366.2021.1901088.

Paper II

Fatema Rahman, Imin Wushur, Nabin Malla, Ove Alexander Høgmoen Åstrand, Pål Rongved, Jan-Olof Winberg and Ingebrigt Sylte. Zinc-Chelating Compounds as Inhibitors of Human and Bacterial Zinc Metalloproteases. *Molecules* **2022**, 27, 56. DOI: 10.3390/molecules27010056.

Paper III

Fatema Amatur Rahman, Imin Wushur, Bibek Chaulagain, Tra-Mi Nguyen, Olayiwola A. Adekoya, Nabin Malla, Jan-Olof Winberg, Ingebrigt Sylte. Interactions of substrates and phosphinyl-containing inhibitors with human MMPs and bacterial virulence factors. (*Manuscript*)

Abbreviations

ACE-2	Angiotensin-converting enzyme-2
Agr	Accessory gene regulator
ALN	Aureolysin
CRP	Carbapenem-resistant <i>Pseudomonas aeruginosa</i>
DNA	Deoxyribonucleic acid
ECM	Extracellular matrix
ES001	Mca-Pro-Leu-Gly-Leu-Dpa-Ala-Arg-NH ₂
ES005	Mca-Arg-Pro-Pro-Gly-Phe-Ser-Ala-Phe-Lys(Dnp)-OH
ESBL	Extended-spectrum beta-lactamase
FDA	Food and Drug Administration
FRET	Fluorescence resonance energy transfer method
GPI	Glycosylphosphatidylinositol
HPX	Haemopexin-like domain
ICM	Internal coordinate mechanics software
IDSA	Infectious diseases society of America
IgG	Immunoglobulin
IMP	Imipenemase type metallo- β -Lactamase
MBLs	Metallo beta lactamases
MD	Molecular dynamics
MDR	Multi-drug resistant
MMPs	Matrix metalloproteases
MPs	Metalloproteases
MRSA	Methicillin-resistant <i>Staphylococcus aureus</i>
MT-MMP	Membrane type-Matrix metalloprotease
NDM-1	New Delhi metallo-beta lactamase
OG domain	O-glycosylated domain
pepSY	Peptidase inhibitor domain
PLN	Pseudolysin
PMN	Polymorpho nuclear leukocytes
POP	Phosphodiester bond

PPC	Pre-peptidase C-terminal extension
PPI	inorganic Pyrophosphate
SAR	Structure-activity relationship
SMPI	Streptomyces metalloprotease inhibitor
SP	Signal peptide
TIMP	Tissue inhibitor of matrix metalloprotease
TLN	Thermolysin
TPA	Tripicolylamine
TPED	Tris pyridine ethylene diamine
VIM	Verona integron-borne metallo- β -lactamase
VIE	Verona integron encoded
VRE	Vancomycin-resistant Enterococcus
WHO	World health organization
Xcp	Extracellular carboxyl proteases
ZA	Zoledronic acid
ZBGs	Zinc-binding group
3D	Three-dimensional

Abstract

Inhibition of bacterial virulence is suggested to be a promising strategy in the development of new antibacterial drugs. The present work has focused on identifying new inhibitors of the bacterial virulence factors thermolysin (TLN), pseudolysin (PLN, LasB) and aureolysin (ALN), which are all zinc metalloproteases (MPs). A chemical group chelating the catalytic zinc ion of MPs, referred to as the zinc-binding group (ZBG) (e.g., phosphinate (PO_2), carboxylate (COO^-), thiolate (S^-) and hydroxamic acid HONH-CO , sulfhydryl, etc.) is important for essential inhibition, and hence this interaction is crucial for the discovery of zinc MP inhibitors as putative new drugs. The strategy in the present work was to use different compounds with a putative ZBG, including compounds with nitrogen as the zinc donor atom. The structure of the active site cleft of the virulence factors is very similar to that of the matrix metalloproteases (MMPs) and other human zinc MPs. Bacterial virulence inhibitors as drugs against bacterial infections should have limited effects on human endogenous zinc MPs. Therefore, we also tested their inhibition of human MMP-9 and MMP-14. Some of the compounds have previously been tested by others for their inhibition of MMP-9 and MMP-14, but were retested in the present study. The reason for retesting was that our experimental conditions were not identical to those previously used. To be able to compare the obtained binding strengths, the experiments needed to be performed under identical conditions.

Enzyme kinetic studies were employed to investigate the inhibitory activities of different compounds and compare their affinities to both human and bacterial zinc MPs. The fluorogenic substrates Mca-Arg-Pro-Pro-Gly-Phe-Ser-Ala-Phe-Lys(Dnp)-OH (ES005) and Mca-Pro-Leu-Gly-Leu-Dpa-Ala-Arg-NH₂ (ES001) were used for bacterial MPs and human MMPs, respectively. Identifying the binding modes of inhibitors in the bacterial and human zinc MPs is important for designing new inhibitors with increased specificity for bacterial zinc MPs. The binding modes were therefore studied by molecular modelling.

Paper I: Catechol and bisphosphonate-containing compounds were tested against TLN, PLN, ALN, MMP-14 and MMP-9 using enzyme inhibition kinetics and *in silico* molecular modelling. The bisphosphonate-containing compound RC2 was identified by both inhibition kinetics and *in silico* studies to bind stronger to the bacterial virulence factors, TLN and PLN than to ALN, MMP-9 and MMP-14. Hence, this compound may be used as

a scaffold to design new and potentially stronger inhibitors of bacterial virulence factors with therapeutic potential. Such compounds may be used alone or as an antibiotic adjuvant that can help prolong the lifespan of available antibiotics by suppressing bacterial resistance or increasing antibiotic efficacy. Catechol-containing compound, BF471 was found to inhibit ALN by more than 50%. Further investigation along with chemical modification for stronger ALN inhibition might be useful in finding potential inhibitors of ALN.

Paper II: Zinc chelators; derivatives of dipicolylamine (DPA), tripicolylamine (TPA), tris pyridine ethylene diamine (TPED), pyridine and thiophene with nitrogen as zinc donor were tested against bacterial MPs (TLN, PLN and ALN) and human MMPs (MMP-9 and MMP-14). Previous studies have shown that TPA is an irreversible and time-dependent inhibitor of metallo- β -lactamases (MBLs). To test if this compound is also a reversible or irreversible time-dependent MP inhibitor, inactivation kinetics combined with a micro-dialysis experimental method were employed with the MMP-14 against TPA. This showed that TPA was a time-dependent reversible inhibitor of MMP-14. Most of the tested compounds were found to inhibit MMP-14 (except for DPA) and PLN more strongly than the other enzymes. DPA inhibited PLN significantly stronger than the other four enzymes. Therefore, these compounds may serve as a scaffold for the development of novel anti-virulence compounds.

Paper III: Phosphinic compounds were tested as inhibitors of TLN, PLN, ALN and the human enzymes MMP-9 and MMP-14 using enzyme kinetics. The binding modes of the strongest inhibitors (compounds H-1 and H-2) were also studied by docking. Molecular dynamics (MD) simulation was performed to predict the cleavage site/sites of the fluorogenic substrate (ES005) in TLN and to identify amino acids constituting the different subpockets of the substrate binding sites. The MD simulations indicated that Gly-Phe amino acids are more favourable P_1 and P_1' residues for TLN than Ala-Phe and, therefore, predicted to be the main cleavage site residues of the TLN/ES005 complex. The H-1 compound was a strong inhibitor of MMP-9 and MMP-14, while the H-2 compound was found to inhibit all five proteases. Therefore, structural modification of H-2 might give rise to a structural scaffold that only inhibits bacterial MPs.

In all three papers, quenching experiments for the compounds showed no quenching effect on the fluorescence product formed during catalysis.

1. Introduction

1.1. The multidrug resistance problem

Bacterial multi-drug resistance (MDR) has become a major health problem worldwide and is prevalent among both Gram-positive and Gram-negative bacteria. Bacterial MDR is defined as a lack of susceptibility to at least one agent in three or more chemical classes of antibiotics [1]. In 2008 a study described the term “ESKAPE”, which was used for the most prevalent MDR bacteria, including *Enterococcus faecium* (*E. faecium*), *Staphylococcus aureus* (*S. aureus*), *Klebsiella pneumoniae* (*K. pneumoniae*), *Acinetobacter baumannii* (*A.baumannii*), *Pseudomonas aeruginosa* (*P. aeruginosa*), and *Enterobacter* species [2]. These bacteria cause the bulk of infections and efficiently “escape” the effects of antibacterial drugs and chemotherapeutic agents.

A systematic review paper from 2022 [3] estimated deaths and disability-adjusted life-years attributable to and associated with bacterial MDR for 23 pathogens and 88 pathogen–drug combinations in 204 countries and territories during 2019. They estimated that around 4.95 million people died from illnesses associated with bacterial MDR in 2019, including 1.27 million deaths attributable to bacterial MDR, mainly caused by ESKAPE pathogens [3]. Vancomycin-resistant *Enterococcus* species (VRE) [4], methicillin-resistant *S. aureus* (MRSA) [5], and carbapenem-resistant *P. aeruginosa* (CRP) [6] are the highest prioritized pathogens by World Health Organization (WHO) for new drug development as they are the most challenging resistant organisms involved in a variety of infections.

Most of the classical antibiotics have been developed based on their ability to kill or inhibit the growth of bacteria. A major limitation of this approach is that it targets bacterial viability and induces a high selection pressure that has driven the rapid emergence of MDR pathogens. Alternative approaches with novel modes of action to the currently available conventional antibiotics are of utmost necessity for encountering extremely MDR bacteria. Otherwise, it would be very difficult to prevent the world from repeating the vulnerable situation of the pre-antibiotic era, where common bacterial infections were seriously life-threatening [7].

1.1.1. Multi-drug resistant bacteria and their virulence factors

The virulence of microbes involves their ability to infect the host and cause clinical symptoms through factors that help bacteria in attachment, colonization and invasion of the host, disrupting host tissue integration, suppressing or escaping from the host immune response, and exhausting nutrients from the host [8-11]. These virulence potencies rely on several different extracellularly secreted factors, among which proteases are considered to be promising novel drug targets [12, 13] as the expression of these virulence factors contributes to the broad spectrum of infections and the frequent ineffectiveness of current therapies [14].

P. aeruginosa secretes several proteases, such as elastase A, elastase B, protease IV, and alkaline proteases [15], among which elastase B or pseudolysin (PLN or LasB) is a key virulence factor of *P. aeruginosa*. PLN is a metalloprotease (MP) that degrades extracellular proteins of the host for the nutrition of the bacteria. PLN is also reported to damage elastin, an essential component of the pulmonary tissue and blood vessels, impairing lung function, triggering pulmonary haemorrhage [16, 17] and causing corneal infections [18]. In patients with cystic fibrosis, *P. aeruginosa* is the most common pathogen [19]. PLN has also a crucial role within the bacterial cell to activate the intracellular pathway that initiates the growth of bacterial biofilm [20, 21]. By adopting a biofilm mode of growth, *P. aeruginosa* can be able to survive and causes fatal and devastating diseases mainly in immunocompromised patients [22].

S. aureus is a dangerous Gram-positive bacterium giving both community-acquired and nosocomial infections [23]. It has now become a major challenge owing to the rise of methicillin-resistant *S. aureus* (MRSA) as well as other bacterial MDR strains [24]. Recently emerged community-acquired MRSA was reported to cause serious infectious diseases, including sepsis and pneumonia [25, 26]. However, several virulence factors produced by *S. aureus* may contribute to the development of infection, including hemolysins, leukocidins, proteases, enterotoxins, exfoliative toxins, and immune-modulatory factors. The accessory gene regulator (*agr*) quorum-sensing system is known to play a central role in the regulation of these virulence factors [27]. The *agr* quorum sensing system is composed of the response regulator AgrA, the sensor histidine kinase and

AgrC that in response to auto-inducing peptides expresses a regulatory RNA [28]. *S. aureus* secretes several proteases such as cysteine proteases, serine proteases, and serine-like proteases and MPs. A skin abscess in the host at the sites of infection serves as a reservoir of peptides. Peptides and free amino acids are important sources of nutrients for the growth of bacteria. A study showed that the MP aureolysin (ALN) secreted by *S. aureus* cleaves collagen into peptide fragments that can support *S. aureus* growth under nutrient-limited conditions [29]. Some virulence factors are also used by *S. aureus* to deteriorate the host immune system [30, 31]. ALN is one of the most important virulence factors reported to actively inhibit the phagocytotic and neutrophilic function of the human complement system facilitating their survival and pathogenicity [32].

The MP thermolysin (TLN) secreted by the Gram-positive thermophilic bacterium *Bacillus thermoproteolyticus* is also known as a bacterial virulence factor involved in bacterial nutrition and sporulation [33]. TLN is well studied both functionally and structurally and has become the prototype of the M4 family of proteases [34]. TLN has been found to cause infections and diseases in humans [35]. The M4 family of proteases contain a zinc ion in the catalytic site, and PLN and ALN are also members of the M4 family. Over the years, TLN has been used as a model system for studying the structure and function of other zinc MPs. Due to structural similarities in the catalytic site, TLN inhibitors have been used in the design of inhibitors of other zinc MPs [36].

1.1.2. Inhibition of bacterial virulence as a new strategy against bacterial infections

As bacterial virulence factors degrade extracellular proteins and peptides as their nutrients before sporulation, the inhibition of the function of these proteases by zinc chelation may prevent the establishment, survival, and maintenance of infection within the host body. The concept of inhibition of virulence is a recently established strategy against bacterial infection [37]. Such a strategy does not attack the bacteria directly and therefore, might apply reduced evolutionary pressure for the development of resistance [37]. Hence, inhibition of the activity of the bacterial virulence factors rather than targeting bacterial growth is suggested to be an alternative new therapeutic strategy against bacterial infections [38]. Molecules capable of selectively inhibiting bacterial zinc MPs in the spread of infection could lead to the development of novel therapeutics. Moreover, because of their mechanism of action, inhibitors of bacterial zinc MPs may as well be used to fight MDR strains [39]. Such

inhibitory agents have been termed “second-generation” antibiotics [40]. This approach has emerged as a promising alternative to classical antibiotics. Alone or in combination with known antibacterial agents, such inhibitors may be effective against bacterial infection and bacterial biofilm formation. Using as an adjuvant, a reduced dose of the antibacterial agent may be effective for the treatment, contributing to less evolutionary pressure for MDR development. Therefore, the virulence factors PLN, ALN, and TLN are promising targets for the development of new antibacterial drugs or in the development of adjuvants to present antibacterial treatment.

1.2 Classification of Proteases

It has been estimated that there are more than sixty thousand different proteases [41] and of which more than 570 different proteases are present in humans [42]. Of the human proteases, approximately 200 are MPs [43]. Proteases target peptide bonds of proteins and cause proteolysis by hydrolysing peptide bonds between amino acids of the proteins [44]. This activity is important for many physiological and pathological processes [45]. Proteases or peptidases are of two types: endoprotease and exoprotease. An endoprotease cuts a bond within a protein/peptide molecule, whereas an exoprotease cleaves off either the carboxy- or the amino-terminal amino acid of the protein/peptide (**Figure 1**).

Based on the mechanism or catalytic residue taking part in the catalysis, proteases in general are divided into six distinct classes namely, aspartate-, glutamate-, metallo-, cysteine-, serine, and threonine-proteases. However, glutamate proteases have not been identified in mammals [46]. As described above, the bacterial virulence factors PLN, TLN, and ALN are all proteases of the MP class [34, 47]. All classes of endoproteases are found both extracellularly and intracellularly (**Figure 1**), but aspartate, threonine and cysteine proteases are mostly intracellular and their proteolytic activity occurs in an acidic environment, whereas serine proteases and MPs are mostly extracellular and hydrolysis occurs optimally at neutral pH [48].

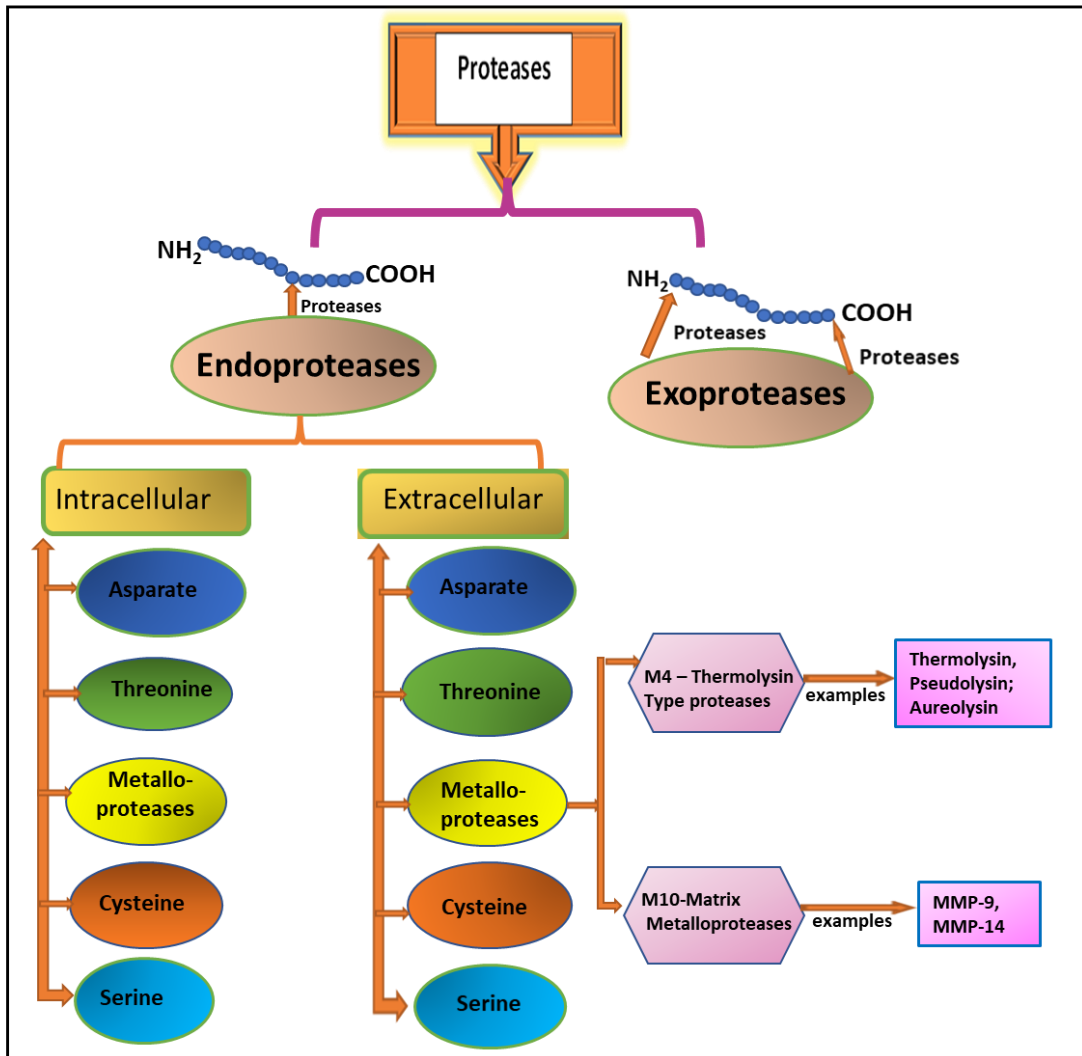


Figure 1: General classification of proteases. The figure was generated based on the text from references 44,46 and 48 by using Powerpoint.

1.2.1 Metalloproteases

Based on sequence similarity and evolutionary distances, MPs are classified hierarchically into more than 90 MP families with subfamilies and clans with subclasses. This is a widely accepted classification provided by the MEROPS database [34]. Most members of the MP class contain two zinc ions and up to four calcium ions. One zinc ion is catalytic, while the other is structural. The calcium ions stabilize the structure [49]. MPs can have metals other than zinc in their catalytic site. For example, cobalt, manganese, or nickel may be anchored at the bottom of the catalytic cleft attached to side chain amino acid residues of the enzyme [50, 51].

MPs with zinc at the catalytic site belong to clan zincin. Generally, three amino acid residues histidine, aspartate, and glutamate are known as zinc-binding residues that are characteristic of particular MPs clans and families [45]. Zincin is the most extensive clan of MPs, which have a relatively common short zinc-binding amino-acid consensus sequence **HEXXH**. This motif is provided by an “active-site helix” and supplies two metal-binding histidines (**H**) and the general base for the reaction which is the glutamic acid (**E**). MPs with this motif belong to two subclans; gluzincin and metzincin. The first one was so named because a glutamic acid (**E**) is the third metal-binding residue whereas the latter one contains a histidine or aspartic acid instead of glutamic acid as the third metal-binding residue. The bacterial MPs TLN, PLN and ALN are all classified into the subclan gluzincin (**HEXXH+E**). In addition, they belong to the M4 family, often called the thermolysin family [52]. The subclan metzincin contains a loop in the active site that is termed the “Met-turn” due to a conserved methionine (**M**) [50, 53]. In metzincins, the catalytic zinc ion is bound to the protein either through three histidine residues or two histidine residues and one aspartic acid residue (**HEXXHXXGXXH/D+M**), depending on the family [54]. Human matrix metalloproteases (MMPs), for example, MMP-9 and MMP-14 belong to this subclan. In addition, the MMPs belong to the M10 family of MPs [55] (**Figure 1**). In MMPs, the catalytic zinc is bound to the enzyme through three histidine residues.

The bacterial MPs TLN, PLN and ALN and the human MMPs MMP-9 and MMP-14 are the MPs studied in the present thesis. They all belong to the clan zincin and have structural similarities in their catalytic sites. There are also structural similarities in molecules inhibiting these enzymes. In the following sections, the active site nomenclature, the structural organization, in addition to the active site topology of these enzymes are presented.

1.3 Catalytic site nomenclature and specificity of the studied proteases

The topology of the active site is important for both specificity and substrate binding. In general, the structural environment of the active site is in a conformational state for performing catalysis before recruiting any substrate. A widely used nomenclature system to describe the molecular interaction of proteases with their substrates was introduced by Schechter and Berger in 1967 [56]. In this system, the active site of a protease to bind a

polypeptide substrate is imagined as a series of subsites (subpockets). Each subsite interacts with one amino acid residue of the substrate. By nomenclature, the substrate amino acid residues that interact with proteases are called P (for peptide) and the subsites on the protease that interact with the amino acid residue of the substrate are called S (for subsite).

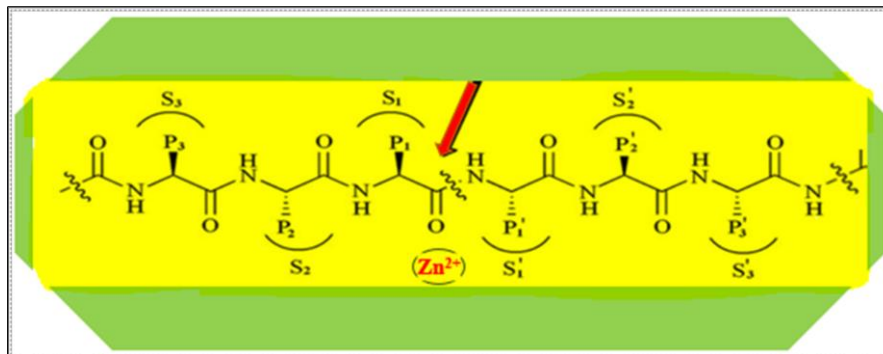


Figure 2: Schematic illustration of different binding subsites of a peptide substrate to the active site cleft in a zinc MP. This nomenclature is used for all proteases. The active site cleft with its sub-sites is denoted as S (S_1 , S_2 , etc.) and the amino acid residues in the peptide substrate that interact with these sub-sites are defined as P (P_1 , P_2 , etc.). The unprimed sites are to the N-terminal and the primed sites are to the C-terminal side of the scissile bond denoted with a red arrow. The zinc ion represents the catalytic residue for most MPs (modified from [56] using Powerpoint).

These subsites interact with the side chains of the residues flanking the scissile or cleavable amide bond. The binding site is subdivided into N-terminal (non-primed) and C-terminal (primed) sites relative to the scissile bond. As shown in **Figure 2**, the substrate side chain upstream (N-terminal) of the cleavable amide bond is termed P_1 , P_2 , P_3 , etc., and downstream (C-terminal) are P_1' , P_2' , P_3' , etc. The corresponding subsites of protease that interact with residues of the substrate are termed S_1 , S_2 , S_3 , and S_1' , S_2' , S_3' , etc., respectively.

The S_1' subsite is the most important for substrate recognition and specificity in many proteases, including MMPs and bacterial MPs of the M4 family. Generally, the S_1' subsite constitutes a hydrophobic site by interacting with hydrophobic or bulky hydrophobic amino

acid side chains of substrates, whereas the S_1 subsite is characterized by hydrophilic residues. The S_2' subsite is also hydrophobic [57]. However, as the active sites of M4 enzymes were found to be structurally quite similar to the endogenous metzincins, for example MMPs belonging to the M10 family, the substrate binding pockets of MMPs present quite similar subsites for the substrates as that of M4 enzymes. Moreover, the depth of the S_1' subsite particularly might represent a specificity factor that may distinguish between the M4 and M10 enzymes [58].

TLN prefers substrate cleavage at the N-terminal side of Leu, Phe, Ile or Val as P_1' residue. Besides, hydrolysis of bonds with Met, His, Tyr, Ala, Asn, Ser, Thr, Gly, Lys, Glu or Asp at P_1' has also been observed. The major specificity site for the substrate of this enzyme is at S_1' , which accepts large hydrophobic residues. Although substrates can interact with residues in the S_1 , S_2 and S_2' subsites, these interactions are less important for specificity [59].

PLN has a significantly more 'open' active-site cleft than TLN. Due to this broader cleft, PLN prefers mostly aromatic residues at the P_1' position as opposed to aliphatic ones favoured by TLN [60]. For ALN, the S_1' site is also the main specificity determinant and is configured to accommodate hydrophobic P_1' residues. In contrast to TLN and PLN, the deep active-site cleft of ALN has a more closed and narrow structure. The presence of a loop segment on top of the active-site cleft makes ALN unique, and because of that ALN lacks elastinolytic activity in comparison to some other members of the M4 family [61].

MMPs generally break peptide bonds N-terminally of a residue with a hydrophobic side chain, for example, Leu, Ile, Met, Phe, or Tyr. The S_1' pocket of variable depth is a well-defined substrate P_1' -binding site in MMPs [62]. Many of the structurally known MMPs possess Leu at their substrate P_1' position (**Figure 2**) and they are classified as "deep and intermediate S_1' pocket MMPs". The S_1' subpocket of MMP-9 is a relatively flat, slightly twisted tunnel-like cavity of predominantly hydrophobic character located in the centre of the active site groove. In MMP-9, this subsite possesses an intermediate-sized pocket, which is neither deep nor shallow and prefers large aliphatic residues in the P_1' position such as Leu and Met [63]. A deep tunnel-like pocket is found in many MMPs like MMP-3, MMP-12, and MMP-14, which can accommodate larger amino acid derivatives, such as

homophenylalanine in the P₁' position and thereby contributing to the substrate specificity [64, 65].

1.4 Thermolysin, pseudolysin and aureolysin

The recent release (Release 9.4) of the MEROPS database shows that the M4 family is a big family of MPs, and its members are mostly bacterial MPs. The main physiological function of secreted bacterial MPs is to degrade host proteins and peptides for bacterial nutrition, and several of them are bacterial virulence factors.

1.4.1 The maturation process

Similar to other secreted MPs, the activation process of bacterial M4 MPs involves the removal of the signal peptide (SP) after the enzyme is secreted [66]. Bacterial M4 MPs are typically translated as propeptides, with a secretory signal sequence at N-terminal to the propeptide and a two-domain peptidase unit. Following the SP in the precursors, a propeptide is present that acts as an intramolecular chaperone (IMC), contributing to the correct folding of the catalytic domain (**Figure 3**). However, the IMC is not required for function [67, 68].

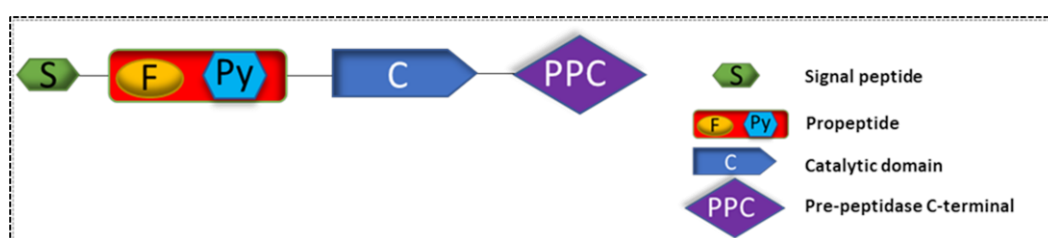


Figure 3: Representation of the domain structure of typical precursor M4 bacterial MPs. The precursor comprises four main parts: a signal peptide S, a propeptide (F and Py), a catalytic domain (C), and PPC domains. The PPC-terminal domain is a type of C-terminal extension in several TLN- like proteases. The figure was created by using Powerpoint.

A recent study revealed that the propeptides contain a peptidase inhibitor domain known as 'pepSY' [69]. In some bacterial MPs, the precursor also contains a C-terminal extension, as

in the *pseudoalteromonas sp.* SM9913, which contains two PPC (Pre-peptidase C-terminal) domains at its C-terminal extension [68]. Both the propeptide and the C-terminal extension are cleaved during maturation. Biochemical studies have revealed that the maturation of bacterial MPs is accomplished by an autocatalytic process, and their prodomain also plays a key role in the maturation [70, 71].

The PLN maturation process has been studied in detail among the M4 family members. After synthesis, prepropseudolysin is secreted into the periplasm and the SP is removed. The resultant proenzyme folds into an un-auto-processed zymogen which is mediated by its prodomain [67]. Then, going through the autocatalysis, the prodomain is rapidly cleaved off. In most cases, the prodomain is cleaved off in the periplasm by full or partial autocatalysis but remains associated non-covalently with a mature peptide which results in the auto-processed complex of PLN [72-74]. Later this auto-processed complex is translocated to the outside of the cells through the outer membrane by the Xcp (extracellular carboxyl proteases) export machinery [75, 76]. Dissociation and degradation of the prodomain by other active PLNs result in the formation of an active PLN [74, 77]. A detailed study by Gao et al. [68] observed that the un-auto-processed zymogen is in an unstable conformational state with high energy basal protease activity. This condition leads to the quick induction of the first autocleavage of the peptide bond between the prodomain and the catalytic domain. Upon this autocleavage a more stable autoprocessed complex of the prodomain and the catalytic domain with lower energy is formed. The C-terminus of the prodomain in the autoprocessed complex inserts into the cleft between the two regions of the catalytic domain. The last histidine residue of the prodomain replaces the activated water molecule in the mature enzyme and acts as a monodentate ligand to zinc. This interaction brings about the inactivation of enzyme activity. Thereafter, C-terminus of the prodomain in the complex is broken into small peptide pieces and is released from the catalytic domain. Another water molecule occupies the fourth coordinating site of the catalytic Zn^{2+} and thereby results in a fully active enzyme [68].

1.4.2 Three-dimensional structure

1.4.2.1 Thermolysin

The very first X-ray crystal structure of TLN revealed that it comprises 316 amino acid residues [78] and has a molecular mass of 34.6 kDa [59]. It contains an N-terminal and C-terminal region, which form the catalytic domain. The N-terminal region is mainly β -pleated sheets, whereas the C-terminal is predominantly α -helical (**Figure 4(b)**). The catalytic centre is an approximate tetrahedral geometry formed with the coordination of Zn^{2+} and its four ligands, His142, His146, Glu166, and the activated water molecule. The Zn^{2+} is located in a deep cleft of the catalytic centre and participates in the hydrolysis process. Therefore, it is named the catalytic Zn^{2+} . Removal of the catalytic Zn^{2+} by a chelator lead to the loss of the activity [79]. Besides the Zn^{2+} , there are four Ca^{2+} ions of which two are located near the catalytic centre and the other two on two surface loops. These are found important for the structural stabilization of TLN by preventing autolysis [80].

1.4.2.2 Pseudolysin

Pseudolysin (PLN) is the most important extracellular endoprotease of *P. aeruginosa*, and has a molecular mass of 33 kDa containing 301 amino acid residues [81]. This enzyme shows considerable sequence homology with TLN, with approximately 48 % overall sequence identity. The identity is especially high in the region between residues 136 and 180, which includes part of the catalytic site [82]. Therefore, the 3D structure of PLN is almost superimposable to that of TLN [83]. Like TLN, PLN also has N-terminal and C-terminal domains that are separated by the cleft of the catalytic site (**Figure 4(a)**). The N-terminal domain contains antiparallel β -strands while the C-terminal domain is α -helical like that of TLN. It contains one zinc atom necessary for the activity, while one calcium ion is required for its stability. PLN contains four cysteine residues which form two disulfide bonds (Cys30–Cys58 and Cys270–Cys297) important for both stability and activity. Cysteine residues are not present in TLN [84].

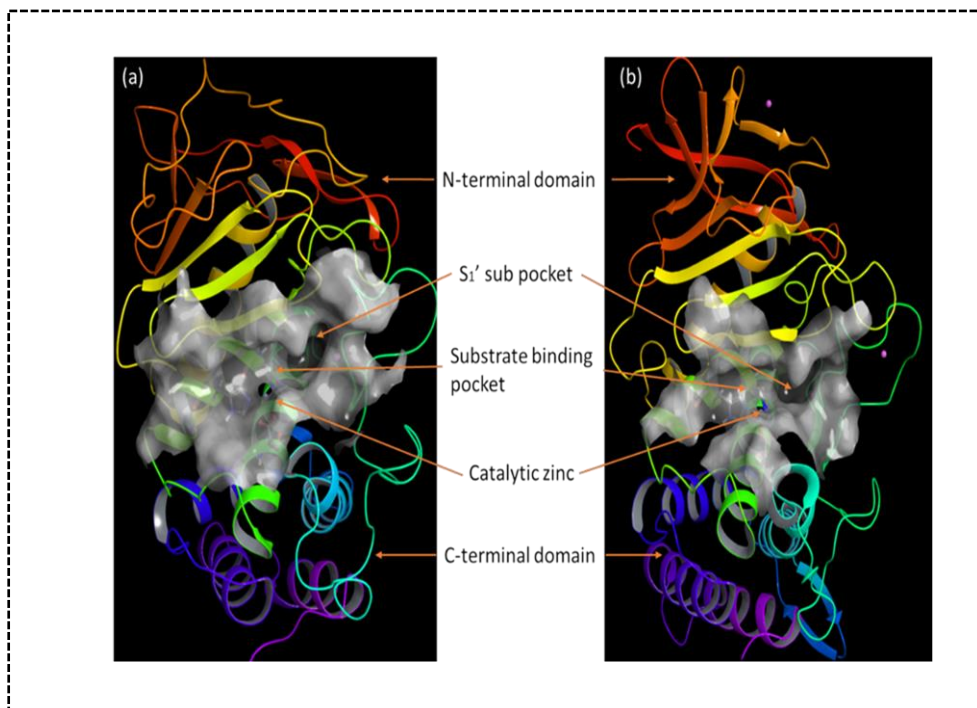


Figure 4: Comparison between the substrate binding site of PLN and TLN. The α -trace of the enzymes are shown. (a) 3D structures of the catalytic domain of PLN (PDB-1u4g) which has a more open and broader active site than TLN. (b) 3D structure of the catalytic domain of TLN (PDB-5dpe) showing the substrate binding site. The figure has been created with the program majestro included in the Schrödinger suit of molecular modelling programs.

1.4.2.3 Aureolysin

ALN is an extracellular zinc-dependent neutral MP secreted by *S. aureus* [85, 86]. It is a single-chain protein that contains 301 amino acid residues with a molecular mass of 38 kDa [87, 88]. It exhibits high sequence similarity to other proteases from the TLN family. ALN is conserved in two allelic forms (type I and II) in *S. aureus* that employs different specific functions. The primary structure of type I ALN shares a sequence homology of 48.6% and 36.7% with TLN and PLN respectively [89]. This enzyme binds one zinc metal ion necessary for activity and three calcium ions essential for its stability.

1.5 Human matrix metalloproteases

The extracellular matrix (ECM) comprises various matrix macromolecules. Major constituents are fibrous-forming proteins such as collagens, elastins, fibronectins, proteoglycans, laminins and glycoproteins. All proteins undergo extensive remodelling or breakdown under many physiological and pathological conditions [90]. The primary enzymes responsible for ECM breakdown are endoproteases belonging to the subclass metzincin of the MP class. The major role of these MPs is the degradation of various ECM and non-ECM molecules to regulate many physiological functions in humans, such as cell growth, angiogenesis, cell apoptosis, tissue repair, blood pressure, coagulation, cell signalling, reproduction, wound healing, hemostasis and homeostasis and immune response [91]. MMPs are also reported to promote cell proliferation, migration, and differentiation [92]. MMPs belong to the M10 family and show optimal proteolytic activity between pH 7 and 8 for most substrates [93]. Dysregulation of one or many of these MMPs can lead to numerous serious health issues, such as cardiovascular diseases, arthritis, and neurodegenerative diseases, as well as various types of cancer [94].

In humans, there are 24 different MMPs (**Figure 5**). Out of these, 16 are secreted and six (MMP-14, -15, -16, -17, -24 and -25) are membrane-anchored/associated also termed MT-MMPs, while -23A and 23B contain a type II transmembrane domain at their N-terminal domain but also an RX(K/R)R motif in front of the catalytic domain. The secreted MMP-9 (gelatinase B) and the membrane-associated MMP-14 are the two most studied [95].

MMPs are classified based on different criteria such as structural homology, substrate preferences, mechanism of enzymatic reaction, and types of domains present. The catalytic domain of all MMPs contains the zinc-binding motif **HEXXHXXGXXH** (E- the catalytic glutamic acid) [92]. The occurrence of additional domains within the C-terminus is the major difference between MMPs [96]. The typical structure of MMPs consists of a prodomain, a catalytic domain, a hinge region and a hemopexin-like domain (HPX) (**Figure 5**) [97].

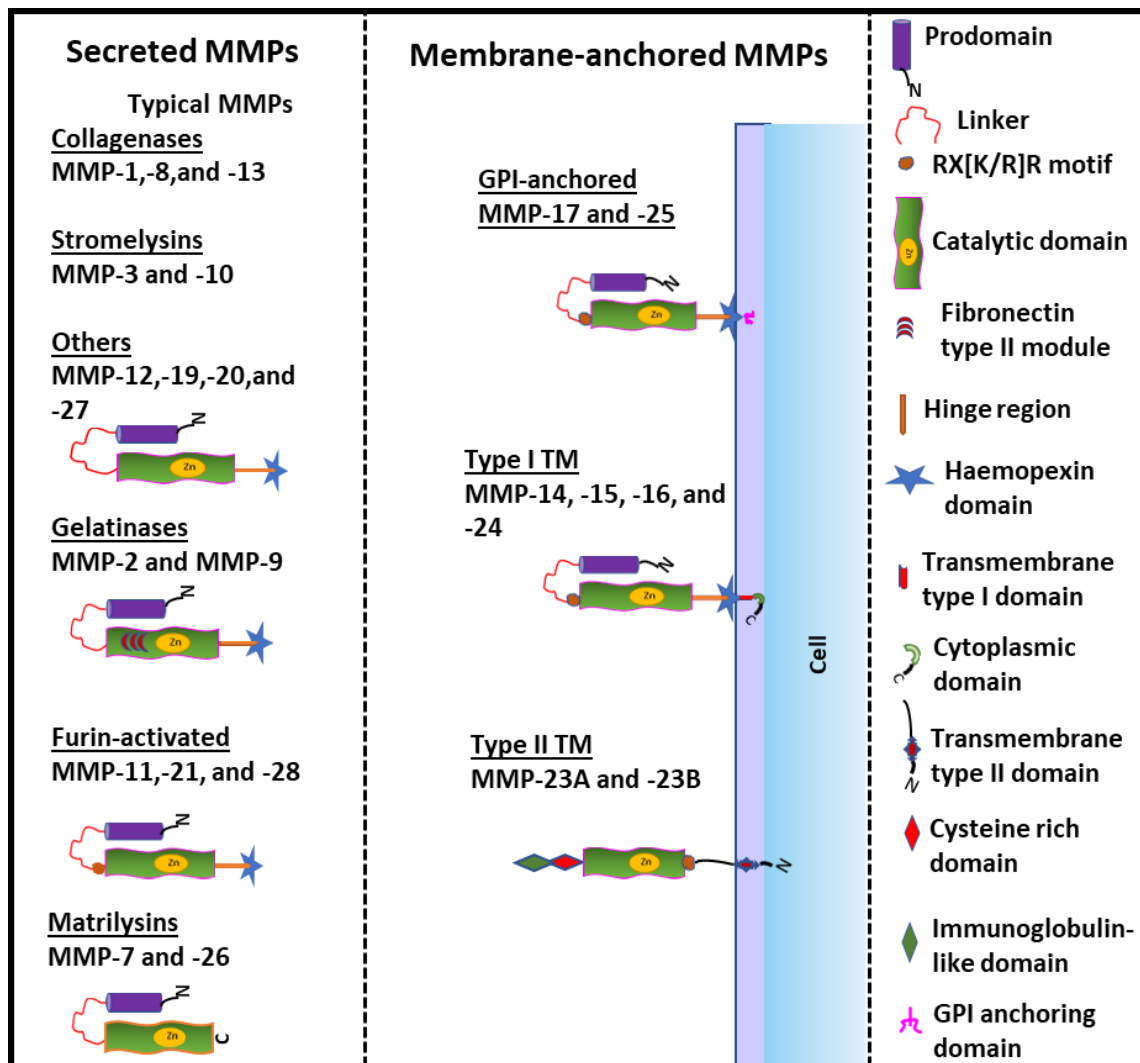


Figure 5: Classification of MMPs with their domain structures. There are four common domain structures found in MMPs: a propeptide domain, a catalytic domain, a hinge region and a hemopexin domain. MMP-7 and MMP-26 do not have haemopexin and hinge regions. MMP-9 contains a heavily O-glycosylated hinge region, while both MMP-9 and MMP-2 have three fibronectin-like repeats in the catalytic domain. RX(K/R)R motif is present at the C-terminal end of the prodomain of both membrane-anchored and furin-activated MMPs) (modified from [96 and 97] using Powerpoint).

1.5.1 Matrix Metalloprotease-9

Matrix metalloprotease - 9 (MMP-9) is known to have gelatin-degrading capacity and hence is called gelatinase. MMP-2 is also known as a gelatinase having the same capacity. MMP-9 is a secreted multidomain enzyme. Human monomer proMMP-9 has a molecular weight of 92 kDa [98]. Like collagenases, stromelysins and MT-MMPs, MMP-9 contains all typical domain structures of MMPs (**Figure 5**), with an additional fibronectin-like module

in the catalytic domain consisting of cysteine-rich repeats that resemble fibronectin type II and enables binding to gelatin (denatured collagen), laminin and collagen types I and IV (**Figure 5**). However, MMP-9 is the most complex MMP identified so far. Having a heavily glycosylated structurally flexible 64 amino acids linker region (OG domain) between its catalytic and HPX domain, it possesses a rather different overall 3D structure compared to MMP-2. Previously this domain was called the type-V-collagen-like domain [99, 100].

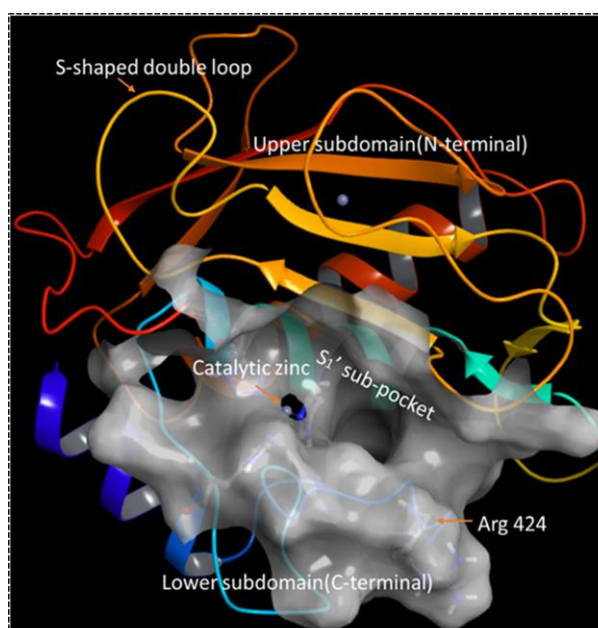


Figure 6: 3D structure of the catalytic domain of MMP-9 (PDB-2OVZ). The α -trace of the catalytic domain is shown. The figure has been created with the program majestro included in the Schrödinger suit of molecular modelling programs.

The catalytic domain of the MMP-9 has an oblate-ellipsoidal shape with a notch at its flat surface which harbours the catalytic zinc. It is separated into small “lower” S_n' ($n'=1, 2, 3\dots$) and large “upper” S_n ($n=1, 2, 3\dots$) subdomains. These subdomains form the substrate binding pocket. The upper subdomain comprises a five-stranded, highly twisted β -sheet, two α -helices, and three surface loops together with the S-shaped double loop, which is attached to the β -sheet by the “structural” zinc ion. The lower subdomain consists of a wide right-handed spiral terminating in the met-turn, the S_1' wall, the specificity loop arcuate around the S_1' pocket, and a C-terminal α -helix (**Figure 6**).

1.5.2 Matrix Metalloprotease-14

Matrix metalloprotease-14 (MMP-14) was the first integral membrane protein found among MMPs. Therefore, it was named membrane-type I matrix metalloprotease (MT1-MMP) [101]. The activated MMP-14 has a molecular mass of 53.7 kDa [102] and was first reported as an efficient activator of proMMP-2 [101]. It can also activate pro-collagenase 3 (proMMP-13) [103]. MMP-14 contains a typical domain structure of MMPs with an additional transmembrane domain and a cytoplasmic tail (**Figure 5**) [101]. Furin was reported to activate proMT1-MMP by cleaving at Arg111-Tyr112 of a decapeptide insert with an RXLR motif upstream of its catalytic domain [104]. It is also reported that by cleaving the same site, trypsin can also activate the human recombinant proMT1-MMP ($\Delta 269-559$, N-MT1-MMP) *in vitro* [105].

1.6. Catalytic mechanism of metalloproteases

A functional zinc ion in the active site of TLN acts as a cofactor and is essential for proteolytic function. The catalytic mechanisms of TLN have been used as a model system to understand different stages of enzyme catalysis in zinc MPs [106]. This mechanism involves the recruitment and positioning of a water molecule before catalysis. The water molecule first interacts with the catalytic zinc ion and forms hydrogen bonds with the general base, a glutamic acid residue adjacent to the first histidine in the zinc-binding motif (**HEXXH+E**) (**Figure 7**). This action polarizes the solvent and increases its nucleophilicity. With a Zn^{2+} -coordinated water molecule, the wide groove separates the enzyme into two large domains and, through the accommodation of an extended peptide chain within the enzyme, results in the Michaelis complex [80, 106]. Once the carbonyl oxygen of the scissile peptide is bound and polarized by the catalytic metal, the carbonyl carbon becomes more susceptible to nucleophilic attack by a water molecule. A proton is accepted by the general base glutamate that is immediately transferred to the nitrogen of the scissile substrate bond. Thus, a gem-diolate tetrahedral reaction intermediate is formed. Again, the glutamic acid serves as a proton shuttle, removing the second proton from the water molecule and delivering this proton to the same amino nitrogen in the substrate. The peptide bond (C-N) is broken, and finally, the release of an amine and an enzyme-carboxylate

complex is resolved from the intermediate. The catalytic cycle is closed by the carboxyl product detachment, probably mediated by the uptake of a new water molecule [107].

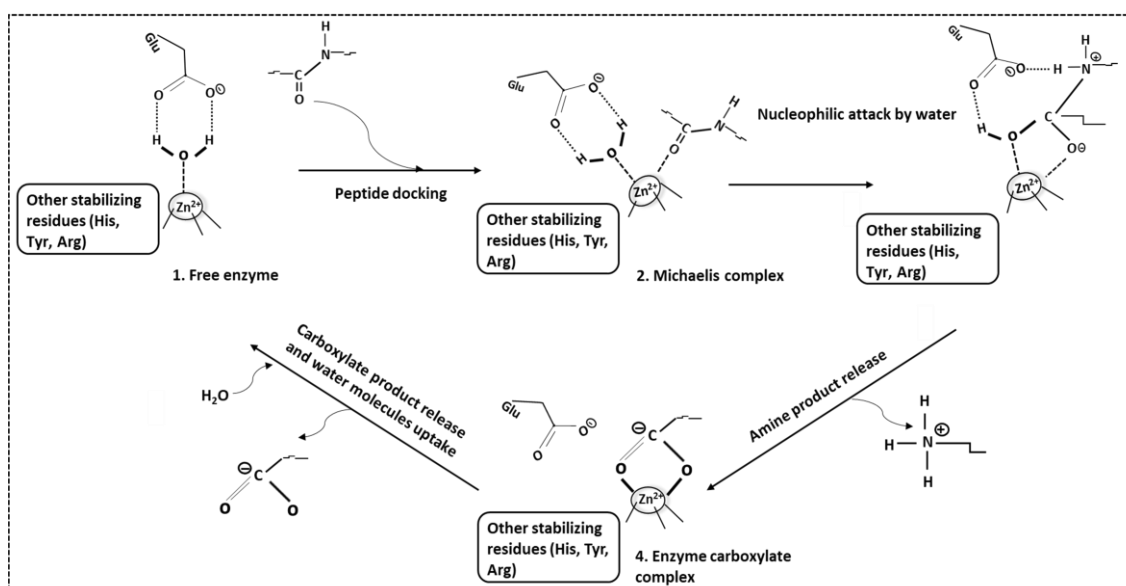


Figure 7: Schematic representation of hydrolytic mechanism for MPs. Most MPs contain two zinc ligands histidine (**HEXXH+E**) and some three, and usually, glutamic acid (**E**) acts as a Lewis acid or base. The fourth ligand is a water molecule that is activated and cleaves peptide bonds through a nucleophilic attack on the carbon atom in the carbonyl group. His, Tyr or Arg residues serve to stabilize the transition phase by forming a hydrogen bond with the oxygen atom on the carbonyl group. Protonation of the amide nitrogen atom results in the bond being split off. Zinc acts as a Lewis acid in the system and becomes penta-coordinated (modified from [80] using Powerpoint).

1.7 Inhibitors of zinc metalloproteases

Enzyme activity can be affected by inhibitors slowing down or stopping an enzymatic reaction. Poisons and drugs often act as enzyme inhibitors. By the 21st century, medical science evolved a lot in discovering drug targets and new drugs were discovered for receptors (e.g. opioids), ion channels (e.g. calcium channel blockers), transporters (e.g. diuretics) and enzymes (e.g. angiotensin-converting-enzyme inhibitors) [108]. Enzymes hold a prominent position among antibacterial drug targets [109, 110]. Enzyme inhibitors have immediate and defined effects that are key criteria for being a good therapeutic agent. Hence, the efforts to identify and optimise drug candidates are made by focusing on the act

of inhibition of specific enzyme targets. Among currently available drugs, 47% are enzyme inhibitors [111].

Zinc MP inhibitors may be endogenous peptides or proteins like the tissue inhibitors of metalloproteases (TIMPs) [112] that inhibit MMPs, and the streptomyces metalloprotease inhibitor (SMPI) that inhibits enzymes of the M4 family [113] or traditional small synthetic molecules. However, both endogenous peptide and protein inhibitors and also small synthetic molecules have a functional group capable of displacing the zinc-coordinating water molecule and interacting with the catalytic zinc, referred to as zinc-binding groups (ZBGs). A lot of effort was put into the development of MMP inhibitors for therapeutical use. Most of the compounds failed in clinical trials. However, over the years, several drug screening campaigns have identified high-affinity inhibitors of human MMPs and other zinc MPs [114]. In addition to high-affinity inhibitors, these screening campaigns also resulted in several compounds with known ZBGs but limited or no activity for the tested target. Phosphinate (PO_2^-), carboxylate (COO^-), thiolate (S^-) and hydroxamic acid HONH-CO were identified as effective ZBG leading to potent inhibition of zinc MPs [115-119]. In addition to zinc interactions, these functional groups may provide hydrogen bonding interactions with the enzyme backbone, and one or more additional groups may form effective Van der Waals interactions with enzyme subsites [114] (**Figure 2**).

Hydroxamic acid is a widely used ZBG for inhibitors of MMPs [120] and is also a common motif in the development of protease inhibitors connected to many diseases [121]. These compounds relied on targeting the zinc ion in the active site of MMPs. However, due to a lack of specificity along with partial instability and hydrolysis of hydroxamate to hydroxylamine and carboxylate derivatives [49,69], these zinc ion chelators failed in the late stages of clinical trials. A precise understanding of the structural details of individual MMPs from the available crystal structures [205, 206], as well as the role of the individual MMPs in normal physiology and disease, is of utmost necessity and requires a lot of investigation to find more potent, and selective ZBGs for the MMPs active site zinc ion to incorporate the inhibition.

Phosphorus-containing drugs have been an important class of therapeutic agents targeting a broad range of diseases. Due to the strong absorption capacity for metal ions and organic molecules, phosphorus-containing compounds were also found to act as good inhibitors of

zinc MPs [122]. The major types of phosphorus-containing functional groups include thiophosphate-containing P=S bonds, phosphoric anhydrides with one or multiple P-O-P units, and bisphosphonate - bearing P-C-P units. BP drugs are bone resorption inhibitors belonging to the class of anti-osteoporotic drugs [123]. Compounds containing a phosphorus atom bound directly to one or more carbon atoms show more hydrophilic character and better chemical stability [122]. However, phosphoramidon is a phosphorus-containing peptide and a naturally occurring potent inhibitor of TLN. A study by Bartlett and Marlowe provided evidence that the different analogs of phosphoramidon were good TLN inhibitors, and not just multi-substrate ground-state analogues but also transition-state analogs [124, 125]. They were found to form tetrahedral intermediates during the hydrolysis of peptide bonds [126].

Since the discovery of penicillins, β -lactam antibiotics have been among the most important antimicrobial drugs [127]. Metallo- β -lactamases (MBLs) have been identified as an important contributing factor to β -lactam resistance in Gram-negative bacteria [128]. To date, at least 200 different types of MBLs have been described [129, 130]. Among them, MBLs- VIM, IMP and NDM-1, produced by clinical isolates of *Enterobacteriaceae* and *P. aeruginosa* have been reported in most geographical regions [131] and become a serious threat to global public health due to their antimicrobial resistance mechanisms. In MBLs, zinc in the active site plays a central role in their activity and catalysis [132]. Therefore, zinc chelation may be an effective strategy to overcome the resistance developed by MBLs [133, 134]. Simultaneously, bacterial zinc MPs like PLN, TLN, and ALN are all zinc-dependent proteases [47, 135]. Therefore, MBL inhibitors or compounds structurally similar to known MBL inhibitors may also be a valuable strategy as zinc MP inhibitors.

Camberlein et al. described the interaction of phosphoramidon with PLN using an antivirulence approach [136]. Their study disclosed phosphoramidon as a PLN inhibitor (K_i value of 0.25 μ M) for the first time, previously reported as a TLN inhibitor (K_i of 30 nM at neutral pH) [137]. They also tested compounds containing metal-chelating moieties thiol and hydroxamate as potential inhibitors of PLN. Though several good lead compounds were reported in this study, unfortunately, none of these compounds has reached the market yet because of their poor chemical stability (oxidation) under physiological conditions and a lack of specificity over human MMPs.

Kessler et al. [138] also tested several amino acid and peptide derivatives containing hydroxamate, phosphoramidate, and thiol as potential inhibitors of PLN. The most effective inhibitors found were P-Leu-Phe, and HSAC-Phe-Leu ($K_i = 0.2 \mu\text{M}$). Similar findings were achieved by Holmquist and Vallee [139] for the inhibition of TLN using analogous derivatives. Nishino and Powers [140] showed that peptides containing thiol and hydroxamic acids were 10-fold more effective as inhibitors of PLN than TLN, as the zinc atom in the active site of PLN has a geometry more favourable for coordination with some ligands than the zinc atom of TLN.

In a recent study by Konstantinović et al. [117], a series of novel thiol-containing succinimide-based derivatives were tested as inhibitors of PLN. They found some potent inhibitors of PLN that sufficiently showed selectivity for the bacterial MPs over human MMPs with low toxicity. However, a drawback of zinc-chelating inhibitors containing the thiol group is the possible oxidation to the respective disulfides, resulting in the inactivation of the compounds [121].

To avoid this possible oxidation issue, Kany et al. [121] synthesized and tested several compounds replacing the thiol with a hydroxamic acid to see the antivirulence effect on PLN. They also aimed to see the effect on biofilm formation and extracellular DNA release by *P. aeruginosa*. One hydroxamate compound was found effective for the purposes; additionally, low cytotoxic effects on mammalian cell lines were also observed [121].

As mercaptoacetamide-based thiols have been reported to inhibit clostridial collagenase, inhibitors with high selectivity toward human MMPs also inhibit PLN [141]. Kany et al. studied the structure-activity relationship (SAR) of N-aryl mercaptoacetamides by testing 35 derivatives of this thiol-containing compound for PLN inhibition by applying a FRET-based *in vitro* assay. Their study revealed some potent inhibitors that could be further developed into drugs for antibacterial infection. The compounds of mercaptoacetamide class contain a prodrug-like thiocarbamate-motif, which releases free thiols as the active form after hydrolysis in the buffer. Unlike thiols, which have the possibilities to be oxidized to disulfides, thiocarbamate prodrugs have the advantage of being stable toward oxidation [142].

As mentioned previously, the structure of the active site clefts of the bacterial virulence factors PLN, TLN and ALN are very similar to that of human MMPs and other zinc MPs.

It is, therefore, reasonable to believe that compounds synthesized during screening for inhibitors of human zinc MPs may inhibit TLN, PLN or ALN. Over the years, our research group has also tested several known MMP inhibitors as inhibitors of PLN, TLN and ALN. Sylte et al.[143] studied two hydroxamate compounds (galardin and compound 1b) for the bacterial zinc MPs, TLN, PLN and ALN, and the two human zinc MMPs, MMP-9 and MMP-14, using experimental binding studies and molecular modelling. Both compounds bound stronger to MMP-9 than to MMP-14, while 1b was a stronger inhibitor than galardin. Only galardin inhibited the bacterial enzymes, but not as strongly as did with human MMPs. Their study also revealed that the size and shape of the ligand structural moiety that enters the S_1' -subpocket is an important determinant for specificity between the human MMPs and bacterial MPs [143].

In our research group, several hydroxamate derivatives were also tested by Sjøli et al. [57] to find inhibitors of TLN and PLN, and the human zinc MPs adamalysin-17 (ADAM-17), MMP-2 and MMP-9 using the same methods as Sylte et al. [143]. Their study showed that these compounds were stronger inhibitors of the MMPs than of the M4 enzymes. However, compound LM2 bound stronger to PLN than to TLN, and stronger to the two bacterial MPs TLN and PLN than to tested human MPs. Molecular modelling revealed that occupation of the S_2' subpocket by an aromatic group was the main reason for stronger interactions with PLN than with TLN [57].

A series of 14 compounds that have previously been investigated for their ability to inhibit different MMPs were also tested for TLN and PLN by Adekoya et al. [33]. Their study showed that only two compounds bound stronger to PLN and TLN than to the MMPs. They also revealed that the structural differences between the bacterial zinc MPs and human MMPs in S_1 , S_1' and S_2 subpockets at the active site and the shape and size of the compounds are important for designing new TLN and PLN inhibitors with low MMP binding affinity [33].

2. Aims of the study

The overall long-term goal of our project is to identify inhibitors of the bacterial virulence factors PLN, ALN and TLN that could be developed into drugs against bacterial infections. Several inhibitors have been identified for TLN and PLN, both by our group and by others, some of which were already mentioned above. However, TLN and PLN inhibitors have so far not been developed into approved drugs. To our knowledge, small molecules as inhibitors of ALN have not been identified either.

In the present thesis, we aimed to test compounds with a ZBG from previous screening campaigns in search of MMP inhibitors for their activity against PLN, ALN and TLN. Both the compounds found to inhibit MMPs and other compounds from the screening campaigns were included [144, 145]. Further, we aimed to test their effects against human MMP-9 and MMP-14 using the same experimental conditions as for the bacterial MPs. In addition, we wanted to test a series of compounds with nitrogen as a donor atom for zinc chelation. These compounds have previously been tested for their binding of MBLs [127, 134, 146].

In that way, we were aiming to obtain information that could enrich the existing knowledge about the inhibition of bacterial zinc MPs. In addition, identify compounds that could be used as lead compounds for the development of anti-virulence drugs or compounds that could be used as adjuvants during antibacterial treatment.

We considered several approaches to achieve the above-mentioned goals:

- Perform enzyme kinetic and inhibition kinetic studies with the different series of compounds to obtain information about the inhibitory activities and compare their affinities to both human and bacterial zinc MPs.
- Study the molecular interaction of various inhibitors with bacterial and human zinc MPs by molecular modelling.
- Study the possible quenching effect of the putative inhibitors on the fluorescence product of the substrate (McaPL-OH) formed during catalysis.
- Predict the cleavage site/sites of the fluorogenic substrate Mca-Arg-Pro-Pro-Gly-Phe-Ser-Ala-Phe-Lys(Dnp)-OH (catalogue # ES005) by TLN, and identify enzyme amino acids constituting the different subpockets of the substrate binding site using molecular dynamics (MD) simulations.

3. Experimental summary

Compounds were tested as inhibitors of the bacterial virulence factors PLN, ALN and TLN and the human MMP-9 and -14 using enzyme kinetics and molecular modelling. By inhibition kinetics, we obtained affinity values of the tested compounds, while molecular modelling of enzyme-compound complexes contributed with structural insight into the affinity values.

The experimental methods applied in the present study were similar for all three papers. The fluorogenic substrates Mca-Arg-Pro-Pro-Gly-Phe-Ser-Ala-Phe-Lys(Dnp)-OH (catalogue # ES005) for bacterial zinc MPs and Mca-Pro-Leu-Gly-Leu-Dpa-Ala-Arg-NH₂ (catalogue # ES001) for MMP-9 and MMP-14 were used for enzyme kinetic studies. First, it was necessary to determine if a compound was an inhibitor and if the compound was a slow or fast binder. In these experiments, 100 μ M compound was mixed and preincubated with the enzyme for different time points (0 – 45 min) at room temperature before the addition of substrate and the determination of enzyme activity. Dose-response curves were performed for compounds that inhibited the enzyme activity by more than 50% and from these curves IC_{50} values were determined. Thereafter, K_i values were determined based on the inhibition mechanism using IC_{50} values and K_m values for the substrates during the conditions used in the inhibitory experiments. The binding modes of the strongest inhibitors of the tested compounds with the TLN, PLN, ALN, MMP-14 and MMP-9 were studied using molecular docking. In **paper I**, the ICM-modelling software [147] was used for docking, while the Schrödinger suite of programs [148] was used for the molecular docking in **paper II** and, and molecular dynamics studies in **paper III**.

Catechol-containing compounds in **paper I** were previously investigated as MMP inhibitors by Tauro et al. [144]. They were tested for binding to MMP-2,-8 and -9, and we wanted to see if these compounds also could inhibit bacterial zinc MPs. Seven catechol derivatives from the previous study by Tauro et al. [144], in addition to ML33 were tested in the present study, focusing on classical SARs. Most of the catechol derivatives had a sulphonylamide group connected to aromatic groups, and we wanted to see how the relative position of the sulfonamide linking group with catechol as well as the hydroxyl groups in the catechol, affected the binding interaction with bacterial zinc MPs and human MMP-9 and MMP-14.

Previously Rubino et al. tested the bisphosphonate compounds RC14, LS4, MT242, and RC2 against MMP-2,-8,-9,-14 [149]. In **paper I**, a total of seven bisphosphonate compounds, including those that Rubino et al. investigated, were also studied against PLN, ALN and TLN and MMP-9 and MMP-14. Quenching effect on the fluorescence product formed during catalysis and time-dependent inhibition were also tested for the compounds.

Several studies have shown that zinc chelators could be used [150] to inhibit MBLs by removing Zn^{2+} from their active site [151, 152]. In **paper II**, twenty different zinc chelators dipicolylamine (DPA), tripicolylamine (TPA), tris pyridine ethylene diamine (TPED), pyridine and thiophene derivatives were tested against TLN, PLN, ALN, MMP-14 and MMP-9 using the same methods as in **paper I**.

Phosphinates were found to be transition state analogues where one oxygen atom of the phosphate binds zinc, and the other oxygen interacts with the catalytic Glu and hence has the position of the water molecule that hydrolysis the peptide bond. Previously, different phosphinyl-containing compounds have been tested against various MMPs and other MPs, such as compound H-1 (RXP470) against MMP-1,-2,-3,-7,-8,-9,-10,-11,-12,-13,-14, ACE, NEP and TACE [153, 154], compound H-2 (RXPO3) against MMP-1,-2,-7,-8,-9,-11,-14 [155] and compound H-4 against the carboxypeptidase Angiotensin Converting Enzyme-2 (ACE-2) [145]. In **paper III**, we tested H-1, H-2 and H-4, in addition to two phosphinyl-containing compounds to check if they were inhibitors of bacterial zinc MPs, and how strongly they inhibited MMP-9 and MMP-14 under the same experimental conditions as used for the bacterial MPs. Besides using the same methodology as in the first two papers for compound testing, two 200 ns MD simulations of TLN/ES005 complexes were performed to find the most favourable cleavage site of ES005 by TLN and identify amino acids within the different substrate binding subsites of TLN. Similar simulations were also performed for complexes of ES001 with MMP-9 and MMP-14 to identify amino acids within the subsites of these enzymes.

4. Summary of Results

Catechol and bisphosphonate compounds (**Paper I**), zinc-chelating compounds (**Paper II**) and phosphinic compounds (**Paper III**) showed no quenching effect on the substrate product (McaPL-OH). Most of the zinc-chelating compounds and some phosphinic compounds expressed background fluorescence, but this did not affect the inhibitory assays or the determination of their IC_{50} and K_i values against the proteases they bound.

An experiment of enzyme inhibition kinetics to check the inhibition mechanism of catechol and bisphosphonate compounds (**Paper I**) revealed that they were bound to the active site of the proteases and are thereby considered to be competitive to the substrates of these proteases. All other tested compounds in the present thesis were also found to be competitive inhibitors, and they were also found to bind to the active site in the docking studies. None of the compounds alone showed stronger binding to the bacterial MPs than human MMPs except for bisphosphonate compounds RC2 (**Paper I**) and the zinc chelator DPA (**Paper II**). The RC2 compound bound stronger to TLN and PLN while the zinc-chelating compound DPA inhibited PLN much stronger than the other proteases, including human MMPs. The zinc-chelating compounds TPA and its derivative Zn148 (**Paper II**) showed strong inhibition of both PLN and MMP-14 with K_i values in the lower μM region. Several catechol-containing compounds, particularly BF471 showed more than 50% inhibition of all five proteases including ALN for which K_i value was around $49 \mu\text{M}$ (**Paper I, Figure 1**). Inactivation experiments along with microdialysis of TPA revealed that it was a time-dependent reversible inhibitor of MMP-14. Molecular docking results revealed that interaction with the S_1' subpocket residue was important for strong binding and inhibition of MPs. The orientation of the side chain of R203 in TLN, R200 in ALN, and R197 in PLN located at the entrance of the S_1' subpocket was found to hinder functional groups from entering deeply into S_1' subpocket of bacterial MPs, and this could be the main reason for weaker interaction with bacterial MPs than with human MMPs. Two 200 ns MD simulations of TLN/ES005 complexes (**Paper III**) were performed to find the putative favourable cleavage site for TLN/ES005 complex. This study revealed that the Gly (P_1) - Phe (P_1') bond was a more favourable cleavage site for TLN/ES005 than between Aln (P_1)-Phe (P_1'). Of the five phosphinic compounds, only H-2 acted as a strong inhibitor against all five enzymes, H-1 only against the two MMPs, while H-3, H-4 and H-5 could not be regarded as good inhibitors of any of the five enzymes.

5. Discussion

Some of the compounds tested in the present studies have previously been tested against MMP-9 and MMP-14. We decided to retest these compounds as our experimental conditions varied from those previously used. The differences in experimental conditions and to which extent these differences resulted in different binding strengths of some of the compounds were depicted in detail in the papers of this thesis, and will not be discussed in the present chapter. The SAR of the tested compounds, including elucidation of the compound binding modes studied by docking, were also discussed in the three papers and will not be discussed in detail here in this chapter. The focus of the present chapter is on the most interesting compounds from these studies, and the use of zinc MP inhibitors as putative antivirulence compounds.

5.1. Antivirulence strategy at the dawn of the post-antibiotic era

In 1969, the general surgeon of the United States declared, “We have closed the chapter on infectious diseases due to antibiotics”. However, we are now in the post-antibiotic era, unfortunately, with many MDR bacteria which are responsible for infectious diseases substantially contributing to high mortality worldwide [8]. Very few new antibiotics are in the late-stage development pipeline, and according to a report from the International Diseases Society of America (IDSA) only one single new antibiotic has been approved by FDA since 2010. This report also concluded that only seven new antibiotics targeting MDR Gram-negative bacilli had completed phase II or phase III trials since 2010 [156]. If this situation continues, the prediction is that by the year 2050, around 10 million people will die yearly because of infections that are difficult to treat with available classical antibiotics [157]. The only way to control the current health crisis caused by MDR bacteria is to develop novel new strategies to fight these pathogens. Research contributing to the development of new antibacterial strategies with high selectivity and specificity to their target may give hope to overcome the critical situation in the coming years.

The present thesis is focusing on a new and promising strategy that targets bacterial virulence rather than viability, by identifying inhibitors of the bacterial virulence factors PLN, ALN and TLN. This strategy may be an alternative sustainable solution to classical

antibiotics to defeat the increasing prevalence of antibiotic-resistant of bacterial infections and has been proposed as one of the most effective solutions to this health crisis that may improve the therapeutic options for bacterial infection [8]. As bacteria-derived proteases are essential for virulence, they are attractive pharmacological targets as they may be specifically inhibited while leaving normal host zinc MPs (including MMPs) functions intact [158]. In addition, anti-virulence agents do not affect commensal bacteria, thereby mitigating secondary infections. Importantly, bacterial SOS responses to their DNA damage are not affected by anti-virulence agents, and hence little side effects may occur compared to the present antibiotic treatment. The bacterial virulence factors PLN, ALN and TLN resemble several human zinc MPs, including the MMPs, in structure and function. Hence finding selective and specific inhibitors which only strongly inhibit bacterial zinc MPs with little or less inhibition of human zinc MPs is challenging, but would be strongly beneficial. The treatment of bacterial infections with MPs inhibitors will most often be for a shorter period of time, some milder side effects may therefore be accepted. In addition, bacterial MP inhibitors could serve as adjuvants, and this potential approach can prolong the lifespan of classical antibiotics by suppressing bacterial resistance or enhancing antibiotic efficacy.

There may be some challenges with anti-virulence activity as well. The disruption of the virulence factor may imply fitness consequences for the bacteria, and this requires a more detailed understanding of the dynamics of action of the targeted virulence factor as well as the dynamics of their production. Chemical modification of the virulence factor might appear over time and can modulate its activity.[159]

5.2. Putative consequences of off-target effects on human matrix metalloproteases

In the present thesis MMP-9 and MMP-14 were chosen as representatives for human MMPs for studying putative off-target binding. The reason was that MMP-9 is the best studied among soluble MMPs, while MMP-14 is the best studied among the MT-MMPs [95]. MMPs are ubiquitously present in the human body and are found to involve in the regulation of many physiological processes. In most typical adult tissues MMPs remain at a balanced level between MMPs and tissue TIMPs, which maintains several biological activities [160]. Inhibition of the virulence factors that in addition create an imbalance between MMPs and

tissue TIMPs may affect several physiological processes such as morphogenesis, angiogenesis, tissue remodelling (e.g., cardiovascular remodelling), embryonic development, regulation of cell growth and death, and wound healing [161, 162]. Dysregulation of one or many of these MMPs (or TIMPs) can cause numerous serious health issues.

In addition, several MMPs were also found to participate in the activation of other pro-MMPs. For example, MMP-10 and MMP-3 have been identified to activate MMP-1, MMP-7, MMP-8, and MMP-9, enhancing ECM degradation [163]. MMP-2 and MMP-13 were found to help in the cleavage of the pro-domain of pro-MMP-9 for its activation [164]. However, MMP-14 activates both MMP-2 and MMP-13 and, in the presence of TIMP-2, affects tumour invasion and metastasis by promoting cell migration [165]. The cross-reactivity and interactions of MMPs can damage the ECM if the tight regulation of MMPs is not optimized [166]. The complex network and cross-reactivity of the MMPs as well as overlapping substrate recognition, make it challenging to understand the individual role of each MMP in the ECM. Off-target effect on one particular subtype of MMP during the treatment of bacterial infection may, therefore, also affect the regulation of other MMPs.

Using MMP knockout mice as a model for examining MMPs *in vivo* is challenging because animal models may not show exact human conditions and mechanisms of diseases [167]. It might show different phenotypes based on different kinds of bacteria, different infection rates or different infection routes. Two individual studies used MMP knockout mice and their conclusion on the role of MMP-9 during infection was found contradictory to each other. Lee et al. showed that MMP-9 had a protective role in infection with *Pseudomonas* [168], whereas McClellan et al. showed the opposite [169]. Though these two studies suggested that MMPs were involved in infections, it is a big challenge for researchers using knockout mice as a model for human health to find when, where and which MMP is beneficial or detrimental during a particular infection, and hence complicates the work on drug discovery.

A wide range of proteases of the M4 family secreted by *P. aeruginosa* is known to activate various pro-MMPs. The virulence factor PLN has been found to strongly activate pro-MMP-1, -8 and -9 *in vitro* [170]. MMP-9 was found to be activated by TLN [49]. The excessive MMP activity results in uncontrolled ECM cleavage, directly contributing to tissue damage

of the host [167] and the dissemination of the bacteria. The level and activities of MMPs during infection depend substantially on different parameters, such as the bacterial species and its types of virulence, the route of infection, and the immune status and age of the host conditions etc. Therefore, one of the benefits of drugs targeting a bacterial zinc MP known to activate one or more human MMPs is that it will also prevent uncontrolled MMP activation and tissue destruction in infected and nearby tissue.

5.3. Promising compounds as a scaffold for future lead compounds

Bacterial arthritis, particularly *S. aureus*-induced arthritis, is a disease with high morbidity leading to rapidly progressive bone resorption [171]. The bisphosphonates are found to be beneficial in clinical trials of osteoporosis as they can regulate bone turnover by suppressing osteoclast activity. Zoledronic acid (ZA) is a third-generation bisphosphonate for the treatment of osteoporosis [172, 173]. All bisphosphonates are synthetic analogues of inorganic pyrophosphate (PPi), which is composed of easily-degraded phosphodiester (P-O-P) bonds that connect the two phosphate groups of PPi. Contrary, bisphosphonates are the natural by-product of numerous metabolic reactions that is present in plasma and urine. Unlike PPi, bisphosphonates contain two phosphate groups joined by stable, covalent bonds to a central carbon atom. Bisphosphonates can bind with a divalent cation such as Ca^{2+} and Zn^{2+} by coordination of two phosphonate groups. Their ability to chelate Zn^{2+} is the basis for the MP-inhibiting property of bisphosphonates [174]. In our study on bisphosphonates (**Paper I**), we found that one of the bisphosphonates (RC2) had a much stronger binding to the two virulent factors (PLN and TLN) than to the two human MMPs (MMP-9 and MMP-14) and the third virulent factor (ALN). Based on the beneficial use of various bisphosphonates in clinical trials on osteoporosis, it appears that further studies including improvement of RC2 and tests against other human MPs and bacterial MP virulence factors would be favourable. RC2 or an RC2-derivative may be used as an antibacterial adjuvant.

The binding strength of the RC2 compound for PLN ($K_i = 22 \pm 3 \mu\text{M}$) was found to be comparable with the recently reported hydroxamate inhibitor of PLN ($K_{iapp} = 12.3 \pm 0.6 \mu\text{M}$) by Kany et al. [121]. The binding modes and interactions with the active site of PLN of these two compounds were found to be very similar (**Figure 8**). They showed that their hydroxamate inhibitor was leaning toward the primed binding sites of PLN, which was

similar to RC2. One of the phosphate groups of the RC2 compound interacted with active site zinc atom, H223 and E141, while the other phosphate group interacted with R198 (two hydrogen bonds) and H223. Kany et al. also showed that the hydroxamate compound interacted with the same residues of PLN as RC2. Both the carbonyl oxygen and the hydroxamate oxygen of the hydroxamate compound coordinated with the zinc of the active site, giving a distorted trigonal bipyramidal geometry of zinc coordination. The carbonyl oxygen had a weaker interaction with His223 and the hydroxamate oxygen forms a hydrogen bond with the adjacent Glu141. The NH-group of RC2 interacted with the backbone of A113, while the amide nitrogen of hydroxamate interacted with the carbonyl group of Ala113. In TLN, we observed a binding pose quite similar to that described for PLN. The NO₂-group of RC2 was located within the S1'-subpocket not deep into the pocket because of the side chain of R198. The aromatic core of hydroxamate compound was found to be away from Arg198 in the S1' binding site which was contradictory to their previous study with thiol-containing inhibitors of PLN [142]. The interaction with Arg198 in the S1' binding site was found to be important for the selectivity of MPs [136, 175] and our present study also revealed the same findings. However, the findings of Kany et al. showed that the selectivity of proteases could indeed be achieved by sparing the S1' pocket [121].

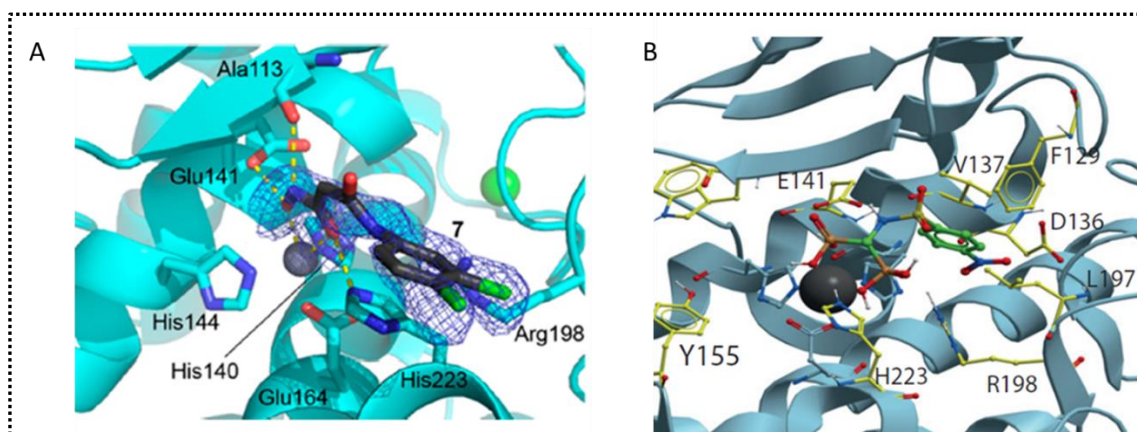


Figure 8: Comparison of the binding mode and interaction with the active site residues of PLN by one hydroxamate compound called compound 7 (panel A) [121], and RC2 in **Paper I Figure 5** (panel B). A. The structure of PLN is complex with compound 7 [121]. The active site zinc ion is grey, and the calcium ion is a green sphere. Residues involved in the binding of 7 are shown as sticks and interactions are represented as yellow dashed lines. B. Structure of PLN in complex with RC2. Zinc is shown as a dark grey sphere and the side chain of zinc coordinating amino acids is shown in blue (**Paper I, Figure 5**).

Hydroxamate is a strong zinc binder and has been used as a ZBG in many zinc MP inhibitors, including inhibitors of MMPs [120]. In addition, several of the more recent good inhibitors of PLN are also hydroxamates [121]. Hydroxamate inhibitors have not been tested in the present study, but previously our group found a promising hydroxamate compound (LM2) that bound stronger to the bacterial zinc MPs than to human MMP-2, MMP-9 and ADAM-17 [57], suggesting that LM2 and LM2 derivatives can be a promising structural scaffold for developing compounds with high specificity against bacterial MPs. Testing of new LM2 derivatives confirmed this assumption (unpublished work).

In a study by Konstantinovic et al., N-aryl-3-mercaptosuccinimide inhibitors showed strong inhibition against PLN with IC_{50} values from 4-6 μM [117]. A study by Camberlein et al. showed moderate inhibition of PLN by N-aryl-3-mercaptoacetamide with an IC_{50} value of 6.6 μM [136]. The IC_{50} values for RC2 in the present study were also in lower micromolar ranges for PLN and TLN. A comparison of the findings of the present study with those of others confirmed that RC2 could be an interesting lead, which could serve as a scaffold for the rational development of selective MPs inhibitors as potential new antibiotics or adjuvants of classical antibiotics.

Peptide-based inhibitor of ALN has been identified by a study where K_i value was found to be 346 nM [176]. The present study described small-molecule inhibitors of ALN. To our knowledge, this is the first time small molecules as ALN inhibitors have been described in the literature. The catechol-containing compound BF471 showed more than 50% inhibition of ALN with K_i value around 49 μM and this finding will hopefully be a good start for developing potential ALN inhibitors with stronger affinity.

Inactivation of the bacterial MBLs by removing the Zn^{2+} was found to be a very effective approach [177]. A highly selective zinc chelator is very important in the construction of an inhibitor of a zinc-dependent enzyme, as the metal chelators are generally toxic to the host cells [127]. In solution, metal chelating groups with nitrogen rather than oxygen as a donor atom are expected to bind weaker to sodium, calcium, potassium, iron and manganese or other relevant biological cation than to zinc [178]. Hence, compounds containing metal chelating groups with nitrogen as donor atoms may therefore show specificity for zinc MPs over other MPs. A study revealed that TPA containing nitrogen as donor atoms are Zn^{2+} chelators of MBLs. They showed that TPA derivatives Zn148 [179] and Zn155 [134]

strongly inhibited MBLs. **In paper II**, we found that some of these MBL inhibitors also inhibited zinc MPs, and the strongest inhibition was seen against PLN and human MMP-14. Therefore, we can conclude that the present inhibitors of MBLs also might be relatively good inhibitors of the bacterial virulence factor PLN. In addition, this inhibition may strengthen the potency of Zn148 and Zn155 as antibacterial adjuvants against *P. aeruginosa* infections.

The phosphinate compound H2 was found to inhibit all five MPs, while compound H1 was found to inhibit MMP-9 and MMP-14 (**Paper III**). Previous X-ray crystallographic studies showed that these compounds interact with both primed and non-primed site residues of the MMPs [118, 180]. Occupation of both primed and non-primed binding sites of the bacterial zinc MPs was confirmed in **paper III** by docking. In addition, phosphinate compounds are transition state analogues and could be excellent small-molecule inhibitors of MPs. Chemical modification of the H-2 compound could give rise to useful inhibitors of bacterial MPs with increased selectivity.

5.4. Putative methodological limitations

The 3D structure of the enzymes is very important for their proper functioning of enzymes. Disruption of the structure by breaking the intermolecular bonds and interaction causes a loss of activity. Temperatures and pH beyond their optimal range can result in enzyme denaturation. Besides substrate and enzyme concentration, optimized pH of around 7.5 of the assay buffer and a temperature of 37° C were maintained during enzyme kinetic experiments. Some very tiny technical errors, for example, pipetting and instrumental errors, might have some effect on the results. Therefore, we conducted each experiment with at least three parallels, sometimes even more, to reduce possible errors. In addition, incubation time, proper mixing of the components and reading the data continuously for 30 minutes were all maintained at the best level to obtain a reliable outcome.

However, accurate prediction of binding conformations and compound activity corresponding to the SAR based on docking is still a big challenge. Many uncertainties are associated with the docking and scoring of compound conformations. These could be a limited resolution of the crystal structure of targets and some inherent uncertainty; for

example, the enzymes themselves are not static. Atoms can vibrate, electron clouds may shift, and the last crystal structure might be an averaged atomistic position considered to be another source of uncertainty. However, though most structures in the PDB have a B-value or temperature factor associated with each atom to model this uncertainty, still, it is a prediction, mimicking the truth. Molecular mechanical parameters for zinc are problematic as zinc can change coordination during the binding and reaction and results in conformational changes. The parameterization of zinc is, therefore, challenging [113].

Due to steric clashes with the protein, compounds might be improperly docked, or even after being docked correctly, the score might be bad due to non-optimal ligand-protein contacts. In addition to problems associated with scoring, induced fit or other conformational changes that occur on binding and the participation of water molecules or ions in protein-ligand interactions are most challenging when it comes to comparing with the actual versatile cellular environment. However, a combined study of molecular modelling and inhibition kinetics to obtain the molecular interaction between ligands and the target was found to be an excellent methodological approach for finding potential inhibitors of bacterial zinc MPs.

6. Conclusion

The strategy of targeting bacterial virulence factors does not directly cause bacterial cell death. Instead, they focus on mechanisms used by bacteria to cause infection and damage the hosts' immune response. This therapeutic strategy has been found promising in reducing and preventing resistance formation within infectious pathogens as this exhibit reduced selective pressure on bacteria compared to traditional antibiotics.

In the present study we have identified new inhibitors of the bacterial virulence factors PLN, TLN and ALN, and in that way obtain information that enriches the existing knowledge about the inhibition of bacterial zinc MPs. The bisphosphonate-containing compound RC2, DPA, and the TPA derivatives Zn148 and Zn155 showed anti-virulence potential against bacterial zinc MPs, especially for PLN, while the catechol-containing compound BF471 was a promising inhibitor of ALN. Both Zn148 and Zn155 have previously been found to inhibit MBLs and the finding in the present study that they also inhibited PLN further support their significance as promising compounds. These compounds may also serve as scaffolds for the development of novel anti-virulence compounds. As an antibiotic adjuvant, these inhibitors can also help prolong the lifespan of available antibiotics by suppressing bacterial resistance or increasing antibiotic efficacy. Overall, the findings of the present study would contribute to enriching the list of potential anti-virulence agents that can be an enormous help against bacterial infection, especially against PLN, the main virulence factor of *P. aeruginosa*.

7. Future perspectives

The molecules that showed promising *in vitro* results by inhibiting the enzymatic activity of bacterial virulence factors need further testing. Testing the efficacy of anti-virulence agents on the biofilm formed by the pathogenic bacteria is in progress in our group. During *P. aeruginosa* infections, the complement system is targeted by PLN. Studying the depletion of complement factors by *P. aeruginosa* in the presence or absence of PLN inhibitors will also give information about their therapeutic value. Such studies have been described previously [181]. However, they should also be tested further *in vivo* to investigate their effects in cell culture and animal models. The artificial liposomes mimicking cell membranes could be used in sequestering bacterial virulence factors in both *in vitro* and *in vivo* studies.

8. References

1. Magiorakos, A. P., Srinivasan, A., Carey, R. B., Carmeli, Y., Falagas, M. E., Giske, C. G., Harbarth, S., Hindler, J. F., Kahlmeter, G., Olsson-Liljequist, B., Paterson, D. L., Rice, L. B., Stelling, J., Struelens, M. J., Vatopoulos, A., Weber, J. T. & Monnet, D. L. (2012) Multidrug-resistant, extensively drug-resistant and pandrug-resistant bacteria: an international expert proposal for interim standard definitions for acquired resistance, *Clin Microbiol Infect.* **18**, 268-81.
2. Rice, L. B. (2008) Federal funding for the study of antimicrobial resistance in nosocomial pathogens: no ESKAPE, *J Infect Dis.* **197**, 1079-81.
3. Collaborators of antimicrobial resistance. (2022) Global burden of bacterial antimicrobial resistance in 2019: a systematic analysis, *Lancet.* **399**, 629-655.
4. Wiener-Kronish, J. P., Albertine, K. H. & Matthay, M. A. (1991) Differential responses of the endothelial and epithelial barriers of the lung in sheep to Escherichia coli endotoxin, *J Clin Invest.* **88**, 864-75.
5. Hanson, M. R. & Chung, C. L. (2009) Antibiotic selection for MRSA: case presentations and review of the literature, *J Drugs Dermatol.* **8**, 281-6.
6. Tacconelli, E., Carrara, E., Savoldi, A., Harbarth, S., Mendelson, M., Monnet, D. L., Pulcini, C., Kahlmeter, G., Kluytmans, J., Carmeli, Y., Ouellette, M., Outtersson, K., Patel, J., Cavalieri, M., Cox, E. M., Houchens, C. R., Grayson, M. L., Hansen, P., Singh, N., Theuretzbacher, U., Magrini, N. & Group, W. H. O. P. P. L. W. (2018) Discovery, research, and development of new antibiotics: the WHO priority list of antibiotic-resistant bacteria and tuberculosis, *Lancet Infect Dis.* **18**, 318-327.
7. <https://apps.who.int/iris/handle/10665/112642> in 11.08.2023
8. Rasko, D. A. & Sperandio, V. (2010) Anti-virulence strategies to combat bacteria-mediated disease, *Nat Rev Drug Discov.* **9**, 117-28.
9. Muhlen, S. & Dersch, P. (2016) Anti-virulence Strategies to Target Bacterial Infections, *Curr Top Microbiol Immunol.* **398**, 147-183.
10. Dickey, S. W., Cheung, G. Y. C. & Otto, M. (2017) Different drugs for bad bugs: antivirulence strategies in the age of antibiotic resistance, *Nat Rev Drug Discov.* **16**, 457-471.
11. Diggle, S. P. & Whiteley, M. (2020) Microbe Profile: Pseudomonas aeruginosa: opportunistic pathogen and lab rat, *Microbiology (Reading).* **166**, 30-33.
12. Gellatly S. L. & Hancock, R. E. W. (2013) Pseudomonas Aeruginosa: New Insights Into Pathogenesis and Host Defenses., *Pathog Dis.* **67**, 159–173.
13. Hauser, A. R. (2009) The type III secretion system of Pseudomonas aeruginosa: infection by injection, *Nat Rev Microbiol.* **7**, 654-65.
14. Veessenmeyer, J. L., Hauser, A. R., Lisboa, T. & Rello, J. (2009) Pseudomonas aeruginosa virulence and therapy: evolving translational strategies, *Crit Care Med.* **37**, 1777-86.
15. Kipnis, E., Sawa, T. & Wiener-Kronish, J. (2006) Targeting mechanisms of Pseudomonas aeruginosa pathogenesis, *Med Mal Infect.* **36**, 78-91.

16. Liu, P. V. (1974) Extracellular toxins of *Pseudomonas aeruginosa*, *J Infect Dis.* **130**, 94-99.
17. Kessler, E., Safrin, M., Abrams, W. R., Rosenbloom, J. & Ohman, D. E. (1997) Inhibitors and specificity of *Pseudomonas aeruginosa* LasA, *J Biol Chem.* **272**, 9884-9.
18. Hobden, J. A. (2002) *Pseudomonas aeruginosa* proteases and corneal virulence, *DNA Cell Biol.* **21**, 391-6.
19. Gibson, R. L., Burns, J. L. & Ramsey, B. W. (2003) Pathophysiology and management of pulmonary infections in cystic fibrosis, *Am J Respir Crit Care Med.* **168**, 918-51.
20. Cathcart, G. R., Quinn, D., Greer, B., Harriott, P., Lynas, J. F., Gilmore, B. F. & Walker, B. (2011) Novel inhibitors of the *Pseudomonas aeruginosa* virulence factor LasB: a potential therapeutic approach for the attenuation of virulence mechanisms in pseudomonal infection, *Antimicrob Agents Chemother.* **55**, 2670-8.
21. Gunn, J. S., Bakaletz, L. O. & Wozniak, D. J. (2016) What's on the Outside Matters: The Role of the Extracellular Polymeric Substance of Gram-negative Biofilms in Evading Host Immunity and as a Target for Therapeutic Intervention, *J Biol Chem.* **291**, 12538-12546.
22. Moskowitz, S. M. & Wiener-Kronish, J. P. (2010) Mechanisms of bacterial virulence in pulmonary infections, *Curr Opin Crit Care.* **16**, 8-12.
23. Chambers, H. F. & Deleo, F. R. (2009) Waves of resistance: *Staphylococcus aureus* in the antibiotic era, *Nat Rev Microbiol.* **7**, 629-41.
24. Venter, J. C., Remington, K., Heidelberg, J. F., Halpern, A. L., Rusch, D., Eisen, J. A., Wu, D., Paulsen, I., Nelson, K. E., Nelson, W., Fouts, D. E., Levy, S., Knap, A. H., Lomas, M. W., Nealson, K., White, O., Peterson, J., Hoffman, J., Parsons, R., Baden-Tillson, H., Pfannkoch, C., Rogers, Y. H. & Smith, H. O. (2004) Environmental genome shotgun sequencing of the Sargasso Sea, *Science.* **304**, 66-74.
25. Berman, D. S., Eisner, W. & Kreiswirth, B. (1993) Community-acquired methicillin-resistant *Staphylococcus aureus* infection, *N Engl J Med.* **329**, 1896.
26. DeLeo, F. R., Otto, M., Kreiswirth, B. N. & Chambers, H. F. (2010) Community-associated methicillin-resistant *Staphylococcus aureus*, *Lancet.* **375**, 1557-68.
27. Cheung, A. L., Bayer, A. S., Zhang, G., Gresham, H. & Xiong, Y. Q. (2004) Regulation of virulence determinants in vitro and in vivo in *Staphylococcus aureus*, *FEMS Immunol Med Microbiol.* **40**, 1-9.
28. Paulander, W., Varming, A. N., Bojer, M. S., Friberg, C., Baek, K. & Ingmer, H. (2018) The agr quorum sensing system in *Staphylococcus aureus* cells mediates death of sub-population, *BMC Res Notes.* **11**, 503.
29. Lehman, M. K., Nuxoll, A. S., Yamada, K. J., Kielian, T., Carson, S. D. & Fey, P. D. (2019) Protease-Mediated Growth of *Staphylococcus aureus* on Host Proteins Is opp3 Dependent, *mBio.* **10**.
30. Sieprawska-Lupa, M., Mydel, P., Krawczyk, K., Wojcik, K., Puklo, M., Lupa, B., Suder, P., Silberring, J., Reed, M., Pohl, J., Shafer, W., McAleese, F., Foster, T., Travis, J. & Potempa, J. (2004) Degradation of human antimicrobial peptide LL-37 by *Staphylococcus aureus*-derived proteinases, *Antimicrob Agents Chemother.* **48**, 4673-9.

31. Smagur, J., Guzik, K., Bzowska, M., Kuzak, M., Zarebski, M., Kantyka, T., Walski, M., Gajkowska, B. & Potempa, J. (2009) Staphylococcal cysteine protease staphopain B (SspB) induces rapid engulfment of human neutrophils and monocytes by macrophages, *Biol Chem.* **390**, 361-71.
32. Jusko, M., Potempa, J., Kantyka, T., Bielecka, E., Miller, H. K., Kalinska, M., Dubin, G., Garred, P., Shaw, L. N. & Blom, A. M. (2014) Staphylococcal proteases aid in evasion of the human complement system, *J Innate Immun.* **6**, 31-46.
33. Adekoya, O. A., Sjoli, S., Wuxiuer, Y., Bילו, I., Marques, S. M., Santos, M. A., Nuti, E., Cercignani, G., Rossello, A., Winberg, J. O. & Sylte, I. (2015) Inhibition of pseudolysin and thermolysin by hydroxamate-based MMP inhibitors, *Eur J Med Chem.* **89**, 340-8.
34. Rawlings, N. D., Barrett, A. J., Thomas, P. D., Huang, X., Bateman, A. & Finn, R. D. (2018) The MEROPS database of proteolytic enzymes, their substrates and inhibitors in 2017 and a comparison with peptidases in the PANTHER database, *Nucleic Acids Res.* **46**, D624-D632.
35. Lamazares, E., MacLeod-Carey, D., Miranda, F. P. & Mena-Ulecia, K. (2021) Theoretical Evaluation of Novel Thermolysin Inhibitors from *Bacillus thermoproteolyticus*. Possible Antibacterial Agents, *Molecules.* **26**.
36. Tiraboschi, G., Jullian, N., Thery, V., Antonczak, S., Fournie-Zaluski, M. C. & Roques, B. P. (1999) A three-dimensional construction of the active site (region 507-749) of human neutral endopeptidase (EC.3.4.24.11), *Protein Eng.* **12**, 141-9.
37. Soares, A., Alexandre, K. & Etienne, M. (2020) Tolerance and Persistence of *Pseudomonas aeruginosa* in Biofilms Exposed to Antibiotics: Molecular Mechanisms, Antibiotic Strategies and Therapeutic Perspectives, *Front Microbiol.* **11**, 2057.
38. Sharma, A. K., Dhasmana, N., Dubey, N., Kumar, N., Gangwal, A., Gupta, M. & Singh, Y. (2017) Bacterial Virulence Factors: Secreted for Survival, *Indian J Microbiol.* **57**, 1-10.
39. Burchacka, E. & Sienczyk, M. (2018) The Lord of the Bacteria: The Fellowship of the Leader and Other Serine Protease Inhibitors, *Curr Pharm Des.* **24**, 4445-4465.
40. Travis, J. & Potempa, J. (2000) Bacterial proteinases as targets for the development of second-generation antibiotics, *Biochim Biophys Acta.* **1477**, 35-50.
41. Artenstein, A. W. & Opal, S. M. (2011) Proprotein convertases in health and disease, *N Engl J Med.* **365**, 2507-18.
42. Overall, C. M. & Blobel, C. P. (2007) In search of partners: linking extracellular proteases to substrates, *Nat Rev Mol Cell Biol.* **8**, 245-57.
43. Sterchi, E. E., Stocker, W. & Bond, J. S. (2008) Meprins, membrane-bound and secreted astacin metalloproteinases, *Mol Aspects Med.* **29**, 309-28.
44. Dufour, A. (2015) Degradomics of matrix metalloproteinases in inflammatory diseases, *Front Biosci (Schol Ed).* **7**, 150-67.
45. Cerda-Costa, N. & Gomis-Ruth, F. X. (2014) Architecture and function of metallopeptidase catalytic domains, *Protein Sci.* **23**, 123-44.

46. Lopez-Otin, C. & Bond, J. S. (2008) Proteases: multifunctional enzymes in life and disease, *J Biol Chem.* **283**, 30433-7.
47. Di Leo, R., Cuffaro, D., Rossello, A. & Nuti, E. (2023) Bacterial Zinc Metalloenzyme Inhibitors: Recent Advances and Future Perspectives, *Molecules.* **28**.
48. Cawston, T. E. & Wilson, A. J. (2006) Understanding the role of tissue degrading enzymes and their inhibitors in development and disease, *Best Pract Res Clin Rheumatol.* **20**, 983-1002.
49. Nagase, H., Visse, R. & Murphy, G. (2006) Structure and function of matrix metalloproteinases and TIMPs, *Cardiovasc Res.* **69**, 562-73.
50. Gomis-Ruth, F. X., Botelho, T. O. & Bode, W. (2012) A standard orientation for metallopeptidases, *Biochim Biophys Acta.* **1824**, 157-63.
51. Renneberg, R., Berkling, V. & Lorocho, V. (2017) Enzymes: Molecular Supercatalysts for Use at Home and in Industry in *Biotechnology for Beginners* (Arnold, L. D., ed) pp. 33, Elsevier Inc.,
52. Rawlings, N. D., Barrett, A. J. & Bateman, A. (2010) MEROPS: the peptidase database, *Nucleic Acids Res.* **38**, D227-33.
53. Cerda-Costa, N. & Gomis-Ruth, F. X. (2014) Architecture and function of metallopeptidase catalytic domains, *Protein Sci.* **23**, 123-44.
54. Rawlings, N. D., Barrett, A. J. & Bateman, A. (2012) MEROPS: the database of proteolytic enzymes, their substrates and inhibitors, *Nucleic Acids Res.* **40**, D343-50.
55. Hadler-Olsen, E., Fadnes, B., Sylte, I., Uhlin-Hansen, L. & Winberg, J. O. (2011) Regulation of matrix metalloproteinase activity in health and disease, *FEBS J.* **278**, 28-45.
56. Schechter, I. & Berger, A. (2012) On the size of the active site in proteases. I. Papain. 1967, *Biochem Biophys Res Commun.* **425**, 497-502.
57. Sjöli, S., Nuti, E., Camodeca, C., Bilotto, I., Rossello, A., Winberg, J. O., Sylte, I. & Adekoya, O. A. (2016) Synthesis, experimental evaluation and molecular modelling of hydroxamate derivatives as zinc metalloproteinase inhibitors, *Eur J Med Chem.* **108**, 141-153.
58. Cuffaro, D., Nuti, E., D'Andrea, F. & Rossello, A. (2020) Developments in Carbohydrate-Based Metzincin Inhibitors, *Pharmaceuticals (Basel).* **13**.
59. Burg, B. V. d. & Eijssink, V. (2013) Thermolysin and Related Bacillus Metallopeptidases in *Handbook of Proteolytic Enzymes* (Rawlings, N. D. & Barrett, A. J., eds) pp. 540-553, Academic press,
60. Adekoya, O. A. & Sylte, I. (2009) The thermolysin family (M4) of enzymes: therapeutic and biotechnological potential, *Chem Biol Drug Des.* **73**, 7-16.
61. Potempa, J., Dubin, A., Korzus, G. & Travis, J. (1988) Degradation of elastin by a cysteine proteinase from *Staphylococcus aureus*, *J Biol Chem.* **263**, 2664-7.
62. Bode, W., Fernandez-Catalan, C., Tschesche, H., Grams, F., Nagase, H. & Maskos, K. (1999) Structural properties of matrix metalloproteinases, *Cell Mol Life Sci.* **55**, 639-52.

63. Netzel-Arnett, S., Sang, Q. X., Moore, W. G., Navre, M., Birkedal-Hansen, H. & Van Wart, H. E. (1993) Comparative sequence specificities of human 72- and 92-kDa gelatinases (type IV collagenases) and PUMP (matrilysin), *Biochemistry*. **32**, 6427-32.
64. Tochowicz, A., Maskos, K., Huber, R., Oltenfreiter, R., Dive, V., Yiotakis, A., Zanda, M., Pourmotabbed, T., Bode, W. & Goettig, P. (2007) Crystal structures of MMP-9 complexes with five inhibitors: contribution of the flexible Arg424 side-chain to selectivity, *J Mol Biol*. **371**, 989-1006.
65. Mucha, A., Cuniasse, P., Kannan, R., Beau, F., Yiotakis, A., Basset, P. & Dive, V. (1998) Membrane type-1 matrix metalloprotease and stromelysin-3 cleave more efficiently synthetic substrates containing unusual amino acids in their P1' positions, *J Biol Chem*. **273**, 2763-8.
66. Wu, J. W. & Chen, X. L. (2011) Extracellular metalloproteases from bacteria, *Appl Microbiol Biotechnol*. **92**, 253-62.
67. McIver, K. S., Kessler, E. & Ohman, D. E. (2004) Identification of residues in the *Pseudomonas aeruginosa* elastase propeptide required for chaperone and secretion activities, *Microbiology (Reading)*. **150**, 3969-77.
68. Gao, X., Wang, J., Yu, D. Q., Bian, F., Xie, B. B., Chen, X. L., Zhou, B. C., Lai, L. H., Wang, Z. X., Wu, J. W. & Zhang, Y. Z. (2010) Structural basis for the autoprocessing of zinc metalloproteases in the thermolysin family, *Proc Natl Acad Sci U S A*. **107**, 17569-74.
69. Yeats, C., Rawlings, N. D. & Bateman, A. (2004) The PepSY domain: a regulator of peptidase activity in the microbial environment?, *Trends Biochem Sci*. **29**, 169-72.
70. Marie-Claire, C., Roques, B. P. & Beaumont, A. (1998) Intramolecular processing of prothermolysin, *J Biol Chem*. **273**, 5697-701.
71. Nickerson, N. N., Joag, V. & McGavin, M. J. (2008) Rapid autocatalytic activation of the M4 metalloprotease aureolysin is controlled by a conserved N-terminal fungalysin-thermolysin-propeptide domain, *Mol Microbiol*. **69**, 1530-43.
72. Kessler, E. & Safrin, M. (1988) Synthesis, processing, and transport of *Pseudomonas aeruginosa* elastase, *J Bacteriol*. **170**, 5241-7.
73. Kessler, E. & Safrin, M. (1988) Partial purification and characterization of an inactive precursor of *Pseudomonas aeruginosa* elastase, *J Bacteriol*. **170**, 1215-9.
74. Kessler, E., Safrin, M., Gustin, J. K. & Ohman, D. E. (1998) Elastase and the LasA protease of *Pseudomonas aeruginosa* are secreted with their propeptides, *J Biol Chem*. **273**, 30225-31.
75. Braun P, B. W., Tommassen (2000) Activation of *Pseudomonas aeruginosa* elastase in *Pseudomonas putida* by triggering dissociation of the propeptide-enzyme complex, *J Microbiol*. **146**, 2565–2572.
76. Filloux A, M. G., Bally M. (1998) GSP-dependent protein secretion in Gram-negative bacteria: the Xcp system of *Pseudomonas aeruginosa*, *FEMS Microbiol Rev* **22**, 177–198.
77. Braun, P., de Groot, A., Bitter, W. & Tommassen, J. (1998) Secretion of elastolytic enzymes and their propeptides by *Pseudomonas aeruginosa*, *J Bacteriol*. **180**, 3467-9.

78. Matthews, B. W., Colman, P. M., Jansonius, J. N., Titani, K., Walsh, K. A. & Neurath, H. (1972) Structure of thermolysin, *Nat New Biol.* **238**, 41-3.
79. Thompson, M. W. (2022) Regulation of zinc-dependent enzymes by metal carrier proteins, *Biometals.* **35**, 187-213.
80. Pelmeshnikov, V., Blomberg, M. R. & Siegbahn, P. E. (2002) A theoretical study of the mechanism for peptide hydrolysis by thermolysin, *J Biol Inorg Chem.* **7**, 284-98.
81. Morihara, K., Tsuzuki, H., Oka, T., Inoue, H. & Ebata, M. (1965) Pseudomonas Aeruginosa Elastase. Isolation, Crystallization, and Preliminary Characterization, *J Biol Chem.* **240**, 3295-304.
82. Fukushima, J., Yamamoto, S., Morihara, K., Atsumi, Y., Takeuchi, H., Kawamoto, S. & Okuda, K. (1989) Structural gene and complete amino acid sequence of Pseudomonas aeruginosa IFO 3455 elastase, *J Bacteriol.* **171**, 1698-704.
83. Thayer, M. M., Flaherty, K. M. & McKay, D. B. (1991) Three-dimensional structure of the elastase of Pseudomonas aeruginosa at 1.5-Å resolution, *J Biol Chem.* **266**, 2864-71.
84. Ogino, H., Uchiho, T., Yokoo, J., Kobayashi, R., Ichise, R. & Ishikawa, H. (2001) Role of intermolecular disulfide bonds of the organic solvent-stable PST-01 protease in its organic solvent stability, *Appl Environ Microbiol.* **67**, 942-7.
85. Arvidson, S., Holme, T. & Wadstrom, T. (1970) Formation of bacteriolytic enzymes in batch and continuous culture of Staphylococcus aureus, *J Bacteriol.* **104**, 227-33.
86. Arvidson, S., Holme, T. & Lindholm, B. (1972) The formation of extracellular proteolytic enzymes by Staphylococcus aureus, *Acta Pathol Microbiol Scand B Microbiol Immunol.* **80**, 835-44.
87. Drapeau, G. R. (1978) Role of metalloprotease in activation of the precursor of staphylococcal protease, *J Bacteriol.* **136**, 607-13.
88. Arvidson, S. (1973) Studies on extracellular proteolytic enzymes from Staphylococcus aureus. II. Isolation and characterization of an EDTA-sensitive protease, *Biochim Biophys Acta.* **302**, 149-57.
89. Potempa, J. & Shaw, L. N. (2013) Aureolysin in *Handbook of Proteolytic Enzymes* pp. 563-569, Academic press,
90. Theocharis, A. D., Skandalis, S. S., Gialeli, C. & Karamanos, N. K. (2016) Extracellular matrix structure, *Adv Drug Deliv Rev.* **97**, 4-27.
91. Wolberg, A. S. & Mast, A. E. (2012) Tissue factor and factor VIIa--hemostasis and beyond, *Thromb Res.* **129 Suppl 2**, S1-4.
92. Cui, N., Hu, M. & Khalil, R. A. (2017) Biochemical and Biological Attributes of Matrix Metalloproteinases, *Prog Mol Biol Transl Sci.* **147**, 1-73.
93. Nagase H & G, M. (2004) Matrix Metalloproteinases in *Encyclopedia of Biological Chemistry* pp. 657-665, Elsevier,
94. Tokito, A. & Jougasaki, M. (2016) Matrix Metalloproteinases in Non-Neoplastic Disorders, *Int J Mol Sci.* **17**.

95. Lee, M. H. & Murphy, G. (2004) Matrix metalloproteinases at a glance, *J Cell Sci.* **117**, 4015-6.
96. Li, K., Tay, F. R. & Yiu, C. K. Y. (2020) The past, present and future perspectives of matrix metalloproteinase inhibitors, *Pharmacol Ther.* **207**, 107465.
97. Gong, Y., Chippada-Venkata, U. D. & Oh, W. K. (2014) Roles of matrix metalloproteinases and their natural inhibitors in prostate cancer progression, *Cancers (Basel).* **6**, 1298-327.
98. Malla, N., Sjoli, S., Winberg, J. O., Hadler-Olsen, E. & Uhlin-Hansen, L. (2008) Biological and pathobiological functions of gelatinase dimers and complexes, *Connect Tissue Res.* **49**, 180-4.
99. Opdenakker, G., Van den Steen, P. E. & Van Damme, J. (2001) Gelatinase B: a tuner and amplifier of immune functions, *Trends Immunol.* **22**, 571-9.
100. Van den Steen, P. E., Van Aelst, I., Hvidberg, V., Piccard, H., Fiten, P., Jacobsen, C., Moestrup, S. K., Fry, S., Royle, L., Wormald, M. R., Wallis, R., Rudd, P. M., Dwek, R. A. & Opdenakker, G. (2006) The hemopexin and O-glycosylated domains tune gelatinase B/MMP-9 bioavailability via inhibition and binding to cargo receptors, *J Biol Chem.* **281**, 18626-37.
101. Sato, H., Takino, T., Okada, Y., Cao, J., Shinagawa, A., Yamamoto, E. & Seiki, M. (1994) A matrix metalloproteinase expressed on the surface of invasive tumour cells, *Nature.* **370**, 61-5.
102. Itoh, Y. & Seiki, M. (2004) Membrane-type matrix metalloproteinase1 Aspartic and Metallo Peptidases in *Handbook of Proteolytic Enzymes* (Barrett, A. J., Woessner, J. F. & Rawlings, N. D., eds) pp. 544-549, Academic press,
103. Knauper, V., Will, H., Lopez-Otin, C., Smith, B., Atkinson, S. J., Stanton, H., Hembry, R. M. & Murphy, G. (1996) Cellular mechanisms for human procollagenase-3 (MMP-13) activation. Evidence that MT1-MMP (MMP-14) and gelatinase a (MMP-2) are able to generate active enzyme, *J Biol Chem.* **271**, 17124-31.
104. Pei, D. & Weiss, S. J. (1995) Furin-dependent intracellular activation of the human stromelysin-3 zymogen, *Nature.* **375**, 244-7.
105. Will, H., Atkinson, S. J., Butler, G. S., Smith, B. & Murphy, G. (1996) The soluble catalytic domain of membrane type 1 matrix metalloproteinase cleaves the propeptide of progelatinase A and initiates autoproteolytic activation. Regulation by TIMP-2 and TIMP-3, *J Biol Chem.* **271**, 17119-23.
106. Rawlings, N. D. & Salvesen, G. (2013) Catalytic mechanism for metallopeptidases in *Handbook of proteolytic enzymes* pp. 370–396, Academic Press,
107. Gomis-Ruth, F. X. (2003) Structural aspects of the metzincin clan of metalloendopeptidases, *Mol Biotechnol.* **24**, 157-202.
108. Rask-Andersen, M., Almen, M. S. & Schioth, H. B. (2011) Trends in the exploitation of novel drug targets, *Nat Rev Drug Discov.* **10**, 579-90.
109. Bakheet, T. M. & Doig, A. J. (2010) Properties and identification of antibiotic drug targets, *BMC Bioinformatics.* **11**, 195.
110. Egorov, A. M., Ulyashova, M. M. & Rubtsova, M. Y. (2018) Bacterial Enzymes and Antibiotic Resistance, *Acta Naturae.* **10**, 33-48.

111. Ramsay, R. R. & Tipton, K. F. (2017) Assessment of Enzyme Inhibition: A Review with Examples from the Development of Monoamine Oxidase and Cholinesterase Inhibitory Drugs, *Molecules*. **22**.
112. Raeeszadeh-Sarmazdeh, M., Do, L. D. & Hritz, B. G. (2020) Metalloproteinases and Their Inhibitors: Potential for the Development of New Therapeutics, *Cells*. **9**.
113. Adekoya, O. A., Willassen, N. P. & Sylte, I. (2006) Molecular insight into pseudolysin inhibition using the MM-PBSA and LIE methods, *J Struct Biol*. **153**, 129-44.
114. Whittaker, M., Floyd, C. D., Brown, P. & Gearing, A. J. (1999) Design and therapeutic application of matrix metalloproteinase inhibitors, *Chem Rev*. **99**, 2735-76.
115. Georgiadis, D. & Yiotakis, A. (2008) Specific targeting of metzincin family members with small-molecule inhibitors: progress toward a multifarious challenge, *Bioorg Med Chem*. **16**, 8781-94.
116. Grobelny, D., Poncz, L. & Galaray, R. E. (1992) Inhibition of human skin fibroblast collagenase, thermolysin, and *Pseudomonas aeruginosa* elastase by peptide hydroxamic acids, *Biochemistry*. **31**, 7152-4.
117. Konstantinovic, J., Yahiaoui, S., Alhayek, A., Haupenthal, J., Schonauer, E., Andreas, A., Kany, A. M., Muller, R., Koehnke, J., Berger, F. K., Bischoff, M., Hartmann, R. W., Brandstetter, H. & Hirsch, A. K. H. (2020) N-Aryl-3-mercaptosuccinimides as Antivirulence Agents Targeting *Pseudomonas aeruginosa* Elastase and *Clostridium* Collagenases, *J Med Chem*. **63**, 8359-8368.
118. Rouanet-Mehouas, C., Czarny, B., Beau, F., Cassar-Lajeunesse, E., Stura, E. A., Dive, V. & Devel, L. (2017) Zinc-Metalloproteinase Inhibitors: Evaluation of the Complex Role Played by the Zinc-Binding Group on Potency and Selectivity, *J Med Chem*. **60**, 403-414.
119. Kaya, C., Walter, I., Yahiaoui, S., Sikandar, A., Alhayek, A., Konstantinovic, J., Kany, A. M., Haupenthal, J., Kohnke, J., Hartmann, R. W. & Hirsch, A. K. H. (2022) Substrate-Inspired Fragment Merging and Growing Affords Efficacious LasB Inhibitors, *Angew Chem Int Ed Engl*. **61**, e202112295.
120. Yadav, R. K., Gupta, S. P., Sharma, P. K. & Patil, V. M. (2011) Recent advances in studies on hydroxamates as matrix metalloproteinase inhibitors: a review, *Curr Med Chem*. **18**, 1704-22.
121. Kany, A. M., Sikandar, A., Yahiaoui, S., Haupenthal, J., Walter, I., Empting, M., Kohnke, J. & Hartmann, R. W. (2018) Tackling *Pseudomonas aeruginosa* Virulence by a Hydroxamic Acid-Based LasB Inhibitor, *ACS Chem Biol*. **13**, 2449-2455.
122. Yu, H., Yang, H., Shi, E. & Tang, W. (2020) Development and Clinical Application of Phosphorus-Containing Drugs, *Med Drug Discov*. **8**, 100063.
123. Drake, M. T., Clarke, B. L. & Khosla, S. (2008) Bisphosphonates: mechanism of action and role in clinical practice, *Mayo Clin Proc*. **83**, 1032-45.
124. Bartlett, P. A., & Marlowe C.K. (1983) Phosphoramidates as Transition State Analog Inhibitors of Thermolysin, *Biochemistry*. **22**, 4618-4624.
125. Tronrud, D. E., Holden, H. M. & Matthews, B. W. (1987) Structures of two thermolysin-inhibitor complexes that differ by a single hydrogen bond, *Science*. **235**, 571-4.

126. Weaver, L. H., Kester, W. R. & Matthews, B. W. (1977) A crystallographic study of the complex of phosphoramidon with thermolysin. A model for the presumed catalytic transition state and for the binding of extended substances, *J Mol Biol.* **114**, 119-32.
127. Prandina, A., Radix, S., Borgne, L. M., Jordheim, L. P., Bousfiha, Z., Frohlich, C., Leiros, H. K. S., Samuelsen, O., Frovold, E., Rongved, P. & Åstrand, O. A. H. (2019) Synthesis and biological evaluation of new dipicolylamine zinc chelators as metallo-beta-lactamase inhibitors. *Tetrahedron.* **75**, 1525–40.
128. Jacoby, G. A. & Munoz-Price, L. S. (2005) The new beta-lactamases, *N Engl J Med.* **352**, 380-91.
129. Paterson, D. L. & Bonomo, R. A. (2005) Extended-spectrum beta-lactamases: a clinical update, *Clin Microbiol Rev.* **18**, 657-86.
130. Malloy, A. M. & Campos, J. M. (2011) Extended-spectrum beta-lactamases: a brief clinical update, *Pediatr Infect Dis J.* **30**, 1092-3.
131. Pitout, J. D. D. (2010) Infections with extended-spectrum beta-lactamase-producing enterobacteriaceae: changing epidemiology and drug treatment choices, *Drugs.* **70**, 313-33.
132. Crowder, M. W., Spencer, J. & Vila, A. J. (2006) Metallo-beta-lactamases: novel weaponry for antibiotic resistance in bacteria, *Acc Chem Res.* **39**, 721-8.
133. Principe, L., Vecchio, G., Sheehan, G., Kavanagh, K., Morroni, G., Viaggi, V., di Masi, A., Giacobbe, D. R., Luzzaro, F., Luzzati, R. & Di Bella, S. (2020) Zinc Chelators as Carbapenem Adjuvants for Metallo-beta-Lactamase-Producing Bacteria: In Vitro and In Vivo Evaluation, *Microb Drug Resist.* **26**, 1133-1143.
134. Schnaars, C., Kildahl-Andersen, G., Prandina, A., Popal, R., Radix, S., Le Borgne, M., Gjoen, T., Andresen, A. M. S., Heikal, A., Okstad, O. A., Frohlich, C., Samuelsen, O., Lauksund, S., Jordheim, L. P., Rongved, P. & Astrand, O. A. H. (2018) Synthesis and Preclinical Evaluation of TPA-Based Zinc Chelators as Metallo-beta-lactamase Inhibitors, *ACS Infect Dis.* **4**, 1407-1422.
135. Rawlings, N. D., Waller, M., Barrett, A. J. & Bateman, A. (2014) MEROPS: the database of proteolytic enzymes, their substrates and inhibitors, *Nucleic Acids Res.* **42**, D503-9.
136. Camberlein, V., Jezequel, G., Haupenthal, J. & Hirsch, A. K. H. (2022) The Structures and Binding Modes of Small-Molecule Inhibitors of *Pseudomonas aeruginosa* Elastase LasB, *Antibiotics (Basel).* **11**.
137. Poncz, L., Gerken, T. A., Dearborn, D. G., Grobelny, D. & Galardy, R. E. (1984) Inhibition of the elastase of *Pseudomonas aeruginosa* by N alpha-phosphoryl dipeptides and kinetics of spontaneous hydrolysis of the inhibitors, *Biochemistry.* **23**, 2766-72.
138. Kessler, E., Israel, M., Landshman, N., Chechick, A. & Blumberg, S. (1982) In vitro inhibition of *Pseudomonas aeruginosa* elastase by metal-chelating peptide derivatives, *Infect Immun.* **38**, 716-23.
139. Holmquist, B. & Vallee, B. L. (1979) Metal-coordinating substrate analogs as inhibitors of metalloenzymes, *Proc Natl Acad Sci U S A.* **76**, 6216-20.
140. Nishino, N. & Powers, J. C. (1980) *Pseudomonas aeruginosa* elastase. Development of a new substrate, inhibitors, and an affinity ligand, *J Biol Chem.* **255**, 3482-6.

141. Schonauer, E., Kany, A. M., Hauptenthal, J., Husecken, K., Hoppe, I. J., Voos, K., Yahiaoui, S., Elsasser, B., Ducho, C., Brandstetter, H. & Hartmann, R. W. (2017) Discovery of a Potent Inhibitor Class with High Selectivity toward Clostridial Collagenases, *J Am Chem Soc.* **139**, 12696-12703.
142. Kany, A. M., Sikandar, A., Hauptenthal, J., Yahiaoui, S., Maurer, C. K., Proschak, E., Kohnke, J. & Hartmann, R. W. (2018) Binding Mode Characterization and Early in Vivo Evaluation of Fragment-Like Thiols as Inhibitors of the Virulence Factor LasB from *Pseudomonas aeruginosa*, *ACS Infect Dis.* **4**, 988-997.
143. Sylte, I., Dawadi, R., Malla, N., von Hofsten, S., Nguyen, T. M., Solli, A. I., Berg, E., Adekoya, O. A., Svineng, G. & Winberg, J. O. (2018) The selectivity of galardin and an azasugar-based hydroxamate compound for human matrix metalloproteases and bacterial metalloproteases, *PLoS One.* **13**, e0200237.
144. Tauro, M., Laghezza, A., Loiodice, F., Piemontese, L., Caradonna, A., Capelli, D., Montanari, R., Pochetti, G., Di Pizio, A., Agamennone, M., Campestre, C. & Tortorella, P. (2016) Catechol-based matrix metalloproteinase inhibitors with additional antioxidative activity, *J Enzyme Inhib Med Chem.* **31**, 25-37.
145. Mores, A., Matziari, M., Beau, F., Cuniase, P., Yiotakis, A. & Dive, V. (2008) Development of potent and selective phosphinic peptide inhibitors of angiotensin-converting enzyme 2, *J Med Chem.* **51**, 2216-26.
146. Kildahl-Andersen, G., Schnaars, C., Prandina, A., Radix, S., Le Borgne, M., Jordheim, L. P., Gjoen, T., Andresen, A. M. S., Lauksund, S., Frohlich, C., Samuelsen, O., Rongved, P. & Astrand, O. A. H. (2019) Synthesis and biological evaluation of zinc chelating compounds as metallo-beta-lactamase inhibitors, *Medchemcomm.* **10**, 528-537.
147. Abagyan R, T. M. K. D. (1994) ICM – a new method for protein modeling and design – applications to docking and structure prediction from the distorted native conformation., *J Comput Chem.* **15**, 488–506.
148. <https://www.schrodinger.com/suites/small-molecule-drug-discovery-suite> in 11.08.2023.
149. Rubino, M. T., Agamennone, M., Campestre, C., Campiglia, P., Cremasco, V., Faccio, R., Laghezza, A., Loiodice, F., Maggi, D., Panza, E., Rossello, A. & Tortorella, P. (2011) Biphenyl sulfonylamino methyl bisphosphonic acids as inhibitors of matrix metalloproteinases and bone resorption, *ChemMedChem.* **6**, 1258-68.
150. Wright, G. D. (2016) Antibiotic Adjuvants: Rescuing Antibiotics from Resistance: (Trends in Microbiology 24, 862-871; October 17, 2016), *Trends Microbiol.* **24**, 928.
151. Rotondo, C. M. & Wright, G. D. (2017) Inhibitors of metallo-beta-lactamases, *Curr Opin Microbiol.* **39**, 96-105.
152. King, A. M., Reid-Yu, S. A., Wang, W., King, D. T., De Pascale, G., Strynadka, N. C., Walsh, T. R., Coombes, B. K. & Wright, G. D. (2014) Aspergillomarasmine A overcomes metallo-beta-lactamase antibiotic resistance, *Nature.* **510**, 503-6.
153. Devel, L., Beau, F., Amoura, M., Vera, L., Cassar-Lajeunesse, E., Garcia, S., Czarny, B., Stura, E. A. & Dive, V. (2012) Simple pseudo-dipeptides with a P2' glutamate: a novel inhibitor family of matrix metalloproteases and other metzincins, *J Biol Chem.* **287**, 26647-56.

154. Devel, L., Rogakos, V., David, A., Makaritis, A., Beau, F., Cuniasse, P., Yiotakis, A. & Dive, V. (2006) Development of selective inhibitors and substrate of matrix metalloproteinase-12, *J Biol Chem.* **281**, 11152-60.
155. Vassiliou, S., Mucha, A., Cuniasse, P., Georgiadis, D., Lucet-Levannier, K., Beau, F., Kannan, R., Murphy, G., Knauper, V., Rio, M. C., Basset, P., Yiotakis, A. & Dive, V. (1999) Phosphinic pseudo-tripeptides as potent inhibitors of matrix metalloproteinases: a structure-activity study, *J Med Chem.* **42**, 2610-20.
156. Boucher, H. W., Talbot, G. H., Benjamin, D. K., Jr., Bradley, J., Guidos, R. J., Jones, R. N., Murray, B. E., Bonomo, R. A., Gilbert, D. & Infectious Diseases Society of, A. (2013) 10 x '20 Progress--development of new drugs active against gram-negative bacilli: an update from the Infectious Diseases Society of America, *Clin Infect Dis.* **56**, 1685-94.
157. O'Neill, J. (2014) Antimicrobial resistance: Tackling a crisis for the health and wealth of nations. in *The Review on Antimicrobial Resistance*
158. Elkington, P. T., O'Kane, C. M. & Friedland, J. S. (2005) The paradox of matrix metalloproteinases in infectious disease, *Clin Exp Immunol.* **142**, 12-20.
159. Totsika, M. (2016) Benefits and Challenges of Antivirulence Antimicrobials at the Dawn of the Post-Antibiotic Era, *Drug Delivery letters.* **6**, 30-37.
160. Baker, A. H., Edwards, D. R. & Murphy, G. (2002) Metalloproteinase inhibitors: biological actions and therapeutic opportunities, *J Cell Sci.* **115**, 3719-27.
161. Azevedo, A., Prado, A. F., Antonio, R. C., Issa, J. P. & Gerlach, R. F. (2014) Matrix metalloproteinases are involved in cardiovascular diseases, *Basic Clin Pharmacol Toxicol.* **115**, 301-14.
162. Hu, J., Van den Steen, P. E., Sang, Q. X. & Opdenakker, G. (2007) Matrix metalloproteinase inhibitors as therapy for inflammatory and vascular diseases, *Nat Rev Drug Discov.* **6**, 480-98.
163. Eckhard, U., Huesgen, P. F., Schilling, O., Bellac, C. L., Butler, G. S., Cox, J. H., Dufour, A., Goebeler, V., Kappelhoff, R., Keller, U. A. D., Klein, T., Lange, P. F., Marino, G., Morrison, C. J., Prudova, A., Rodriguez, D., Starr, A. E., Wang, Y. & Overall, C. M. (2016) Active site specificity profiling of the matrix metalloproteinase family: Proteomic identification of 4300 cleavage sites by nine MMPs explored with structural and synthetic peptide cleavage analyses, *Matrix Biol.* **49**, 37-60.
164. Konopka, J. A., DeBaun, M. R., Chang, W. & Dragoo, J. L. (2016) The Intracellular Effect of Relaxin on Female Anterior Cruciate Ligament Cells, *Am J Sports Med.* **44**, 2384-92.
165. Shogan, B. D., Belogortseva, N., Luong, P. M., Zaborin, A., Lax, S., Bethel, C., Ward, M., Muldoon, J. P., Singer, M., An, G., Umanskiy, K., Konda, V., Shakhsheer, B., Luo, J., Klabbers, R., Hancock, L. E., Gilbert, J., Zaborina, O. & Alverdy, J. C. (2015) Collagen degradation and MMP9 activation by *Enterococcus faecalis* contribute to intestinal anastomotic leak, *Sci Transl Med.* **7**, 286ra68.
166. Andreini, C., Banci, L., Bertini, I., Elmi, S. & Rosato, A. (2005) Comparative analysis of the ADAM and ADAMTS families, *J Proteome Res.* **4**, 881-8.
167. Vanlaere, I. & Libert, C. (2009) Matrix metalloproteinases as drug targets in infections caused by gram-negative bacteria and in septic shock, *Clin Microbiol Rev.* **22**, 224-39.

168. Lee, M. M., Yoon, B. J., Osiewicz, K., Preston, M., Bundy, B., van Heeckeren, A. M., Werb, Z. & Soloway, P. D. (2005) Tissue inhibitor of metalloproteinase 1 regulates resistance to infection, *Infect Immun.* **73**, 661-5.
169. McClellan, S. A., Huang, X., Barrett, R. P., Lighvani, S., Zhang, Y., Richiert, D. & Hazlett, L. D. (2006) Matrix metalloproteinase-9 amplifies the immune response to *Pseudomonas aeruginosa* corneal infection, *Invest Ophthalmol Vis Sci.* **47**, 256-64.
170. Okamoto, T., Akaike, T., Suga, M., Tanase, S., Horie, H., Miyajima, S., Ando, M., Ichinose, Y. & Maeda, H. (1997) Activation of human matrix metalloproteinases by various bacterial proteinases, *J Biol Chem.* **272**, 6059-66.
171. Shirliff, M. E. & Mader, J. T. (2002) Acute septic arthritis, *Clin Microbiol Rev.* **15**, 527-44.
172. Reid, I. R., Brown, J. P., Burckhardt, P., Horowitz, Z., Richardson, P., Trechsel, U., Widmer, A., Devogelaer, J. P., Kaufman, J. M., Jaeger, P., Body, J. J., Brandi, M. L., Broell, J., Di Micco, R., Genazzani, A. R., Felsenberg, D., Happ, J., Hooper, M. J., Ittner, J., Leb, G., Mallmin, H., Murray, T., Ortolani, S., Rubinacci, A., Saaf, M., Samsioe, G., Verbruggen, L. & Meunier, P. J. (2002) Intravenous zoledronic acid in postmenopausal women with low bone mineral density, *N Engl J Med.* **346**, 653-61.
173. Chung, G. & Keen, R. W. (2003) Zoledronate treatment in active Paget's disease, *Ann Rheum Dis.* **62**, 275-6.
174. Russell, R. G., Watts, N. B., Ebetino, F. H. & Rogers, M. J. (2008) Mechanisms of action of bisphosphonates: similarities and differences and their potential influence on clinical efficacy, *Osteoporos Int.* **19**, 733-59.
175. Fabre, B., Ramos, A. & de Pascual-Teresa, B. (2014) Targeting matrix metalloproteinases: exploring the dynamics of the s1' pocket in the design of selective, small molecule inhibitors, *J Med Chem.* **57**, 10205-19.
176. Mendes, S. R., Eckhard, U., Rodriguez-Banqueri, A., Guevara, T., Czermak, P., Marcos, E., Vilcinskis, A. & Gomis-Ruth, F. X. (2022) An engineered protein-based submicromolar competitive inhibitor of the *Staphylococcus aureus* virulence factor aureolysin, *Comput Struct Biotechnol J.* **20**, 534-544.
177. Sychantha, D., Rotondo, C. M., Tehrani, K., Martin, N. I. & Wright, G. D. (2021) Aspergillomarasmine A inhibits metallo-beta-lactamases by selectively sequestering Zn(2), *J Biol Chem.* **297**, 100918.
178. Robert, D. H. & Martell, A. E. (1989) Ligand design for selective complexation of metal ions in aqueous solution, *Chem Rev.* **89**, 1875-1914.
179. Samuelson, O., Astrand, O. A. H., Frohlich, C., Heikal, A., Skagseth, S., Carlsen, T. J. O., Leiros, H. S., Bayer, A., Schnaars, C., Kildahl-Andersen, G., Lauksund, S., Finke, S., Huber, S., Gjoen, T., Andresen, A. M. S., Okstad, O. A. & Rongved, P. (2020) ZN148 Is a Modular Synthetic Metallo-beta-Lactamase Inhibitor That Reverses Carbapenem Resistance in Gram-Negative Pathogens In Vivo, *Antimicrob Agents Chemother.* **64**.
180. Gall, A. L., Ruff, M., Kannan, R., Cuniasso, P., Yiotakis, A., Dive, V., Rio, M. C., Basset, P. & Moras, D. (2001) Crystal structure of the stromelysin-3 (MMP-11) catalytic domain complexed with a phosphinic inhibitor mimicking the transition-state, *J Mol Biol.* **307**, 577-86.

181. Laarman, A. J., Bardoel, B. W., Ruyken, M., Fernie, J., Milder, F. J., van Strijp, J. A. & Rooijackers, S. H. (2012) *Pseudomonas aeruginosa* alkaline protease blocks complement activation via the classical and lectin pathways, *J Immunol.* **188**, 386-93.

Paper I



Inhibition of bacterial and human zinc-metalloproteases by bisphosphonate- and catechol-containing compounds

Fatema Rahman, Tra-Mi Nguyen, Olayiwola A. Adekoya, Cristina Campestre, Paolo Tortorella, Ingebrigt Sylte & Jan-Olof Winberg

To cite this article: Fatema Rahman, Tra-Mi Nguyen, Olayiwola A. Adekoya, Cristina Campestre, Paolo Tortorella, Ingebrigt Sylte & Jan-Olof Winberg (2021) Inhibition of bacterial and human zinc-metalloproteases by bisphosphonate- and catechol-containing compounds, Journal of Enzyme Inhibition and Medicinal Chemistry, 36:1, 819-830, DOI: [10.1080/14756366.2021.1901088](https://doi.org/10.1080/14756366.2021.1901088)

To link to this article: <https://doi.org/10.1080/14756366.2021.1901088>



© 2021 The Author(s). Published by Informa UK Limited, trading as Taylor & Francis Group.



Published online: 23 Mar 2021.



Submit your article to this journal [↗](#)



Article views: 1812



View related articles [↗](#)



View Crossmark data [↗](#)







Citing articles: 3 View citing articles [↗](#)

RESEARCH PAPER



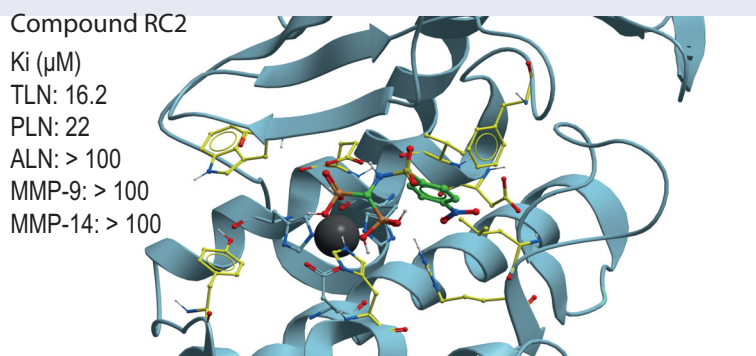
Inhibition of bacterial and human zinc-metalloproteases by bisphosphonate- and catechol-containing compounds

Fatema Rahman^a, Tra-Mi Nguyen^b, Olayiwola A. Adekoya^b, Cristina Campestre^c , Paolo Tortorella^d , Ingebrigt Sylte^a  and Jan-Olof Winberg^a 

^aDepartment of Medical Biology, Faculty of Health Sciences, UiT-The Arctic University of Norway, Tromsø, Norway; ^bDepartment of Pharmacy, Faculty of Health Sciences, UiT-The Arctic University of Norway, Tromsø, Norway; ^cDepartment of Pharmacy, University of “G. d’Annunzio” Chieti, Chieti, Italy; ^dDepartment of Pharmacy, Science of Pharmacy, University “A. Moro” Bari, Bari, Italy

ABSTRACT

Compounds containing catechol or bisphosphonate were tested as inhibitors of the zinc metalloproteases, thermolysin (TLN), pseudolysin (PLN) and aureolysin (ALN) which are bacterial virulence factors, and the human matrix metalloproteases MMP-9 and -14. Inhibition of virulence is a putative strategy in the development of antibacterial drugs, but the inhibitors should not interfere with human enzymes. Docking indicated that the inhibitors bound MMP-9 and MMP-14 with the phenyl, biphenyl, chlorophenyl, nitrophenyl or methoxyphenyl ringsystem in the S₁'-subpocket, while these ringsystems entered the S₂'- or S₁-subpockets or a region involving amino acids in the S₁'- and S₂'-subpockets of the bacterial enzymes. An arginine conserved among the bacterial enzymes seemed to hinder entrance deeply into the S₁'-subpocket. Only the bisphosphonate containing compound RC2 bound stronger to PLN and TLN than to MMP-9 and MMP-14. Docking indicated that the reason was that the conserved arginine (R203 in TLN and R198 in PLN) interacts with phosphate groups of RC2.



ARTICLE HISTORY

Received 8 November 2020
Revised 12 February 2021
Accepted 4 March 2021

KEYWORDS

Zinc proteases; bacterial virulence factors; matrix metalloproteases; enzyme inhibition; docking and scoring

Introduction

It is estimated that there are more than 60000 different proteases^{1,2}. In vertebrates they are involved in regulation of physiologic processes such as cell growth, angiogenesis, blood pressure, coagulation, cell signalling, reproduction, wound repair, hemostasis and homeostasis^{2–7}. Proteases are either secreted from cells or localised inside cells. They are divided into classes and clans depending on the active site residues taking part in the catalytic reaction (Merops database)^{8–10}. The major classes found in all organisms are aspartate-, threonine-, cysteine-, serine- and metallo-proteases, but in addition the classes glutamate-, asparagine- and mixed-proteases have been detected in microorganisms (Merops database)¹⁰.

Dysregulation of one or several proteases in humans is often associated with disease^{3,4,11–14} and several proteases are potential

targets for therapeutic interventions^{15–18}. In humans there are around 570 different proteases and approximately 190 of these are metalloproteases¹⁹. Of around 280 cell-secreted human proteases, approximately 120 are metalloproteases^{2,19,20}. Matrixins or matrix metalloproteases (MMPs) is a family of secreted and membrane associated calcium dependent metalloproteases which contains a catalytic and a structural zinc ion¹¹. MMPs belong to the M10 family of proteases. In humans there are 23 different MMPs, and MMP-9 and -14 are two of the members¹¹. One or several members of the MMP family are overexpressed and functionally involved in pathological conditions such as chronic venous disease, fibrotic disorders, inflammation, liver diseases, lung diseases, neurological diseases, osteoarthritis, viral infection, cardiovascular diseases and in various cancer forms²¹. Several investigators both in academia and industry have developed MMP inhibitors

CONTACT Ingebrigt Sylte  ingebrigt.sylte@uit.no; Jan-Olof Winberg  jan.o.winberg@uit.no  Department of Medical Biology, Faculty of Health Sciences, UiT-The Arctic University of Norway, Tromsø, Norway

© 2021 The Author(s). Published by Informa UK Limited, trading as Taylor & Francis Group.

This is an Open Access article distributed under the terms of the Creative Commons Attribution License (<http://creativecommons.org/licenses/by/4.0/>), which permits unrestricted use, distribution, and reproduction in any medium, provided the original work is properly cited.

interacting with the active site. However, in clinical tests the vast majority of MMP inhibitors have failed²². The most likely reason is that the MMPs are of major importance in many physiological processes such as cell apoptosis, embryogenesis, immune response, morphogenesis, tissue remodelling, tooth enamel formation, reproduction, menstruation, wound healing, angiogenesis and axonal growth^{13,21,23}. MMPs are tightly regulated and expressed in all human tissues and organs^{13,22,23}, and therefore an uncontrolled activity regulation of one or several MMPs by an inhibitor should be avoided. In microorganisms, proteases are involved in processes such as generation of nutrition, growth, survival and invasion into host organisms^{24–30}. Bacterial infectious diseases claim millions of casualties each year, and the spreading of antibiotic multi-resistance among central human pathogenic bacteria is recognised as a major global health concern and a pressing societal challenge. Development of new antibiotics with novel modes of action and innovative strategies to efficiently fight bacterial infections are urgently needed. Inhibition of bacterial virulence rather than directly targeting bacterial growth and viability has gained increasing interests in anti-infective drug discovery^{31,32}. Such compounds may impose less evolutionary pressure for resistance development than classical antibiotics, and have limited impact on the host commensal flora. Several proteases are bacterial virulent factors and therapeutically interesting as putative antibacterial drug targets^{26–29,33}. However, compounds targeting bacterial virulence have so far not been approved as drugs^{34,35}.

MMP-9 (gelatinase B) is secreted, while MMP-14 belongs to the membrane type metalloproteases (MT-MMPs), and is also called membrane type 1 metalloprotease (MT1-MMP). The MT-MMPs contain either a transmembrane domain or a GPI-membrane anchor, with the catalytic site located outside the cell in the extracellular environment¹¹. The MMPs are constituted of different structural domains, and both MMP-9 and MMP-14 contain an N-terminal prodomain, followed by a catalytic domain, a hinge region and a C-terminal hemopexin like (HPX) domain. In MMP-14, the HPX domain is followed by the transmembrane domain, while MMP-9 contains three fibronectin-III like (FnIII) repeats in the catalytic domain¹¹. The MMPs belong to the clan metzincins and the catalytic zinc ion is bound to the protein through three histidines of the segment (HEXXHXXGXXH/D + M)^{8,9}. The fourth zinc ligand in the inactive proform is the cysteine in the PRCGV motif of the pro-domain^{36,37}. The fourth zinc ligand in the activated MMPs is a water molecule, that also binds to the side chain of the glutamate that follows the first histidine in the zinc binding segment^{8,9}. MMP-9 can be activated in the extracellular environment by naturally occurring proteases such as trypsin, kallikrein, MMP-2 and MMP-3, but also by mercurial and organomercurial compounds such as HgCl₂ and APMA (p-aminophenylmercuric acetate) and bacterial metalloproteases such as thermolysin (TLN) and pseudolysin (PLN)³⁷. MMP-14, like the other MT-MMPs, are activated inside cells by the serine protease furin¹¹. MMP-14 is the most studied enzyme among membrane-linked MMPs, while MMP-9 (gelatinase B) is the most studied among secreted MMPs^{14,38}. Binding of inhibitors to the active site of MMP-14 and MMP-9 have been extensively studied both by kinetic and X-ray crystallography^{39–47}. The active sites of the MMPs are similar but not identical. Their S₁'-subpocket determines the substrate cleavage site, and they all prefer hydrophobic amino acids in this pocket^{48,49}.

TLN from *Bacillus thermoproteolyticus* is the model enzyme of the M4 family of proteases, which is also termed the thermolysin family⁵⁰. These enzymes have a zinc ion in the catalytic site, which has tetrahedral coordination. Two histidines of a HEXXH motif and

a glutamic acid located 18–72 residues C-terminal to the HEXXH motif are the three ligands that anchor the zinc ion to the enzyme, while the fourth ligand is a water molecule as in the MMPs, which also binds the side chain of the glutamate following the first histidine in the zinc binding segment^{8,9,50}. Inhibitors containing a metal binding group replace the catalytic water molecule on the zinc ion when they bind the catalytic site⁵¹. TLN, PLN from *Pseudomonas aeruginosa* (LasB or elastase of *P. aeruginosa*) and aureolysin (ALN) from *Staphylococcus aureus* belong to the subclass MA(E) of the M4 family, also known as the "Gluzincins"^{8,9,50}. These three proteases have several similarities despite a modest sequence identity (28% between TLN and PLN)^{52,53}. The three dimensional (3D) structures of PLN and TLN have been extensively studied, also in complex with inhibitors, and reveal large similarities in the overall structure. The main structural differences are that PLN consists of a slightly more open substrate binding cleft than TLN, and that PLN has one structural calcium while TLN has three^{53–55}. For ALN only the 3D-structure of the free enzyme is known⁵⁶. Although PLN is not as well characterised as TLN, it appears that the slight difference in substrate specificity between the two enzymes is mainly due to the size of the S₁'-subpocket and a more open substrate binding cleft in PLN than in TLN. PLN has a broader substrate specificity than most other M4 family members including TLN, although all these enzymes prefer a hydrophobic amino acid at the P₁' position. Furthermore, for substrate degradation four subsites of PLN require to be occupied^{50,53,55}.

PLN, TLN and ALN are secreted bacterial virulence factors, and inhibitors may be new antibacterial drugs, either alone or used as adjuvant to traditional antibacterial treatment. PLN, TLN and ALN have structural resemblance with human MMPs. In order to have a therapeutic value, compounds targeting these virulence factors should not interfere strongly with the function of human MMPs, due to the importance of MMPs in physiological processes. Identifying structural determinants for strong binding to the bacterial M4 proteases and human MMPs would therefore be of pivotal importance for the development of new antibacterial drugs. In this study, we have studied several catechol containing and bisphosphonate containing compounds for their inhibition of TLN, PLN, ALN, MMP-9 and MMP-14 in order to identify new M4 inhibitors and investigate structural determinants that might be important for selective binding using inhibition kinetic and molecular modelling.

Results and discussion

K_m values for the fluorescence quenched substrates

At conditions used in the present work (1% DMSO in all assays), the *K_m* values of the substrate McaPLGL(Dpa)AR-NH₂ with APMA-activated recombinant MMP-9 (rMMP-9(A)), trypsin-activated MMP-9 from THP-1 cells (MMP-9(T)) and MMP-14 were 4 ± 1, 6 ± 2 and 4.9 ± 0.4 μM, while the *K_m* values of the substrate McaRPPGFSAFK(Dnp)-OH with ALN, PLN and TLN were 76 ± 7, 24 ± 8 and 6 ± 1 μM, respectively. The estimated *K_m* values for ALN and PLN must be regarded as uncertain since the highest substrate concentration used was 10 μM due to quenching. The obtained *K_m* values are very similar to those previously obtained for these enzymes without DMSO⁵⁷ or with a DMSO concentration of 5%⁵⁸. Previously it was reported that TLN is inactivated in most organic cosolvents, but can tolerate up to 10% DMSO to enhance substrate solubility⁵⁹. For TLN, the *K_m* value was also determined with a DMSO concentration of 2%. This resulted in a

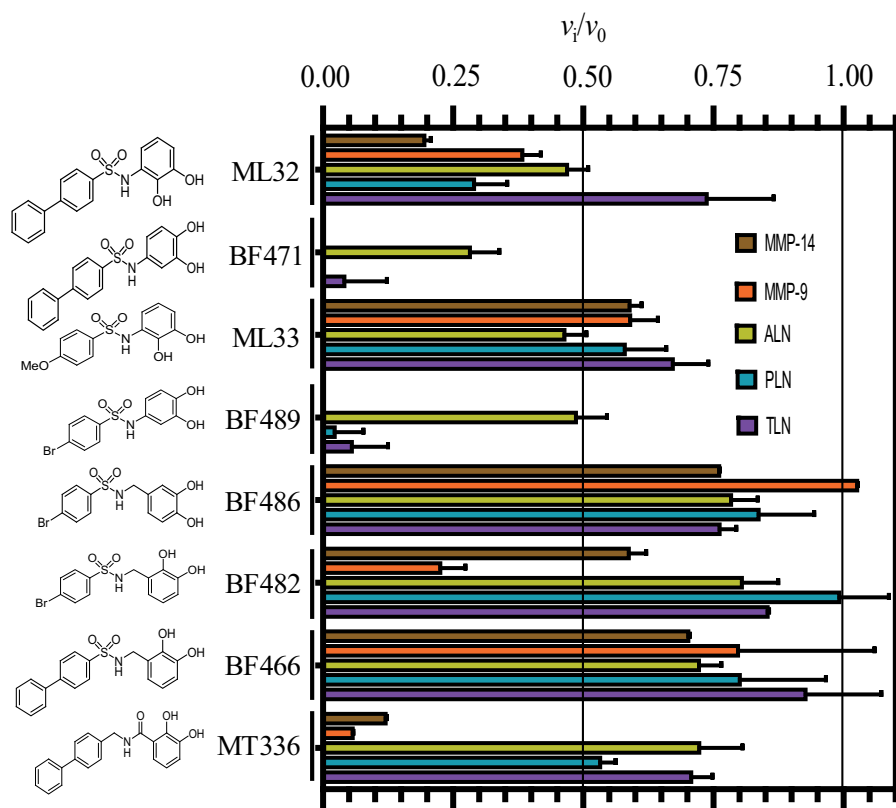


Figure 1. Inhibitory effect of 100 μM of the catechol containing compounds on the activity of the human metalloproteases, MMP-9 and MMP-14, and the bacterial metalloproteases TLN, PLN and ALN. The inhibition experiments were performed by using a fixed concentration of 4 μM of both the MMP-9 and MMP-14 substrate McaPLGL(Dpa)AR-NH₂ and the ALN, PLN and TLN substrate McaRPPGFSAFK(Dnp)-OH. The v_i/v_0 (mean \pm sd) were based on 4–6 experiments.

K_m value of $7 \pm 1 \mu\text{M}$ which is not significantly different from the value obtained in the presence of 1% DMSO.

Quenching experiments with catechol containing compounds and bisphosphonates

All compounds were first tested for possible quenching of the formed fluorescence product. The experiments were performed with varying concentrations of the putative inhibitors (0 – 100 μM) against varying fluorescence product (McaPL-OH) concentration as previously described for PAC-1 and Isatin derivatives⁵⁸, and as described in the experimental section. These experiments revealed that in contrast to the PAC-1 and Isatin derivatives⁵⁸, neither the catechol derivatives nor the bisphosphonates used in the present work quenched the fluorescence product. However, some of the compounds showed fluorescence at the emission and excitation wavelength used, but that did not affect the inhibitory assays as enzymatic reactions were followed continuously.

Inhibitory effects of catechol containing compounds

The inhibitory power of 100 μM of the eight catechol containing compounds was tested against the two human metalloproteases MMP-9(T) and MMP-14 and the three bacterial metalloproteases ALN, PLN and TLN (Figure 1). In order to detect putative slow and slow-tight binding, the catechol derivatives were first incubated along with the enzyme for 15 min at 37 °C. In controls without inhibitor present, enzymes and buffer were preincubated under identical conditions. Thereafter, the enzyme reaction was started by adding the relevant chromogenic substrate and the rate was

followed continuously for 30 min. Except for BF486, which did not affect MMP-9, and BF482 which did not affect PLN, all catechol containing compounds showed inhibition of the five proteases (Figure 1). Both BF471 and BF489 showed more than 50% inhibition of all five proteases, while ML32 reduced the activity more than 50% for four of the proteases (not for TLN). The activity was reduced with more than 50%, by MT336 for the two MMPs, by BF482 for MMP-9(T) and by ML33 for ALN (Figure 1). In all other inhibitory studies with catechol containing compounds, the activity was reduced between 0 and 45%.

X-ray crystallography studies showed that BF471 binds to the active site of MMP-8⁶⁰, and hence we could expect that all tested catechol derivatives should bind the active site. To assure that this is correct, the inhibitors BF471 and BF489 were tested against varying McaRPPGFSAFK(Dnp)-OH using TLN as described in the Experimental section. The results showed that the two catechol derivatives competed with the substrate (data not shown) and the K_i values obtained were $57 \pm 6 \mu\text{M}$ for BF471 and $73 \pm 11 \mu\text{M}$ for BF489. It should be noted that the reaction was started by adding the enzyme to the substrate-inhibitor mixtures. In the case of slow binding, the full potential of these inhibitors would not be realised by this inhibitory assay. When the activity was reduced by more than 60%, experiments were performed with varying concentrations of the catechol derivatives. IC₅₀ values were obtained from dose response plots, and K_i values were determined from the IC₅₀ values based on substrate competitive inhibition. By the use of K_i values, we can compare the binding strength of the compounds for the different enzymes and not only comparing the compounds ability to bind one enzyme. The obtained K_i values of the catechol containing compounds for the five tested proteases are given in Table 1. There are several possible explanations for

Table 1. K_i values of the catechol containing compounds for TLN, PLN, ALN, MMP-14, and MMP-9(T).

Compound	$K_i \pm \text{sd}$ (μM)				
	McaRPPGFSAFK(Dnp)-OH			McaPLGL(Dpa)AR-NH ₂	
	TLN	PLN	ALN	MMP-14	MMP-9(T)
ML32	N.D.	38 ± 8	N.D.	19 ± 0.8	51 ± 17
BF471	13 ± 2	9 ± 3	49 ± 5	6.6 ± 0.6	13 ± 2
BF489	14 ± 5	16 ± 3	N.D.	8.3 ± 0.6	12.6 ± 0.6
MT336	N.D.	N.D.	N.D.	12 ± 1	13 ± 1

K_i values determined for both bacterial and human metalloproteases using two different fluorescence quenched peptide substrates, McaRPPGFSAFK(Dnp)-OH (for TLN, PLN, and ALN) and McaPLGL(Dpa)AR-NH₂ (for MMP-9(T) and MMP-14). The concentration of the substrates used was 4 μM and the highest concentration of tested inhibitors was 100 μM . Compounds included are only those where 100 μM of the compound reduced the enzymatic activity by 60% or more as described in the text. The K_i values are based on 4–6 experiments. N.D.: not determined.

the deviation in determined K_i value of BF471 and BF489 for TLN from the dose response plots and the double inverse plots. One possible explanation is that the catechol compounds are slow binders, and hence less inhibitory activity is observed without preincubation of enzyme and inhibitor.

Figure 1 and Table 1 show that the position of the OH-groups in the catechol moiety affects the binding. Moving the OH-group from position 2 to position 4 (ML32 vs. BF471 and ML33 vs. BF489) largely strengthen the binding for four of the enzymes, while the effect was less for ALN. Another striking effect occurs with the addition of a methylene group between the catechol moiety and the sulphonamide group, which resulted in weaker binding (BF489 vs. BF486 and ML32 vs. BF466). Changing the sulphonyl group to a methylene group and the methylene between the catechol moiety and the sulphonylamide moiety to a carbonyl (BF466 vs. MT336) resulted in stronger binding for the two MMPs, but with only limited activity changes for the bacterial enzymes. Overall, it appeared that the structural differences between the catechol derivatives had little effect on the ALN activity, while the activity of the other four enzymes varied correspondingly. None of the catechol derivatives showed stronger binding to the bacterial than the human enzymes. The largest differences in binding strengths between the human MMPs and the bacterial proteases were seen for MT336.

Except for ML33, all catechol derivatives have previously been tested for binding to MMP-2, MMP-8 and MMP-9⁶⁰. For six of them, IC_{50} values for the enzymes between 2 and 12 μM were reported. The exception was MT336, which had IC_{50} values between 4 and 56 μM . The K_i values for MMP-9 in the present study were higher than the IC_{50} values in the previous study, the exception was MT336 for which we obtained a lower value. It is not easy to point out a single factor in the experiments contributing to deviations between the studies. Both studies used a pH of 7.5 but the buffer compositions were slightly different. In the present study, we used MMP-9 purified from THP-1 cells and activated by trypsin, and hence the enzyme has its C-terminal hemopexin domain intact⁵⁷. Tauro et al.⁶⁰ used a commercial active MMP-9 produced in *E-coli* that only contained the catalytic domain and the fibronectin-like (FnII) module. We do not believe that the use of the two different variants of MMP-9 should affect binding of the catechol derivatives, as we previously have shown that small MMP inhibitors, like galardin and an azasugar-based hydroxamate compound had, the same strength of binding to different N- and C-terminal truncated variants of recombinant MMP-9 and trypsin activated MMP-9 from THP-1 cells⁵⁷. A factor that may contribute to differences is that after preincubation of MMP-9

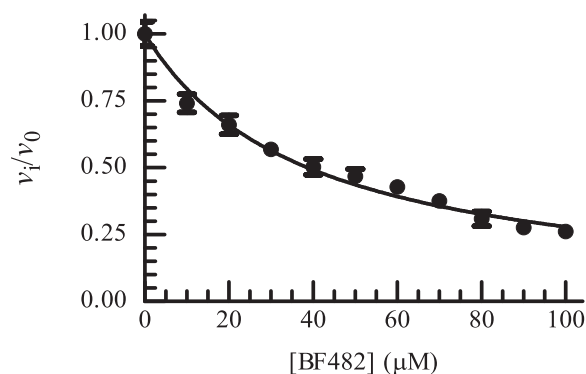


Figure 2. Dose response plot of BF482 for MMP-9(A). The enzyme with and without inhibitor was pre-incubated for 30 min at room temperature and the reaction was started by adding McaPLGL(Dpa)AR-NH₂ (4 μM in assay). The reaction was allowed to proceed for 4 h at 37 °C and stopped by the addition of EDTA (10 mM end concentration). The relative fluorescence was determined with the Clariostar plate reader as described in the Experimental Section, where v_i and v_0 are the reaction rates in the presence and absence of BF482, respectively. Each point on the curve shows the mean \pm sd ($N=5$ for all points except for two points where $N=4$). The regression coefficient r^2 is 0.97, with a determined IC_{50} value of $38.8 \pm 0.9 \mu\text{M}$ and a K_i value of $19.4 \pm 0.4 \mu\text{M}$.

with catechol derivatives and adding of the substrate for starting the reaction, we followed the reaction continuously for 30 min, while Tauro et al.⁶⁰ used an endpoint assay allowing the reaction to proceed for 2 to 4 h before the fluorescence was measured. We did some tests to determine if some of these differences could affect the binding results. In the test experiments, we used rMMP-9(A) which differs from the MMP-9(T) by a slightly different N-terminal and a largely truncated C-terminal HPX domain⁵⁷. One hundred μM of BF466 was tested where the 0.1 M Hepes buffer pH 7.5 was exchanged to a 0.1 M Tris-HCl buffer pH 7.5. The rMMP-9(A) was preincubated with BF466 for 0, 15 and 30 min at 37 °C and the reaction was started by the addition of the substrate McaPLGL(Dpa)AR-NH₂ (4 μM in the assay) following the reaction continuously for 3 h. The controls without BF466 were treated identically. The obtained v_i/v_0 values for the three time points were 0.74 ± 0.04 ($N=4$), 0.68 ± 0.02 ($N=4$) and 0.73 ± 0.05 ($N=4$). These results fit well with obtained data for MMP-9(T) in Hepes buffer (Figure 1) suggesting that neither the buffer nor the origin of the MMP-9 affected the binding of this inhibitor. Further, the compound could not be regarded as a slow binder of MMP-9. We also tested if the use of an end point assay could affect the results. Here rMMP-9(A) was preincubated with different concentrations of BF482 for 30 min in 0.1 M Hepes pH 7.5 and the reaction was started by the addition of McaPLGL(Dpa)AR-NH₂ (4 μM in the assay). The reaction was allowed to proceed for 4 h, and the reaction was stopped by addition of EDTA (end concentration 10 mM) and the relative fluorescence intensity determined. This resulted in an IC_{50} value of $40 \pm 1 \mu\text{M}$ and a K_i value of $20.1 \pm 0.7 \mu\text{M}$ (Figure 2), while the v_i/v_0 value for 100 μM inhibitor was similar to that in Figure 1. This suggests that the use of either initial rate assays or end point assays is not a reason for the obtained differences between this study and that of Tauro et al.⁶⁰.

Docking

Docking of the catechol containing compounds into the X-ray structure of MMP-9 (PDB ID: 5cuh) and MMP-14 (PDB ID: 1bqq) showed that the biphenyl, bromophenyl and methoxyphenyl group of the compounds enter the S_1' -subpocket. The interaction modes of BF471 in MMP-9 and MMP-14 were very similar to that observed in the X-ray structure of BF471 with MMP-8⁶⁰. In

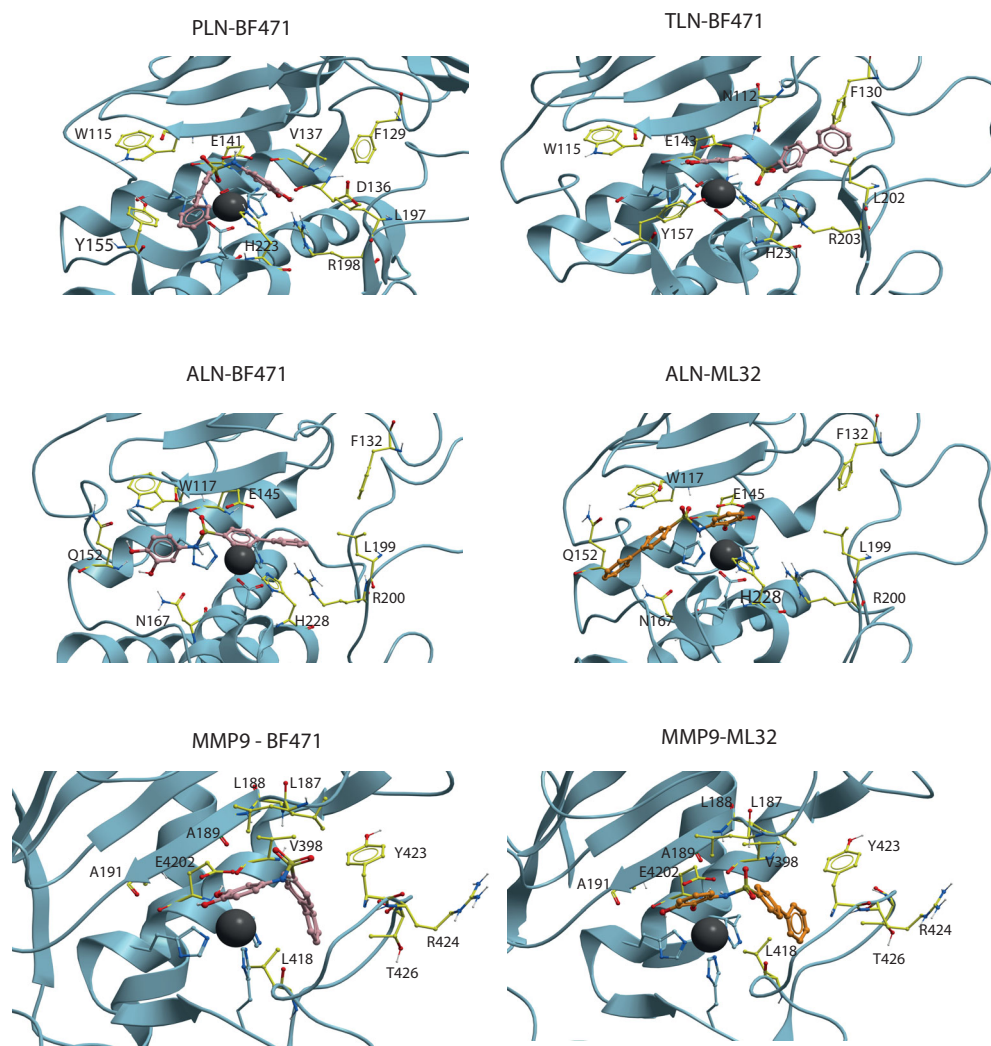


Figure 3. BF471 docked into PLN, TLN, ALN and MMP-9, and ML32 docked into ALN and MMP-9. Zinc is shown in dark grey. The side chain of zinc coordinating amino acids are shown in blue. The side chains of some amino acids of importance for ligand binding are displayed with the following colour coding of atoms: oxygen: red; nitrogen: blue; carbon: yellow; hydrogen: grey. Colour coding of ligand atoms: oxygen: red; sulphur: green; nitrogen: blue; hydrogen: grey; carbon (BF471): pink; carbon (ML32): orange.

contrast, docking catechol containing compounds into TLN (PDB ID: 5dpe) and PLN (PDB ID: 1u4g) showed docking poses both with the diphenyl, bromophenyl and methoxyphenyl groups entering the S_1 - or the S_1'/S_2' -subpockets. The catechol containing compounds bind quite weak to ALN, and docking indicated binding modes quite different from the other proteases (Figure 3). It seems like the side chain of R203 in TLN, corresponding to R200 in ALN and R197 in PLN, is the main reason for the binding pose differences between the human and bacterial proteases. For most of the compounds, the arginine side chain orientation hinders the biphenyl, bromophenyl and methoxyphenyl groups of the compounds to enter deeply into the S_1' -subpocket (Figure 3). This arginine is known as functionally important for TLN-like proteases, and is suggested to interact with a backbone carbonyl group of the substrates⁶¹ and is located at the border between the S_1' - and S_2' -subpockets. Table 2 shows the most important amino acids in the different protease subpockets for binding the compounds in the present study.

The highest scored pose of BF471 with TLN was with the diphenyl moiety into the S_2' -subpocket, with the sulphonamide group interacting between the side chain of R203, the side chain of N112 in the S_2' -subpocket and H231 (Figure 3). Both hydroxyl groups of the BF471 catechol ring interacted with the Zn atom,

while the hydroxyl group in position 3 also created a hydrogen bond with E143. However, the best pose of BF489 in TLN had the bromophenyl entirely into the S_1' -subpocket, while a hydroxyl of the catechol ring interacted with the backbone of W115 (S_1 -subpocket) and the amide with E143, thereby obtaining a binding pose quite similar to that observed for BF471 and the other catechol containing compounds in MMP-9 and MMP-14 (Figure 3).

The highest scored pose of BF471 in PLN was with the diphenyl moiety into the S_1 -subpocket interacting close to Y155, while the catechol moiety entered into the region between the S_1' - and S_2' -subpocket with the hydroxyl groups interacting with R198 (Figure 3). The NH-group formed a hydrogen bond with E141. Moving the hydroxyl group from position 2 (ML32) to position 4 (BF471) of the catechol moiety resulted in increased binding affinity towards all enzymes. In PLN the change allowed interactions between both hydroxyl groups of BF471 and R198, while only one hydroxyl group of ML32 interacted with R198 which may explain the higher PLN affinity of BF471 than of ML32.

The compounds showed weak affinity for ALN (Figure 1), and only BF471 reduced the enzymatic activity with more than 60% at a concentration of 100 μM and a K_i value of 49 μM was determined. BF471 obtained a docking pose in ALN quite different from those in the other enzymes (Figure 3). The catechol hydroxyl

Table 2. Functionally important amino and amino acids in the S_{1-} , $S_{1'}$ - and $S_{2'}$ -subpockets of TLN, PLN, ALN, MMP-9, and MMP-14 contributing to the binding of catechol or bisphosphonate containing compounds tested in the present study.

	TLN	PLN	ALN	MMP-9	MMP-14
S_1 -subpocket	W115, Y157	W115, Y155	W117, Q152, N167	H190, P193	F204
S_1' -subpocket	L133, V139, H142, I188	L132, V137, H140, I190	V137, H144, I186, V189	L397, V398, H401, L418, Y420, P421, Y423, R424, T426	L199, E219, W221, N231, H239
S_2' -subpocket	N111, F130, Y193, L202	E111, F129, L197	N114, F132, L199	G186, L187, Y218	L235, V236, Y261, Q262
Catalytic Glu	E143	E141	E145	E402	E240
Known inhibitor binding residues	N112, A113, F114, R203, H231	E111, N112, A113, R198, H223	N112, Y114, R200, H228	A189, H190, A191	A200, H201
Zn ²⁺ ligated	H142, H146, E166	H140, H144, E164	H144, H148, E168	H401, H405, H411	H239, H243, H248

The subpocket amino acids of MMP-9 in the table are based on the X-ray structure of the inactive MMP-9 mutant E402A lacking the pro, Fnnl, hinge and HPX domains bound to a chromogenic substrate (PDB id: 4JJJ)⁷¹, while the numbering is as in the PDB id: 1l6j, which includes the three Fnnl-like repeats in the catalytic site⁷². The subpocket amino acids of TLN are based on Krimmer et al.⁷³. Subpocket amino acids of the other enzymes are based on structural superimposition with TLN (PLN and ALN) and MMP-9 (MMP-14).

groups formed hydrogen bonds with Q152 and N167 in the S_1 -subpocket, while the NH group formed hydrogen bonds with the backbone of W117 and with the biphenyl ring-system located above the Zn²⁺ and R200. The possibility of two hydrogen bonds (with Q152 and N167) is perturbed for ML32 with the hydroxyl group in position 2 (Figure 3). Instead the hydroxyl groups of ML32 were occupied with Zn²⁺, while diphenyl ring system was highly exposed to solvent without clear interactions with amino acids in ALN. Based on the docking it was not easy to explain the increased binding affinity of BF471 for ALN compared with ML32. Both compounds docked quite similar into the enzyme. However, the meta-hydroxyl group (position 3) of ML32 was located further from Y157 in the S_1 -subpocket without the possibility of a hydrogen bond, and in addition the sulphonamide group in ML32 was located further from H231 than the corresponding group in BF471.

Docking indicated that ML32 and ML33 bound similarly to MMP-9 and -14. The hydroxyl group in position 2 of both compounds formed hydrogen bonds with the two oxygen atoms of the side chain carboxyl group of E402 (MMP-9 numbering). The hydroxyl group in position 2 seems to replace the zinc-bound water in the free enzyme, as it also interacted with the catalytic zinc. The two oxygen atoms at the sulphonylamide group formed hydrogen bonds with the main chain NH groups of L187 and A189, while the amide hydrogen of the compounds formed hydrogen bonds with the main chain carbonyl of P421. Thus the main difference in binding strength between ML32 and ML33 for MMP-9 and -14 is mainly attributed to the difference in interaction with the S_1' -subpocket by the diphenyl and the methoxyphenyl group.

The position of the OH- groups in the catechol in relation to the position of the amide nitrogen bound to the catechol seemed important for inhibitory capacity of the compounds. Moving the hydroxyl in position 2 of ML32 and ML33 into position 4 (BF471 and BF489) seemed to strengthen binding to MMP-9 and MMP-14 (Table 1, Figure 1). BF471 docked into MMP-9 with the hydroxyl group in position 3 forming a hydrogen bond with the side chain of E402, while the hydroxyl group in position 4 interacted with the backbone CO of A191. Both hydroxyl groups of BF471 and BF489 also interacted with Zn²⁺, while only the hydroxyl group in position 2 of ML32 and ML33 interacted with Zn²⁺. Introduction of a methyl group between sulphonylamide moiety and the catechol ring of BF489 giving compound BF486 resulted in decreased inhibition of all enzymes (Figure 1). Docking indicated that the bromophenyl group of BF486 was deeper into the S_1' -subpocket of MMP-9 and -14 than that of BF489, and one of the oxygen at the sulphonylamide group formed a hydrogen bond with the main chain nitrogen of Y423 and not with A189 and L188 as seen

for BF489. Furthermore, one side chain carbonyl oxygen of E402 formed a hydrogen bond with the NH group of the sulphonylamide moiety of BF486, while the other E402 carbonyl oxygen interacted with the hydroxyl group in position 3 of the catechol. In addition, the position 3 hydroxyl group interacted with the backbone CO of A191. These overall changes result in weaker binding of BF486 than of BF489.

MT336 differs from BF466 in that the sulphonyl group of BF466 is replaced by a methylene group, and the methyl group between the sulphonylamide moiety and the catechol ring by a carbonyl group. Hence MT336 contains an amide bond, which improved the binding for MMP-9 and MMP-14 compared to BF466, but not for the bacterial enzymes (Figure 1 and Table 1). Docking into MMP-9 and MMP-14 showed that the carbonyl of MT336 was much closer to the catalytic zinc atom than any of the oxygen atoms of the sulphonylamide moiety of BF466, and in addition, the hydroxyl group in position 2 of the catechol was also closer to Zn²⁺.

Inhibitory effects of bisphosphonates

Figure 4 shows the inhibition of 100 μ M of the seven bisphosphonates. Replacing the catechol moiety of ML32 and BF471 with a bisphosphonate giving MT242, and the catechol moiety of ML33 giving LS4, had either no effect or reduced the binding (Figures 1 and 4). Adding a methoxy group to position 4 of the phenyl group (RC14 to LS4) had almost no effect of the binding, except for PLN where the binding was strengthened. The addition of a strong electron withdrawing group (NO₂) at the position 4 of the phenyl group, giving RC2 resulted in a much stronger binding to PLN and TLN than to the two MMPs (Figure 4 and Table 3). However, for ALN the binding strength was almost similar to that without the NO₂ group (RC14) or with a methoxy group at the phenyl ring (LS4) (Figure 4). The binding of RC2 to ALN was even weaker than for the two human MMPs (Figure 4). Removal of the sulphonyl group from the bisphosphonate of RC14 giving GD16 had limited effect on the binding of the five proteases (Figure 4). Addition of a chloride ion at position 4 of the phenyl group of GD16 giving ML45 resulted in enhanced binding to all proteases except for TLN (Figure 4 and Table 3). Addition of an additional phenyl ring to position 4 of the phenyl group of GD16, giving MT363, gave much stronger binding for four of the proteases. However, the binding was reduced for ALN (Figure 4 and Table 3). Most bisphosphonates bound weaker to ALN than to the other proteases.

The seven bisphosphonate compounds were also previously tested against various MMPs including MMP-9 and MMP-14^{62,63}. As for the catechol derivatives, the results for some of the

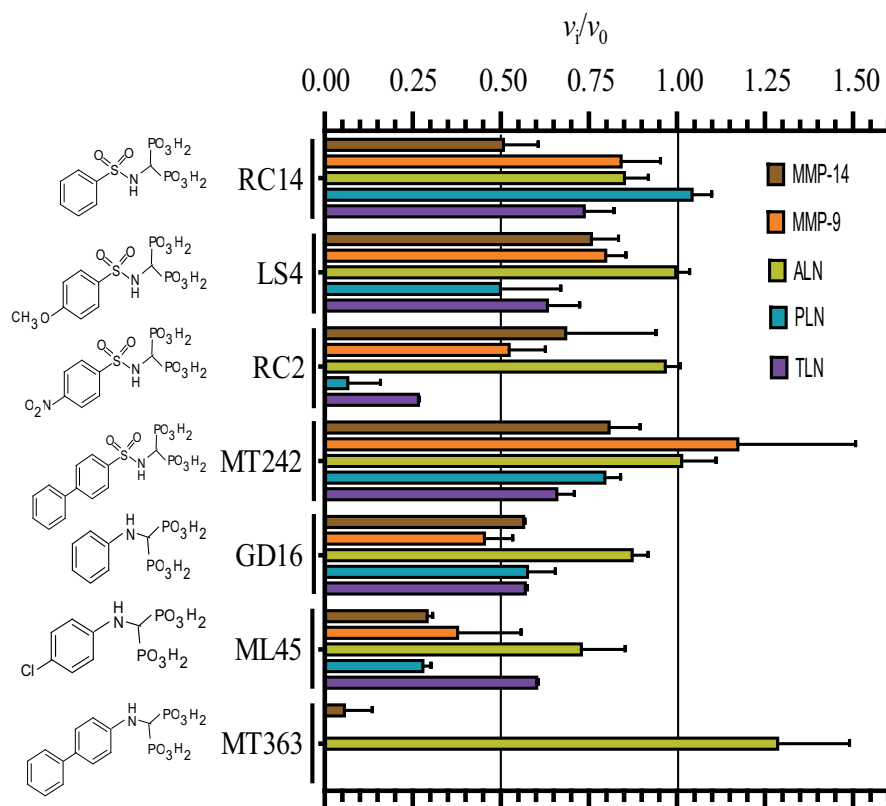


Figure 4. Inhibitory effect of 100 μM bisphosphonate containing compounds on the activity of the human metalloproteases, MMP-9 and MMP-14, and the bacterial metalloproteases TLN, PLN, and ALN. The inhibition experiments were performed by using a fixed concentration of 4 μM of both the MMP-9 and MMP-14 substrate McaPLGL(Dpa)AR-NH₂ and the ALN, PLN and TLN substrate McaRPPGFSAFK(Dnp)-OH. The v_i/v_0 (mean \pm sd) were based on 4–6 experiments.

Table 3. The obtained K_i values of the various bisphosphonate containing compounds for TLN, PLN, ALN, MMP-14 and MMP-9.

Compounds	$K_i \pm \text{sd}$ (μM)				
	McaRPPGFSAFK(Dnp)			McaPLGL(Dpa)AR-NH ₂	
	TLN	PLN	ALN	MMP-14	MMP-9(T)
LS4	N.D.	58 \pm 4	N.D.	N.D.	N.D.
RC2	16.2 \pm 0.4	22 \pm 3	N.D.	N.D.	N.D.
ML45	N.D.	37 \pm 6	N.D.	17 \pm 1	N.D.
MT363	7 \pm 1	12 \pm 4	N.D.	7.2 \pm 0.6	6.6 \pm 0.4

The K_i values for both bacterial and human metalloproteases were measured with two different fluorescence quenched substrates, McaPLGL(Dpa)AR-NH₂ (for MMP-9 and MMP-14) and McaRPPGFSAFK(Dnp)-OH (for TLN, PLN and ALN). The concentration of the substrates used was 4 μM and the highest concentration of the inhibitor compounds tested was 100 μM . Compounds tested were only those where 100 μM of the compound reduced the enzymatic activity by 60% or more. The K_i values are based on 4–6 experiments. N.D.: not determined.

compounds varied slightly from the present results for MMP-9 and MMP-14. A difference between the assays was that in the present study we used a preincubation time of 15 min at 37 $^{\circ}\text{C}$, while Rubino et al. 2011⁶² and Tauro et al. 2013⁶³ used 30 min at 25 $^{\circ}\text{C}$. Another important difference was that in the present work we followed the reaction continuously for 30 min after preincubation, while Rubino et al. 2011⁶² and Tauro et al. 2013⁶³ used an end point assay where the reaction was stopped by adding 3% of acetic acid after 2–4 h of incubation, followed by fluorescence measurements. These differences in assay conditions are not likely

explanations for the small differences in the obtained binding values as previously discussed for the catechol derivatives.

Docking

Docking indicated that like the catechol containing compounds, the bisphosphonates bind MMP-9 and MMP-14 with the phenyl, biphenyl, chlorophenyl, nitrophenyl or methoxyphenyl ringsystem into the S₁'-subpocket (Figure 5). The phosphate and sulphonamide groups were located in the region of Zn²⁺, E402, A189, L187, L188, and V398 (MMP-9 numbering). However, docking into TLN and PLN was not conclusive, and docking poses with these ringsystems into the S₁- or S₁'/S₂'-subpockets of TLN and PLN were observed for most of the compounds. Notable features from the binding studies were that RC2 inhibits TLN and PLN stronger than ALN and the two human MMPs, while MT363 is a decent inhibitor of all enzymes, except ALN (Figure 4, Table 3).

Docking of RC2 into PLN showed that one of the phosphate groups interacted with Zn²⁺, H223 and E141, while the other phosphate group interacted with R198 (two hydrogen bonds) and H223. The NH-group interacted with the backbone of A113. The NO₂-group was located within the S₁'-subpocket close to the side chain R198, the backbone NH-group of G187 and the side chain of the zinc-coordinating H140 (Figure 5). However, docking poses in PLN with the nitrophenyl group of RC2 in the S₁-subpocket were also observed. In TLN, poses quite similar to that described in PLN were observed, but the highest scored was with the nitrophenyl group into the S₁-subpocket interacting with Y157 and with the nitro group exposed to solvent. The sulphonamide group interacted with N112 and H231. One of the phosphate groups interacted with Zn²⁺, and the side chains of R203

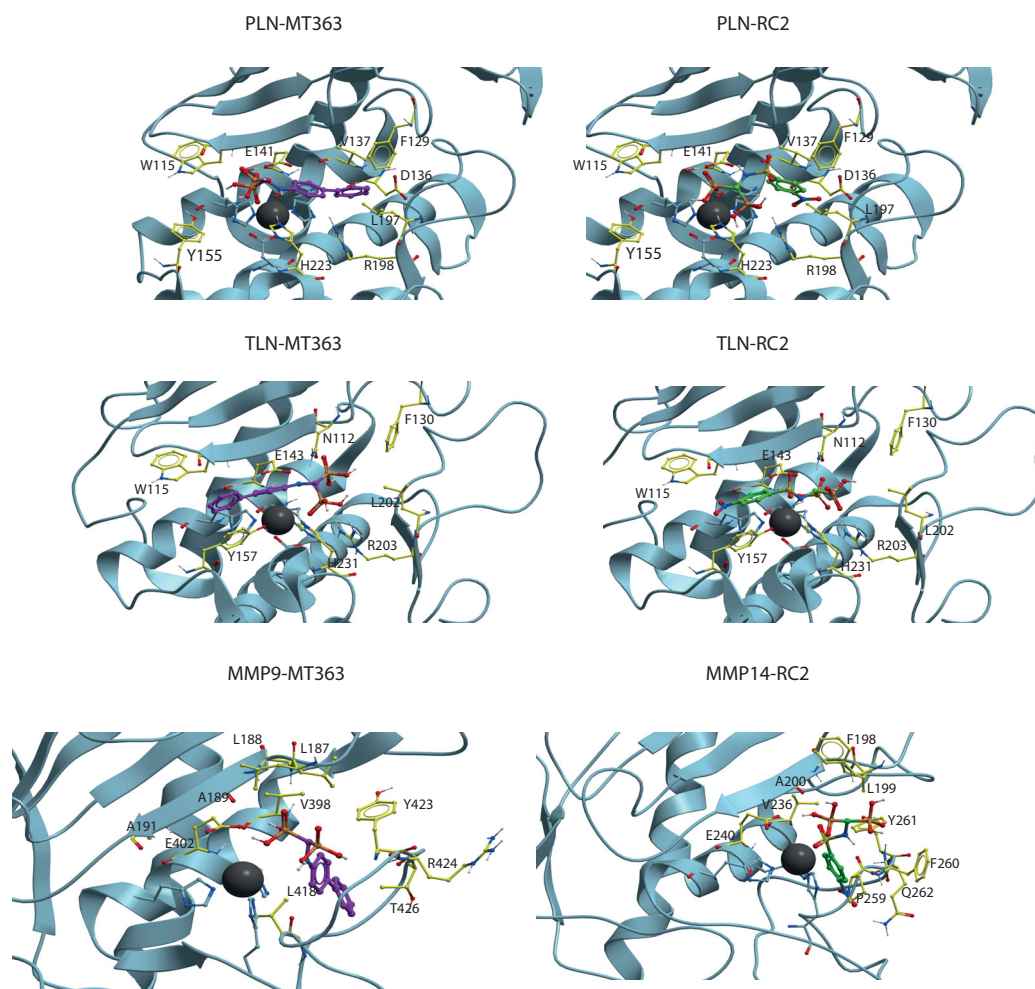


Figure 5. MT363 and RC2 docked into PLN, TLN MMP-9 (MT363) and MMP-14 (RC2). TLN, PLN and MMP-9. Zinc is shown in dark grey. The side chain of zinc coordinating amino acids are shown in blue. The side chains of some amino acids of importance for ligand binding are displayed with the following colour coding of atoms: oxygen: red; nitrogen: blue; carbon: yellow; hydrogen: grey. Colour coding of ligand atoms: oxygen: red; sulphur: green; nitrogen: blue; phosphate: orange; hydrogen: grey; carbon – MT363: purple; carbon – ML32: orange.

and E143, while the other interacted with the side chain of R203 and N112. In MMP-9 and -14, RC2 bound with the nitrophenyl group into the S_1' -subpocket (Figure 5). In MMP-14, the phosphate groups were involved in a network of interactions with Zn^{2+} and E240, backbone NH and CO of A200, and the backbone NH groups of L199 and Y261, in addition to being exposed to solvent. The phosphate groups of RC2 had fewer strong interactions with the enzyme in the MMPs than in PLN and TLN, which may contribute to stronger interactions of RC2 with TLN and PLN than with the MMP-9 and -14.

Except for ALN, MT363 binds quite strong to all enzymes. In PLN the biphenyl group of MT363 was located within the S_2' -subpocket, while one of the phosphate groups interacted with Zn^{2+} , E141 and the backbone NH of W115, while the other interacted with N112, F114, in addition to being quite solvent exposed. However, docking poses with the biphenyl group into the S_1' -subpocket were also obtained. In TLN, MT363 docked best with the biphenyl group into the S_1' -subpocket obtaining stacking interactions with Y157, while also poses with the biphenyl into the S_2' -subpocket were obtained. In the best docking pose the phosphate groups interacted with Zn^{2+} , R203 and H231, while the other pointed into the S_2' -subpocket and interacted with N112 (Figure 5). In the MMPs, the biphenyl moiety was in the S_1' -subpocket, while the bisphosphonate group interacted with Zn^{2+} , the side

chain of E402 (MMP-9 numbering), V398, the backbone of A189, in addition to being exposed to the solvent.

Conclusion

Several of the tested MMP-inhibitors were identified as strong TLN and PLN inhibitors, while only BF471 inhibited ALN activity with more than 60%. Both tested catechol containing compounds and bisphosphonates bound MMP-9 and -14 with the phenyl, biphenyl, chlorophenyl, bromophenyl, nitrophenyl or methoxyphenyl ringsystem into the structurally flexible S_1' -subpocket. In TLN, PLN and ALN, the contribution of a positively charged arginine (TLN; R203, PLN; R198, ALN; R200) at the entrance of the S_1' -subpocket hinders that these functional groups fully enter the S_1' -subpocket of the bacterial enzymes. Instead these groups occupy the S_1' - or the S_2' -subpocket, or are located at the entrance of the S_1' -subpocket. However, interactions with the arginine seem to be an important factor for strong binding to the bacterial proteases. RC2-bound stronger to TLN and PLN than to the MMPs. RC2 may be used as a scaffold to identify new compounds that bind much stronger to the bacterial virulence factors TLN and PLN than to the human MMPs, and hence have a therapeutic potential as

virulence factor inhibitors and represent a new strategy in the fight against drug resistant bacterial infections.

Experimental section

Materials

TRIS, DMSO, Na₂HPO₄ and sodium acetate were from Merck (Darmstadt, Germany). EDTA was from Fluka (Buchs, Switzerland). Acrylamide, Commaissie Brilliant Blue G-250 and Triton X-100 were from BDH (Poole, UK). RPMI 1640, streptomycin, penicillin, phorbol 12-myristate 13-acetate (PMA), Hepes, Brij-35, Silver nitrate, alkaline phosphatase-conjugated antibodies and gelatine were purchased from Sigma (St Louis, MO, USA). Gelatine-Sepharose, Q-Sepharose and Sephadex G-50 (fine) were from GE-Healthcare (Uppsala, Sweden). DC Protein Assay and unlabelled molecular weight standards were from BioRad (Richmond, CA, USA). Magic Marker molecular weight standards were from Invitrogen (Carlsbad, CA, USA). Western Blotting Luminol reagent and HRP-conjugated donkey anti-goat secondary antibody were from Sancta Cruz (Santa Cruz, CA, USA). HRP-conjugated goat anti-rabbit secondary antibody was from Southern Biotech (Birmingham, AL, USA). Foetal bovine serum was from Biochrom AG (Berlin, Germany). Human MT1-MMP/MMP-14 (catalytic domain), TLN and PLN were from Calbiochem (San Diego, CA, USA) and Aureolysin was from BioCentrum Ltd (Kraków, Poland). McaPLGL(Dpa)AR-NH₂ (E5001) and McaRPPGFSAFK(Dnp)-OH (E5005) were from R&D Systems (Minneapolis, MN, USA).

Synthesis of compounds

Synthesis of compounds tested in the present study was reported previously^{60,62,63}.

Biosynthesis of proMMP-9

The human leukemic monocyte cell-line THP-1 was a kind gift from Dr. K. Nilsson, Department of Pathology, University of Uppsala, Sweden. The cells were cultured in RPMI 1640 medium with 10% foetal bovine serum, 50 µg/ml of streptomycin, and 100 units/ml of penicillin. To isolate secreted cell-synthesized proMMP-9, the cells were washed 3 times in serum-free medium and then cultured for 72 h in serum-free RPMI 1640 medium with 0.1 µM PMA as described previously^{64,65}. Conditioned medium was harvested, loose cells were pelleted by centrifugation at 1200 rpm (200 g) for 10 min. ProMMP-9 was thereafter isolated and detected as described below.

Purification and activation of proMMP-9 from the THP-1 cells

The proMMP-9 in conditioned medium from the THP-1 cells was partly purified as described previously^{57,65,66}. SDS-electrophoresis under reducing conditions, followed by either silver or Coomassie Blue staining, showed two bands, a major band at 92 kDa and a minor band at 28 kDa. Western blotting revealed that the 92 kDa band was proMMP-9, and the 28 kDa band was TIMP-1. The amount of proMMP-9 was estimated spectrophotometrically at 280 nm using $\epsilon_{280\text{nm}}=114,360 \text{ M}^{-1} \text{ cm}^{-1}$ ⁶⁷, ignoring the contribution of TIMP-1.

The purified proMMP-9 was activated by trypsin, by mixing approximately 300 µg of proMMP-9 with trypsin (31 µg/ml) for 10 min at 37 °C in 0.1 M Hepes pH 7.5, 0.005% Brij35% and 10 mM CaCl₂. The activation and processing of MMP-9 were terminated

by adding a 50 times excess of SBTI (2.7 mg/ml) in relation to trypsin and after 10 min incubation at room temperature, the mixture was transferred and kept on ice during the kinetic and inhibition kinetic measurements. After activation, the activity was determined with 10 µM of McaPLGL(Dpa)AR-NH₂ in 0.1 M Hepes pH 7.5, 0.005% Brij35% and 10 mM CaCl₂ in a total assay volume of 100 µL, at 37 °C. Initial rates were measured at an excitation wavelength of 320 nm and an emission wavelength of 405 nm with a slit width of 10 nm using a Perkin Elmer LS 50 Luminescence spectrometer and the FL WinLab Software Package (Perkin Elmer). The amount of active MMP-9 was determined by active site titration using galardin as described previously⁵⁷.

Expression, purification and activation of recombinant human proMMP-9 in Sf9 insect cells

The expression and purification of recombinant human full-length proMMP-9 (rpMMP-9) from Sf9 insect cells were performed as described previously⁵⁷. The amount of proMMP-9 was estimated spectrophotometrically at 280 nm using $\epsilon_{280\text{nm}}=114,360 \text{ M}^{-1} \text{ cm}^{-1}$ ⁵⁷. Activation of the recombinant proMMP-9 was performed with APMA (auto-activation) as described previously⁵⁷. The amount of active MMP-9 was determined by active site titration using galardin also described previously⁵⁷.

Determination of K_m values

K_m values were determined for McaPLGL(Dpa)AR-NH₂ with APMA-activated recombinant MMP-9 (rMMP-9(A)), trypsin-activated MMP-9 from THP-1 cells (MMP-9(T)) and MMP-14, and for McaRPPGFSAFK(Dnp)-OH with ALN, PLN and TLN. Substrate concentrations used were 1–10 µM in a total volume of 100 µL of 0.1 M Hepes pH 7.5 containing 10 mM CaCl₂, 0.005% Brij-35 and 1.0% DMSO. Substrate concentrations above 10 µM resulted in quenching as reported previously⁵⁸. Initial rate experiments were performed as described above for the determination of enzyme activity of MMP-9 during activation and the same excitation and emission wavelengths were used for both substrates.

Determination of IC₅₀ and K_i values

The various inhibitors were dissolved in 100% DMSO giving an inhibitor concentration of 10 mM. All the inhibitory and control experiments contained a total and fixed concentration of 1.0% DMSO. The inhibitory constant IC₅₀ of the various compounds were performed with inhibitor concentrations ranging from 10⁻¹⁰ to 10⁻⁴ M in the assay, with a fixed substrate concentration of 4.0 µM in a total volume of 100 µL 0.1 M Hepes pH 7.5, 10 mM CaCl₂, 0.005% Brij-35 and 1.0% DMSO, except for ALN where the substrate concentration was 5.0 µM. The fixed enzyme concentration were as follows; 0.28 nM MMP-9(T), 0.05 nM MMP-9(A), 1.0 nM MMP-14, 1.4 nM ALN, 0.5 nM PLN and 0.21 nM TLN. Enzymes with and without inhibitors were pre-incubated for 15 min at 37 °C, the initial rate assays were started by adding the substrate and the reaction was followed for 30 min. Assays were performed using a Spectra Max Gemini EM micro-plate reader (Molecular Devices) or a Clario Star micro plate reader (CLARIOstar® BMG LABTECH). Assays were performed at 37 °C, using an excitation wavelength of 320 nm and an emission wavelength of 405 nm with a slit width of 10 nm. The IC₅₀ values were calculated either in Sigma Plot (Enzyme kinetics 1.3 module) or in Graph Pad Prism 5 using Equations (1) or (2) depending on the concentration span of the

used inhibitor:

$$\frac{v_i}{v_0} = \frac{1}{(1 + 10^{(pI/C_{50}-pI)})} \quad (1)$$

$$\frac{v_i}{v_0} = \frac{1}{\left(1 + \frac{[I]}{IC_{50}}\right)} \quad (2)$$

where v_i is the enzyme activity in the presence of inhibitor, v_0 the activity in the absence of inhibitor, $pI = -\log [\text{Inhibitor}]$ in M and $pIC_{50} = -\log IC_{50}$ in M. All experiments were performed in at least triplicate.

For substrate competitive inhibitors, Equations (3) shows the relation between IC_{50} and K_i values based on the fixed concentration of substrate used and the enzymes K_m value for the substrate:

$$IC_{50} = K_i (1 + [S]/K_m) \quad (3)$$

Quenching experiments

Some of the catechol and biphosphate derivatives showed a concentration dependent fluorescence at wavelengths used for the McaPLGL(Dpa)AR-NH₂ and McaRPPGFSAFK(Dnp)-OH substrates. To determine to which extent these derivatives could quench the time dependent enzymatic increase in the fluorescence product of the processed substrate, quenching experiments were performed as described previously⁵⁸. Briefly, the fluorescence ($\lambda_{ex}=320$ nm, $\lambda_{em}=405$ nm, slit width = 10 nm) of various concentrations of the fluorescent product of the substrate McaPLGL(Dpa)AR-NH₂, McaPL-OH (0–100 nM), was determined in absence and presence of various concentrations of the catechol and bisphosphonate derivatives (0–100 μ M). Primary and secondary plots were used to determine whether the catechol and bisphosphonate derivatives quenched the McaPL-OH fluorescence.

Docking

The internal Coordinate Mechanics (ICM) program version⁶⁸ was used for docking of catechol containing compounds (ML32, BF471, ML33, BF489, BF486, BF482, BF466, MT336) and bisphosphonate containing compounds (RC14, LS4, RC2, MT242, GD16, ML45, MT363) into the target proteases. The X-ray crystal structures of PLN (PDB-code:1u4g), TLN (PDB-code: 5dpe), MMP-9 (PDB-code: 5cuh, ALN (PDB-code: 1bqb) and MMP-14 (PDB-code:1bqq) were collected from the PDB database and used for docking. Crystallographic water molecules were removed along with the co-crystallized small molecule inhibitors. Hydrogen atoms were added and optimised using the ECEPP/3 force field before the structures were refined and minimised. The various inhibitors were built using ICM and minimised before docking. The binding modes of the inhibitors in the X-ray structure complexes PLN (1u4g), TLN (5dpe) and MMP-9 (5cuh) were used to define the binding pocket for docking into these enzymes, using grid maps that included all amino acids within 5 Å of the cocrystallized inhibitors. However, X-ray crystal structures with small molecule inhibitors were not available for ALN and MMP-14. For ALN, the X-ray structure without inhibitor (1bqb) was superimposed with the PLN complex (1u4g) and the inhibitor in the PLN complex was used to create docking grids including all amino acids within 5 Å of the PLN inhibitor. For MMP-14, the X-ray crystal structure of MMP-8 with the inhibitor BF471 (PDB id: 5h8x) was superimposed with the MMP-14 structure in complex with TIMP-2 (1bqq) and binding mode of BF471 in MMP-8 was used to create docking grids within

5 Å of BF471. After ceating grid maps, semi-flexible docking was performed where the enzymes were kept rigid while the ligands were structurally flexible. Each docking was run in three parallels. Ligand conformer sampling *in vacuo* and Monte Carlo global energy optimisation were used to generate docking poses⁶⁹, while the poses were scored using the Virtual Ligand Scoring (VLS) module of the ICM program. The VLS scoring function uses steric, entropic, hydrogen bonding, hydrophobic and electrostatic terms to calculate the score and also includes a correction term proportional to the number of atoms in the ligand to avoid bias towards larger ligands⁷⁰.

Disclosure statement

No potential conflict of interest was reported by the author(s).

Funding

This work was supported by Northern Norway Health Authorities (HelseNord) under [grant number HNF 1514–20] and Tromsø Forskningsstiftelse.

ORCID

Cristina Campestre  <http://orcid.org/0000-0001-5870-7509>
 Paolo Tortorella  <http://orcid.org/0000-0003-1358-7376>
 Ingebrigt Sylte  <http://orcid.org/0000-0002-3290-3736>
 Jan-Olof Winberg  <http://orcid.org/0000-0001-7165-6056>

References

1. Artenstein AW, Opal SM. Proprotein convertases in health and disease. *N Engl J Med* 2011;365:2507–18.
2. Winberg JO, Matrix Proteinases: biological significance in health and disease. In: Karamanos NK, ed. *Extracellular matrix: pathobiology and signaling*. Berlin: de Gruyter; 2012: 235–238.
3. De Groef L, Van Hove I, Dekeyser E, et al. MMPs in the neuroretina and optic nerve: modulators of glaucoma pathogenesis and repair? *Invest Ophthalmol Vis Sci* 2014;55: 1953–64.
4. Quiros PM, Langer T, Lopez-Otin C. New roles for mitochondrial proteases in health, ageing and disease. *Nat Rev Mol Cell Biol* 2015;16:345–59.
5. Ricard-Blum S, Vallet SD. Proteases decode the extracellular matrix cryptome. *Biochimie* 2016;122:300–13.
6. Rodriguez D, Morrison CJ, Overall CM. Matrix metalloproteinases: what do they not do? New substrates and biological roles identified by murine models and proteomics. *Biochim Biophys Acta* 2010;1803:39–54.
7. Wolberg AS, Mast AE. Tissue factor and factor VIIa-hemostasis and beyond. *Thromb Res* 2012;129:S1–S4.
8. Cerda-Costa N, Gomis-Ruth FX. Architecture and function of metallopeptidase catalytic domains. *Protein Sci* 2014;23: 123–44.
9. Gomis-Ruth FX, Botelho TO, Bode W. A standard orientation for metallopeptidases. *Biochim Biophys Acta* 2012;1824: 157–63.
10. Rawlings ND, Barrett AJ, Thomas PD, et al. The MEROPS database of proteolytic enzymes, their substrates and


- inhibitors in 2017 and a comparison with peptidases in the PANTHER database. *Nucleic Acids Res* 2018;46:D624–D632.
11. Hadler-Olsen E, Fadnes B, Sylte I, et al. Regulation of matrix metalloproteinase activity in health and disease. *Febs J* 2011;278:28–45.
 12. Hadler-Olsen E, Winberg JO, Uhlin-Hansen L. Matrix metalloproteinases in cancer: their value as diagnostic and prognostic markers and therapeutic targets. *Tumour Biol* 2013;34:2041–51.
 13. Kessenbrock K, Plaks V, Werb Z. Matrix metalloproteinases: regulators of the tumor microenvironment. *Cell* 2010;141:52–67.
 14. Sbardella D, Fasciglione GF, Gioia M, et al. Human matrix metalloproteinases: an ubiquitous class of enzymes involved in several pathological processes. *Mol Aspects Med* 2012;33:119–208.
 15. Geurts N, Opendakker G, Van den Steen PE, Van den Steen PE. Matrix metalloproteinases as therapeutic targets in protozoan parasitic infections. *Pharmacol Ther* 2012;133:257–79.
 16. Gialeli C, Theocharis AD, Karamanos NK. Roles of matrix metalloproteinases in cancer progression and their pharmacological targeting. *Febs J* 2011;278:16–27.
 17. Vandembroucke RE, Libert C. Is there new hope for therapeutic matrix metalloproteinase inhibition? *Nat Rev Drug Discov* 2014;13:904–27.
 18. Yadav L, Puri N, Rastogi V, et al. Matrix metalloproteinases and cancer – roles in threat and therapy. *Asian Pac J Cancer Prev* 2014;15:1085–91.
 19. Overall CM, Blobel CP. In search of partners: linking extracellular proteases to substrates. *Nat Rev Mol Cell Biol* 2007;8:245–57.
 20. Theocharis AD, Gialeli C, Hascall V, Karmanos N, Extracellular matrix: a functional scaffold. In Karamanos NK, ed. *Extracellular matrix: pathobiology and signaling*. Berlin: de Gruyter; 2012: 3–19.
 21. Cui N, Hu M, Khalil RA. Biochemical and biological attributes of matrix metalloproteinases. *Prog Mol Biol Transl Sci* 2017;147:1–73.
 22. Overall CM, Lopez-Otin C. Strategies for MMP inhibition in cancer: innovations for the post-trial era. *Nat Rev Cancer* 2002;2:657–72.
 23. Kessenbrock K, Wang CY, Werb Z. Matrix metalloproteinases in stem cell regulation and cancer. *Matrix Biol* 2015; 44–46: 184–90.
 24. Ballok AE, O'Toole GA. Pouring salt on a wound: *Pseudomonas aeruginosa* virulence factors alter Na⁺ and Cl⁻ flux in the lung. *J Bacteriol* 2013;195:4013–9.
 25. Dubin G. Extracellular proteases of *Staphylococcus* spp. *Biol Chem* 2002;383:1075–86.
 26. Jensen LM, Walker EJ, Jans DA, Ghildyal R. Proteases of human rhinovirus: role in infection. *Methods Mol Biol* 2015; 1221:129–41.
 27. Maeda H. Role of microbial proteases in pathogenesis. *Microbiol Immunol* 1996;40:685–99.
 28. Matsumoto K. Role of bacterial proteases in pseudomonal and serratial keratitis. *Biol Chem* 2004;385:1007–16.
 29. Shinoda S, Miyoshi S. Proteases produced by vibrios. *Biocontrol Sci* 2011;16:1–11.
 30. Silva-Almeida M, Pereira BAS, Ribeiro-Guimarães ML, Alves CR. Proteinases as virulence factors in *Leishmania* spp. infection in mammals. *Parasit Vectors* 2012;5:160.
 31. Dickey SW, Cheung GYC, Otto M. Different drugs for bad bugs: antivirulence strategies in the age of antibiotic resistance. *Nat Rev Drug Discov* 2017;16:457–71.
 32. Munguia J, Nizet V. Pharmacological targeting of the host-pathogen interaction: alternatives to classical antibiotics to combat drug-resistant superbugs. *Trends Pharmacol Sci* 2017;38:473–88.
 33. Brotz-Oesterhelt H, Sass P. Bacterial caseinolytic proteases as novel targets for antibacterial treatment. *Int J Med Microbiol* 2014;304:23–30.
 34. Hauser AR, Meccas J, Moir DT. Beyond antibiotics: new therapeutic approaches for bacterial infections. *Clin Infect Dis*. 2016;63:89–95.
 35. Zambelloni R, Marquez R, Roe AJ. Development of antivirulence compounds: a biochemical review. *Chem Biol Drug Des* 2015;85:43–55.
 36. Nagase H, Woessner JF. Matrix metalloproteinases. *J Biol Chem* 1999;274:21491–4.
 37. Woessner Jr., JF, Nagase H, Matrix metalloproteinases and TIMPs. Oxford: Oxford University Press; 2000.
 38. Vandooren J, Van den Steen PE, Opendakker G. Biochemistry and molecular biology of gelatinase B or matrix metalloproteinase-9 (MMP-9): the next decade. *Crit Rev Biochem Mol Biol* 2013;48:222–72.
 39. Antoni C, Vera L, Devel L, et al. Crystallization of bi-functional ligand protein complexes. *J Struct Biol* 2013;182:246–54.
 40. Fernandez-Catalan C, Bode W, Huber R, et al. Crystal structure of the complex formed by the membrane type 1-matrix metalloproteinase with the tissue inhibitor of metalloproteinases-2, the soluble progelatinase A receptor. *Embo J* 1998; 17:5238–48.
 41. Grossman M, Tworowski M, Dym O, et al. The intrinsic protein flexibility of endogenous protease inhibitor TIMP-1 controls its binding interface and affects its function. *Biochemistry* 2010;49:6184–92.
 42. Nuti E, Cantelmo RA, Gallo C, et al. N-O-isopropyl sulfonamido-based hydroxamates as matrix metalloproteinase inhibitors: hit selection and *in vivo* antiangiogenic activity. *J Med Chem* 2015;58:7224–40.
 43. Nuti E, Casalini F, Avramova SI, et al. N-O-isopropyl sulfonamido-based hydroxamates: design, synthesis and biological evaluation of selective matrix metalloproteinase-13 inhibitors as potential therapeutic agents for osteoarthritis. *J Med Chem* 2009;52:4757–73.
 44. Nuti E, Casalini F, Avramova SI, et al. Potent arylsulfonamide inhibitors of tumor necrosis factor-alpha converting enzyme able to reduce activated leukocyte cell adhesion molecule shedding in cancer cell models. *J Med Chem* 2010;53:2622–35.
 45. Nuti E, Panelli L, Casalini F, et al. Design, synthesis, biological evaluation, and NMR studies of a new series of arylsulfones as selective and potent matrix metalloproteinase-12 inhibitors. *J Med Chem* 2009;52:6347–61.
 46. Rowsell S, Hawtin P, Minshull CA, et al. Crystal structure of human MMP9 in complex with a reverse hydroxamate inhibitor. *J Mol Biol* 2002;319:173–81.
 47. Tochowicz A, Maskos K, Huber R, et al. Crystal structures of MMP-9 complexes with five inhibitors: contribution of the flexible Arg424 side-chain to selectivity. *J Mol Biol* 2007;371:989–1006.
 48. Eckhard U, Huesgen PF, Schilling O, et al. Active site specificity profiling of the matrix metalloproteinase family:

- Proteomic identification of 4300 cleavage sites by nine MMPs explored with structural and synthetic peptide cleavage analyses. *Matrix Biol* 2016;49:37–60.
49. Fabre B, Ramos A, de Pascual-Teresa B. Targeting matrix metalloproteinases: exploring the dynamics of the S₁' pocket in the design of selective, small molecule inhibitors. *J Med Chem* 2014;57:10205–19.
 50. Adekoya OA, Sylte I. The thermolysin family (M4) of enzymes: therapeutic and biotechnological potential. *Chem Biol Drug Des* 2009;73:7–16.
 51. Englert L, Biela A, Zayed M, et al. Displacement of disordered water molecules from hydrophobic pocket creates enthalpic signature: binding of phosphoramidate to the S₁'-pocket of thermolysin. *Biochim Biophys Acta* 2010;1800:1192–202.
 52. Bever RA, Iglewski BH. Molecular characterization and nucleotide sequence of the *Pseudomonas aeruginosa* elastase structural gene. *J Bacteriol* 1988;170:4309–14.
 53. Galloway DR. *Pseudomonas aeruginosa* elastase and elastolysis revisited: recent developments. *Mol Microbiol* 1991;5:2315–21.
 54. Pauptit RA, Karlsson R, Picot D, et al. Crystal structure of neutral protease from *Bacillus cereus* refined at 3.0 Å resolution and comparison with the homologous but more thermostable enzyme thermolysin. *J Mol Biol* 1988;199:525–37.
 55. Thayer MM, Flaherty KM, McKay DB. Three-dimensional structure of the elastase of *Pseudomonas aeruginosa* at 1.5-Å resolution. *J Biol Chem* 1991;266:2864–71.
 56. Banbula A, Potempa J, Travis J, et al. Amino-acid sequence and three-dimensional structure of the *Staphylococcus aureus* metalloproteinase at 1.72 Å resolution. *Structure* 1998;6:1185–93.
 57. Sylte I, Dawadi R, Malla N, et al. The selectivity of galardin and an azasugar-based hydroxamate compound for human matrix metalloproteinases and bacterial metalloproteinases. *PLOS One* 2018;13:e0200237.
 58. Sjoli S, Nuti E, Camodeca C, et al. Synthesis, experimental evaluation and molecular modelling of hydroxamate derivatives as zinc metalloproteinase inhibitors. *Eur J Med Chem* 2016;108:141–53.
 59. Yang JJ, Van Wart HE. Kinetics of hydrolysis of dansyl peptide substrates by thermolysin: analysis of fluorescence changes and determination of steady-state kinetic parameters. *Biochemistry* 1994;33:6508–15.
 60. Tauro M, Laghezza A, Loiodice F, et al. Catechol-based matrix metalloproteinase inhibitors with additional antioxidative activity. *J Enzyme Inhib Med Chem* 2016;31:25–37.
 61. Holden HM, Tronrud DE, Monzingo AF, et al. Slow- and fast-binding inhibitors of thermolysin display different modes of binding: crystallographic analysis of extended phosphoramidate transition-state analogues. *Biochemistry* 1987;26:8542–53.
 62. Rubino MT, Agamennone M, Campestre C, et al. Biphenyl sulfonylamino methyl bisphosphonic acids as inhibitors of matrix metalloproteinases and bone resorption. *ChemMedChem* 2011;6:1258–68.
 63. Tauro M, Laghezza A, Loiodice F, et al. Arylamino methylene bisphosphonate derivatives as bone seeking matrix metalloproteinase inhibitors. *Bioorg Med Chem* 2013;21:6456–65.
 64. Malla N, Berg E, Moens U, et al. Biosynthesis of promatrix metalloproteinase-9/chondroitin sulphate proteoglycan heteromer involves a Rottlerin-sensitive pathway. *PLOS One* 2011;6:e20616.
 65. Malla N, Berg E, Uhlir-Hansen L, Winberg JO. Interaction of pro-matrix metalloproteinase-9/proteoglycan heteromer with gelatin and collagen. *J Biol Chem* 2008;283:13652–65.
 66. Dawadi R, Malla N, Hegge B, et al. Molecular interactions stabilizing the promatrix metalloproteinase-9. *Serglycin Heteromer Int J Mol Sci* 2020;21:4205.
 67. Murphy G, Crabbe T. Gelatinases A and B. *Methods Enzymol* 1995;248:470–84.
 68. Abagyan R, Totrov M, Kuznetsov D. ICM – a new method for protein modeling and design – applications to docking and structure prediction from the distorted native conformation. *J Comput Chem* 1994;15:488–506.
 69. Abagyan R, Kufareva I. The flexible pocketome engine for structural chemogenomics. *Methods Mol Biol* 2009;575:249–79.
 70. Schapira M, Abagyan R, Totrov M. Nuclear hormone receptor targeted virtual screening. *J Med Chem* 2003;46:3045–59.
 71. Tranchant I, Vera L, Czarny B, et al. Halogen bonding controls selectivity of FRET substrate probes for MMP-9. *Chem Biol* 2014;21:408–13.
 72. Elkins PA, Ho YS, Smith WW, et al. Structure of the C-terminally truncated human ProMMP9, a gelatin-binding matrix metalloproteinase. *Acta Crystallogr D Biol Crystallogr* 2002;58:1182–92.
 73. Krimmer SG, Cramer J, Betz M, et al. Rational design of thermodynamic and kinetic binding profiles by optimizing surface water networks coating protein-bound ligands. *J Med Chem* 2016;59:10530–48.

Paper II

Article

Zinc-Chelating Compounds as Inhibitors of Human and Bacterial Zinc Metalloproteases

Fatema Rahman¹, Imin Wushur¹, Nabin Malla¹, Ove Alexander Høgmoen Åstrand², Pål Rongved², Jan-Olof Winberg¹ and Ingebrigt Sylte^{1,*} 

¹ Molecular Pharmacology and Toxicology, Department of Medical Biology, Faculty of Health Sciences, UiT—The Arctic University of Norway, NO-9037 Tromsø, Norway; fatema.rahman@uit.no (F.R.); imin.wushur@uit.no (I.W.); nabin.malla@uit.no (N.M.); jan.o.winberg@uit.no (J.-O.W.)

² Department of Pharmaceutical Chemistry, School of Pharmacy, University of Oslo, NO-0316 Oslo, Norway; alexander.astrand@gmail.com (O.A.H.Å.); pal.rongved@farmasi.uio.no (P.R.)

* Correspondence: ingebrigt.sylte@uit.no; Tel.: +47-7764-4705

Abstract: Inhibition of bacterial virulence is believed to be a new treatment option for bacterial infections. In the present study, we tested dipicolylamine (DPA), tripicolylamine (TPA), tris pyridine ethylene diamine (TPED), pyridine and thiophene derivatives as putative inhibitors of the bacterial virulence factors thermolysin (TLN), pseudolysin (PLN) and aureolysin (ALN) and the human zinc metalloproteases, matrix metalloprotease-9 (MMP-9) and matrix metalloprotease-14 (MMP-14). These compounds have nitrogen or sulfur as putative donor atoms for zinc chelation. In general, the compounds showed stronger inhibition of MMP-14 and PLN than of the other enzymes, with K_i values in the lower μM range. Except for DPA, none of the compounds showed significantly stronger inhibition of the virulence factors than of the human zinc metalloproteases. TPA and Zn230 were the only compounds that inhibited all five zinc metalloproteinases with a K_i value in the lower μM range. The thiophene compounds gave weak or no inhibition. Docking indicated that some of the compounds coordinated zinc by one oxygen atom from a hydroxyl or carbonyl group, or by oxygen atoms both from a hydroxyl group and a carbonyl group, and not by pyridine nitrogen as in DPA and TPA.

Keywords: bacterial virulence factors; matrix metalloproteases; zinc chelators; enzyme inhibition; docking; molecular interactions



Citation: Rahman, F.; Wushur, I.; Malla, N.; Åstrand, O.A.H.; Rongved, P.; Winberg, J.-O.; Sylte, I. Zinc-Chelating Compounds as Inhibitors of Human and Bacterial Zinc Metalloproteases. *Molecules* **2022**, *27*, 56. <https://doi.org/10.3390/molecules27010056>

Academic Editor: Elisa Nuti

Received: 24 November 2021

Accepted: 20 December 2021

Published: 22 December 2021

Publisher's Note: MDPI stays neutral with regard to jurisdictional claims in published maps and institutional affiliations.



Copyright: © 2021 by the authors. Licensee MDPI, Basel, Switzerland. This article is an open access article distributed under the terms and conditions of the Creative Commons Attribution (CC BY) license (<https://creativecommons.org/licenses/by/4.0/>).

1. Introduction

Proteases (proteinases, peptidases, proteolytic enzymes) are involved in a variety of biological processes and comprise many enzymes in different families with structural and catalytic diversity. All proteases have a common ability to hydrolyze peptide bonds [1–3]. In humans, proteases are associated with different physiological processes including cellular signaling and growth, angiogenesis, blood pressure regulation, coagulation, intestinal absorption of nutrition, reproduction, wound repair, hemostasis, and homeostasis [3–7]. In microorganisms, proteases are involved in processes such as generation of nutrition, growth, survival, virulence, and formation of biofilm [8,9]. Dysregulation of human proteases may contribute to disease, and several human proteases are targets for therapeutic interventions [10–12], while several bacterial proteases are considered as important targets for the next generation of antibacterial drugs [10,13,14].

Metalloproteases are a heterogeneous group of proteases using a metal ion to bind the substrate and polarize a water molecule to perform the hydrolytic reaction. One of the human enzyme families that utilize a zinc-ion in the hydrolytic reactions is the matrix metalloproteases (MMPs). They belong to the M10 family of proteases [15], are calcium-dependent, and contain both a catalytic and a structural zinc ion [16]. The catalytic zinc is coordinated by three histidine residues and a water molecule in activated MMPs [17,18], and

they are classified by the MEROPS database in the subclan metzincins [15]. MMPs are often overexpressed and functionally involved in a wide range of pathological conditions and are considered important drug targets [10,11,19–22]. However, the development of clinically relevant MMP inhibitors for therapeutic interventions has so far shown limited success, with a lack of efficacy and severe side effects in clinical trials [23,24]. More knowledge about the regulation of MMPs in different tissues and organs may be necessary so that compounds that promote positive effects and inhibit deleterious effects of specific MMPs for disease may be developed. In humans, there are 23 different MMPs. Most of them are secreted from cells as inactive proenzymes, while six are membrane-anchored through a type I transmembrane domain or a glycosyl-phosphatidyl-inositol (GPI) moiety [16]. Membrane-anchored MMPs have the catalytic site extracellularly and are also called membrane-type metalloproteases (MT-MMPs). MMP-9 (gelatinase B) is the most studied secreted MMP, while MMP-14 (also called MT1-MMP) is the most studied MT-MMP. Several three dimensional (3D) structures of MMP-9 with and without inhibitors are known from X-ray crystallography [25], while 3D structures of MMP-14 in complex with a small molecular inhibitor are not published, but a complex of MMP-14 with the tissue inhibitor-2 of matrix metalloproteases (TIMP-2) is deposited in the PDB-database (PDB id: 1BQQ).

The zinc-metalloproteases thermolysin (TLN) from *Bacillus thermoproteolyticus*, pseudolysin (PLN) from *Pseudomonas aeruginosa* (LasB, or elastase of *P. aeruginosa*) and aureolysin (ALN) from *Staphylococcus aureus* are secreted bacterial virulence factors that belong to the M4 family of proteases [13,15]. In the active enzymes, the catalytic zinc is coordinated by two histidines, a glutamic acid and a water molecule. In addition to the catalytic zinc, TLN has four calcium ions, while ALN has three and PLN has two. These enzymes are classified by the MEROPS database in the subclan gluzincins [15]. The secreted virulence factors degrade extracellular proteins and peptides of the host for bacterial nutrition and contribute to biofilm formation. The spread of antibiotic multi-resistance among central human pathogens is recognized by the World Health Organization (WHO) as a major global health concern and a pressing societal challenge, and new treatment options are needed to combat the spread [26]. Compounds inhibiting the virulence and not directly targeting the growth and viability may be an alternative treatment to present antibiotics, either alone or as an adjuvant to antibacterial drugs [27–30], and PLN, TLN and ALN are therefore interesting drug targets. The 3D structures of TLN and PLN were extensively studied with and without inhibitor [25], while only the 3D structure of the free enzyme is known for ALN (PDB id: 1BQB).

The ratio of the effect on virulence factors over effects on human zinc metalloproteases should be optimized to increase the therapeutic value of potential antibacterial drug candidates. The zinc metalloproteases cleave protein and peptide substrates at the N-terminal side of the amino acid occupying the S_1' -subpocket. MMPs and virulence factors of the M4 family preferentially accept hydrophobic amino acids in the S_1' -subpocket as shown in the MEROPS database [15], indicating structural similarities in their catalytic sites. X-ray structures of the enzymes show that the region around the catalytic zinc ion has structural similarities. Identifying potent inhibitors with high selectivity is therefore challenging.

Small molecules that inhibit zinc metalloproteases contain a chemical group that replaces the zinc coordinating water molecule in the catalytic site of the active enzymes and coordinates the zinc ion. Phosphinate (PO_2^-), carboxylate (COO^-), thiolate (S^-) and hydroxamic acid HONH-CO have shown to be effective zinc-binding groups leading to potent inhibition of zinc metalloproteases [31–35]. In solution, metal chelating groups with oxygen as donor atom are expected to be quite unselective for the chelating cation, while chelating groups with nitrogen as donor atom are expected to bind weaker to sodium, calcium, potassium, iron and manganese or other relevant biological cation than to zinc [36]. Compounds containing metal chelating groups with nitrogen as donor atom may therefore show selectivity for zinc enzymes in front of other metalloenzymes. Derivatives of the zinc chelators di(2-pyridinemethyl)amine (dipicolylamine, DPA) and tri(2-pyridinemethyl)amine

(tripicolylamine, TPA) with nitrogen as putative donor atom were found to inhibit metallo- β -lactamases (MBLs) [37–40]. MBLs are a group of zinc-dependent hydrolytic enzymes responsible for breaking down β -lactam antibiotics, including carbapenems, penicillins and cephalosporins [41]. Their most likely mechanism of inhibition is by interference with zinc in the active site giving irreversible inhibition [42,43]. In the present study derivatives of DPA, TPA, tris pyridine ethylene diamine (TPED), pyridine and thiophene were tested for their inhibition of MMP-9 as a representative of secreted MMPs, and MMP-14 as a representative of MT-MMPs, and against the bacterial virulence factors TLN, PLN and ALN.

2. Results and Discussion

Twenty TPA, DPA, TPED, pyridine and thiophene derivatives were studied using inhibition kinetics and molecular modeling. Some of the TPA and DPA analogs were previously shown to be slow or irreversible inhibitors of MBLs [38–40]. Therefore, we decided to test if the 20 compounds are time-dependent inhibitors of the bacterial virulence factors TLN, PLN and ALN and two human zinc metalloproteases, MMP-9 and MMP-14. In addition, we tested if TPA is a reversible or irreversible time-dependent inhibitor of MMP-14. The compounds were also tested for putative quenching of the fluorescence product formed during catalytic cleavage. The binding modes of the compounds in the five enzymes were studied by docking the compounds into the catalytic site of the five zinc metalloproteases.

2.1. Quenching

Quenching experiments were performed with varying concentrations of the compounds (0–100 μ M) against varying fluorescence product (McaPL-OH) concentrations as previously described for procaspase-activating compounds (PACs), isatin derivatives, bisphosphonate and catechol containing compounds [44,45]. Primary and secondary quenching plots revealed that none of the compounds quenched the fluorescence of the product. Most of the 20 compounds gave a background fluorescence at the wavelengths used, but this did not affect the inhibitory assays as enzymatic reactions were followed continuously.

2.2. The Inhibition of MMP-14 by TPA

We tested if TPA is a time-dependent irreversible or reversible inhibitor of MMP-14. In these experiments, two different concentrations of MMP-14 (45 and 5.6 nM) were pre-incubated up to 48 min at 37 °C with 10.0 and 11.1 μ M of TPA, respectively, as described in Materials and Methods. As controls, the same amount of MMP-14 (without TPA but with the same concentration of DMSO) was identically pre-incubated at 37 °C. In the activity assay (10 μ M of the substrate McaPLGL(Dpa)AR-NH₂) the pre-incubation mixture with or without TPA and with a high concentration of MMP-14 was diluted 10 times which resulted in a TPA concentration in the activity assay of 1 μ M, while the mixture with the low concentration of MMP-14 was only diluted 1.1 times, and hence the TPA concentration in the activity assay was 10 μ M. Figure 1A shows that the MMP-14 control without inhibitor present was stable during the entire pre-incubation period, while the presence of TPA resulted in a time-dependent inhibition of the enzyme. In the presence of 100 μ M TPA, v_i/v_0 was 0.61 after 2 min and 0.03 after 11 min pre-incubation at 37 °C. To determine whether the observed time-dependent inhibition was due to reversible or irreversible inhibition, a solution of 45 nM MMP-14 was first pre-incubated for approximately 40 min at 37 °C with 10 μ M TPA (1% DMSO in assay buffer, pH 7.5). As a control, MMP-14 (without TPA but with the same concentration of DMSO) was also pre-incubated for approximately 40 min at 37 °C. Thereafter, aliquots (20 or 30 μ L) of MMP-14 control and MMP-14/TPA mixture were applied to micro-dialysis at 4 °C as described in Materials and Methods. Figure 1B shows results from two representative independent micro-dialysis experiments. The activity (v_i/v_0) increased after dialysis, and hence TPA is slowly released from the MMP-14/TPA complex. This indicates that TPA is a slow, reversible inhibitor of

MMP-14, and therefore we assume the tested TPA, DPA, TPED, pyridine and thiophene derivatives most probably are not inactivators/irreversible inhibitors of the tested zinc metalloproteinases, in contrast to the previous observations for MBLs [38–40].

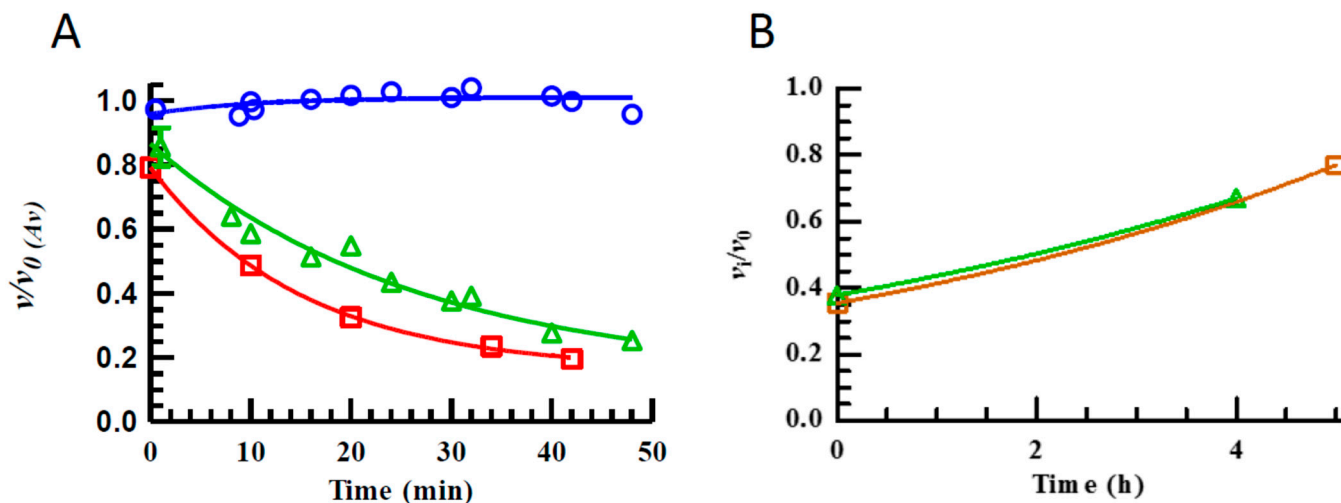


Figure 1. Time-dependent reversible inhibition of MMP-14 with TPA. (A): MMP-14 (45 (Δ) and 5.6 (\square) nM) was pre-incubated at 37 °C with 10 and 11.1 μ M TPA, respectively, while controls were without TPA (\circ). Aliquots were withdrawn and the enzymatic activity determined. Initial rate velocities (v) at the different time points were divided by the average of the control velocities ($v_{0(Av)}$). The results for the high concentration of MMP-14 in the pre-incubation assay are from two independent experiments. (B): Two independent experiments (Δ and \square) of micro-dialysis (4 °C) of MMP-14 (45 nM) pre-incubated at 37 °C. Aliquots were withdrawn after various time points and the initial rate velocities determined. The velocity ratio v_i/v_0 was determined for each time point where v_i is the initial rate of the MMP-14/TPA sample and v_0 of the MMP-14 control at the same dialysis time point.

2.3. Inhibitory Effects

A total of 100 μ M of the compounds was either pre-incubated with the protease for 15, 30 and 45 min at room temperature and the enzymatic reaction was started by adding the substrate, or not pre-incubated, i.e., the reaction was started by adding the protease to a mixture of substrate and compound as described in Materials and Methods. The controls were performed in the same way but without inhibitor present. Figures 2 and 3 show the relative binding strength at 100 μ M of the 20 compounds to MMP, MMP-14, ALN, PLN and TLN. For compounds showing fast inhibition, each bar represents the mean of the results after 0–30 or 0–45 min pre-incubation. When time-dependent/slow inhibition was seen, the bars represent the mean of time points after the time curve has flattened out, and the slope of the curve is approximately zero (enzyme and inhibitors have reached an equilibrium) (supplementary material, Figures S1 and S2). For compounds where the time curve was still decreasing after 45 min pre-incubation, the mean of the 30 and 45 min pre-incubation time was used to give an impression of the relative binding strength of the compound.

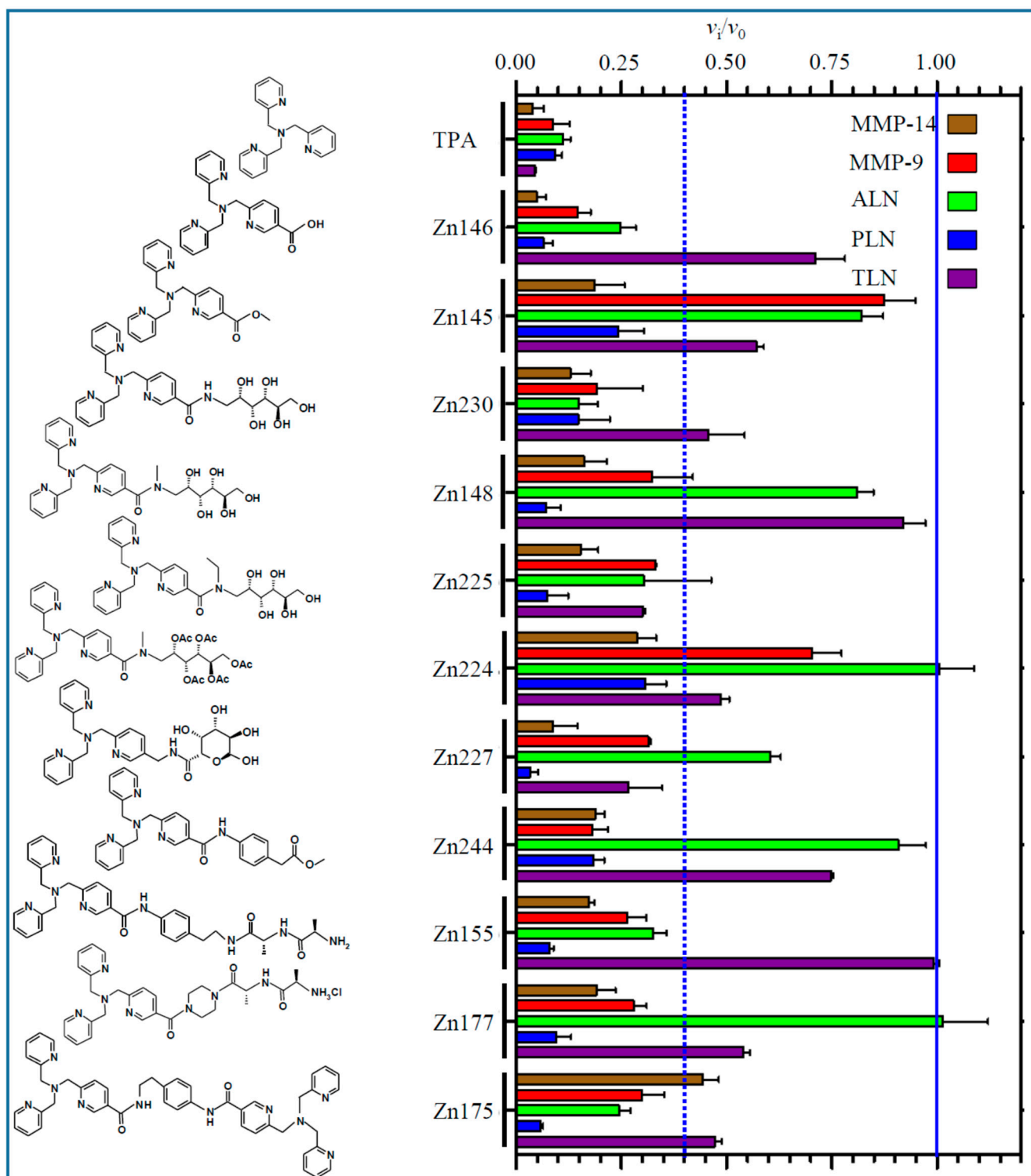


Figure 2. Inhibitory effect of 100 μM of TPA derivatives on the activity of MMP-9, MMP-14, TLN, PLN and ALN. For compounds with fast inhibitory binding, the v_1/v_0 (mean \pm s.e.m.) was based on the mean values after 0–45 or 0–30 min pre-incubation. For compounds with time-dependent slow inhibition the v_1/v_0 (mean \pm s.e.m.) was based on pre-incubation time points where the time curve in supplementary material Figure S1 flattens out. For compounds where the time curve was not flattening out after 45 min of pre-incubation (not reached equilibrium), the mean value was for 30 and 45 min pre-incubation.

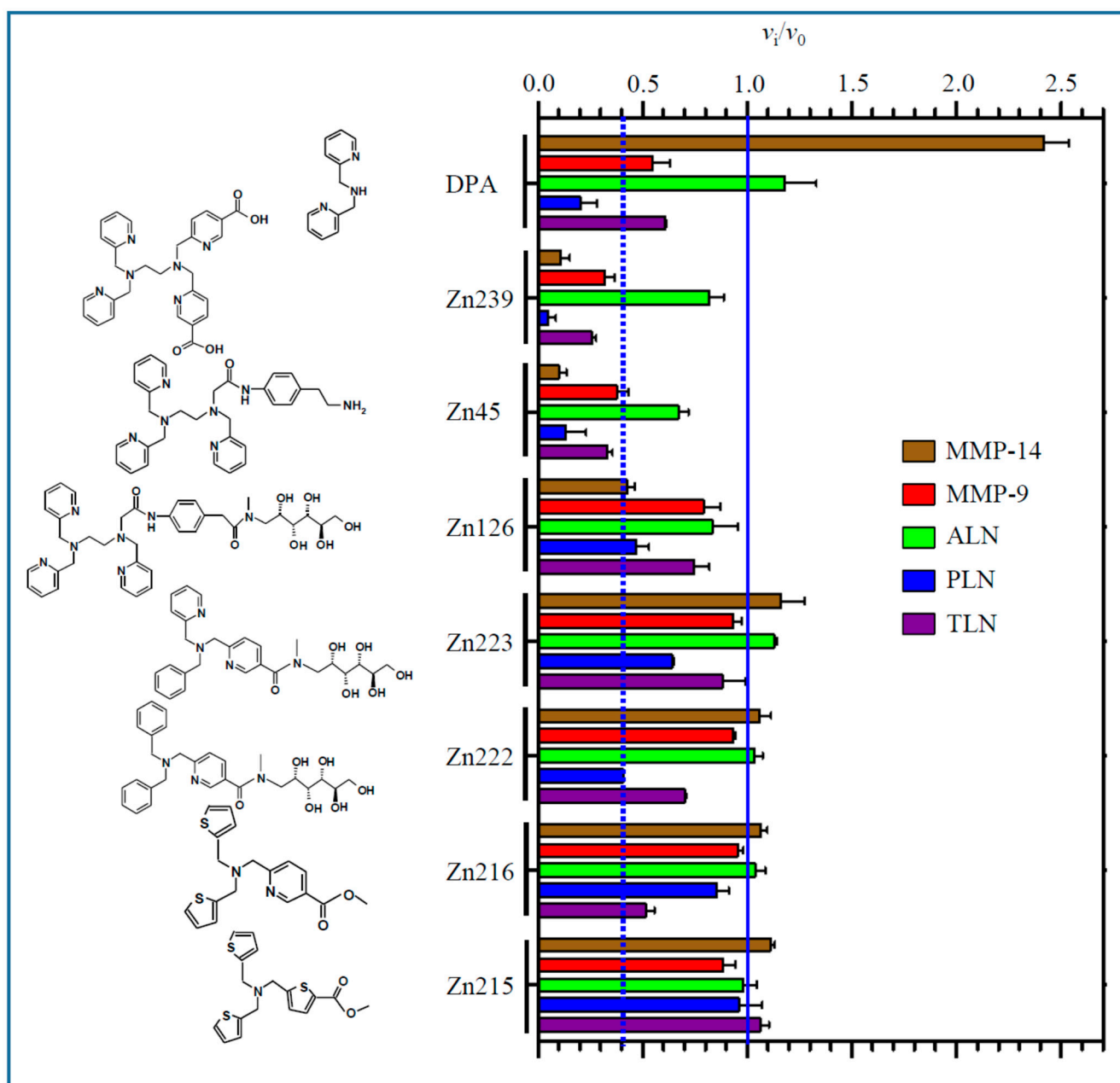


Figure 3. Inhibitory effect of 100 μM of DPA, TPEN, pyridine and thiophene derivatives on the activity of MMP-9, MMP-14, TLN, PLN and ALN. For compounds with fast inhibitory binding, the v_i/v_0 (mean \pm s.e.m.) was based on the mean values after 0–45 or 0–30 min pre-incubation. For compounds with time-dependent slow inhibition, the v_i/v_0 (mean \pm s.e.m.) was based on the pre-incubation time points where the time curve in Figure S2 flattens out. For compounds where the time curve was not flattening out after 45 min of pre-incubation (not reached equilibrium), the mean value was for 30 and 45 min pre-incubation.

As shown for some of the compounds in supplementary material Figures S1 and S2, the same compound had completely different effects on the five zinc metalloproteases. One compound that did not give any effect on the activity of one enzyme, could be a fast binding inhibitor with different binding strengths on other enzymes and be a slow and time-dependent inhibitor of another. One of the compounds (DPA) had a surprising effect on MMP-14, where the rate of the enzymatic substrate cleavage was greatly enhanced at all the different incubation time points (supplementary material Figure S2). The mechanism behind this was not further investigated. For most compounds with time-dependent

inhibition, the inhibitory v_i/v_0 curve was flattening out after 15 or 30 min, but for a few compounds the curve did not flatten out, indicating that the enzyme/inhibitor complex had not reached an equilibrium (supplementary material, Figures S1 and S2). The reason might be a very slow, reversible binding. This was not further investigated.

When 100 μM of the test compound gave an inhibition of 60% or more ($v_i/v_0 \leq 0.4$) at 30 min pre-incubation, further experiments were performed to obtain dose–response curves and K_i values calculated from the obtained IC_{50} values. To ensure comparable results, all IC_{50} and K_i values were based on 30 min pre-incubation of the enzyme and tested compound. Figure 4A,B show typical dose–response curves for Zn244 and Zn148 against PLN. Equation (1) in the Materials and Methods section was used to calculate IC_{50} values.

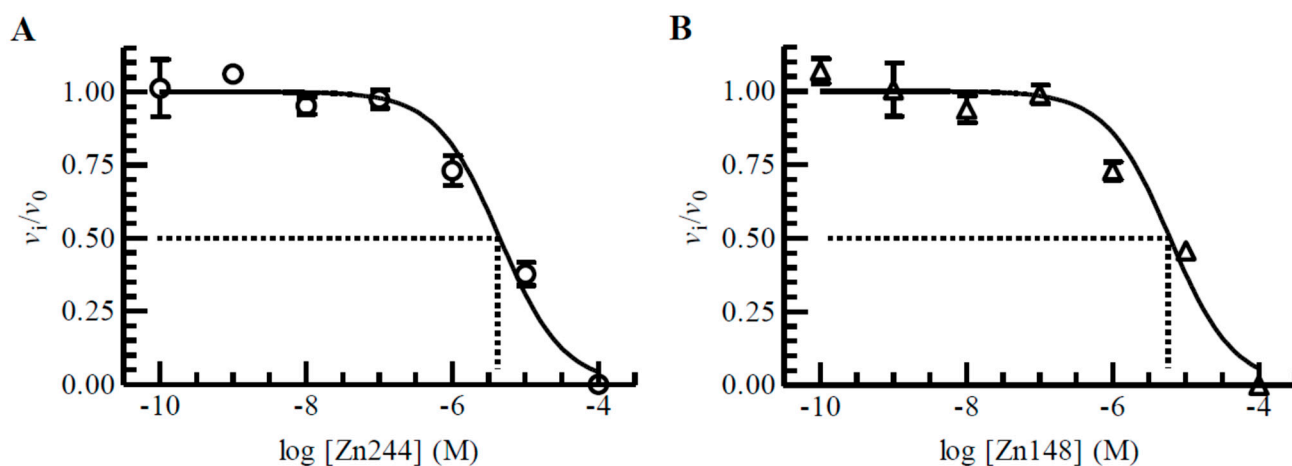


Figure 4. Dose–response plots of Zn244 (A) and Zn148 (B) for PLN. The enzyme with and without inhibitor was pre-incubated for 30 min at room temperature and the reaction started by adding McaRPPGFSAFK(Dnp)-OH (4 μM in assay), where v_i and v_0 are initial reaction rates in the presence and absence of Zn244 and Zn148. Each point on the curve shows the mean \pm s.d. ($N = 3$ for all points in (A) and $N = 4$ for all points in (B) with regression coefficients r^2 of 0.97 in (A) and 0.95 in (B), giving an IC_{50} value of $4.46 \pm 0.05 \mu\text{M}$ and a K_i value of $4 \pm 1 \mu\text{M}$ for Zn244 (A) and an IC_{50} value of $6.07 \pm 0.08 \mu\text{M}$ and a K_i value of $5 \pm 2 \mu\text{M}$ for Zn148 (B). The large s.d. of the K_i values compared to the IC_{50} values is due to the large s.d. in the K_m value of the substrate in absence of an inhibitor.

For calculating K_i values from the obtained IC_{50} values it is necessary to know the K_m value for the enzyme with the substrate at the conditions in the inhibition experiments. Equation (2) in Materials and Methods shows the relation between K_i and IC_{50} values for a competitive inhibitor. K_m values for the enzymes at the conditions used in the present work were determined previously [44]. To summarize, the K_m values of the substrate McaPLGL(Dpa)AR-NH₂ with MMP-9 and MMP-14 were 4 ± 1 , and $4.9 \pm 0.4 \mu\text{M}$, respectively, while the K_m values of the substrate McaRPPGFSAFK(Dnp)-OH with ALN, PLN and TLN were 76 ± 7 , 24 ± 8 and $6 \pm 1 \mu\text{M}$, respectively. Estimated K_m values for ALN and PLN must be regarded as uncertain since the highest substrate concentration was 10 μM due to quenching. Table 1 shows the obtained K_i values. None of the compounds were tight binders, i.e., K_i values close to or less than the enzyme concentration in the assay. Most of the compounds showed inhibition of PLN and MMP-14 in the lower μM region, while only 30–50% of the compounds had K_i values in the lower μM region for MMP-9, TLN and ALN.

Table 1. K_i values of the TPA, DPA and TPED derivatives for MMP-14, MMP-9, ALN, PLN and TLN. K_i values determined for both bacterial and human metalloproteases using two different fluorescence quenched peptide substrates, McaRPPGFSAFK(Dnp)-OH (for TLN, PLN and ALN) and McaPLGL(Dpa)AR-NH₂ (for MMP-9 and MMP-14). The concentration of the substrates used was 4 μ M except for ALN where it was 5 μ M and the highest concentration of the inhibitor compounds tested was 100 μ M. K_i values were only obtained for compounds where 100 μ M of the compound reduced the enzymatic activity by 60% or more, as described in the main text. Compound and enzyme were pre-incubated for 30 min at room temperature and the reaction was started by the addition of substrate as described in Materials and Methods.

Compound	$K_i \pm$ s.d. (μ M)				
	McaPLGL(Dpa)AR-NH ₂		McaRPPGFSAFK(Dnp)-OH		
	MMP-14	MMP-9	ALN	PLN	TLN
TPA	1.2 \pm 0.1	15 \pm 4	16 \pm 1	5 \pm 2	5.5 \pm 0.9
Zn146	3.8 \pm 0.3	21 \pm 5	25 \pm 2	4 \pm 1	n.d. ^a
Zn145	1.5 \pm 0.1	n.d.	n.d.	12 \pm 4	n.d.
Zn230	3.5 \pm 0.3	22 \pm 6	20 \pm 2	1.1 \pm 0.3	12 \pm 2
Zn148	8.6 \pm 0.7	n.d.	n.d.	5 \pm 2	n.d.
Zn225	4.5 \pm 0.4	28 \pm 7	n.d.	5 \pm 2	9 \pm 2
Zn224	4.5 \pm 0.4	n.d.	n.d.	13 \pm 4	n.d.
Zn227	4.8 \pm 0.4	77 \pm 19	n.d.	9 \pm 3	11 \pm 2
Zn244	4.0 \pm 0.3	22 \pm 6	n.d.	4 \pm 1	n.d.
Zn155	2.4 \pm 0.2	26 \pm 6	60 \pm 6	6 \pm 2	n.d.
Zn177	11.2 \pm 0.9	56 \pm 14	n.d.	11 \pm 4	n.d.
Zn175	n.d.	6 \pm 2	14 \pm 1	7 \pm 2	n.d.
DPA	n.d.	n.d.	n.d.	4 \pm 1	n.d.
Zn239	6.1 \pm 0.5	58 \pm 14	n.d.	5 \pm 2	32 \pm 5
Zn45	2.5 \pm 0.2	n.d.	n.d.	2.8 \pm 0.9	7 \pm 1

^a n.d., not determined.

None of the compounds showed selective inhibition favoring bacterial zinc metalloproteases over the two human MMPs, but DPA inhibited PLN much stronger than the other enzymes. In general, the compounds showed quite similar inhibition of PLN and MMP-14, and in general, the K_i values for these enzymes were lower than for the other enzymes (Table 1).

The TPA derivative Zn148 (K_d (zinc) = 10^{-12} M), which is an irreversible inhibitor of the MBLs VIM-2 and NDM-1, was shown to reverse carbapenem resistance in Gram-negative pathogens in vivo without acute toxicity in female BALB/c mice [39]. These authors also showed that Zn148 derivatives with reduced zinc-binding, Zn222 (K_d (zinc) = 10^{-6} M) and Zn223 (K_d (zinc) = 10^{-7} M), lacked the ability to reverse carbapenem resistance in Gram-negative pathogens. The former compound did not inactivate the two MBLs, while the latter showed a reduced capability to inactivate the two MBLs compared to Zn148. The present results show that Zn148 is a decent inhibitor of the PLN and MMP-14, while 100 μ M of the compound had no or only a limited effect on the other two bacterial proteases (Table 1, Figure 2, supplementary material Figure S1). This compound reacts slower with human MMP-9 than with MMP-14 and PLN, and the time curve did not flatten out after 45 min (supplementary material, Figure S1). It was also notable that the two compounds where one or two pyridine groups were replaced by a benzene ring (Zn223 and Zn222) resulted in weaker binding than Zn148 to PLN, MMP-14 and MMP-9, and no effect on TLN and ALN (Figures 3 and S2).

Although our results suggest that the TPA derivatives are not irreversible inhibitors of the five zinc metalloproteases, there are similarities with their effects on MBLs, as the strongest zinc chelator binds strongest to both the proteases and the MBLs. PLN, the elastase of *P. aeruginosa* is known to play a pivotal role in pseudomonal infections, and the inhibition of PLN by Zn148 (K_i of 5 μ M) suggests that this inhibition may strengthen the potential of Zn148 as an antibacterial adjuvant against *P. aeruginosa* infections. In most

human tissues, MMP-14 is constitutively expressed while MMP-9 is induced, and both are involved in several physiological processes. The present results encourage further investigations into off-target effects of this class of putative antibacterial adjuvants [39].

2.4. Enzyme Interactions

Of the 20 compounds, only TPA and Zn230 showed strong binding to all five proteases (Figure 1, Table 1). In solution, TPA has a K_d for zinc of approximately 10^{-11} M [40,46]. Docking showed that the binding mode of TPA was quite similar in all five zinc metalloproteases (Figure 5). In PLN, the nitrogen atom in one of the pyridine rings coordinated zinc. His223 formed a hydrogen bond with the same nitrogen atom and had pi-pi stacking interactions with the pyridine ring. Another pyridine ring interacted within the S_1' -subpocket forming hydrophobic interactions with the side chains of Leu132, Val137 and Ile190. This pyridine ring also formed pi-pi stacking interactions with His140 and pi-cation interactions with Arg198. The third pyridine ring was in the direction of the S_1 -subpocket, being more exposed to solvent than the other pyridine rings. In addition, this pyridine ring formed pi-pi stacking interactions with His223 and pi-cation interactions with Arg198. The amine nitrogen atom interacted with Glu141 and Asn112.

The introduction of a carboxylic acid functionality (Zn146) and its methyl ester (Zn145) reduced the binding to MMP-9, TLN and ALN compared with TPA, but not to MMP-14 and PLN (Figure 2, Table 1). Docking of Zn146 showed that the carboxylic acid was responsible for coordinating the zinc in all enzymes, and not any of the pyridine nitrogen atoms (Figure 6). In PLN, one pyridine ring was into the S_1 -subpocket forming pi-pi stacking interactions with Tyr114, while another was exposed to solvent. Similar binding modes were also seen in the other enzymes. In MMP-14 pi-pi stacking interactions were formed with Phe198 (S_1' -subpocket), in addition to a hydrogen bond between pyridine nitrogen and Leu199 (S_1' -subpocket), for one of the pyridine rings. Zn239 contains two carboxylic acid groups (Figure 3), and docking indicated that the carboxylic acid group not interacting with zinc, interacted with Glu111 in PLN, while one pyridine ring had pi-pi stacking with Tyr155 (S_1 -subpocket), another with His223, while one pyridine nitrogen formed a hydrogen bond with Asn112. Docking of Zn145 showed that the nitrogen atom of the pyridine ring containing the methyl ester functionality ligated zinc, while the methyl ester group was exposed to solvent in both PLN and MMP-14 (Figure 6). However, in PLN docking poses of Zn145 with the methyl ester group interacting with Arg198 were also obtained during the docking experiments, but still, the pyridine nitrogen coordinated zinc. MMP-14 is lacking an arginine corresponding to Arg198 in PLN, and that may be the reason that only one orientation of Zn145 was obtained with MMP-14. The reason for zinc coordination by pyridine nitrogen in Zn145 that contains the carboxylic acid ester functionality may be that the carboxylic acid ester is less polar and bulkier than the carboxylic acid functionality in Zn146 giving steric hindrances.

Removal of one 2-methylpyridine group of TPA gives DPA. DPA is a weaker zinc-binder ($K_d \sim 10^{-8}$ M) than TPA ($K_d \sim 10^{-11}$ M) [37,46], and its inhibition of the five proteases was largely reduced compared to TPA, except for PLN where DPA and TPA were equally effective (Figures 2 and 3, Table 1). Moderately strong inhibition of DPA was only seen for PLN (Figure 3, Table 1). Docking of DPA into PLN showed that pyridine nitrogen coordinated the zinc. The zinc interacting pyridine ring also had pi-pi stacking interactions with His223. The other pyridine ring interacted with hydrophobic amino acids (Val137, Ile186, Gly187, Ile190) and Asp136 in the S_1' -subpocket and formed pi-pi stacking interactions with the zinc ligated amino acid His140. In addition, the amine nitrogen atom interacted with the catalytic amino acid Glu141 (Figure 7). Similar binding modes were also seen in TLN and MMP-9. As previously mentioned, DPA increased the rate of the substrate cleavage by MMP-14 at all pre-incubation time points (Supplementary, Figure S2). Interestingly, docking into MMP-14 indicated a binding mode different from that in PLN. The docking program did not recognize any clear zinc binding, and the distance between zinc and the closest pyridine nitrogen was approximately 3 Å in the highest scored docking pose, while

the corresponding distance in PLN was approximately 2 Å. The pyridine ring containing this nitrogen atom had pi–pi stacking interactions with the zinc ligated amino acid His239 (as in PLN). In addition, an amine hydrogen atom formed a pi–cation interaction with His239 and a hydrogen bond with Pro259 (S_1' -subpocket), while the other pyridine ring interacted with Tyr261 (pi–pi stacking) in the S_1' -subpocket. The binding mode indicated that the substrate may interact within the substrate binding cleft despite bound DPA. A putative explanation for the increased rate of substrate cleavage may be that the position of the pyridine ring closest to zinc may contribute to a more favorable binding mode of the substrate McaPLGL(Dpa)AR-NH₂ for cleavage.

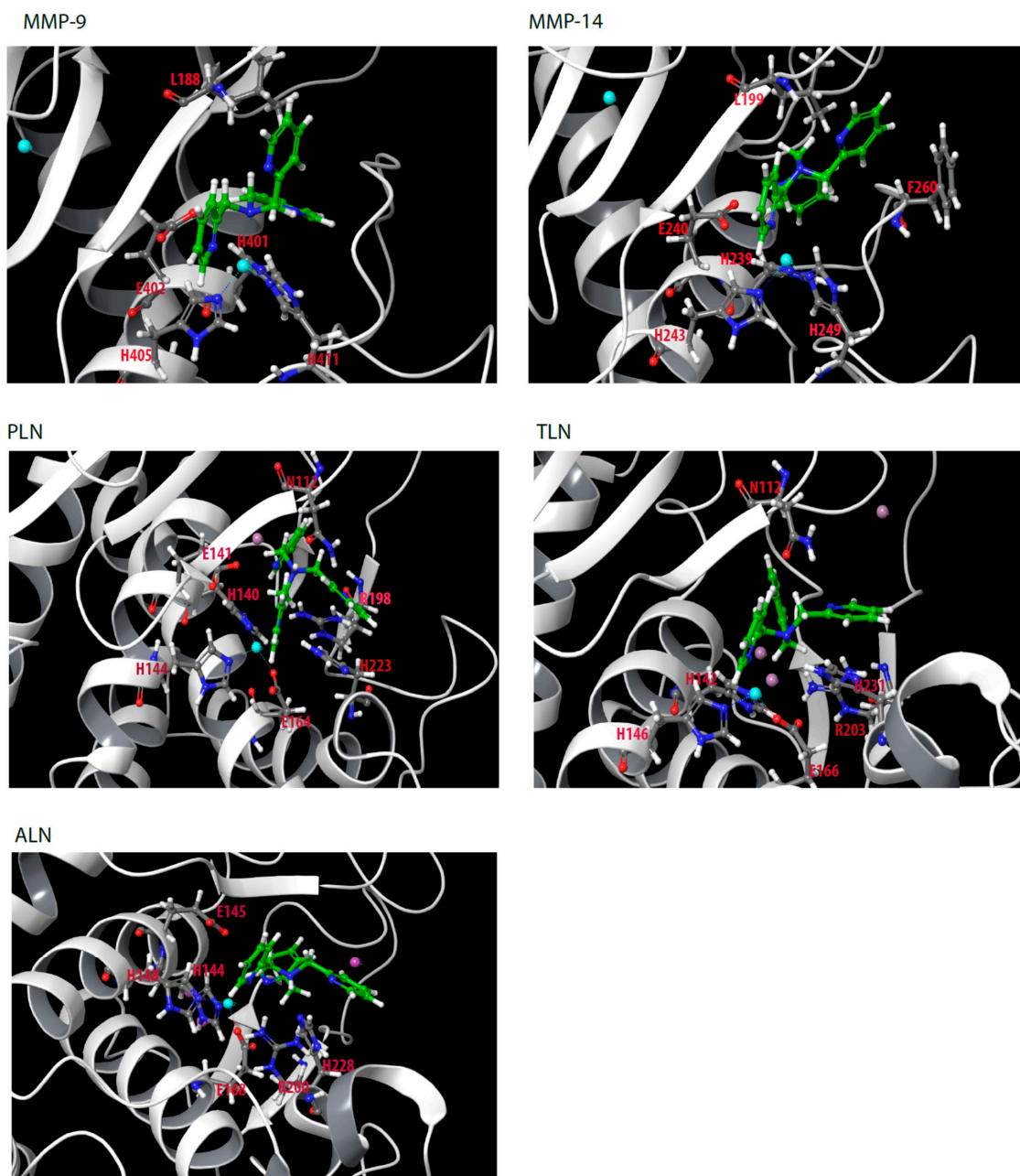
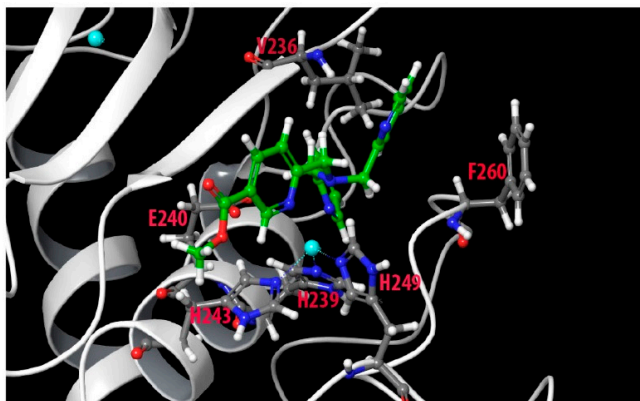
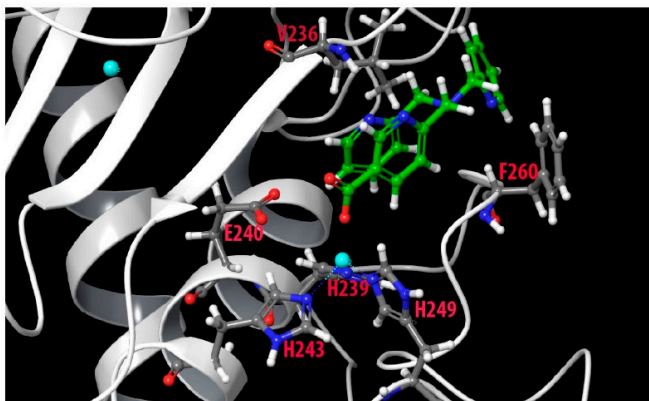


Figure 5. TPA docked into the catalytic site of MMP-9, MMP-14, PLN, TLN and ALN. Some of the most important amino acids for TPA binding are shown. Color coding of amino acids: carbon; grey, oxygen; red, nitrogen; dark blue, hydrogen; white. Color coding of TPA: carbon; green, nitrogen; blue, hydrogen; white. Color coding of ions: zinc; light blue sphere, calcium; pink sphere.

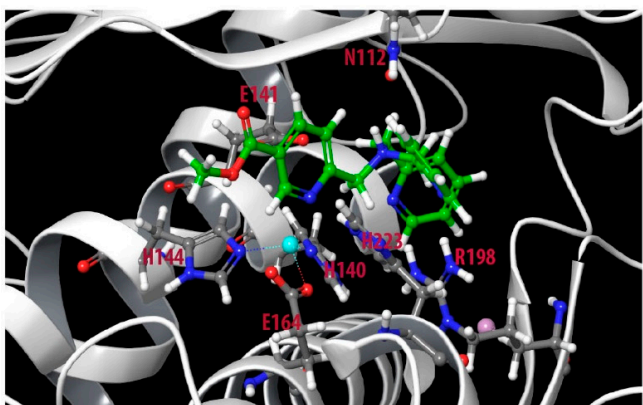
MMP-14/Zn145



MMP-14/Zn146



PLN/Zn145



PLN/Zn146

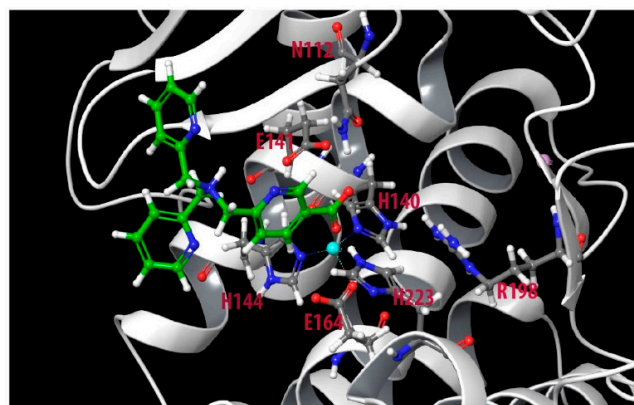
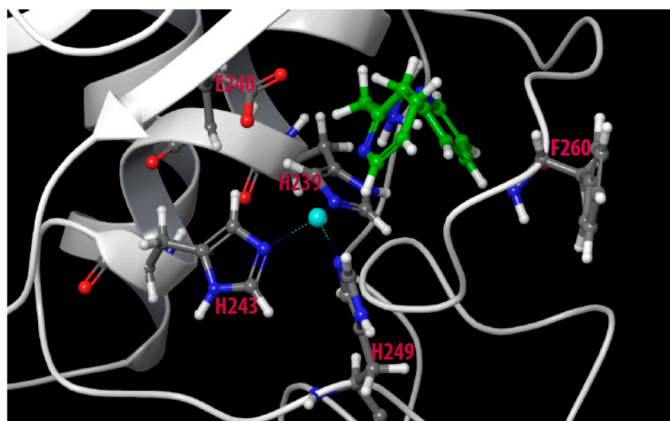


Figure 6. Zn145 and Zn146 docked into the catalytic site of MMP-14 and PLN. Some of the most important amino acids for binding Zn145 and Zn146 are shown. Color coding as in Figure 5.

MMP-14



PLN

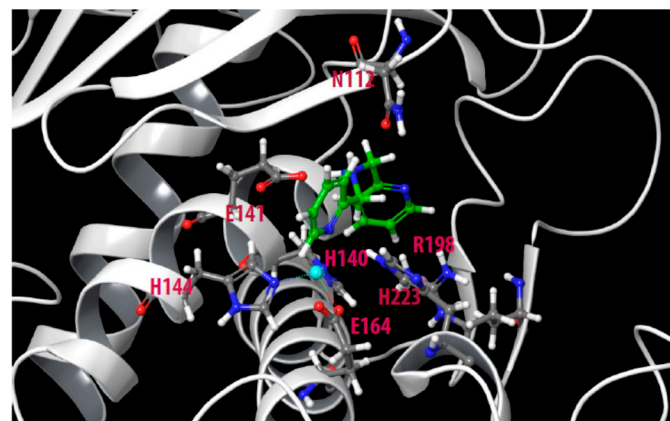


Figure 7. Docking of DPA into the catalytic site of MMP-14 and PLN. Some of the most important amino acids for binding DPA are shown. Color coding as in Figure 5.

Putative scaffolds for zinc chelation in most of the compounds are the DPA or TPA molecules, with nitrogen as the expected donor atom for zinc coordination. However, during docking, the derivatives containing carboxylic acid (Zn146 and Zn239) coordinated

zinc via the carboxylic acid. Zn230, Zn148 and Zn225 have the hydrophilic methyl-amino glycosyl side chain linked to the TPA molecule via an amide bond that is either unmodified (Zn230), methylated (Zn148) or ethylated (Zn225). Except for PLN, reduced inhibition relative to TPA was obtained for these derivatives, but their difference in inhibition of PLN and MMP-14 was small (Figure 2, Table 1). Derivatives with a structural change of one of the 2-methylpyridine groups of TPA had little effect on the enzyme activity of MMP-14 and PLN. That may suggest that their main interactions with PLN and MMP-14 are mainly through the 2-methylpyridine groups. However, this suggestion is contradictory to the docking results that indicated that, in addition to Zn146 and Zn239, derivatives containing the methyl-amino glycosyl side chain (Zn230, Zn148 and Zn225, Zn126) also coordinated by one or more oxygen atoms, either via one hydroxyl group, the carbonyl group, or both a hydroxyl group and the carbonyl group. Docking indicated that all other TPA and DPA derivatives, including those containing a carboxylic acid ester functionality (Zn145, Zn244) coordinated zinc by pyridine nitrogen. The exception was Zn45 (Figure 2), which coordinated zinc by the carbonyl group.

An interesting feature was when one or both the two unmodified 2-methylpyridine groups of Zn148 were replaced by a benzylic group (Zn223 and Zn222) the MMP-14 binding was prevented compared with Zn148 (Figures 2 and 3). This suggests that the nitrogen in both these 2-methylpyridine groups is needed for MMP-14 binding. Similarly, these two modifications weaken but do not prevent the binding to PLN. The importance of the two unmodified 2-methylpyridine groups for the binding to MMP-14 and PLN is also shown by the weak inhibition or lack of inhibition by the two compounds Zn216 and Zn215, where the 2-methylpyridine groups are replaced by 2-methylthiophene groups. That may suggest that the pyridine nitrogen atoms of Zn148 are directly involved in binding or that the electron distribution of the pyridine rings is important. Docking of Zn148 into MMP-14 (Figure 8) showed that the zinc-binding was both by the carbonyl group and a hydroxyl group, and not by pyridine nitrogen. However, the pyridine rings were still important for interactions, as one pyridine nitrogen interacted with Phe204 in the S_1 -subpocket, while Phe204 also formed pi–pi stacking interactions with another pyridine ring, while the third pyridine ring formed pi–pi stacking with Tyr203. The sugar chain also formed hydrogen bonds with the catalytic residue Glu240 and with Ala200 (S_1' -subpocket) and Pro259 (S_1' -subpocket).

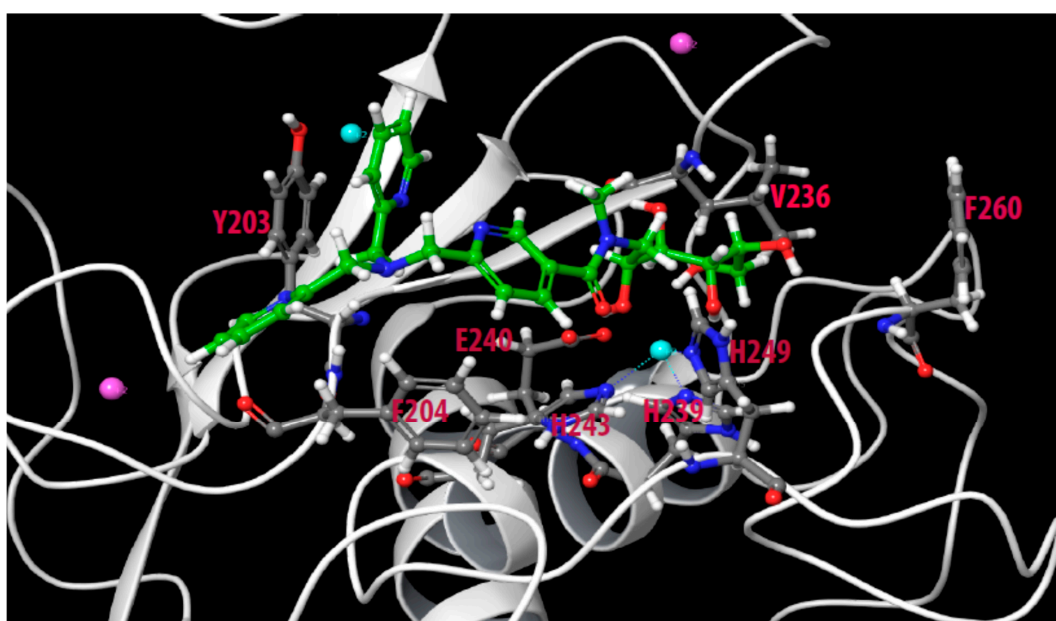


Figure 8. Docking of Zn148 into the catalytic site of MMP-14. Some of the most important amino acids for binding Zn148 are shown. Color coding as in Figure 5.

3. Materials and Methods

3.1. Materials

Dimethyl sulfoxide (DMSO), TRIS, sodium hydrogen phosphate (Na_2HPO_4), and sodium acetate (CH_3COONa) were from Merck (Darmstadt, Germany). Ethylenediaminetetraacetic acid was from Fluka (Buchs, Switzerland). Acrylamide, Coomassie Brilliant Blue G-250 and Triton X-100 were from BDH (Poole, UK). Hepes, Brij-35, Silver nitrate, alkaline phosphatase-conjugated antibodies and gelatin were from Sigma (St. Louis, MO, USA). Gelatin-Sepharose, was from GE-Healthcare (Uppsala, Sweden). DC Protein Assay and unlabeled molecular weight standards were from BioRad (Richmond, CA, USA). Sf9 insect cells and Magic Marker molecular weight standards were from Invitrogen (Carlsbad, CA, USA). Western Blotting Luminol reagent and HRP-conjugated donkey anti-goat secondary antibody were from Sancta Cruz (Santa Cruz, CA, USA). HRP-conjugated goat anti-rabbit secondary antibody was from Southern Biotech (Birmingham, AL, USA). Fetal bovine serum was from Biochrom AG (Berlin, Germany). Galardin (Gm6001), human MT1-MMP/MMP-14 (catalytic domain), TLN and PLN were from Calbiochem (San Diego, CA, USA) and Aureolysin was from BioCentrum Ltd. (Kraków, Poland). McaPLGL(Dpa)AR-NH₂ (ES001) and McaRPPGFSAFK(Dnp)-OH (ES005) were from R&D Systems (Minneapolis, MN, USA).

3.2. Compounds for Testing

Twenty TPA, DPA, TPEN, pyridine and thiophene derivatives were tested as putative inhibitors of MMP-9, MMP-14, PLN, TLN and ALN. Synthesis of the compounds was reported previously [37–40]. The structure of the compounds is shown in Figures 2 and 3.

3.3. Expression, Purification and Activation of Recombinant Human proMMP-9 in Sf9 Insect Cells

The expression and purification of recombinant human full-length proMMP-9 (rpMMP-9) from Sf9 insect cells were performed as described previously [47]. The amount of proMMP-9 was estimated spectrophotometrically at 280 nm using $\epsilon_{280 \text{ nm}} = 114.36 \text{ mM}^{-1} \text{ cm}^{-1}$ [48]. Activation of the recombinant proMMP-9 was performed with APMA (auto-activation) as described previously [47]. The amount of active MMP-9 was determined by active site titration using galardin also described previously [47].

3.4. Determination of Reaction Velocities

McaPLGL(Dpa)AR-NH₂ was used as a substrate for MMP-9 and MMP-14, while McaRPPGFSAFK(Dnp)-OH was used as substrate for ALN, PLN and TLN. The reaction velocities/initial rates (v) were determined at 37 °C, at an excitation wavelength of 320 nm and an emission wavelength of 405 nm with a slit width of 10 nm using either a Perkin Elmer LS 50 Luminescence spectrometer and the FL WinLab Software Package (Perkin Elmer) or a Clario Star microplate reader (CLARIOstar[®] BMG LABTECH).

The test compounds were dissolved in 100% DMSO giving a concentration of 10 mM. A fixed substrate concentration of 4.0 μM in a total volume of 100 μL 0.1 M Hepes pH 7.5, 10 mM CaCl_2 , 0.005% Brij-35 and 1.0% DMSO, were used in all assays, except for ALN where the substrate concentration was 5.0 μM . The fixed enzyme concentrations were as follows; 0.05 nM MMP-9, 1.0 nM MMP-14, 1.4 nM ALN, 0.5 nM PLN and 0.21 nM TLN. Time-dependent inhibitory experiments without and with 100 μM of testing compounds were performed as follows. Compounds were either pre-incubated with the proteases for 15, 30 and 45 min at room temperature and the enzymatic reaction was started by adding the substrate, or not pre-incubated, i.e., the reaction was started by adding the protease to the mixture of substrate and compound. Control tests without compound present were performed in the same way. The reaction was followed for 30 min at 37 °C.

3.5. Testing of Slow, Reversible/Irreversible Binding of TPA

In pre-incubation tests with high concentration of MMP-14, 90 μL 50 nM MMP-14 was mixed with 9.0 μL 110 μM TPA (dissolved in 0.1 M Hepes pH 7.5 containing 10 mM CaCl_2 , 0.005% Brij-35 and 10% DMSO) and incubated at 37 $^\circ\text{C}$ for up to 48 min. As a control, 90 μL 50 nM MMP-14 was mixed with 9.0 μL 0.1 M Hepes pH 7.5 containing 10 mM CaCl_2 , 0.005% Brij-35 and 10% DMSO. At different time points, 10 μL of the enzyme (with and without TPA) was added to 90 μL of 0.1 M Hepes pH 7.5 containing 10 mM CaCl_2 , 0.005% Brij-35 and 11.1 μM ES001 and the initial rate reaction velocity (v) was determined as described in Section 3.4. using a Perkin Elmer LS 50 Luminescence spectrometer. The reaction was followed for 1 min (10 data points collected per second). The TPA concentration was 10 μM in the pre-incubation assay and 1.0 μM in the reaction rate assay.

In pre-incubation tests with a low concentration of MMP-14, 60 μL 50 nM MMP-14 was mixed with 420 μL 0.1 M Hepes pH 7.5 (containing 10 mM CaCl_2 , 0.005% Brij-35) and 60 μL of either 0.1 M Hepes pH 7.5 containing 10 mM CaCl_2 , 0.005% Brij-35 and 10% DMSO (control) or 60 μL 100 μM TPA (dissolved in 0.1 M Hepes pH 7.5 containing 10 mM CaCl_2 , 0.005% Brij-35 and 10% DMSO). At different time points, 90 μL of the enzyme (with and without TPA) was mixed with 10 μL 100 μM ES001 and the initial rate of the reaction was determined as described above. The TPA concentration is 11.1 μM in the pre-incubation assay and 10 μM in the reaction rate assay.

3.6. Microdialysis

Ninety μL of 50 nM MMP-14 was mixed with 9.0 μL of either 0.1 M Hepes pH 7.5 containing 10 mM CaCl_2 , 0.005% Brij-35 and 10% DMSO (control) or 110 μM TPA (dissolved in 0.1 M Hepes pH 7.5 containing 10 mM CaCl_2 , 0.005% Brij-35 and 10% DMSO) and incubated at 37 $^\circ\text{C}$ for approximately 40 min. After 0 and 40 min pre-incubation, 10 μL of an enzyme (with and without TPA) was mixed with 90 μL of 0.1 M Hepes pH 7.5 containing 10 mM CaCl_2 , 0.005% Brij-35 and 11.1 μM ES001 and the reaction velocity was determined as described above (Section 3.5). Samples pre-incubated for 40 min at 37 $^\circ\text{C}$ were added to microdialysis at 4 $^\circ\text{C}$. For that, 1 mL Eppendorf pipette tips were cut and sealed with a dialysis membrane (cut-off 14 kDa) that were boiled and rinsed in Milli-Q water. Twenty or 30 μL of the sample (with and without TPA) was added to each tip and samples with and without TPA were dialyzed for up to 4 or 5 h in 100 mL of 50 mM Hepes pH 7.5 containing 5 mM CaCl_2 and 0.005% Brij-35. After dialysis, the sample (with and without TPA) in the tip was removed and the total volume of the dialyzed sample was determined. If a sample at a time point contained more than added (i.e., >20 or 30 μL), the dilution was determined and compared with the other sample at that time point. At each time point, the initial rate was determined for an equal amount of enzyme (with and without TPA) based on the dilution factor. The reaction rate was determined as described above, where 10 μL sample (after correct dilution) was added to 90 μL of 0.1 M Hepes pH 7.5 containing 10 mM CaCl_2 , 0.005% Brij-35 and 11.1 μM ES001.

3.7. Determination of IC_{50} and K_i Values

The inhibitory constant IC_{50} of the various compounds were performed with concentrations ranging from 10^{-10} to 10^{-4} M in the assay, with a fixed substrate, enzyme and buffer concentration as described above. Enzymes with and without inhibitor were pre-incubated for 30 min at room temperature, and initial rate assays were performed as described above. Assays were performed using a Clario Star microplate reader (CLARIOstar[®] BMG LABTECH). The IC_{50} values were calculated in Graph Pad Prism 5 using Equation (1):

$$\frac{v_i}{v_0} = \frac{1}{(1 + 10^{(pIC_{50} - pI)})} \quad (1)$$

where v_i is the enzyme activity in the presence of inhibitor, v_0 the activity in the absence of inhibitor, $pI = -\log [\text{Inhibitor}]$ in M and $pIC_{50} = -\log IC_{50}$ in M. All experiments were performed in at least triplicate.

Equation (2) shows the relation between IC_{50} and K_i values for substrate competitive inhibitors based on the used fixed substrate concentration and the enzymes K_m value for the substrate:

$$IC_{50} = K_i (1 + [S]/K_m) \quad (2)$$

3.8. Quenching Experiments

To determine to which extent the compounds quench the time-dependent enzymatic increase in the fluorescence product of the processed substrate, quenching experiments were performed as described previously [45]. Briefly, the fluorescence ($\lambda_{\text{ex}} = 320$ nm, $\lambda_{\text{em}} = 405$ nm, slit width = 10 nm) of various concentrations of the fluorescent product McaPL-OH (0–100 nM) of the substrate McaPLGL(Dpa)AR-NH₂ was determined in the absence and presence of various concentrations of the test compounds (0–100 μM). Primary and secondary plots were used to determine whether these compounds quenched the McaPL-OH fluorescence.

3.9. Docking

The following enzyme structures in the PDB-database were used for docking: TLN; 5DPE, PLN; 1U4G, ALN; 1BQB, MMP-14; 1BQQ, MMP-9; 5CUH. All five X-ray structures were optimized using the Protein preparation Wizard in Schrodinger Suites (version 2021-1) with default setting [49]. Water molecules at the binding site were deleted. Overlapping atoms were corrected using restrained minimization with the OPLS4 force field [50]. Grid maps were generated for each structure with a van der Waals radius scaling factor of 1 Å and a partial cut-off of 0.25 Å. The co-crystallized ligands were used as the centroid of the grid map generation for PLN, TLN and MMP-9, while the catalytic zinc atom was the centroid for ALN and MMP-14. The 20 selected derivatives were prepared with the Ligprep program, using ionization states in the pH range of 7.4 ± 0.2 , generation of tautomers and retaining the specified chirality. The compounds were docked into the five enzyme structures using Glide Standard Precision (SP) docking with enhanced sampling and generation of maximum 10 poses per compound. The docking result was ranked using docking score. Docking of the compounds was performed in triplicate. The best results were determined using both docking score and ligand orientation in the binding site.

4. Conclusions

Inhibition of bacterial virulence is believed to be a new treatment option for bacterial infections. Here we tested DPA, TPA, and derivatives of DPA, TPA, TPEN, pyridine and thiophene as putative inhibitors of the bacterial virulence factors TLN, PLN and ALN, the human zinc metalloproteases MMP-9 and MMP-14. The compounds showed stronger inhibition of PLN and MMP-14 than of the other enzymes, with K_i values in the lower μM range. TPA and Zn230 were the only compounds that inhibited all five zinc metalloproteinases with a K_i value in the lower μM range. Docking studies indicated that Zn146 and Zn239 coordinated zinc by the carboxylic acid functionality, while derivatives containing the methyl-amino glycosyl side chain (Zn230, Zn148 and Zn225, Zn126) also coordinated by one or more oxygen atoms, either via one hydroxyl group, the carbonyl group, or both a hydroxyl group and the carbonyl group. The other compounds coordinated zinc by pyridine nitrogen. Our studies indicated that TPA is a slow, reversible inhibitor of MMP-14, and it is therefore reasonable to believe that the tested compounds are not inactivators/irreversible inhibitors of the tested zinc metalloproteinases, in contrast to the previous observations for MBLs [38–40].

Several of the tested compounds including Zn148 were previously found to irreversibly inhibit MBLs by chelating the catalytic zinc and were suggested to be promising as adjuvants to antibacterial treatment with β -lactam antibiotics. Zn148 (Figure 2) was

also found to reverse the carbapenem resistance in Gram-negative pathogens in vivo with limited in vivo toxicity [39]. PLN is the key zinc metalloproteinase virulence factor secreted by the opportunistic Gram-negative pathogen *P. aeruginosa*, which is characterized by the WHO as a critical pathogen for which new treatment options are urgently needed. The reversible inhibition of PLN by Zn148 and other compounds in the present study indicates that they may inhibit *P. aeruginosa* virulence and have potential as adjuvants in the treatment of pseudomonas infections.

Supplementary Materials: The following are available online. Figure S1: Time-dependent inhibitory effect of 100 μ M of TPA derivatives on MMP-9, MMP-14, TLN, PLN and ALN. Figure S2: Time-dependent inhibitory effect of 100 μ M of DPA, TPEN, pyridine and thiophene derivatives on the activity of MMP-9, MMP-14, TLN, PLN and ALN.

Author Contributions: Conceptualization, O.A.H.Å., P.R., J.-O.W. and I.S.; methodology, F.R., I.W., N.M., J.-O.W. and I.S.; software, F.R., I.W., J.-O.W. and I.S.; validation, F.R., J.-O.W. and I.S.; formal analysis, F.R., I.W. and N.M.; investigation, F.R., I.W. and N.M.; resources, J.-O.W. and I.S.; data curation, F.R., I.W. and N.M.; writing—original draft preparation, F.R., I.W., J.-O.W. and I.S.; writing—review and editing, O.A.H.Å., P.R., J.-O.W. and I.S.; visualization, F.R., I.W., J.-O.W. and I.S.; supervision, J.-O.W. and I.S.; project administration, J.-O.W. and I.S.; funding acquisition, J.-O.W. and I.S.; All authors have read and agreed to the published version of the manuscript.

Funding: The present work was funded by the Northern Norway Health Authorities (HelseNord) grant number HNF1514-20, The Tromsø Research Foundation, and by The UiT The Arctic University of Norway.

Institutional Review Board Statement: Not applicable.

Informed Consent Statement: Not applicable.

Data Availability Statement: Not applicable.

Conflicts of Interest: The authors declare no conflict of interest.

References

1. Artenstein, A.W.; Opal, S.M. Proprotein convertases in health and disease. *N. Engl. J. Med.* **2011**, *365*, 2507–2518. [[CrossRef](#)] [[PubMed](#)]
2. Ordonez, G.R.; Puente, X.S.; Quesada, V.; Lopez-Otin, C. Proteolytic systems: Constructing degradomes. *Methods Mol. Biol.* **2009**, *539*, 33–47. [[CrossRef](#)] [[PubMed](#)]
3. Winberg, J.O. Matrix Proteinases: Biological significance in health and disease. In *Extracellular Matrix: Pathobiology and Signaling*; Karamanos, N.K., Ed.; De Gruyter: Berlin, Germany, 2012; pp. 235–238.
4. De Groef, L.; Van Hove, I.; Dekeyster, E.; Stalmans, I.; Moons, L. MMPs in the neuroretina and optic nerve: Modulators of glaucoma pathogenesis and repair? *Investig. Ophthalmol. Vis. Sci.* **2014**, *55*, 1953–1964. [[CrossRef](#)] [[PubMed](#)]
5. Lopez-Otin, C.; Bond, J.S. Proteases: Multifunctional enzymes in life and disease. *J. Biol. Chem.* **2008**, *283*, 30433–30437. [[CrossRef](#)] [[PubMed](#)]
6. Quiros, P.M.; Langer, T.; Lopez-Otin, C. New roles for mitochondrial proteases in health, ageing and disease. *Nat. Rev. Mol. Cell Biol.* **2015**, *16*, 345–359. [[CrossRef](#)]
7. Wolberg, A.S.; Mast, A.E. Tissue factor and factor VIIa—hemostasis and beyond. *Thromb. Res.* **2012**, *129* (Suppl. 2), S1–S4. [[CrossRef](#)]
8. Ballok, A.E.; O’Toole, G.A. Pouring salt on a wound: *Pseudomonas aeruginosa* virulence factors alter Na^+ and Cl^- flux in the lung. *J. Bacteriol.* **2013**, *195*, 4013–4019. [[CrossRef](#)]
9. Jensen, L.M.; Walker, E.J.; Jans, D.A.; Ghildyal, R. Proteases of human rhinovirus: Role in infection. *Methods Mol. Biol.* **2015**, *1221*, 129–141. [[CrossRef](#)]
10. Chen, A.Y.; Adamek, R.N.; Dick, B.L.; Credille, C.V.; Morrison, C.N.; Cohen, S.M. Targeting Metalloenzymes for Therapeutic Intervention. *Chem. Rev.* **2019**, *119*, 1323–1455. [[CrossRef](#)]
11. Vandenbroucke, R.E.; Libert, C. Is there new hope for therapeutic matrix metalloproteinase inhibition? *Nat. Rev. Drug Discov.* **2014**, *13*, 904–927. [[CrossRef](#)]
12. Verhelst, S.H.L. Intramembrane proteases as drug targets. *FEBS J.* **2017**, *284*, 1489–1502. [[CrossRef](#)]
13. Adekoya, O.A.; Sylte, I. The thermolysin family (M4) of enzymes: Therapeutic and biotechnological potential. *Chem. Biol. Drug Des.* **2009**, *73*, 7–16. [[CrossRef](#)]
14. Culp, E.; Wright, G.D. Bacterial proteases, untapped antimicrobial drug targets. *J. Antibiot. (Tokyo)* **2017**, *70*, 366–377. [[CrossRef](#)]

15. Rawlings, N.D.; Barrett, A.J.; Thomas, P.D.; Huang, X.; Bateman, A.; Finn, R.D. The MEROPS database of proteolytic enzymes, their substrates and inhibitors in 2017 and a comparison with peptidases in the PANTHER database. *Nucleic Acids Res.* **2018**, *46*, D624–D632. [[CrossRef](#)] [[PubMed](#)]
16. Hadler-Olsen, E.; Fadnes, B.; Sylte, I.; Uhlin-Hansen, L.; Winberg, J.O. Regulation of matrix metalloproteinase activity in health and disease. *FEBS J.* **2011**, *278*, 28–45. [[CrossRef](#)] [[PubMed](#)]
17. Cerda-Costa, N.; Gomis-Ruth, F.X. Architecture and function of metallopeptidase catalytic domains. *Protein Sci.* **2014**, *23*, 123–144. [[CrossRef](#)] [[PubMed](#)]
18. Gomis-Ruth, F.X.; Botelho, T.O.; Bode, W. A standard orientation for metallopeptidases. *Biochim. Biophys. Acta* **2012**, *1824*, 157–163. [[CrossRef](#)]
19. Cathcart, J.M.; Cao, J. MMP Inhibitors: Past, present and future. *Front. Biosci. (Landmark Ed.)* **2015**, *20*, 1164–1178. [[CrossRef](#)] [[PubMed](#)]
20. Fields, G.B. The Rebirth of Matrix Metalloproteinase Inhibitors: Moving Beyond the Dogma. *Cells* **2019**, *8*, 984. [[CrossRef](#)]
21. Fields, G.B. Mechanisms of Action of Novel Drugs Targeting Angiogenesis-Promoting Matrix Metalloproteinases. *Front. Immunol.* **2019**, *10*, 1278. [[CrossRef](#)]
22. Gialeli, C.; Theocharis, A.D.; Karamanos, N.K. Roles of matrix metalloproteinases in cancer progression and their pharmacological targeting. *FEBS J.* **2011**, *278*, 16–27. [[CrossRef](#)]
23. Fingleton, B. MMPs as therapeutic targets—Still a viable option? *Semin. Cell Dev. Biol.* **2008**, *19*, 61–68. [[CrossRef](#)]
24. Winer, A.; Adams, S.; Mignatti, P. Matrix Metalloproteinase Inhibitors in Cancer Therapy: Turning Past Failures Into Future Successes. *Mol. Cancer Ther.* **2018**, *17*, 1147–1155. [[CrossRef](#)]
25. RCSB PDB Protein Databank. Available online: <http://www.rcsb.org> (accessed on 18 December 2021).
26. Antibiotic Resistance (WHO). Available online: <https://www.who.int> (accessed on 18 December 2021).
27. Dickey, S.W.; Cheung, G.Y.C.; Otto, M. Different drugs for bad bugs: Antivirulence strategies in the age of antibiotic resistance. *Nat. Rev. Drug Discov.* **2017**, *16*, 457–471. [[CrossRef](#)] [[PubMed](#)]
28. Kany, A.M.; Sikandar, A.; Yahiaoui, S.; Haupenthal, J.; Walter, I.; Empting, M.; Kohnke, J.; Hartmann, R.W. Tackling *Pseudomonas aeruginosa* Virulence by a Hydroxamic Acid-Based LasB Inhibitor. *ACS Chem. Biol.* **2018**, *13*, 2449–2455. [[CrossRef](#)] [[PubMed](#)]
29. Munguia, J.; Nizet, V. Pharmacological Targeting of the Host-Pathogen Interaction: Alternatives to Classical Antibiotics to Combat Drug-Resistant Superbugs. *Trends Pharmacol. Sci.* **2017**, *38*, 473–488. [[CrossRef](#)] [[PubMed](#)]
30. Schütz, C.; Ho, D.-K.; Hamed, M.M.; Abdelsamie, A.S.; Röhrig, T.R.; Herr, C.; Kany, A.M.; Rox, K.; Schmelz, S.; Siebenbürger, L.; et al. A new PqsR inverse agonist potentiates tobramycin efficacy to eradicate *Pseudomonas aeruginosa* biofilms. *Adv. Sci.* **2021**, *8*, 2004369. [[CrossRef](#)]
31. Georgiadis, D.; Yiotakis, A. Specific targeting of metzincin family members with small-molecule inhibitors: Progress toward a multifarious challenge. *Bioorg. Med. Chem.* **2008**, *16*, 8781–8794. [[CrossRef](#)]
32. Grobelny, D.; Poncz, L.; Galarzy, R.E. Inhibition of Human Skin Fibroblast Collagenase, Thermolysin, and *Pseudomonas aeruginosa* Elastase by Peptide Hydroxamic Acids. *Biochemistry* **1992**, *31*, 7152–7154. [[CrossRef](#)]
33. Konstantinovic, J.; Yahiaoui, S.; Alhayek, A.; Haupenthal, J.; Schonauer, E.; Andreas, A.; Kany, A.M.; Muller, R.; Koehnke, J.; Berger, F.K.; et al. N-Aryl-3-mercaptosuccinimides as Antivirulence Agents Targeting *Pseudomonas aeruginosa* Elastase and *Clostridium* Collagenases. *J. Med. Chem.* **2020**, *63*, 8359–8368. [[CrossRef](#)]
34. Rouanet-Mehouas, C.; Czarny, B.; Beau, F.; Cassar-Lajeunesse, E.; Stura, E.A.; Dive, V.; Devel, L. Zinc-Metalloproteinase Inhibitors: Evaluation of the Complex Role Played by the Zinc-Binding Group on Potency and Selectivity. *J. Med. Chem.* **2017**, *60*, 403–414. [[CrossRef](#)] [[PubMed](#)]
35. Kaya, C.; Walter, I.; Yahiaoui, S.; Sikandar, A.; Alhayek, A.; Konstantinović, J.; Kany, A.M.; Haupenthal, J.; Köhnke, J.; Hartmann, R.W.; et al. Substrate-inspired fragment merging and growing affords efficacious LasB inhibitors. *Angew. Chem. Int. Ed. Engl.* **2021**, e202112295. [[CrossRef](#)] [[PubMed](#)]
36. Hancock, R.D.; Martell, A.E. Ligand Design for Selective Complexation of Metal-Ions in Aqueous-Solution. *Chem. Rev.* **1989**, *89*, 1875–1914. [[CrossRef](#)]
37. Kildahl-Andersen, G.; Schnaars, C.; Prandina, A.; Radix, S.; Le Borgne, M.; Jordheim, L.P.; Gjoen, T.; Andresen, A.M.S.; Lauksund, S.; Frohlich, C.; et al. Synthesis and biological evaluation of zinc chelating compounds as metallo-beta-lactamase inhibitors. *Medchemcomm* **2019**, *10*, 528–537. [[CrossRef](#)]
38. Prandina, A.; Radix, S.; Le Borgne, M.; Jordheim, L.P.; Bousfiha, Z.; Frohlich, C.; Leiros, H.K.S.; Samuelsen, O.; Frovold, E.; Rongved, P.; et al. Synthesis and biological evaluation of new dipicolylamine zinc chelators as metallo-beta-lactamase inhibitors. *Tetrahedron* **2019**, *75*, 1525–1540. [[CrossRef](#)]
39. Samuelsen, O.; Astrand, O.A.H.; Frohlich, C.; Heikal, A.; Skagseth, S.; Carlsen, T.J.O.; Leiros, H.S.; Bayer, A.; Schnaars, C.; Kildahl-Andersen, G.; et al. ZN148 Is a Modular Synthetic Metallo-beta-Lactamase Inhibitor That Reverses Carbapenem Resistance in Gram-Negative Pathogens In Vivo. *Antimicrob. Agents Chemother.* **2020**, *64*, e02415-19. [[CrossRef](#)]
40. Schnaars, C.; Kildahl-Andersen, G.; Prandina, A.; Popal, R.; Radix, S.; Le Borgne, M.; Gjoen, T.; Andresen, A.M.S.; Heikal, A.; Okstad, O.A.; et al. Synthesis and Preclinical Evaluation of TPA-Based Zinc Chelators as Metallo-beta-lactamase Inhibitors. *ACS Infect. Dis.* **2018**, *4*, 1407–1422. [[CrossRef](#)]
41. Palzkill, T. Metallo-beta-lactamase structure and function. *Ann. N. Y. Acad. Sci.* **2013**, *1277*, 91–104. [[CrossRef](#)] [[PubMed](#)]

42. King, A.M.; Reid-Yu, S.A.; Wang, W.; King, D.T.; De Pascale, G.; Strynadka, N.C.; Walsh, T.R.; Coombes, B.K.; Wright, G.D. Aspergillomarasmine A overcomes metallo-beta-lactamase antibiotic resistance. *Nature* **2014**, *510*, 503–506. [[CrossRef](#)]
43. Rotondo, C.M.; Wright, G.D. Inhibitors of metallo-beta-lactamases. *Curr. Opin. Microbiol.* **2017**, *39*, 96–105. [[CrossRef](#)]
44. Rahman, F.; Nguyen, T.M.; Adekoya, O.A.; Campestre, C.; Tortorella, P.; Sylte, I.; Winberg, J.O. Inhibition of bacterial and human zinc-metalloproteases by bisphosphonate- and catechol-containing compounds. *J. Enzym. Inhib. Med. Chem.* **2021**, *36*, 819–830. [[CrossRef](#)] [[PubMed](#)]
45. Sjøli, S.; Solli, A.I.; Akselsen, O.; Jiang, Y.; Berg, E.; Hansen, T.V.; Sylte, I.; Winberg, J.O. PAC-1 and isatin derivatives are weak matrix metalloproteinase inhibitors. *Biochim. Biophys. Acta* **2014**, *1840*, 3162–3169. [[CrossRef](#)] [[PubMed](#)]
46. Blackman, A.G. The coordination chemistry of tripodal tetraamine ligands. *Polyhedron* **2005**, *24*, 1–39. [[CrossRef](#)]
47. Sylte, I.; Dawadi, R.; Malla, N.; von Hofsten, S.; Nguyen, T.M.; Solli, A.I.; Berg, E.; Adekoya, O.A.; Svineng, G.; Winberg, J.O. The selectivity of galardin and an azasugar-based hydroxamate compound for human matrix metalloproteases and bacterial metalloproteases. *PLoS ONE* **2018**, *13*, e0200237. [[CrossRef](#)] [[PubMed](#)]
48. Murphy, G.; Crabbe, T. Gelatinease A and B. *Methods Enzymol.* **1995**, *248*, 470–484. [[CrossRef](#)] [[PubMed](#)]
49. Madhavi, S.G.; Adzhigirey, M.; Day, T.; Annabhimoju, R.; Sherman, W. Protein and ligand preparation: Parameters, protocols, and influence on virtual screening enrichments. *J. Comput.-Aided Mol. Des.* **2013**, *27*, 221–234. [[CrossRef](#)]
50. Lu, C.; Wu, C.; Ghoreishi, D.; Chen, W.; Wang, L.; Damm, W.; Ross, G.A.; Dahlgren, M.K.; Russell, E.; Von Bargen, C.D.; et al. OPLS4: Improving Force Field Accuracy on Challenging Regimes of Chemical Space. *J. Chem. Theory Comput.* **2021**, *17*, 4291–4300. [[CrossRef](#)] [[PubMed](#)]

Supplementary Material

Zinc-chelating compounds as inhibitors of human and bacterial zinc metalloproteases

Fatema Rahman¹, Imin Wushur¹, Nabin Malla¹, Ove Alexander Høgmoen Åstrand², Pål Rongved², Jan-Olof Winberg¹ and Ingebrigt Sylte^{1,*}

¹Molecular Pharmacology and Toxicology, Department of Medical Biology, faculty of Health Sciences, UiT – The Arctic University of Norway, NO-9037 Tromsø, Norway; fatema.rahman@uit.no (FR); imin.wushur@uit.no (IW); nabin.malla@uit.no (NM); ingebrigt.sylte@uit.no (IS); jan.o.winberg@uit.no (JOW).

²Department of Pharmaceutical Chemistry, School of Pharmacy, University of Oslo, PO Box 9 1068 Blindern, N-0316 Oslo, Norway; alexander.aastrand@gmail.com (OAHÅ); pal.rongved@farmasi.uio.no (PR).

Correspondence: ingebrigt.sylte@uit.no; Tel.: +47-77644705

Supplementary figure S1

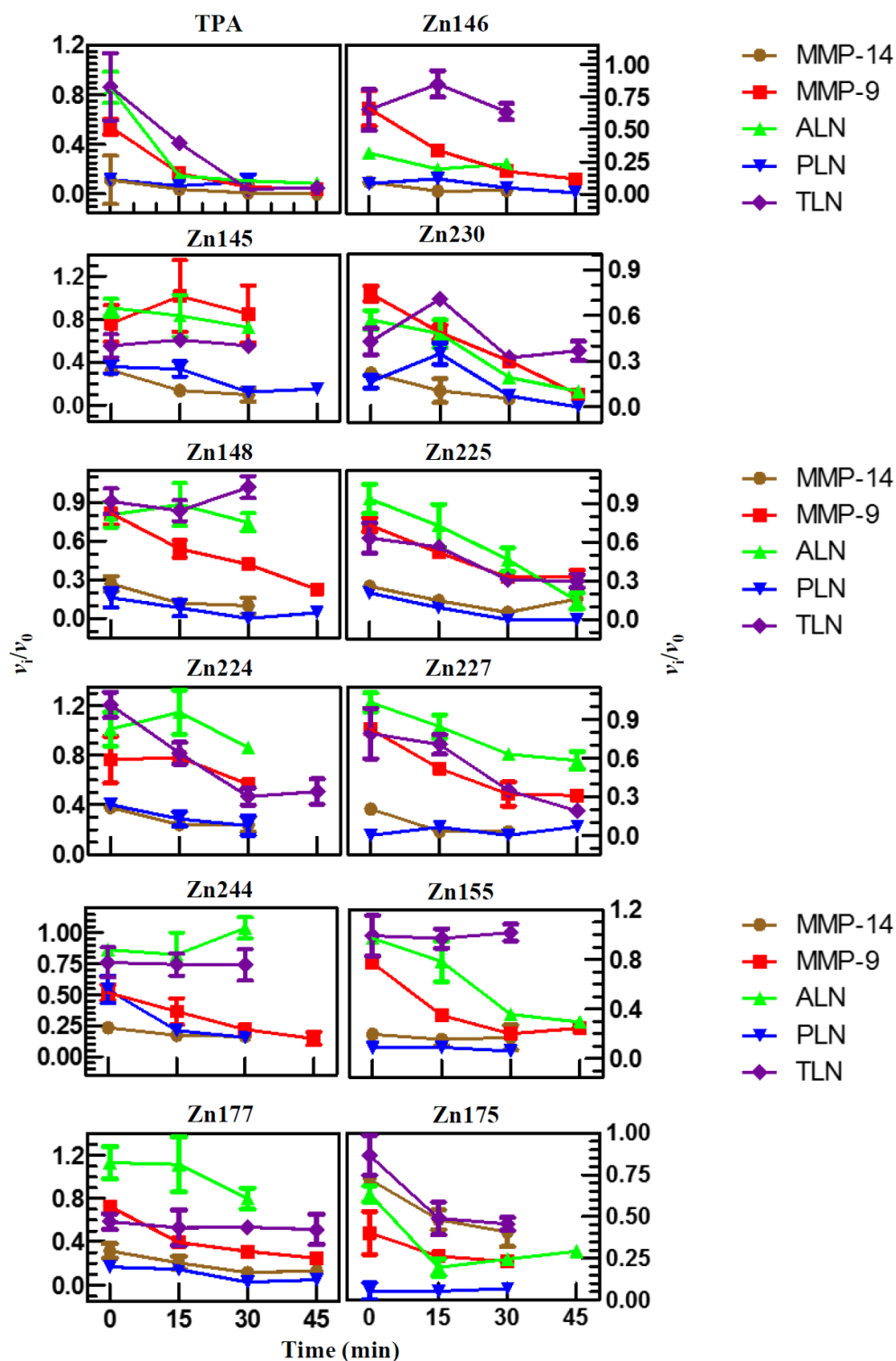


Figure S1. Time dependent inhibitory effects of 100 μM TPA derivatives on the activity of MMP-9, MMP-14, TLN, PLN and ALN. The inhibition experiments were performed as described in Materials and Methods using a concentration of 4 μM of the MMP-9 and MMP-14 substrate McaPLGL(Dpa)AR-NH₂ and the ALN, PLN and TLN substrate McaRPPGFSAFK(Dnp)-OH, except for ALN, where 5 μM was used. The v_i/v_0 (mean \pm s.d.) were based on 3-6 experiments.

Supplementary figure S2

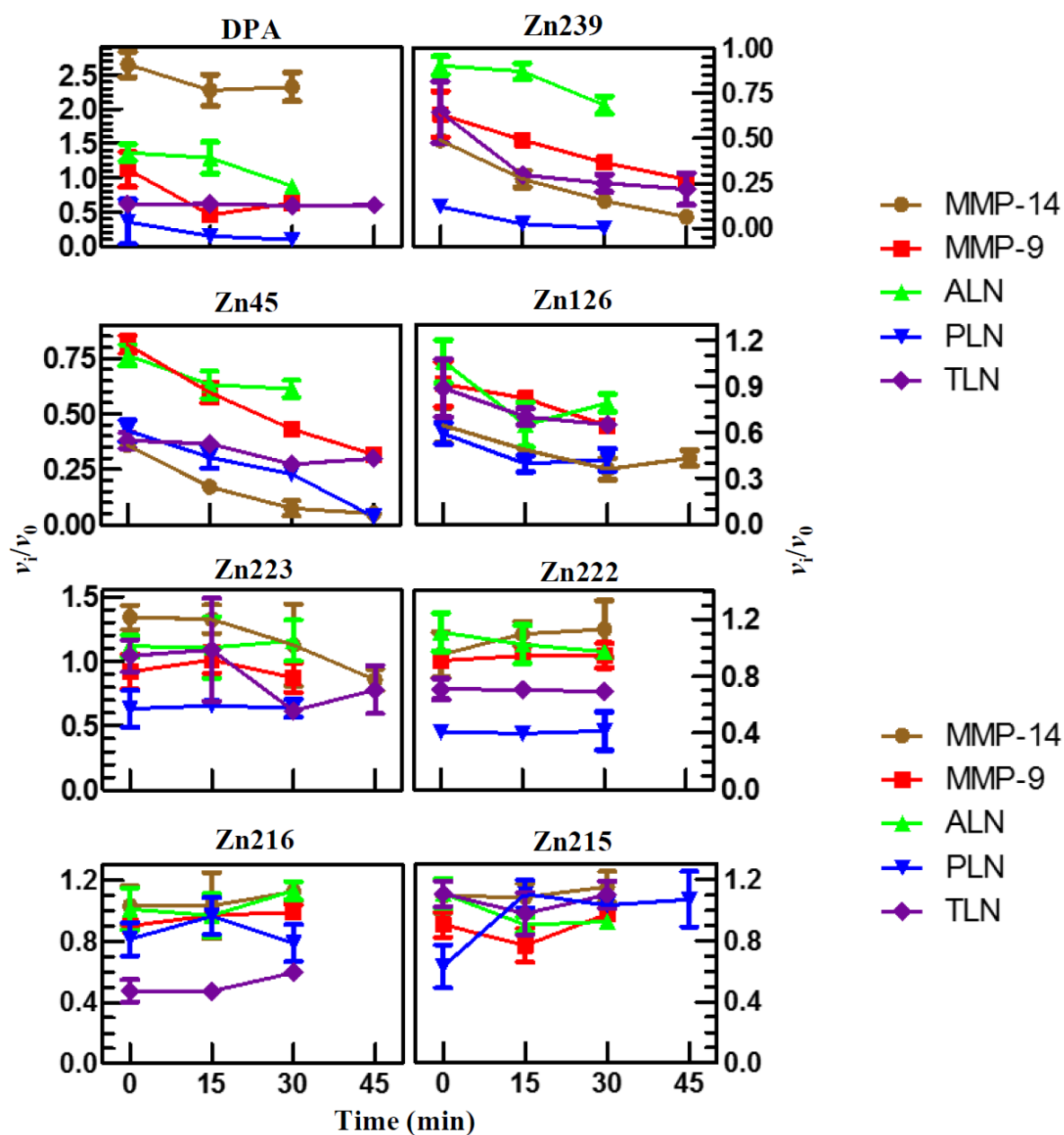


Figure S2. Time dependent inhibitory effects of 100 μM DPA, TPEN, pyridine and thiophene derivatives on the activity of MMP-9, MMP-14, TLN, PLN and ALN. The inhibition experiments were performed as described in Materials and Methods using a fixed concentration of 4 μM of the MMP-9 and MMP-14 substrate McaPLGL(Dpa)AR-NH₂ and the ALN, PLN and TLN substrate McaRPPGFSAFK(Dnp)-OH. For ALN 5 μM was used. The v_t/v_0 (mean \pm s.d.) were based on 3-6 experiments.

Paper III

Interactions of substrates and phosphinyl containing inhibitors with human MMPs and bacterial virulence factors

Fatema Amatur Rahman¹, Imin Wushur¹, Bibek Chaulagain¹, Tra-Mi Nguyen¹, Olayiwola A. Adekoya², Nabin Malla¹, Jan-Olof Winberg¹, Ingebrigt Sylte^{1,3*}

¹ Molecular Pharmacology and Toxicology, Department of Medical Biology, Faculty of Health Sciences, UiT The Arctic University of Norway, NO-9037 Tromsø, Norway

² Centre for Pharmacy, Department of Clinical Science, Faculty of Medicine, University of Bergen, Norway

³ Center for Research and Education, University Hospital of North Norway (UNN)

*Corresponding author: Ingebrigt Sylte, Molecular Pharmacology and Toxicology, Department of Medical Biology, Faculty of Health Sciences, UiT The Arctic University of Norway, NO-9037 Tromsø, Norway. Email: ingebrigt.sylte@uit.no

Abstract

The human matrix metalloproteases MMP-9 and MMP-14, and the bacterial virulence factors thermolysin (TLN), pseudolysin (PLN, LasB) and aureolysin (ALN) are all zinc metalloproteases. In the present study, molecular dynamics (MD) simulations were used to study the interactions of the substrate McaPLGL(Dpa)AR-NH₂ (ES001) with MMP-9 and MMP-14, and of the substrate McaRPPGFSAFK(Dnp)-OH (ES005) with TLN. The MD simulations identified amino acids within the primed and unprimed substrate binding sites and indicated that the P₁ and P₁' residues of ES005 most probably are the Gly-Phe residues. Enzyme inhibition kinetic studies were used to test 5 compounds containing phosphinyl as the putative zinc binding group as inhibitors of MMP-9, MMP-14, TLN, PLN and ALN using the same substrates as in the MD simulations. These studies indicated that the compound H-1 inhibited MMP-14 and two different forms of MMP-9 with inhibition constants ranging from 0.89 to 30 μM, but not the bacterial enzymes. Induced fit docking indicated that the aromatic group of H-1 entering the S₁'-sub-pocket of the MMPs was too big for the S₁'-subpocket of the bacterial enzymes. Compound H-2 inhibited the MMPs with inhibition constants ranging from 0.53 μM (MMP-9) to 3.0 μM (MMP-14) and the bacterial enzymes with inhibition constants ranging from 2.5 μM (TLN) to 80 μM (ALN). Induced fit docking indicated that H-2 bound differently to the human and bacterial protease. The three other compounds did not inhibit any of the proteases.

1. Introduction

Proteases have fundamental roles in all kingdoms of life where they cleave substrates by hydrolyzing peptide bonds (1, 2). Most proteases are found in microorganisms being involved in many processes including generation of nutrition, growth, survival, virulence, and formation of biofilm (3-6). In humans there are more than 570 different proteases involved in variety of physiological processes including cellular signaling and growth, angiogenesis, blood pressure regulation, coagulation, intestinal absorption of nutrition, reproduction, wound repair, hemostasis, and homeostasis (7-12). Alteration in their regulation or structure may have dramatic consequences for organisms, and in human lead to different human pathologies including cancer and neurodegenerative diseases (13).

Metalloproteases (MPs) form the largest family of proteases utilizing 33 % of the human degradome, the complete set of proteases produced by human cells (1). MPs comprise a heterogeneous group of proteases using a metal ion to bind the substrate and polarize a water molecule to perform the hydrolytic reaction. For most MPs, the metal ion is a zinc. In the present paper we are focusing on the human matrix MPs (MMPs), MMP-9 and MMP-14, that belong to the M10 family of proteases and the bacterial MPs thermolysin (TLN), aureolysin (ALN) and pseudolysin (LasB elastase, PLN) of the M4 family of proteases (5). All these enzymes utilize a zinc ion for the hydrolytic cleavage. The metal ion is usually coordinated with the polypeptide backbone through the binding to two histidines and a third residue which can be another histidine as in the MMPs (14), or a glutamic acid as in TLN, PLN and ALN, or an aspartic acid (15). An amino acid serving as a general base in the catalytic reaction is also necessary. The general base accepts a proton from the polarized water molecule and transfer the proton to the nitrogen of the scissile bond. In both the MMPs and the bacterial M4 family enzymes, the general base is the glutamic acid of the conserved HExxH motif, while the histidines of the motif are zinc coordinating (1, 15).

Human MMPs constitute a family of MPs with important functions in many physiological processes and are over-expressed in various diseases. MMPs may have a dual role by promoting the initiation and progression of a disease or by preventing the disease (14, 16-19). MMPs were considered as interesting drug targets, and several compounds that to a certain

extent selectively inhibited the activity of MMPs were developed both by pharmaceutical companies and academia (20-29). However, clinical trials with MMP inhibitors were disappointing, resulting in a reduced focus of MMPs as promising drug targets (30). Based on recent progress in understanding their physiological role and their duality in different diseases, there has been a rebirth for the development of new MMP inhibitors as putative new therapeutics (30, 31).

PLN, ALN and TLN are secreted bacterial virulence factors (15). Inhibition of bacterial virulence is a promising new strategy in the treatment of bacterial infections, either alone or as an adjuvant to antibacterial drugs (32-34). PLN (LasB) is the principle extracellular virulence factor of the Gram negative pathogen *Pseudomonas Aeruginosa* (*P. aeruginosa*) (6). *P. aeruginosa* causes severe infections of lungs, skin, eyes, soft tissues, urinary tract, and bloodstream, and is the etiologic agent of chronic airway infections in patients with chronic bronchitis, bronchiectasis, and cystic fibrosis (6, 35). The pathogen is listed in the category “critical” on the World Health Organization’s (WHO) priority list of bacterial pathogens for which research and development of new antibiotics are urgently needed (36). ALN is secreted by the Gram positive bacterium *Staphylococcus aureus* (*S.aureus*) that may cause serious infections if it enters the bloodstream or internal tissues. *S. aureus* is implicated in several different infections ranging from mild skin-related infections to more severe life-threatening and systemic infections such as bacteremia (37, 38). *S. aureus* is one of the most harmful human pathogens and is connected to the methicillin resistance (39). TLN is a thermostable protease of industrial use secreted by the Gram positive bacteria *Bacillus thermoproteolyticus* (15). The enzyme is the prototype of the M4 family of proteases, and the M4 family is also termed the thermolysin family.

A lot of the knowledge about inhibition of zinc MPs in general is based on MMP inhibitors. Most compounds that inhibit MMPs contain a zinc binding group (ZBG) in addition to a scaffold that interacts with the active site cleft, and common ZBGs are hydroxamic acid (HONH-CO), carboxylate (CO₂⁻), thiolate (S⁻) and phosphinyl (PO₂⁻) (40, 41). Hydroxamic acid and thiolate are stronger zinc binders than carboxylate and phosphinyl groups (41, 42). The scaffold of inhibitors with hydroxamic acid, carboxylate, or thiolate (S⁻) targets the primed (essentially) or unprimed subsites, while X-ray crystallography studies suggested that compounds with the phosphinyl may act as transition state analogues allowing interactions of the connecting

scaffold with both primed and unprimed parts of the active site, and thereby increasing the possibility for selectivity (25, 27, 41-44). In most studies where the goal was to obtain selective MMP inhibitors, the ZBG was fixed while the scaffold of the inhibitors was varying. However, in one study, the contribution of different ZBG to MMP binding was studied by using a scaffold that was combined with phosphinyl, carboxyl or hydroxamic acid as ZBG (41). The scaffold in combination with phosphinyl as ZBG resulted in the compound RXP470 (compound H-1 in the present study). The study showed that the different ZBGs affected binding affinity and selectivity, the dynamics of binding and the position of the inhibitor at the binding site (41). RXP470 interacted both with primed and unprimed sites, while replacements of the phosphinyl group with carboxylic acid or hydroxamic acid as ZBG, in addition to removal of a p-bromophenyl group gave inhibitors that interacted with primed parts of the active site, only (41). The binding strength of inhibitors containing phosphinyl, carboxylic acids or thiolates as ZBG are pH dependent in contrast to those with a hydroxamic acid group (41, 42).

In the present study we performed molecular dynamics (MD) simulations of the substrate McaPLGL(Dpa)AR-NH₂ (ES001) with MMP-9 and MMP-14, and of the substrate McaRPPGFSAFK(Dnp)-OH (ES005) with TLN (Figure 1). The aims of these simulations were to study molecular interactions between the substrates and the enzymes and identify amino acids within primed and unprimed binding sites of the enzymes. In addition, we wanted to identify the most probable cleavage site of ES005 by bacterial MPs. In order to identify structural determinants for selectivity between bacterial zinc MPs and human MMPs, we have in several papers tested compounds with different ZBGs (15, 45-49) as inhibitors, including compounds with nitrogen as donor atom for zinc chelation (50). In the present paper, we are testing RXP470 (compound H-1, Figure 2) and four other compounds with phosphinyl as ZBG as inhibitors of MMP-9, MMP-14, TLN, PLN, and ALN. ES001 was used as substrate in the inhibition kinetics studies with MMP-9 and MMP-14, while ES005 was as substrate in the studies with TLN, PLN and ALN. Phosphinyl compounds were also studied by induced fit docking into the MPs.

2. Results and Discussion

2.1 Molecular dynamics simulations of substrate – enzyme interactions

The binding mode of a substrate probe molecule to a mutated mini-variant of MMP-9 has been studied by X-ray crystallography (51). The structure of the probe molecule is very similar to that of ES001. We have used this X-ray complex as a starting point to obtain more information about the binding of ES001 to MMP-9 and MMP-14 and ES005 to TLN. To study the interactions between these substrates and the enzymes, we performed 200 ns molecular dynamics (MD) simulations. Aims of the MDs were to study the stability of the complexes, identify amino acids constituting the most important sub-pockets of these enzymes and investigate putative cleavage sites of ES005 by TLN. TLN is known to prefer hydrophobic amino acids within the S_1' sub-pocket, but where TLN cleaves ES005 is not exactly known. For ES005 with TLN we performed two 200 ns MD simulations. One simulation with Gly and Phe as respectively P_1 and P_1' residues, and another with Aln and Phe as P_1 and P_1' residues (Figure 1).

The root means square deviations (RMSDs) of the protein and substrate from the starting enzyme/substrate complexes are shown in Supplementary Figure S1 and S2. These figures indicate that the complexes were stable during MD simulations. Table 1 shows amino acids of the enzymes that interacted with the P_1 , P_2 , P_1' and P_2' residues of the substrates, and others being close to these residues during MD simulations of ES001 with MMP-9 and MMP-14 and during the ES005/TLN simulation with the Gly as P_1 residue and the Phe as P_1' residue (Figure 1). Enzyme/substrate contacts during simulations are shown in supplementary Figures S3 and S4.

2.1.1. The binding of ES001 with MMP-9 and MMP-14

The only structural difference between ES001 and a substrate probe molecule that was co-crystallized with MMP-9 (51) is the P_1' residue, which is a Leu in ES001 and a 4-iodo-Phe in the substrate probe (Figure 1). The X-ray crystal structure indicated that the substrate probe binds MMP-9 in an elongated conformation with the N-terminal Mca group (Figure 1) in the unprimed direction and the C-terminal arginine in primed direction. ES001 was docked into MMP-9 in a similar starting orientation such that the Gly was occupying the S_1 -subpocket and

Leu the S_1' -subpocket. During 200 ns simulations both with MMP-9 and MMP-14 the substrate kept the orientation and elongated conformation within the binding site cleft throughout simulations. The terminal parts of ES001 showed largest structural flexibility during the MD simulations, and Figure 2 shows that the N-terminal Mca and the Dpa in the C-terminal of the substrate were most exposed to solvent during MD.

Figure 2 shows that Ala191 interacted with the backbone NH group of Leu in P_2 position of ES001, while the catalytic zinc ion of MMP-9 interacted with the CO group of the Gly in P_1 position and with one of the negatively charged oxygen atoms and a nitrogen of Dpa for most of the simulation. The catalytic glutamic acid (Glu402) also interacted with the backbone NH of the P_1' residue for 30 % of the frames, while the backbone CO of Pro421 interacted with the backbone NH group and a side chain nitrogen of Dpa in P_2' position. A water molecule was bridging between Leu188 and the backbone CO in P_1' -position, while Tyr423 interacted with the backbone CO in P_2' -position for more than 30 % of the frames (Figure 2). Altogether, ES001 obtained a hydrogen bonding network with MMP-9 very similar to that of the substrate probe in the X-ray complex with MMP-9 (51). In MMP-14, the interactions of the central parts around the cleavages site were very similar to that in MMP-9, and ES001 had similar interactions with the catalytic zinc ion and the catalytic glutamic acid (Glu240) as in MMP-9 (Figure 2). However, the interactions around the P_2 and P_2' positions were quite different from that in MMP-9 for most of the frames (Figure 2).

2.1.2 The binding of ES005 with TLN

ES005 is larger than ES001 and the substrate probe that was co-crystallized with MMP-9 (51), and the docking process of ES005 into the catalytic site of TLN was quite problematic, such that the starting complex for the MD simulations may be more uncertain than those for ES001 in MMP-9 and MMP-14. The RMSD of substrate and enzyme during MD are shown in supplementary Figure 2. These plots show that ES005 was quite stable during both simulations. However, for the simulation with Ala and Phe (AF complex) in S_1 and S_1' subpockets, respectively, the substrate obtained an extremely stable conformation after approximately 100 ns and stayed in that conformation for the rest of the simulation. During the first 100 ns of this simulation the N-terminal parts of ES005 did not have binding partners

within the enzyme and large portions of the substrate (especially in the N-terminal parts) were strongly exposed to solvent. After 100 ns the N-terminal Mca group folds against the C-terminal Dnp group giving a folded and very stable conformation of the substrate (Figure 3).

The simulation with Gly and Phe (GF complex) in S_1 and S_1' sub-pockets, respectively, retained a quite elongated conformation for the entire simulation, with the N-terminal Mca in unprimed direction and the C-terminal Dnp in primed direction (Figure 3), as seen for ES001 with MMP-9 and MMP-14, and in the X-ray structure of the substrate probe with MMP-9 (51). In the GF complex, the catalytic zinc interacted with the backbone CO-group of both the Pro in P_2 position and the Gly in P_1 position. Asn112 interacted with the backbone NH group of both Phe in P_1' and Ser in P_2' position, while Arg203 interacted with backbone CO in P_1' position. Asn111 interacted with side chain of Ser in P_2' , while His142 was stacking with the side chain Phe in P_1' position (Figure 3). In the AF complex, unprimed residues of ES005 were more important for forming interactions with amino acids in TLN than in the GF complex (Figure 3). The backbone CO group of Gly now in the P_4 position obtained hydrogen bonding interactions with Asn116, while the backbone NH of Ser now in P_2 position interacted with Trp115. The side chain of Phe now in P_3 position was stacking with Phe114. The backbone CO of P_2 (Ser) and P_1 (Ala) interacted with the catalytic zinc. The backbone NH of P_1' (Phe) interacted with Asn112, while the side chain was stacking with His142. The C-terminal Dnp interacted with Asn11 and Arg203 (Figure 3).

During catalytic cleavage, the incoming substrate is presumed to displace a water molecule coordinated to the catalytic zinc, such that the general base (Glu143 of the HEXXH motif) can accept a proton from the zinc polarized water molecule and transfer it to the leaving nitrogen of the scissile bond (52, 53). During the cleavage process the side chain oxygen of Asn112 in TLN and the backbone carbonyl of Ala113 are suggested to accept hydrogen bonds from the protonated nitrogen (P_1' position) of the scissile bond. In both simulations Asn112 formed hydrogen bonds with the backbone NH of the P_1' residue, and Glu143 is also located near the NH group of the P_1' residue. Based on that both cleavage sites may be possible. In both complexes the central P_1 and P_1' residues form favourable interactions with the enzyme that can facilitate proton transfer and substrate cleavage. In the GF complex the ES005 structure is more elongated than in the AF complex and in a conformation more similar to the conformation of ES001 in MMP-9 and MMP-14 (Figure 2) and to the conformation of the

substrate probe with MMP-9 than in the AF complex. In addition, TLN is classified as an endopeptidase (15), and an Ala-Phe cleavage will result in a dipeptide product. Altogether, this may suggest that the Gly-Phe is a more realistic cleavage site of ES005 in TLN than Ala-Phe. However, based on the present simulations we cannot rule out that ES005 is cleaved both at Gly-Phe and Ala-Phe by TLN.

2.1.3 Sub-pocket amino acids

The amino acids within the substrate sub-pockets during MD of ES001 with MMP-9 and MMP-14 and ES005 with TLN (Gly-Phe cleavage site) are shown in Table 1. Amino acids in direct contact with the substrate, in addition to amino acids in close vicinity of substrate side chains have been included in the table. Amino acids in PLN and ALN corresponding sub-pocket amino acids in TLN are also shown. These amino acids have been identified by amino acids sequence alignments of the catalytic domain of TLN, PLN and ALN (Supplementary figure S5). The identification of amino acids with the different sub-pockets was not easy, especially for the S_1 sub-pocket, since the substrate amino acid entering this pocket were a glycine in both ES001 and the GF-simulation of ES005 with TLN. In addition, for amino acids located at the boarder of two sub-pockets it is a definition if the amino acid belongs to one or the other sub-pocket. Table 1 is therefore slightly differing from a corresponding table based on docking of inhibitors by Rahman et al. 2021 (45).

2.2 K_m values of fluorescence quenched substrates

At experimental conditions in the present work (1 % DMSO in all assays), the K_m value of ES001 with recombinant Mag-Trypsin activated MMP-9 (MMP-9(MT)) was $2.7 \pm 0.5 \mu\text{M}$. K_m values of ES001 for MMP-9(A) and MMP-14, and of ES005 for TLN, PLN and ALN at experimental conditions as in the present work were determined previously (45). To summarize, the K_m values of ES001 with MMP-9(A) and MMP-14 were 4 ± 1 and $4.9 \pm 0.4 \mu\text{M}$, respectively, while the K_m values of ES005 with ALN, PLN and TLN were 76 ± 7 , 24 ± 8 and $6 \pm 1 \mu\text{M}$, respectively. The estimated K_m values for ALN and PLN in that study must be regarded as uncertain since the highest substrate concentration used was $10 \mu\text{M}$ due to quenching. The K_m values were

very similar to those previously obtained for these enzymes without DMSO (48) or with a DMSO concentration of 5 % (47).

2.3 Quenching experiments with phosphinic compounds

All compounds were first tested for possible quenching of the formed fluorescence product. The experiments were performed with varying concentrations of the putative inhibitors (0 - 100 μ M) against varying concentrations of the fluorescence product (McaPLG-OH) of ES001 as previously described for PAC-1 and isatin derivatives (47), and as described in Materials and Methods. These experiments revealed that neither of the phosphinic compounds quenched the fluorescence product. However, some of the compounds showed background fluorescence at the emission and excitation wavelength used, but that did not affect the inhibitory assays as enzymatic reactions were followed continuously. These results were similar to our previous results with bisphosphonate and catechol containing compounds (45) dipicolylamine (DPA), tripicolylamine (TPA), tris pyridine ethylene diamine (TPED), pyridine and thiophene derivatives (50), but in large contrast to PAC-1 and isatin derivatives which rarely quenched the fluorescence product (47).

2.4 Inhibitory effects of the phosphinic compounds

To determine the inhibitory power of the phosphinic compounds and if they were slow or fast binders, enzymes and 100 μ M of the compounds were pre-incubated for either 15 or 30 min at room temperature. Thereafter, the reaction was started by adding substrate, and the reaction was followed for 30 min at 37 °C. Experiments without pre-incubation were also performed, where the reaction was started by adding the enzyme to the mixture of substrate and phosphinic compound and the reaction was followed as described above. Control experiments without phosphinic compounds were performed identically. As shown in Supplementary Figure S6, these compounds were not slow binder to any of the human and bacterial proteases, except H-3 against MMP-14 where it appeared that the inhibition was stabilized after 15 min pre-incubation.

Figure 4 shows that only compound H-2 is a strong inhibitor of all five proteases, and strongest inhibition was seen with MMP-9 and MMP-14. Compound H-1 was a strong inhibitor of only

the two human proteases, while the other three compounds (H-3, H-4 and H-5) showed only weak to no inhibition of the five proteases. K_i values were determined for the enzymes where 100 μ M of a phosphinic compounds resulted in an inhibition of 50 % or more. Table 2 summarizes these results. H-2 binds strongest to the two MMP-9 activated variants (MMP-9(MT) and MMP-9(A) with K_i values around 0.5 μ M. This compound bound approximately equally good to MMP-14 and TLN, although the binding was weaker than to MMP-9. A much weaker binding was observed to PLN and ALN, although the binding was stronger to the former enzyme.

Induced fit docking of H-2 into MMP-9 is shown in Figure 5. The highest scored pose of H-2 with MMP-9 is shown in gold-yellow and had a scoring of -16.3 kcal/mol. All different enantiomers were initially docked however, the RSS enantiomer (Figure 4 and Figure 5C) was the highest scored and was also the one used for the inhibition kinetics studies. The X-ray structure of the SSS enantiomer with MMP-11 is known (PDB id: 1hv5) (54) and is superimposed with the MMP-9/H2 complex in Figure 5A. The figure shows large similarities between the complexes. In both, H-2 interacts both with primed and unprimed pockets, and the propylphenyl group occupies the S_1' sub-pocket and penetrates quite deeply into the pocket. The most striking difference is that the indole ring occupies the S_2' sub-pocket in the X-ray complex (SSS enantiomer), while in the best docked complex (RSS enantiomer) the ring is more in the direction of the S_3' sub-pocket (Figure 5B). In addition, the positions of the other phenyl rings were also different. The position of H-2 (RSS) in MMP-14 was quite similar to that in MMP-9, but in the best pose the indole ring was in the direction of the S_2' -sub-pocket (Figure 6), more similar to the X-ray complex of the SSS-enantiomer with MMP-11 than in MMP-9. The scoring in MMP-14 was - 14.9 kcal/mol.

The induced fit docking complexes of H-2 with PLN, ALN and TLN are shown in Figures 7-9. The scoring values with these enzymes were as follows; PLN: -13.0 kcal/mol, ALN: -13.0 kcal/mol, TLN: -13.4 kcal/mol. In agreement with the obtained K_i values, the induced fit docking studies show that H-2 binds weaker to TLN, PLN and ALN than to MMP-9 and MMP-14 (Table 2). The main differences between the bacterial MPs and the human MMPs was that the phenyl ring of H-2 closest to the phosphinyl group entered the S_1' -sub-pocket in the bacterial MPs (Figure 7, 8 and 9), while the propylphenyl group (Figure 4) entered this pocket in the MMP-9 (Figure 5) and MMP-14 (Figure 6). In the bacterial enzymes the propylphenyl group was in the

direction of unprimed sites. These results indicate that the propyl chain with the phenyl ring that occupies this sub-pocket in MMP-9 and MMP-14 and in the X-ray structure of MMP-11 is too long to enter the S_1' sub-pocket of the virulence factors, and therefore the shorter phenylalanine enters this sub-pocket. This agrees with our previous studies on compounds with hydroxamic acid as ZBG, showing that the S_1' sub-pockets of the MMPs can occupy larger groups than the corresponding sub-pocket of TLN, PLN and ALN (46, 48, 49). H-2 interacted both with prime and unprimed sub-sites in the bacterial MPs. This agreed with the docking into MMP-9 and MMP-14 and indicate that H-2 and other phosphinyl compounds also may mimic substrate transition states while interacting with bacterial zinc MPs.

H-1 binds stronger to MMP-14 than to the two variants of MMP-9, with K_i values of 0.89 μ M, 19 μ M and 30 μ M, respectively (Table 2). (41). Induced fit docking of H-1 into MMP-9 and MMP-14 were performed both with the RSS and SSS enantiomer. The difference between the enantiomers was at the chiral centre closest to the phosphinyl group (Figure 4). The X-ray structure complex of the SSS enantiomer with MMP-12 is known (PDB id: 5czm) (41). In that complex the big isoxazolyl side chain of H-1 (Figure 4) enters deeply into the S_1' -subpocket of MMP-12. Docking of the RSS and SSS enantiomers into MMP-9 (Figure 10) and MMP-14 (Figure 11) showed that this group of H-1 also enters the S_1' -subpocket of MMP-9 and MMP-14. Both the SSS and RSS-enantiomer could be docked into the active site of MMP-9 and MMP-14, but the SSS-enantiomer showed best scoring in both, with a scoring value of -13.2 kcal/mol in MMP-9 and -9.2 kcal/mol in MMP-14. The corresponding scoring values for the RSS-enantiomer was -7.2 kcal/mol for MMP-9 and -6.3 kcal/mol for MMP-14. These scoring values indicated that H-1 binds stronger to MMP-9 than MMP-14, which is contradictory to the calculated K_i values (Table 2). In the bacterial enzymes, isoxazolyl side chain seems too big to enter the S_1' -subpocket, and no clear interactions with any of the enzyme sub-sites were observed, which may explain why H-1 did not bind PLN, TLN and ALN (Figure 4).

Previously, H-1 (RXP470) (Figure 4) have been tested as inhibitor of various metalloproteases (MMP-1,-2,-3,-7,-8,-9,-10,-11,-12,-13,-14, ACE, NEP and TACE) (55, 56). In agreement with our results, they found that H-1 binds stronger to MMP-14 than MMP-9 with K_i values of 0.14 and 1.3 μ M, respectively (56). Noticeable, the previously obtained K_i values H-1 and H-2 for MMP-9 and MMP-14 were lower than the values we obtained in the present study. H-2 (RXPO₃) were also previously tested as an inhibitor against various matrix metalloproteases (MMP-1,-

2,-7,-8,-9,-11,-14) (44). In agreement with our results, H-2 bound stronger to MMP-9 than to MMP-14 with K_i values of 10 and 40 nM, respectively. Another study showed that the RSS enantiomer of H-2 bound stronger to MMP-14 than the RRS enantiomer, with K_i values of 90 and 386 nM, respectively (43). In both these studies, the reported K_i values were lower than those obtained for these two enzymes in the present study with the RSS enantiomer of H-2. Differences in the experimental setup between the present study and the previous studies of H-1 and H-2 (43, 44, 56) may explain the differences in obtained K_i values. Buffer compositions, pH, in addition to assay reaction temperature were different. Previous studies showed that the binding of H-1 (RXP470) to MMP-12 is pH dependent and the K_i value increased approximately ten times with one unit increase in buffer pH (41, 42). The assay reaction temperature may have an effect of the obtained K_i values. In a previous study with the enzyme *Drosophila lebanonensis* alcohol dehydrogenase (ADH), it was shown that the dissociation constant ($K_{EO,i}$) of pyrazole from the ternary enzyme-NAD⁺-pyrazole complex increased with increasing temperature in the pH region 7-10 (57). Both the buffer pH and assay temperature were higher in our experiments compared to the previous studies, which at least in part may contribute the higher K_i values obtained in our study.

The phosphinic di- and tri-peptide compounds H3-H5 with a carboxylic acid or a carboxylic ethyl ester at the C-terminal P₁' position (Figure 4), were previously studied as potential carboxypeptidase inhibitors. H4 was one of several phosphinic di- and tri-peptide compounds designed and tested against angiotensin-converting enzyme 2 (ACE2), carboxypeptidase A and angiotensin-converting enzyme (ACE) (58). Thus, it was not unexpected that compounds H3-H5 showed weak to no inhibition of the five proteases in the present work (Figure 4).

3. Material and Methods

3.1 Materials

Dimethyl sulfoxide (DMSO), TRIS, sodium hydrogen phosphate (Na₂HPO₄), and sodium acetate (CH₃COONa) were from Merck (Darmstadt, Germany). Ethylenediaminetetraacetic acid was from Fluka (Buchs, Switzerland). Acrylamide, Coomassie Brilliant Blue G-250 and Triton X-100

were from BDH (Poole, UK). Hepes, Brij-35, Silver nitrate, alkaline phosphatase-conjugated antibodies, p-aminophenylmercuric acetate (APMA) and gelatin were from Sigma (St Louis, MO, USA). Magnetic trypsin beads (Mag-Trypsin) were purchased from Takera (Gothenburg, Sweden). Gelatin-Sepharose, was from GE-Healthcare (Uppsala, Sweden). DC Protein Assay and unlabelled molecular weight standards were from BioRad (Richmond, CA, USA). Sf9 and High FiveTM insect cells and Magic Marker molecular weight standards were from Invitrogen (Carlsbad, CA, USA). Western Blotting Luminol reagent and HRP-conjugated donkey anti-goat secondary antibody were from Sancta Cruz (Santa Cruz, CA, USA). HRP-conjugated goat anti-rabbit secondary antibody was from Southern Biotech (Birmingham, AL, USA). Fetal bovine serum was from Biochrom AG (Berlin, Germany). Galardin (Gm6001), human MT1-MMP/MMP-14 (catalytic domain), TLN and PLN were from Calbiochem (San Diego, CA, USA) and Aureolysin was from BioCentrum Ltd (Kraków, Poland). McaPLGL(Dpa)AR-NH₂ (ES001) and McaRPPGFSAFK(Dnp)-OH (ES005) were from R&D Systems (Minneapolis, MN, USA). Mca-PL-OH was from Bachem AG (Basel, Switzerland).

The phosphinic compounds were a kind gift from professor Athanasio Yiotakis, University of Athens, Greece. Synthesis of these compounds have been described in previous papers (42-44, 54, 56, 58, 59). Structures of the phosphinic compounds tested in the present study are shown in Figure 4.

3.2 Expression, purification and activation of recombinant human proMMP-9

The expression of recombinant full length proMMP-9 (rpMMP-9) in Sf9 and High Five insect cells and the purification were performed as previously described (48, 60). The amount of proMMP-9 was estimated spectrophotometrically at 280 nm using $\epsilon_{280\text{nm}} = 114.36 \text{ M}^{-1}\text{cm}^{-1}$ (61) for the full length enzyme. Activation of the recombinant proMMP-9 was performed with APMA (auto-activation) and Mag-Trypsin as previously described (48), while the amount of active MMP-9 was determined by active site titration using galardin, also described previously (48).

3.3 Enzyme inhibition studies of phosphinic compounds

3.3.1 Determination of reaction velocities

The substrate McaPLGL(Dpa)AR-NH₂ (ES001) were used for APMA activated MMP-9 (MMP-9(A)), Mag-Trypsin activated MMP-9 (MMP-9(MT)) and MMP-14, while the substrate McaRPPGFSAFK(Dnp)-OH (ES005) were used for ALN, PLN and TLN. The reaction velocities/initial rates (v) were determined at 37 °C, at an excitation wavelength of 320 nm and an emission wavelength of 405 nm with a slit width of 10 nm using either a Perkin Elmer LS 50 Luminescence spectrometer and the FL WinLab Software Package (Perkin Elmer) or a Clario Star micro plate reader (CLARIOstar® BMG LABTECH).

The phosphinic compounds were dissolved in 100 % DMSO giving a concentration of 10 mM. In all assays, a fixed substrate concentration of 4.0 μM in a total volume of 100 μL 0.1 M HEPES pH 7.5, 10 mM CaCl₂, 0.005 % Brij-35 and 1.0 % DMSO. Fixed enzyme concentrations were as follows; 0.05 nM MMP-9(A), 0.05 nM MMP-9(MT), 1.0 nM MMP-14, 1.4 nM ALN, 0.5 nM PLN and 0.21 nM TLN. Time dependent inhibitory experiments without and with 100 μM of phosphinic compounds were performed as follows: Compounds were either pre-incubated with proteases for 15 and 30 minutes at room temperature and the enzymatic reaction was started by adding the substrate, or not pre-incubated, i.e., the reaction was started by adding the protease to the mixture of substrate and compound. Control tests without compound present were performed in the same way. The reaction was followed for 30 minutes at 37 °C.

3.3.2 Determination of K_m values

K_m values were determined for ES001 with Mag-Trypsin activated recombinant MMP-9 (MMP-9(MT)). Substrate concentrations used were 1-10 μM in a total volume of 100 μL of 0.1 M HEPES pH 7.5 containing 10 mM CaCl₂, 0.005 % Brij-35 and 1.0 % DMSO. Substrate concentrations above 10 μM resulted in quenching as reported previously (47). Initial rate experiments were performed as described above for the determination of enzyme reaction velocities using a Perkin Elmer LS 50 Luminescence spectrometer and the FL WinLab Software Package (Perkin Elmer). K_m values of ES001 for MMP-9(A) and MMP-14, and of ES005 for TLN,

TLN and ALN at same experimental conditions as in the present work were determined previously (45). As described previously, in these experiments the reactions were followed for one minute, only, and initial reaction velocities were determined from the activity curves.

3.3.3 Determination of IC_{50} and K_i values

The inhibitory constant IC_{50} of the phosphinic compounds were performed with concentrations ranging from 10^{-10} to 10^{-4} M in the assay or 8 concentrations that resulted in inhibition between 10 - 90%, using a fixed substrate, and concentrations of enzyme and buffer as described above. Enzymes with and without inhibitor were either pre-incubated for 30 minutes at room temperature, or not pre-incubated, and initial rate assays were performed as described above. Assays were performed using a Clario Star microplate reader (CLARIOstar® BMG LABTECH). The IC_{50} values were calculated with Graph Pad Prism 5 using equation 1 or 2, depending on concentration ranges of phosphinic compounds used.

$$\frac{v_i}{v_0} = \frac{1}{(1 + 10^{(pIC_{50}-pI)})} \quad (1)$$

$$\frac{v_i}{v_0} = \frac{1}{(1 + \frac{[I]}{IC_{50}})} \quad (2)$$

In equation 1 and 2, v_i is the enzyme activity in presence of inhibitor, v_0 the activity in absence of inhibitor, $pI = -\log [Inhibitor]$ in M and $pIC_{50} = -\log IC_{50}$ in M. All experiments were performed in at least triplicate. Equation (3) shows the relation between IC_{50} and K_i values for substrate competitive inhibitors based on the fixed substrate concentration used and the enzymes K_m value for the substrate:

$$IC_{50} = K_i (1 + [S] / K_m) \quad (3)$$

3.3.4 Quenching experiments

To determine to which extent the tested compounds quenched the time dependent enzymatic increase in the fluorescence product of processed substrates, quenching experiments were performed as described previously (47). Briefly, the fluorescence ($\lambda_{\text{ex}}=320\text{nm}$, $\lambda_{\text{em}}=405\text{ nm}$, slit width =10 nm) at various concentrations of the Mca-fluorescent product of ES001 and ES005 (0-100 nM), was determined in absence and presence of various concentrations of the phosphinic compounds (0-100 μM). Primary and secondary plots were used to determine if these compounds quenched the McaPL-OH fluorescence.

3.4 Molecular modelling

The Schrödinger 2021-2 suit of programs (Schrödinger, Inc., New York, USA, 2021) were used for molecular modelling. Induced fit docking of H-1 and H-2 (Figure 1) was performed into the active site cleft of MMP-9, MMP-14, TLN, ALN and PLN. The Desmond program (62) running on the graphics processing unit (GPU) of our workstations was used for molecular dynamics simulations of ES001 with MMP-9 and MMP-14, and of ES005 with TLN.

3.4.1 Induced fit docking of H1 and H2

The 2D structures of H-1 and H-2 were drawn, converted to 3D by the 3D builder tools of Maestro 12.8. Different enantiomeric states of H-1 and H-2 were generated and optimized with the LigPrep module using the OPLS4 force field (63). The obtained low energy conformations were used for induced fit docking (IFD).

The following X-ray crystal structures were used for docking: MMP-9; PDB id **2ovz** (a Glu402Gln mutant of MMP-9). MMP-14; PDB id **1bqq**, complexed with TIMP-2, an X-ray crystal structure of MMP-14 with a small molecular inhibitor is lacking in the PDB-database. PLN; PDB id **3dbk**, complex with the inhibitor phosphoramidone. TLN; PDB id **1t1p**, complex with a phosphoramidate inhibitor. ALN; PDB id **1bqb**, structure of the enzyme without inhibitor, an ALN-inhibitor complex is lacking in the PDB-database.

Gln402 in the MMP-9 structure were mutated back to Glu402 as in the wild type MMP-9. Enzyme structures were protonated at pH 7.4 ± 0.2 using the Epik tool, missing hydrogen atoms were added, and structures were optimized using the OPLS4 force field (63). An atomic distance of 12 Å around the center of the co-crystallized inhibitors were used to generate the 3D grid box for docking. For PDB structures without a small molecular inhibitor (MMP-14 and ALN), the catalytic zinc atom was used as center of the 3D grid box. IFD was performed for the H1 and H2 into the enzyme structures using default parameters and standard sampling, retaining 20 poses of each ligand. The IFD scores were calculated to rank the different poses.

3.4.2 Construction of enzyme-substrate complexes

The X-ray structure complex of an inactive mutated form of MMP-9 (the Glu227Ala mutant corresponding to Glu402Ala in the present manuscript) in complex with a substrate probe molecule (PDB id: **4jjj**), together with an X-ray crystal structure of MMP-9 that contains the prodomain, the catalytic domain and the three FnII (fibronectin type II) modules (PDB id: **1l6j**) were used as starting points for generating MMP-9/ES001, MMP-14/ES001 and TLN/ES005 complexes. The prodomain was deleted from the 1l6j structure giving Phe107 as the new N-terminal amino acids, as observed in trypsin and MMP-3 activated MMP-9 (64).

The length of ES001 is similar to that of the substrate probe (Figure 1), and the only structural difference is that the substrate probe contains a phenylalanine with an iodine atom in para-position (51), while ES001 has a leucine in the corresponding position (Figure 1). The iodinated phenylalanine occupies the S_1' binding cavity of MMP-9 (51), and the corresponding leucine in ES001 is therefore most probably the P_1' - position of ES001 (Figure 1). Crystallographic water molecules were removed from both structures, and an initial MMP-9 - ES001 complex was constructed from the MMP-9 – substrate probe complex (PDB id: 4jjj) by mutating the iodinated phenylalanine in P_1' - position of the substrate probe to the leucine in ES001. Thereafter the MMP-9 -ES001 complex were superimposed with the 1l6j structure lacking the prodomain, and ES001 was transferred into the catalytic site of the modified 1l6j structure. The 1l6j structure was chosen since the three FnII domains also may influence the structural dynamics of MMP-9.

An initial complex of MMP-14 with ES001 was constructed by superimposition the X-ray structure of MMP-14 (PDB id: **1bqq**) without crystallographic water molecules with the generated MMP-9 - ES001 complex, and thereafter transferring the ES001 structure into the active site cleft of MMP-14 in a position similarly to the position in MMP-9.

Construction of complexes of TLN with ES005 was a bit more problematic. ES005 is longer than ES001 and the substrate probe (Figure 1) and generating the ES005 structure directly from the substrate probe was therefore problematic. The X-ray structure of MMP-9 with the substrate probe was superimposed with the X-ray structure of TLN (PDB id: **1tlp**), without crystallographic water molecules, and the substrate probe was transferred into the TLN structure. Thereafter ES005 was drawn, converted to 3D by the 3D builder tools of Maestro 12.8, and optimized with the LigPrep module using the OPLS4 force field (63). The exact cleavage site(s) of TLN in ES005 are not known, but TLN prefers quite large and hydrophobic amino acids within the S_1' -pocket (15), and the P_1' -position of ES005 was therefore anticipated to be one of the two phenylalanine residues (Figure 1). Two complexes of ES005 with TLN were therefore constructed, by manually position the ES005 on top of the substrate probe in the TLN structure. In both complexes a phenylalanine of ES005 was superimposed with the 4-iodo-phenylalanine in the substrate probe such that in one of the complexes, the glycine of ES005 was the P_1 -amino acid, while in the other the alanine of ES005 was the P_1 -amino acid (Figure 1). Manual adjusts of some of the side chains of ES005 were necessary to avoid structural clashes.

The enzyme structure complexes of ES001 with MMP-9 and MMP-14, and the two complexes of ES005 with TLN were protonated at pH 7 ± 2 using the Epik tool, missing hydrogen atoms were added, and complexes were optimized using the OPLS4 force field (63).

3.4.3 Molecular dynamics simulations

The four energy optimized complexes from section 2.5.2 were used as starting points for 200 ns of MD simulations using graphics processing unit (GPU) technology as implemented in the Desmond program ([https://www.deshawresearch.com/publications/Desmond-GPU Performance April 2021.pdf](https://www.deshawresearch.com/publications/Desmond-GPU%20Performance%20April%202021.pdf)) version 6.7 (Schrödinger, Inc., New York, USA, 2021). The OPLS4 force field (63) was also used for MD simulations. Molecular systems were solvated

within an orthorhombic box by using the TIP4P water model with a region of 10 Å between the surface of the enzyme – substrate complexes and the walls of the box. Chloride ions were added to neutralise the molecular system. Equilibration of the molecular systems were performed by the recommended default relaxation protocol that includes 100 ps of Brownian dynamics at constant temperature (10 K) and pressure with restraints on solute heavy atoms, followed gradually heating of the system from 0 to 300 K. A cut-off radius of 9 Å was used for short range electrostatic and van der Waals interactions. Long range electrostatic interactions were treated by the smooth particle mesh Ewald method (65). After convergence, MD simulations for 200 ns were performed using isothermal-isobaric ensemble (NPT) (temperature 300 K, pressure 1.01325 bar) with time steps of 2 fs. A Nose-Hoover thermostat and the Martyna-Tobias-Klein barostat were used to maintain constant temperature and pressure (66). Coordinates were written every 100 ps, giving all together 2000 frames in each trajectory.

Acknowledgements

The present work was supported by Helse Nord (project 1514-20).

References

- (1) Ugalde, A. P., Ordonez, G. R., Quiros, P. M., Puente, X. S., and Lopez-Otin, C. (2010) Metalloproteases and the degradome, *Methods Mol Biol* 622, 3-29.
- (2) Ordonez, G. R., Puente, X. S., Quesada, V., and Lopez-Otin, C. (2009) Proteolytic systems: constructing degradomes, *Methods Mol Biol* 539, 33-47.
- (3) Ballok, A. E., and O'Toole, G. A. (2013) Pouring salt on a wound: *Pseudomonas aeruginosa* virulence factors alter Na⁺ and Cl⁻ flux in the lung, *J Bacteriol* 195, 4013-4019.
- (4) Jensen, L. M., Walker, E. J., Jans, D. A., and Ghildyal, R. (2015) Proteases of human rhinovirus: role in infection, *Methods Mol Biol* 1221, 129-141.
- (5) Rawlings, N. D., Barrett, A. J., Thomas, P. D., Huang, X., Bateman, A., and Finn, R. D. (2018) The MEROPS database of proteolytic enzymes, their substrates and inhibitors in 2017 and a comparison with peptidases in the PANTHER database, *Nucleic Acids Res* 46, D624-D632.
- (6) Jurado-Martin, I., Sainz-Mejias, M., and McClean, S. (2021) *Pseudomonas aeruginosa*: An Audacious Pathogen with an Adaptable Arsenal of Virulence Factors, *Int J Mol Sci* 22.
- (7) De Groef, L., Van Hove, I., Dekeyser, E., Stalmans, I., and Moons, L. (2014) MMPs in the neuroretina and optic nerve: modulators of glaucoma pathogenesis and repair?, *Invest Ophthalmol Vis Sci* 55, 1953-1964.
- (8) Lopez-Otin, C., and Bond, J. S. (2008) Proteases: multifunctional enzymes in life and disease, *J Biol Chem* 283, 30433-30437.
- (9) Overall, C. M., and Blobel, C. P. (2007) In search of partners: linking extracellular proteases to substrates, *Nat Rev Mol Cell Biol* 8, 245-257.

- (10) Quiros, P. M., Langer, T., and Lopez-Otin, C. (2015) New roles for mitochondrial proteases in health, ageing and disease, *Nat Rev Mol Cell Biol* 16, 345-359.
- (11) Winberg, J. O. (2012) *Matrix proteinases: biological significance in health and disease*. In: Karmanos NK, ed. *Extracellular matrix: Pathobiology and Signalling.*, De Gruyter, Berlin, Germany, 235-238.
- (12) Wolberg, A. S., and Mast, A. E. (2012) Tissue factor and factor VIIa--hemostasis and beyond, *Thromb Res* 129 Suppl 2, S1-4.
- (13) Puente, X. S., Sanchez, L. M., Overall, C. M., and Lopez-Otin, C. (2003) Human and mouse proteases: a comparative genomic approach, *Nat Rev Genet* 4, 544-558.
- (14) Hadler-Olsen, E., Fadnes, B., Sylte, I., Uhlin-Hansen, L., and Winberg, J. O. (2011) Regulation of matrix metalloproteinase activity in health and disease, *FEBS J* 278, 28-45.
- (15) Adekoya, O. A., and Sylte, I. (2009) The thermolysin family (M4) of enzymes: therapeutic and biotechnological potential, *Chem Biol Drug Des* 73, 7-16.
- (16) Cui, N., Hu, M., and Khalil, R. A. (2017) Biochemical and Biological Attributes of Matrix Metalloproteinases, *Prog Mol Biol Transl Sci* 147, 1-73.
- (17) Kessenbrock, K., Plaks, V., and Werb, Z. (2010) Matrix metalloproteinases: regulators of the tumor microenvironment, *Cell* 141, 52-67.
- (18) Tokito, A., and Jougasaki, M. (2016) Matrix Metalloproteinases in Non-Neoplastic Disorders, *Int J Mol Sci* 17.
- (19) Zhang, X., Huang, S., Guo, J., Zhou, L., You, L., Zhang, T., and Zhao, Y. (2016) Insights into the distinct roles of MMP-11 in tumor biology and future therapeutics (Review), *Int J Oncol* 48, 1783-1793.
- (20) Biasone, A., Tortorella, P., Campestre, C., Agamennone, M., Preziuso, S., Chiappini, M., Nuti, E., Carelli, P., Rossello, A., Mazza, F., and Gallina, C. (2007) alpha-Biphenylsulfonfylamino 2-methylpropyl phosphonates: enantioselective synthesis and selective inhibition of MMPs, *Bioorg Med Chem* 15, 791-799.
- (21) Campestre, C., Agamennone, M., Tortorella, P., Preziuso, S., Biasone, A., Gavuzzo, E., Pochetti, G., Mazza, F., Hiller, O., Tschesche, H., Consalvi, V., and Gallina, C. (2006) N-Hydroxyurea as zinc binding group in matrix metalloproteinase inhibition: mode of binding in a complex with MMP-8, *Bioorg Med Chem Lett* 16, 20-24.
- (22) Campestre, C., Tortorella, P., Agamennone, M., Preziuso, S., Biasone, A., Nuti, E., Rossello, A., and Gallina, C. (2008) Peptidyl 3-substituted 1-hydroxyureas as isosteric analogues of succinylhydroxamate MMP inhibitors, *Eur J Med Chem* 43, 1008-1014.
- (23) Cuniasse, P., Devel, L., Makaritis, A., Beau, F., Georgiadis, D., Matziari, M., Yiotakis, A., and Dive, V. (2005) Future challenges facing the development of specific active-site-directed synthetic inhibitors of MMPs, *Biochimie* 87, 393-402.
- (24) Devel, L., Garcia, S., Czarny, B., Beau, F., LaJeunesse, E., Vera, L., Georgiadis, D., Stura, E., and Dive, V. (2010) Insights from selective non-phosphinic inhibitors of MMP-12 tailored to fit with an S1' loop canonical conformation, *J Biol Chem* 285, 35900-35909.
- (25) Dive, V., Georgiadis, D., Matziari, M., Makaritis, A., Beau, F., Cuniasse, P., and Yiotakis, A. (2004) Phosphinic peptides as zinc metalloproteinase inhibitors, *Cell Mol Life Sci* 61, 2010-2019.
- (26) Dive, V., Lucet-Levannier, K., Georgiadis, D., Cotton, J., Vassiliou, S., Cuniasse, P., and Yiotakis, A. (2000) Phosphinic peptide inhibitors as tools in the study of the function of zinc metalloproteinases, *Biochem Soc Trans* 28, 455-460.
- (27) Georgiadis, D., and Yiotakis, A. (2008) Specific targeting of metzincin family members with small-molecule inhibitors: progress toward a multifarious challenge, *Bioorg Med Chem* 16, 8781-8794.
- (28) Jacobsen, J. A., Major Jourden, J. L., Miller, M. T., and Cohen, S. M. (2010) To bind zinc or not to bind zinc: an examination of innovative approaches to improved metalloproteinase inhibition, *Biochim Biophys Acta* 1803, 72-94.
- (29) Rubino, M. T., Agamennone, M., Campestre, C., Fracchiolla, G., Laghezza, A., Loiodice, F., Nuti, E., Rossello, A., and Tortorella, P. (2009) Synthesis, SAR, and biological evaluation of alpha-

- sulfonylphosphonic acids as selective matrix metalloproteinase inhibitors, *ChemMedChem* **4**, 352-362.
- (30) Fields, G. B. (2019) The Rebirth of Matrix Metalloproteinase Inhibitors: Moving Beyond the Dogma, *Cells* **8**.
- (31) Fields, G. B. (2019) Mechanisms of Action of Novel Drugs Targeting Angiogenesis-Promoting Matrix Metalloproteinases, *Front Immunol* **10**, 1278.
- (32) Dickey, S. W., Cheung, G. Y. C., and Otto, M. (2017) Different drugs for bad bugs: antivirulence strategies in the age of antibiotic resistance, *Nat Rev Drug Discov* **16**, 457-471.
- (33) Kany, A. M., Sikandar, A., Yahiaoui, S., Haupenthal, J., Walter, I., Empting, M., Kohnke, J., and Hartmann, R. W. (2018) Tackling *Pseudomonas aeruginosa* Virulence by a Hydroxamic Acid-Based LasB Inhibitor, *ACS Chem Biol* **13**, 2449-2455.
- (34) Munguia, J., and Nizet, V. (2017) Pharmacological Targeting of the Host-Pathogen Interaction: Alternatives to Classical Antibiotics to Combat Drug-Resistant Superbugs, *Trends Pharmacol Sci* **38**, 473-488.
- (35) Gellatly, S. L., and Hancock, R. E. (2013) *Pseudomonas aeruginosa*: new insights into pathogenesis and host defenses, *Pathog Dis* **67**, 159-173.
- (36) Tacconelli, E., Carrara, E., Savoldi, A., Harbarth, S., Mendelson, M., Monnet, D. L., Pulcini, C., Kahlmeter, G., Kluytmans, J., Carmeli, Y., Ouellette, M., Outterson, K., Patel, J., Cavaleri, M., Cox, E. M., Houchens, C. R., Grayson, M. L., Hansen, P., Singh, N., Theuretzbacher, U., Magrini, N., and Group, W. H. O. P. P. L. W. (2018) Discovery, research, and development of new antibiotics: the WHO priority list of antibiotic-resistant bacteria and tuberculosis, *Lancet Infect Dis* **18**, 318-327.
- (37) Lowy, F. D. (1998) Staphylococcus aureus infections, *N Engl J Med* **339**, 520-532.
- (38) Roberts, S., and Chambers, S. (2005) Diagnosis and management of Staphylococcus aureus infections of the skin and soft tissue, *Intern Med J* **35 Suppl 2**, S97-105.
- (39) Jaradat, Z. W., Ababneh, Q. O., Sha'aban, S. T., Alkofahi, A. A., Assaleh, D., and Al Shara, A. (2020) Methicillin Resistant Staphylococcus aureus and public fomites: a review, *Pathog Glob Health* **114**, 426-450.
- (40) Konstantinovic, J., Yahiaoui, S., Alhayek, A., Haupenthal, J., Schonauer, E., Andreas, A., Kany, A. M., Muller, R., Koehnke, J., Berger, F. K., Bischoff, M., Hartmann, R. W., Brandstetter, H., and Hirsch, A. K. H. (2020) N-Aryl-3-mercaptosuccinimides as Antivirulence Agents Targeting *Pseudomonas aeruginosa* Elastase and Clostridium Collagenases, *J Med Chem* **63**, 8359-8368.
- (41) Rouanet-Mehouas, C., Czarny, B., Beau, F., Cassar-Lajeunesse, E., Stura, E. A., Dive, V., and Devel, L. (2017) Zinc-Metalloproteinase Inhibitors: Evaluation of the Complex Role Played by the Zinc-Binding Group on Potency and Selectivity, *J Med Chem* **60**, 403-414.
- (42) Czarny, B., Stura, E. A., Devel, L., Vera, L., Cassar-Lajeunesse, E., Beau, F., Calderone, V., Fragai, M., Luchinat, C., and Dive, V. (2013) Molecular determinants of a selective matrix metalloprotease-12 inhibitor: insights from crystallography and thermodynamic studies, *J Med Chem* **56**, 1149-1159.
- (43) Makaritis, A., Georgiadis, D., Dive, V., and Yiotakis, A. (2003) Diastereoselective solution and multipin-based combinatorial array synthesis of a novel class of potent phosphinic metalloprotease inhibitors, *Chemistry* **9**, 2079-2094.
- (44) Vassiliou, S., Mucha, A., Cuniasse, P., Georgiadis, D., Lucet-Levannier, K., Beau, F., Kannan, R., Murphy, G., Knauper, V., Rio, M. C., Basset, P., Yiotakis, A., and Dive, V. (1999) Phosphinic pseudo-tripeptides as potent inhibitors of matrix metalloproteinases: a structure-activity study, *J Med Chem* **42**, 2610-2620.
- (45) Rahman, F., Nguyen, T. M., Adekoya, O. A., Campestre, C., Tortorella, P., Sylte, I., and Winberg, J. O. (2021) Inhibition of bacterial and human zinc-metalloproteases by bisphosphonate- and catechol-containing compounds, *J Enzyme Inhib Med Chem* **36**, 819-830.
- (46) Sjoli, S., Nuti, E., Camodeca, C., Bilotto, I., Rossello, A., Winberg, J. O., Sylte, I., and Adekoya, O. A. (2016) Synthesis, experimental evaluation and molecular modelling of hydroxamate derivatives as zinc metalloproteinase inhibitors, *Eur J Med Chem* **108**, 141-153.

- (47) Sjoli, S., Solli, A. I., Akselsen, O., Jiang, Y., Berg, E., Hansen, T. V., Sylte, I., and Winberg, J. O. (2014) PAC-1 and isatin derivatives are weak matrix metalloproteinase inhibitors, *Biochim Biophys Acta* 1840, 3162-3169.
- (48) Sylte, I., Dawadi, R., Malla, N., von Hofsten, S., Nguyen, T. M., Solli, A. I., Berg, E., Adekoya, O. A., Svineng, G., and Winberg, J. O. (2018) The selectivity of galardin and an azasugar-based hydroxamate compound for human matrix metalloproteases and bacterial metalloproteases, *PLoS One* 13, e0200237.
- (49) Adekoya, O. A., Sjoli, S., Wuxiuer, Y., Bילו, I., Marques, S. M., Santos, M. A., Nuti, E., Cercignani, G., Rossello, A., Winberg, J. O., and Sylte, I. (2015) Inhibition of pseudolysin and thermolysin by hydroxamate-based MMP inhibitors, *Eur J Med Chem* 89, 340-348.
- (50) Rahman, F., Wushur, I., Malla, N., Astrand, O. A. H., Rongved, P., Winberg, J. O., and Sylte, I. (2021) Zinc-Chelating Compounds as Inhibitors of Human and Bacterial Zinc Metalloproteases, *Molecules* 27.
- (51) Tranchant, I., Vera, L., Czarny, B., Amoura, M., Cassar, E., Beau, F., Stura, E. A., and Dive, V. (2014) Halogen bonding controls selectivity of FRET substrate probes for MMP-9, *Chem Biol* 21, 408-413.
- (52) Hangauer, D. G., Monzingo, A. F., and Matthews, B. W. (1984) An interactive computer graphics study of thermolysin-catalyzed peptide cleavage and inhibition by N-carboxymethyl dipeptides, *Biochemistry-U S A* 23, 5730-5741.
- (53) Holden, H. M., and Matthews, B. W. (1988) The binding of L-valyl-L-tryptophan to crystalline thermolysin illustrates the mode of interaction of a product of peptide hydrolysis, *J Biol Chem* 263, 3256-3260.
- (54) Gall, A. L., Ruff, M., Kannan, R., Cuniasse, P., Yiotakis, A., Dive, V., Rio, M. C., Basset, P., and Moras, D. (2001) Crystal structure of the stromelysin-3 (MMP-11) catalytic domain complexed with a phosphinic inhibitor mimicking the transition-state, *J Mol Biol* 307, 577-586.
- (55) Devel, L., Beau, F., Amoura, M., Vera, L., Cassar-Lajeunesse, E., Garcia, S., Czarny, B., Stura, E. A., and Dive, V. (2012) Simple pseudo-dipeptides with a P2' glutamate: a novel inhibitor family of matrix metalloproteases and other metzincins, *J Biol Chem* 287, 26647-26656.
- (56) Devel, L., Rogakos, V., David, A., Makaritis, A., Beau, F., Cuniasse, P., Yiotakis, A., and Dive, V. (2006) Development of selective inhibitors and substrate of matrix metalloproteinase-12, *J Biol Chem* 281, 11152-11160.
- (57) Winberg, J. O., Brendskag, M. K., Sylte, I., Lindstad, R. I., and McKinley-McKee, J. S. (1999) The catalytic triad in Drosophila alcohol dehydrogenase: pH, temperature and molecular modelling studies, *J Mol Biol* 294, 601-616.
- (58) Mores, A., Matziari, M., Beau, F., Cuniasse, P., Yiotakis, A., and Dive, V. (2008) Development of potent and selective phosphinic peptide inhibitors of angiotensin-converting enzyme 2, *J Med Chem* 51, 2216-2226.
- (59) Matziari, M., Dellis, D., Dive, V., Yiotakis, A., and Samios, J. (2010) Conformational and solvation studies via computer simulation of the novel large scale diastereoselectively synthesized phosphinic MMP inhibitor RXP03 diluted in selected solvents, *J Phys Chem B* 114, 421-428.
- (60) Dawadi, R., Malla, N., Hegge, B., Wushur, I., Berg, E., Svineng, G., Sylte, I., and Winberg, J. O. (2020) Molecular Interactions Stabilizing the Promatrix Metalloprotease-9.Serglycin Heteromer, *Int J Mol Sci* 21.
- (61) Murphy, G., and Crabbe, T. (1995) Gelatinases A and B, *Methods Enzymol* 248, 470-484.
- (62) K. J. Bowers, E. C., H. Xu, R. O. Dror, M. P. Eastwood, B. A. Gregersen, J. L. Klepeis, I. Kolossvary, M. A. Moraes, F. D. Sacerdoti, J. K. Salmon, Y. Shan, and D. E. Shaw. (2006) Scalable Algorithms for Molecular Dynamics Simulations on Commodity Clusters, In *SC '06: International Conference for High Performance Computing, Networking, Storage and Analysis* (Horner-Miller, B., Ed.), Tampa, Florida, USA.
- (63) Lu, C., Wu, C., Ghoreishi, D., Chen, W., Wang, L., Damm, W., Ross, G. A., Dahlgren, M. K., Russell, E., Von Bargen, C. D., Abel, R., Friesner, R. A., and Harder, E. D. (2021) OPLS4: Improving

- Force Field Accuracy on Challenging Regimes of Chemical Space, *J Chem Theory Comput* 17, 4291-4300.
- (64) Woessner, J., Nagase, H. (2000) *Matrix metalloproteases and TIMPs*, Oxford University Press, Oxford.
- (65) Piana, S., Lindorff-Larsen, K., Dirks, R. M., Salmon, J. K., Dror, R. O., and Shaw, D. E. (2012) Evaluating the effects of cutoffs and treatment of long-range electrostatics in protein folding simulations, *PLoS One* 7, e39918.
- (66) Martyna, G. K., ML. Tuckerman,. (1992) Nosé–Hoover chains: The canonical ensemble via continuous dynamics, *J Chem Phys* 97, 2635-2643.

Table 1. Amino acids within the sub-pockets of MMP-9, MMP-14, TLN, PLN and ALN. Amino acids included are those in the vicinity of substrate side chains during MD simulations. Sub-pocket amino acids of PLN and ALN are based on amino acid sequence alignments with TLN (Figure S5).

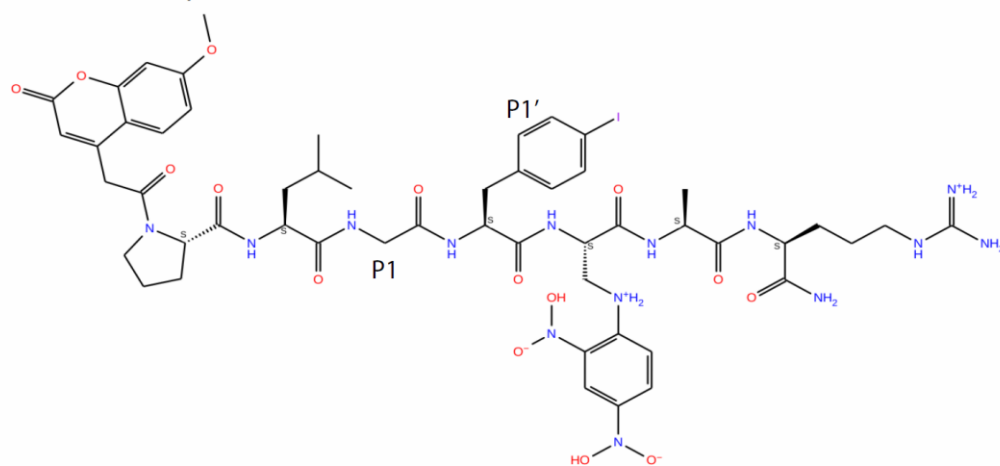
Sub-pocket	MMP-9	MMP-14	TLN	PLN	ALN
S ₁	H190, A191, E402, H405	F198, A200, A202, E240, H243	A113, F114, Y157	A113, Y114, Y155	A115, A116, Y159
S ₁ '	Y393, S394, F396, L397, V398, H401, L418, Y420, P421, M422, Y423, R424, T426	L199, L235, N231, V236, V238, H239, F260, Y261, Q262, F263	N112, M120, S134, D138, V139, H142, G189, L202, R203	N112, M120, L132, D136, V137, H140, G187, L197, R198	N114, M122, S136, D140, V141, H144, G186, L199, R200
S ₂	A191, P193	H201, Y203, F204	W115, E143, H146	W115, E141, H144	W117, E145, H148
S ₂ '	G186, L187, Y218, H411	H249, S250, S251, P259	N111, F130, L133, Y193	E111, Y130, L132, K191	N113, F132, L135, Y190

Table 2. K_i values of the phosphinic compounds H-1 and H-2 for MMP-14, MMP-9(A), MMP-9(MT), ALN, PLN and TLN. The table is showing K_i ± s.d. values determined for both bacterial and human metalloproteases using two different fluorescence quenched peptide substrates, McaRPPGFSAFK(Dnp)-OH (for TLN, PLN and ALN) and McaPLGL(Dpa)AR-NH₂ (for MMP-9(MT), MMP-9(A) and MMP-14). The concentration of the substrates was 4.0 μM and highest concentration of the test compounds was 100 μM. Compounds reducing the enzymatic activity by 50 % or more at a concentration 100 μM are included. Compound and enzyme were pre-incubated for 30 min and the reaction was started by the addition of substrate as described in the Materials and Methods. The s.d. of the K_i values is the sum of the s.d. from both IC₅₀ and K_m, where the added s.d. value of K_m have the same relative weight as the contribution of [S] / K_m to the obtained K_i value from IC₅₀ (eqn. 3).

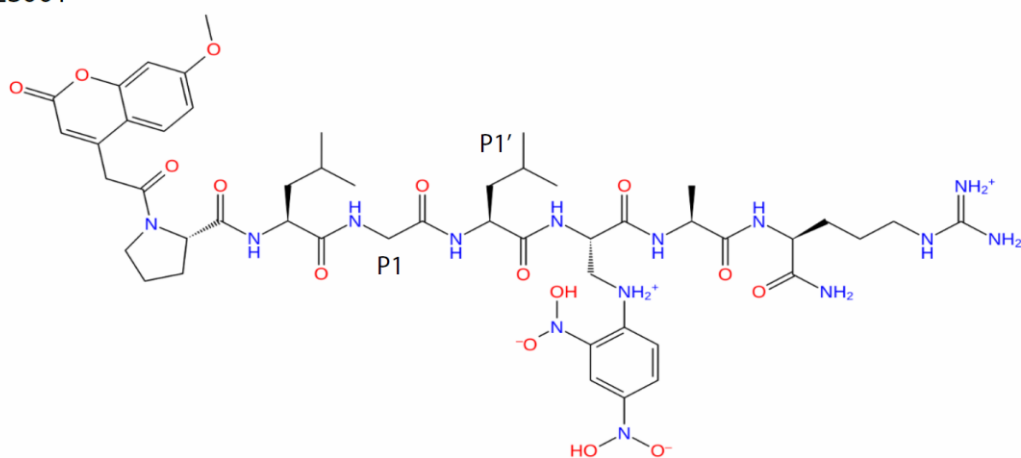
Compound	K _i ± s.d. (μM)					
	McaPLGL(Dpa)AR-NH ₂			McaRPPGFSAFK(Dnp)-OH		
	MMP-14	MMP-9(A)	MMP-9(MT)	ALN	PLN	TLN
H-1	0.89 ± 0.04	19 ± 3	30 ± 4	<i>n.d.</i> ^a	<i>n.d.</i>	<i>n.d.</i>
H-2	3.0 ± 0.1	0.56 ± 0.07	0.53 ± 0.06	80 ± 4	40 ± 2	2.5 ± 0.2

^a*n.d.*, not determined

MMP-9 substrate probe



ES001



ES005

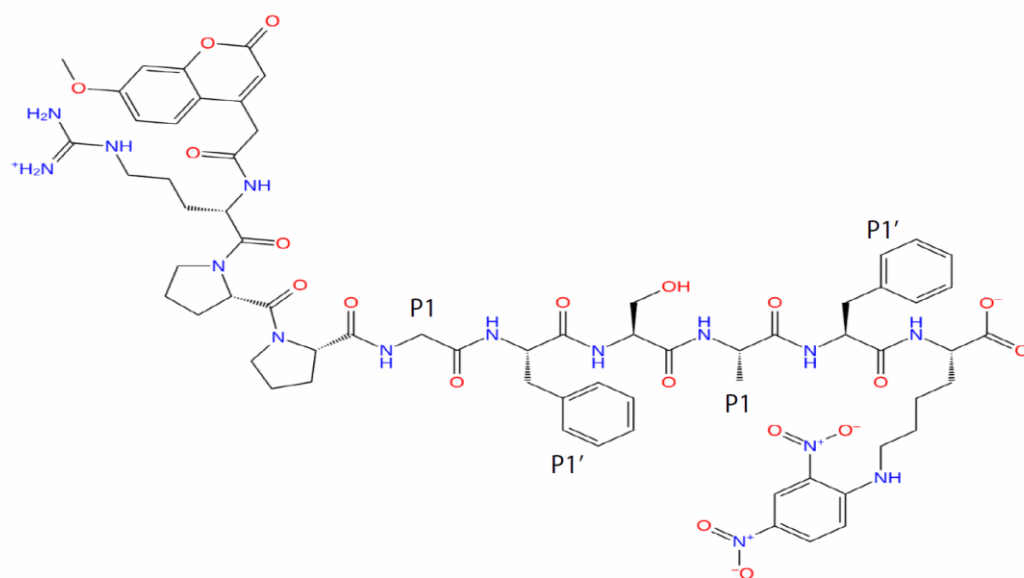


Figure 1. Two dimensional (2D) illustrations of the substrate probe from the X-ray crystallographic complex with MMP-9 (PDB id: 4JIJ), McaPLGL(Dpa)AR-NH₂ (ES001) that was used as substrate for MMP-9 and MMP-14 in the binding assays, and McaRPPGFSAFK(Dnp)-OH (ES005) that was used as substrate for TLN, PLN and ALN.

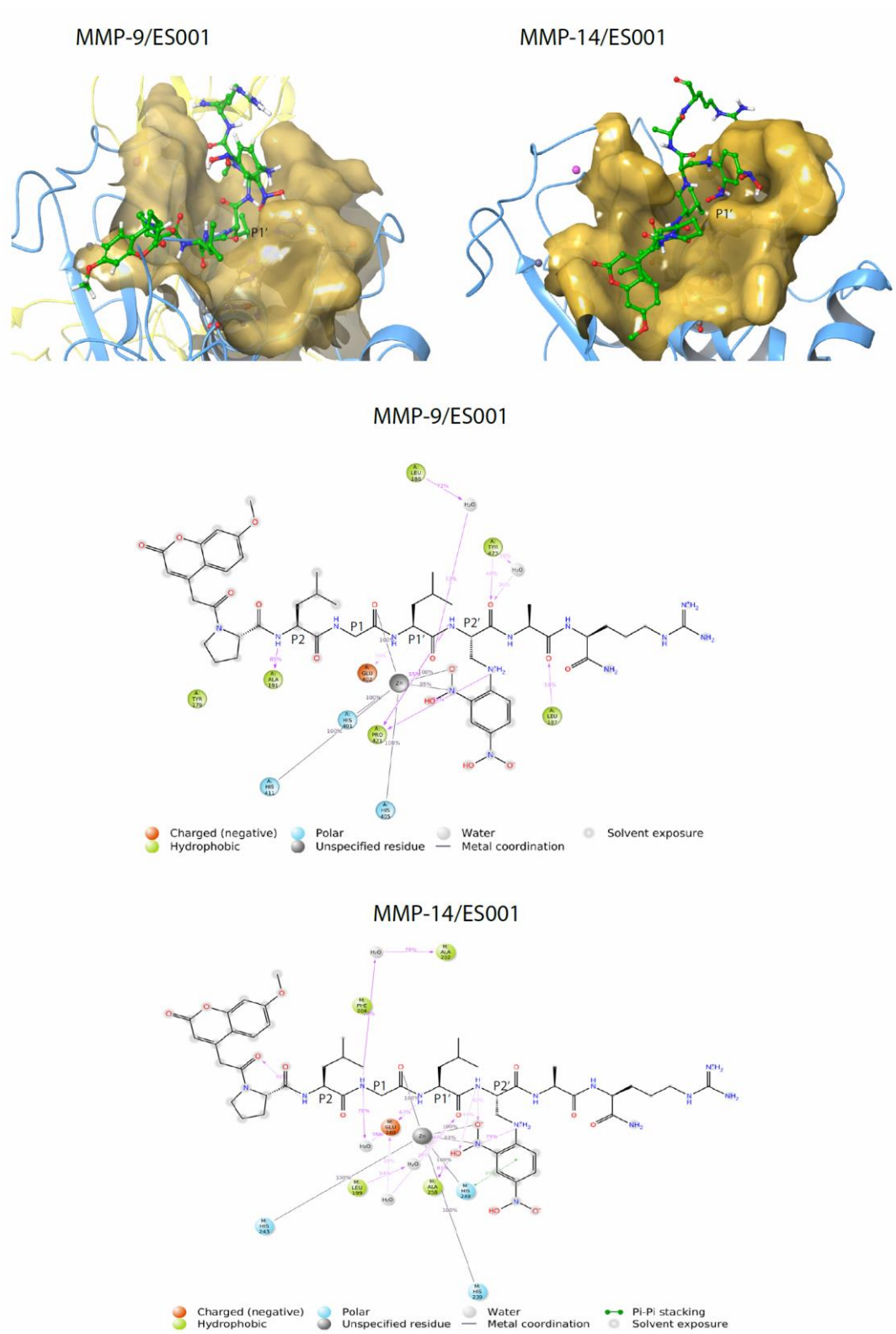


Figure 2. Molecular interactions of ES001 with MMP-9 and MMP-14. A: Close up of the binding cleft of the catalytic site of MMP-9 and MMP-14 with ES001 (green) at the catalytic site. The surface of binding cleft (yellow) is shown and the P₁' residue is indicated. The C α -trace of the backbone of the catalytic part is indicated in blue. The coordinate sets after 161 ns of simulation with MMP-9 and after 125 ns with MMP-14 which represent stable periods of the simulations are used for illustration. The yellow backbone C α of MMP-9 indicates the fibronectin repeats of MMP-9. B and C: 2D illustration of the complexes in A. Amino acids within 4 Å of the substrates are included.

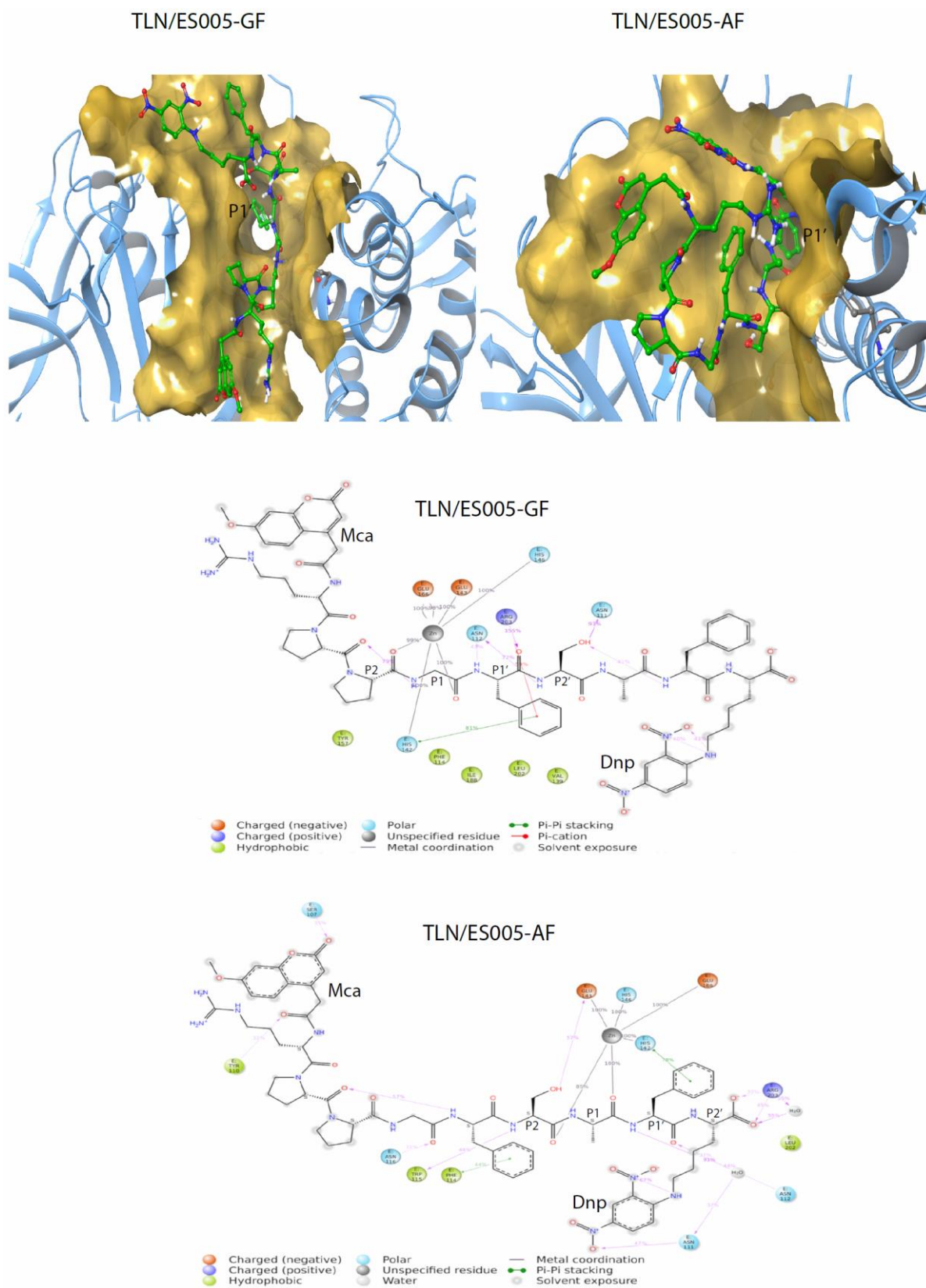


Figure 3. Molecular interactions of ES005 with TLN. Close ups of the substrate binding cleft. A complex from each of the two MD simulation (TLN/ES005-GF and TLN/ES005-AF) representing stable complex structures are shown. The coordinate sets after 137 ns and 160 ns are shown for TLN/ES005-GF and TLN/ES005-AF, respectively. The binding cleft surface is shown in yellow with the C α -trace in blue. ES005 in green.

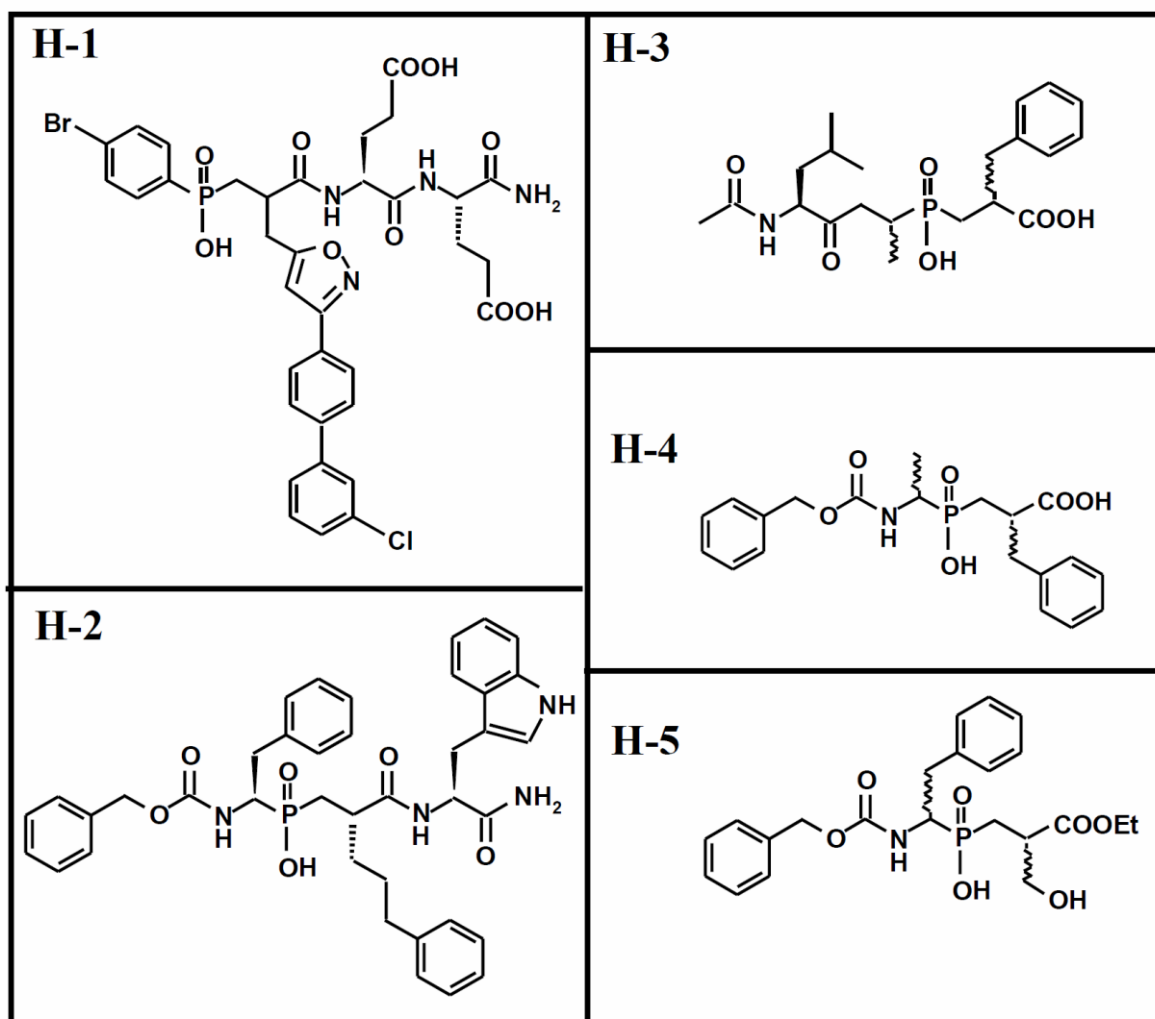
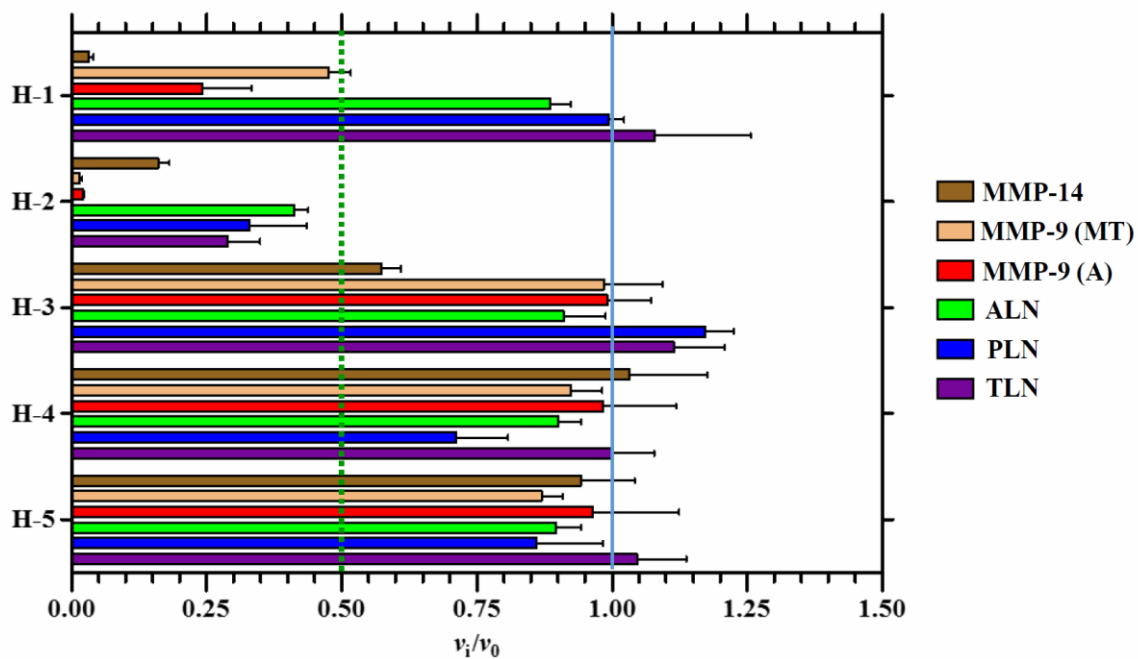


Figure 4. The molecular structures and inhibitory effect of 100 μ M of the H-compounds on the activity of MMP-9, MMP-14, TLN, PLN and ALN.

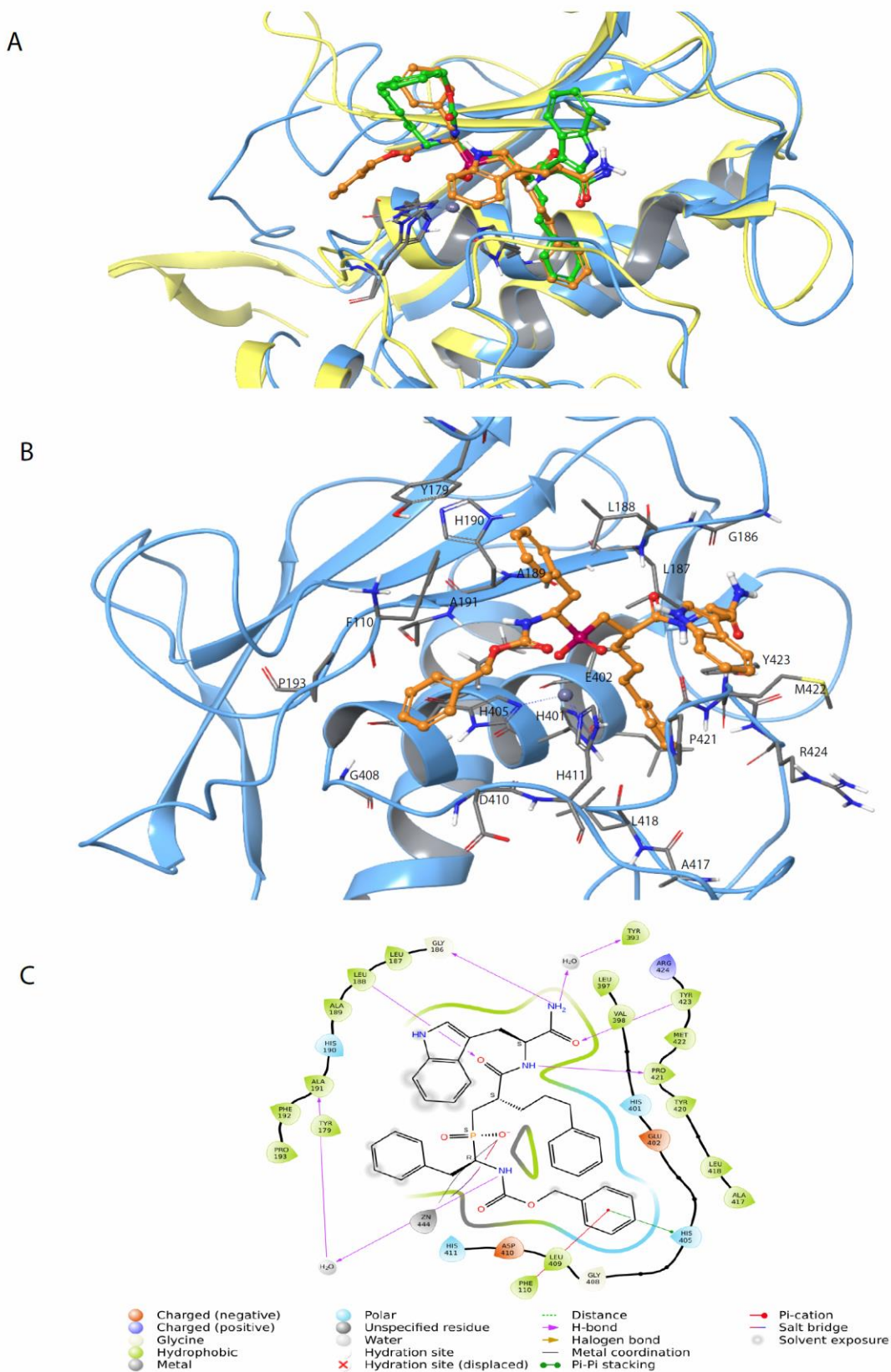


Figure 5. Induced fit docking of H-2 with MMP-9. **A:** The docked complex of H-2 (gold-yellow, RSS enantiomer) with MMP-9 (blue Ca-trace) superimposed with the X-ray structure complex (PDB id: 1HV5) of MMP-11 (yellow Ca-trace) in complex with H-2 (green, SSS enantiomer). H-2 oxygens in red, H-2 nitrogens in blue, H-2 phosphate in dark-red. The RSS enantiomer of H-2 was used in the enzyme kinetics studies. **B:** H-2 with MMP-9, colour coding as in A. **C:** 2D illustrations of the interactions. Amino acids within 4 Å of H-2 are included.

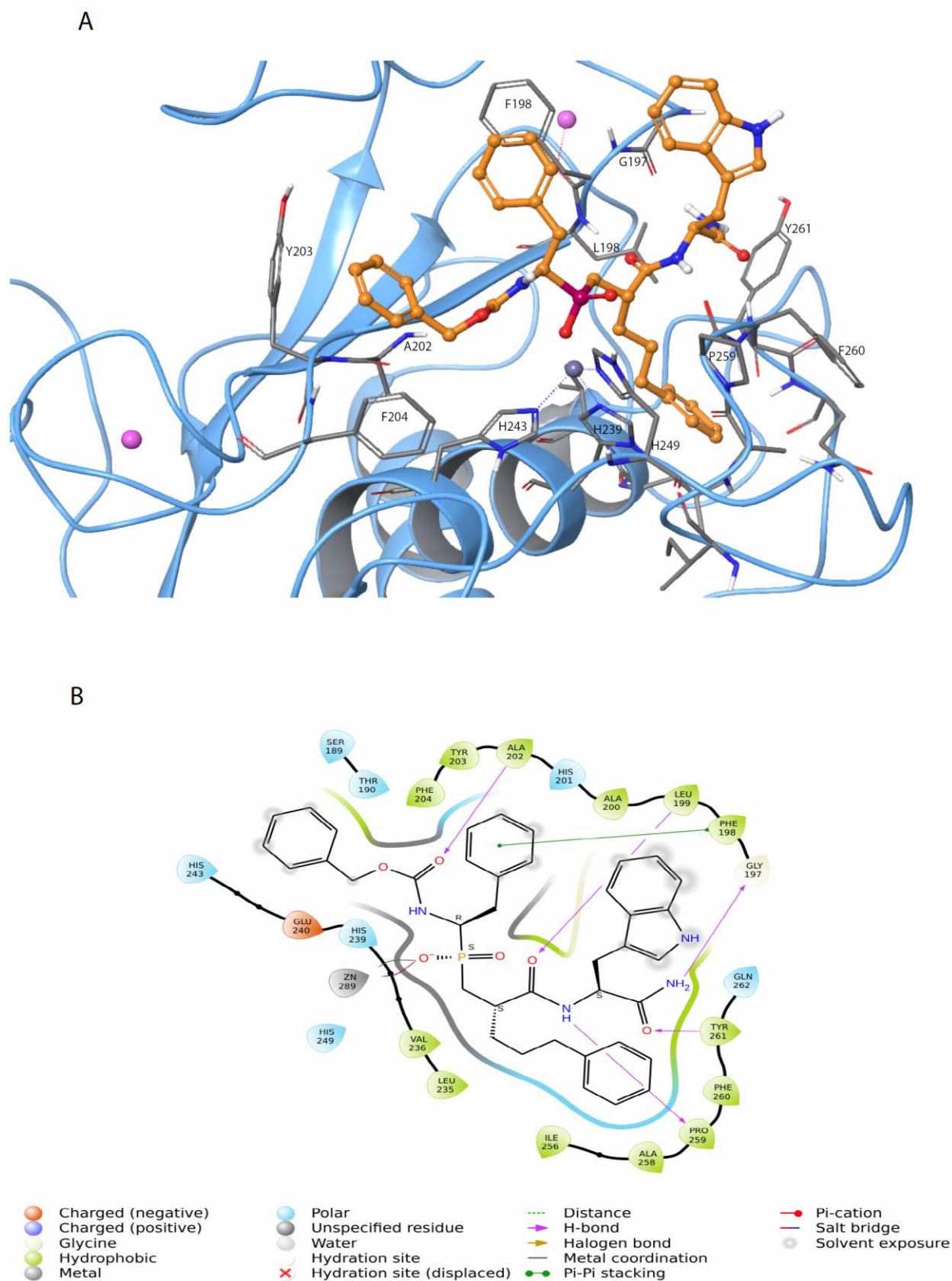


Figure 6. Induced fit docking of H-2 with MMP-14. A: The docked complex of H-2 (RSS enantiomer) with MMP-14. The colour coding is like in Figure 5. B: 2D illustrations of the interactions. Amino acids within 4 Å of H-2 are included.

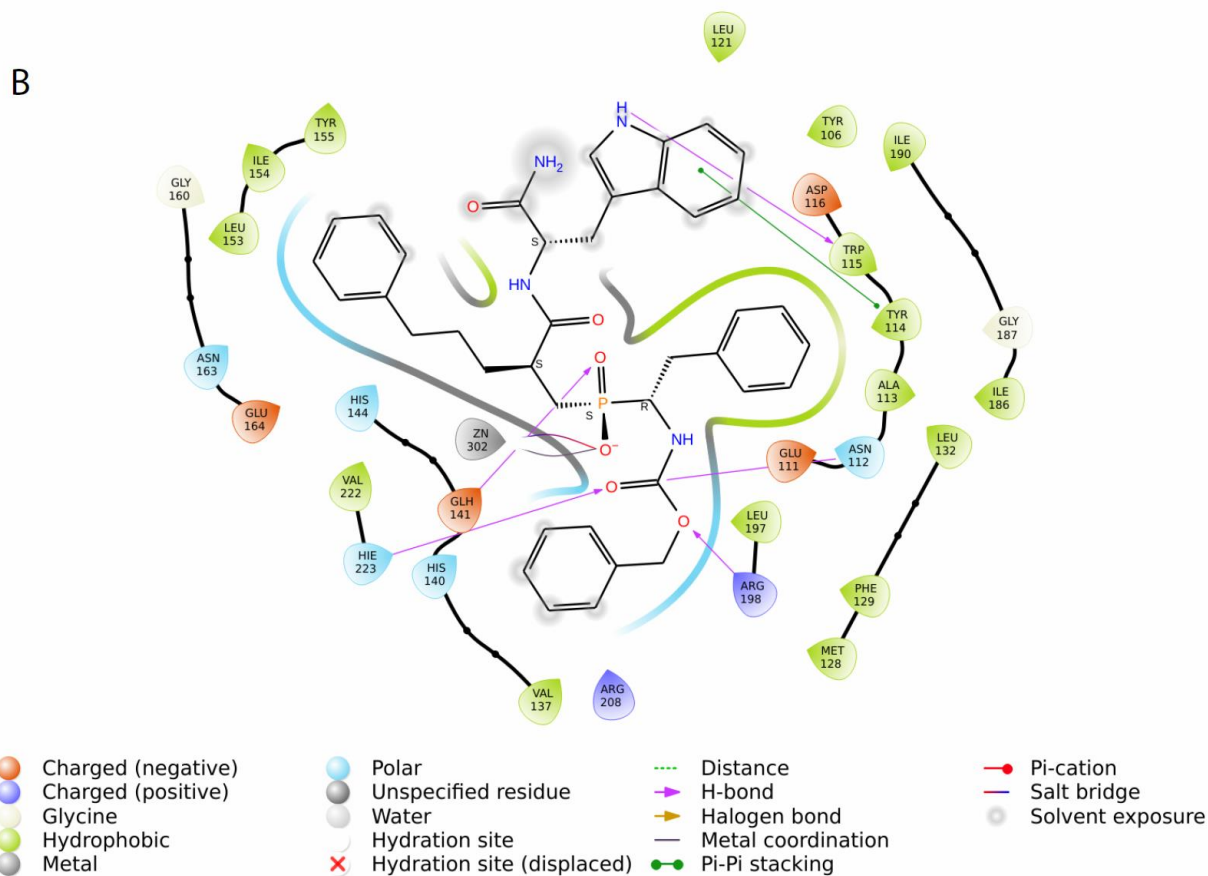
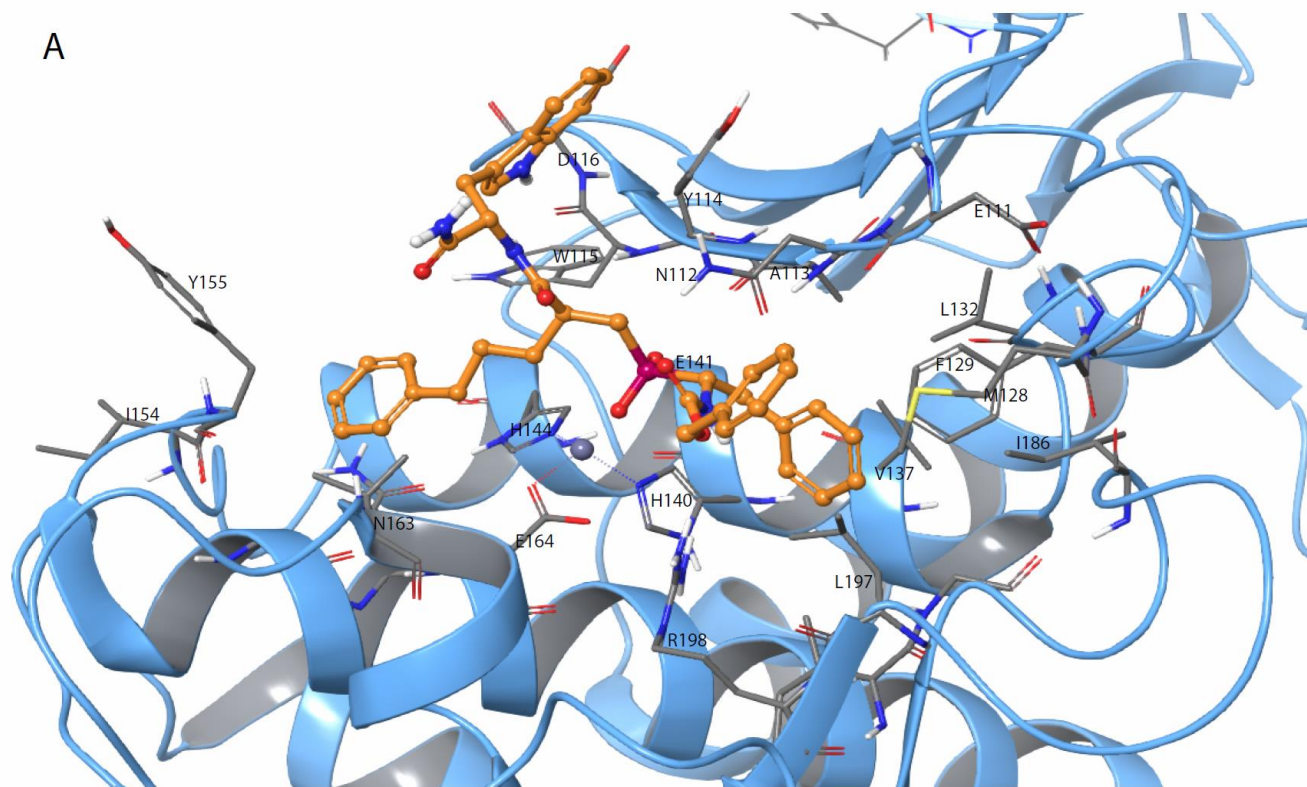


Figure 7. Induced fit docking of H-2 with PLN. A: The docked complex of H-2 (RSS enantiomer) with PLN. The colour coding is like in Figure 5. B: 2D illustrations of the interactions. Amino acids within 4 Å of H-2 are included.

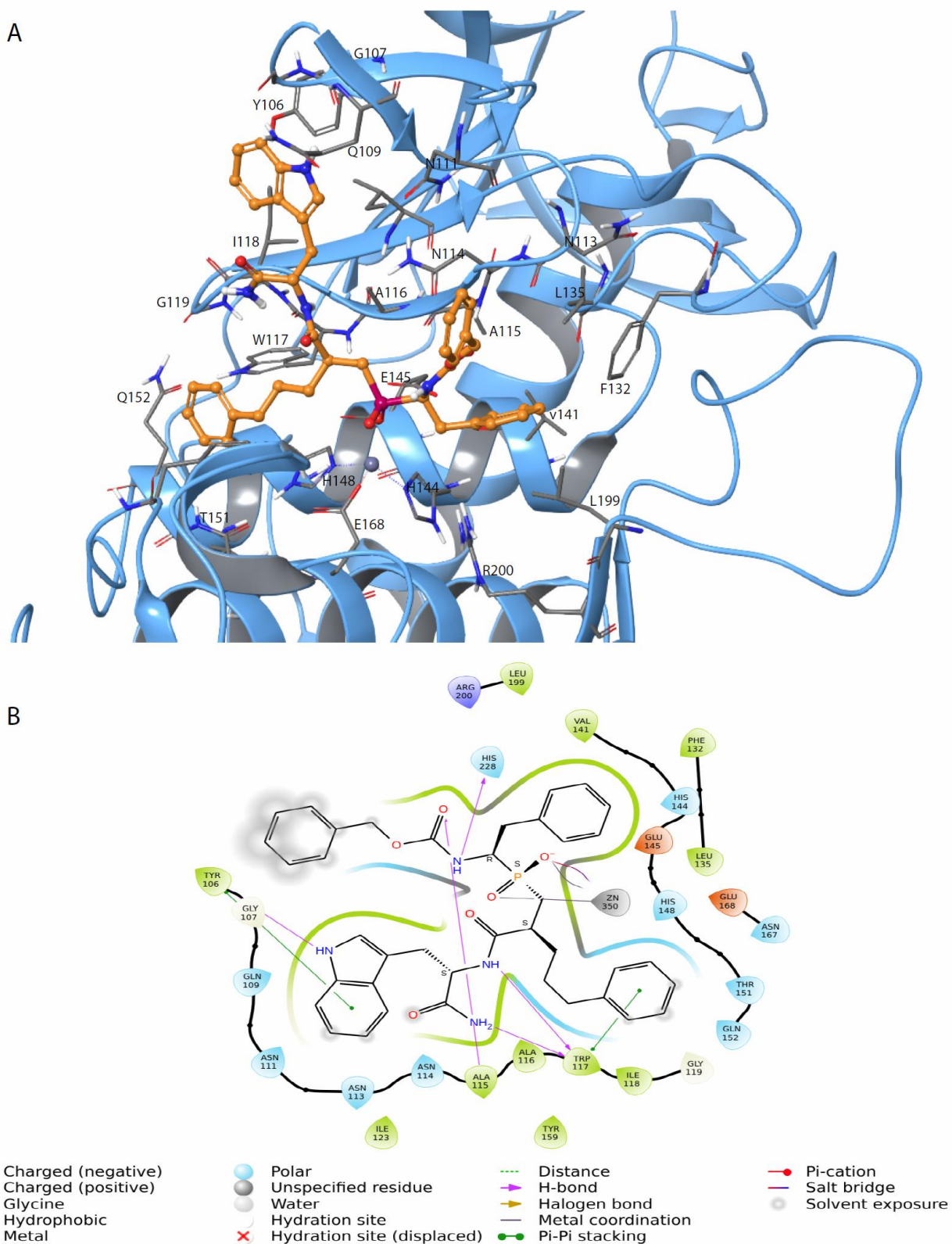


Figure 8. Induced fit docking of H2 with ALN. A: The docked complex of H-2 (RSS enantiomer) with ALN. The colour coding is like in Figure 5. B: 2D illustrations of the interactions. Amino acids within 4 Å of H-2 are included.

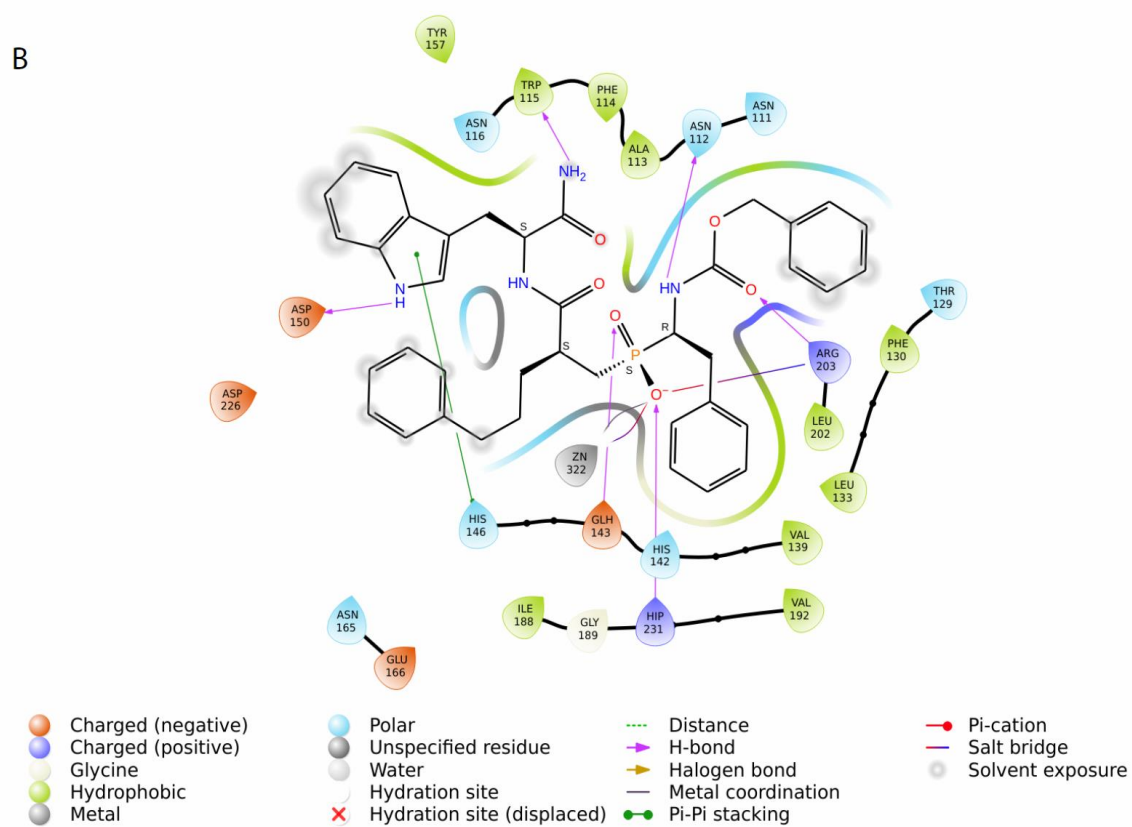
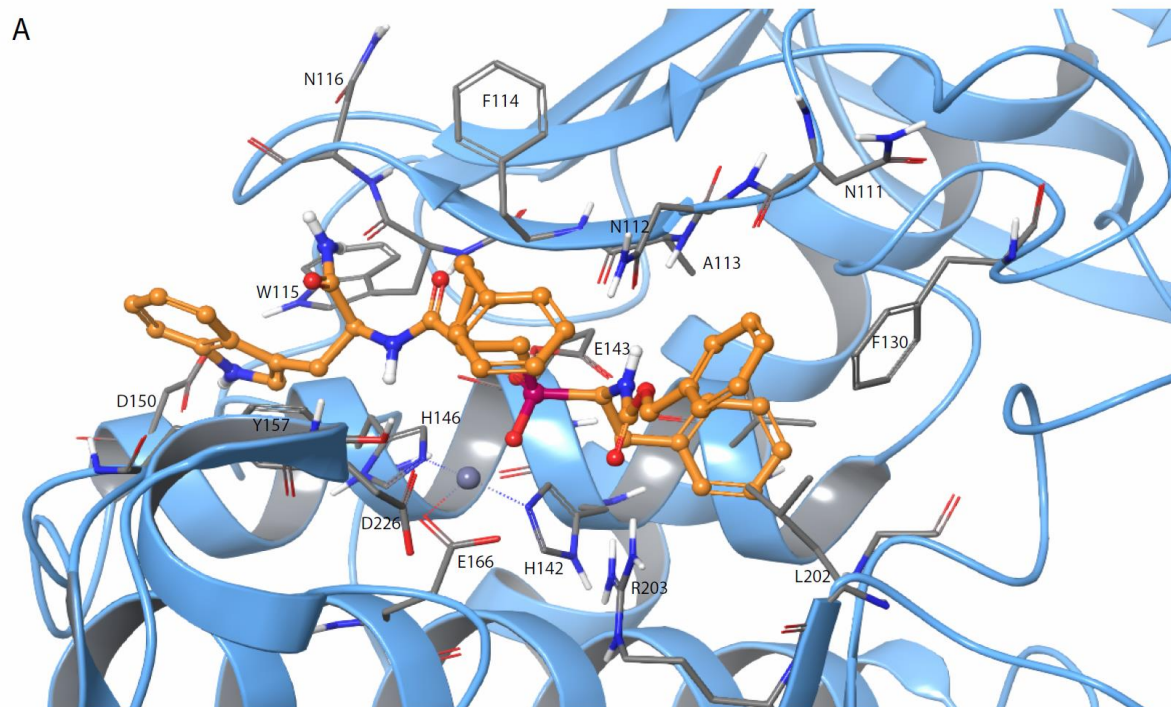


Figure 9. Induced fit docking of H-2 with TLN. A: The docked complex of H-2 (RSS enantiomer) with TLN. The colour coding is like in Figure 5. B: 2D illustrations of the interactions. Amino acids within 4 Å of H-2 are included.

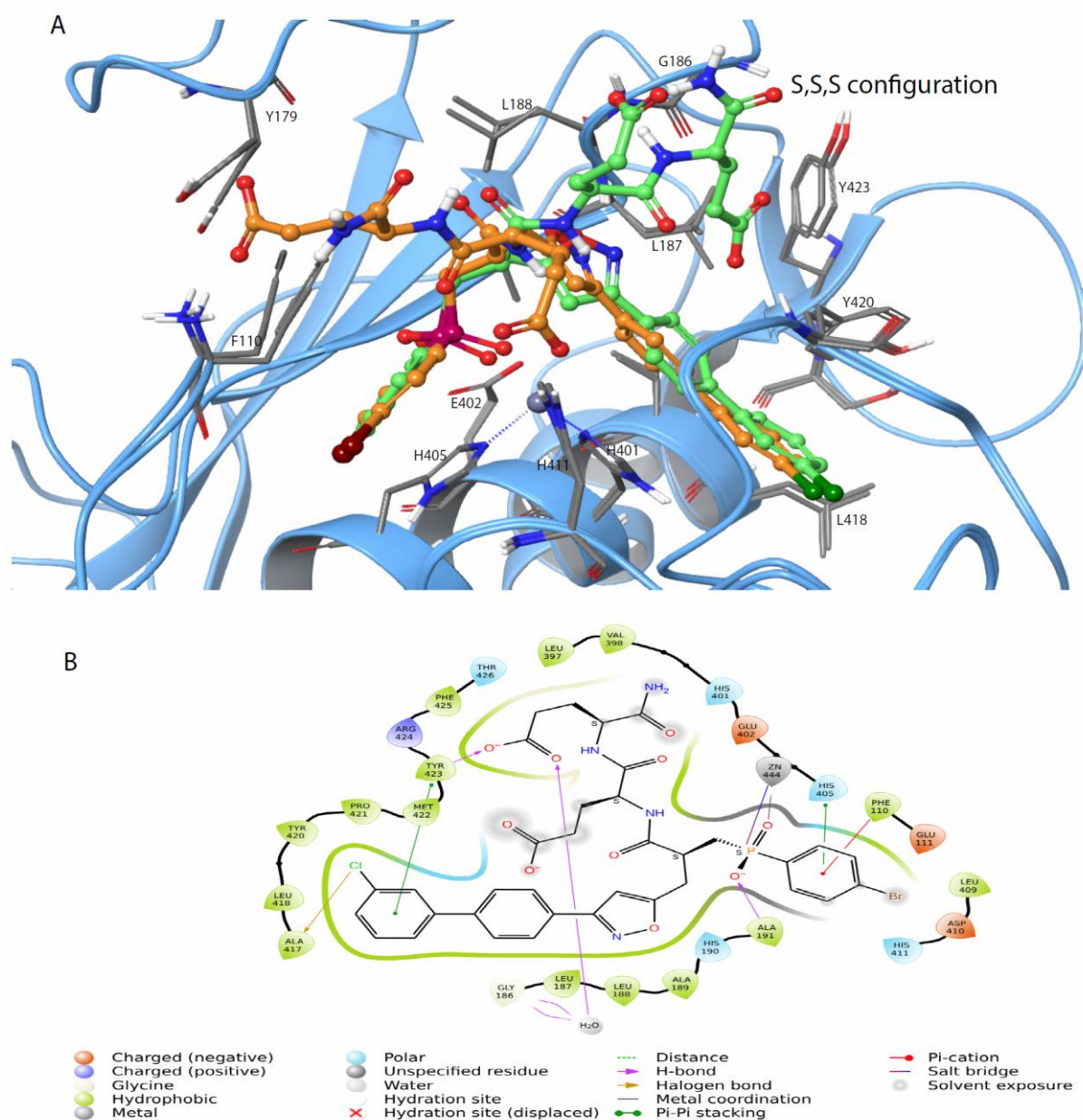


Figure 10. Induced fit docking of H-1 with MMP-9. A: The MMP-9/SSS enantiomer complex superimposed with the MMP-9/RSS enantiomer complex after induced fit docking. SSS enantiomer in green and RSS enantiomer in gold-yellow. Colour coding of enzyme and ligand atoms is like in Figure 5. The chloride of H-1 in dark-green and the bromide in dark-red. B: 2D illustrations of the interactions of the SSS-enantiomer of H-1 with amino acids in MMP-9. Amino acids within 4 Å of H-1 are included.

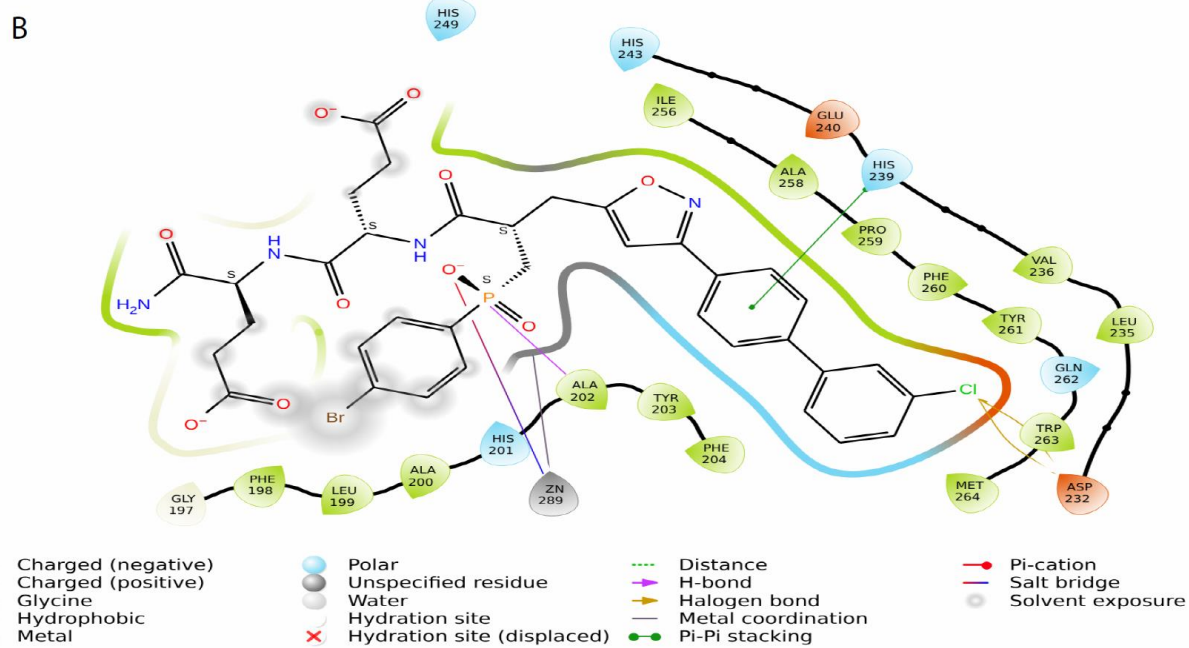
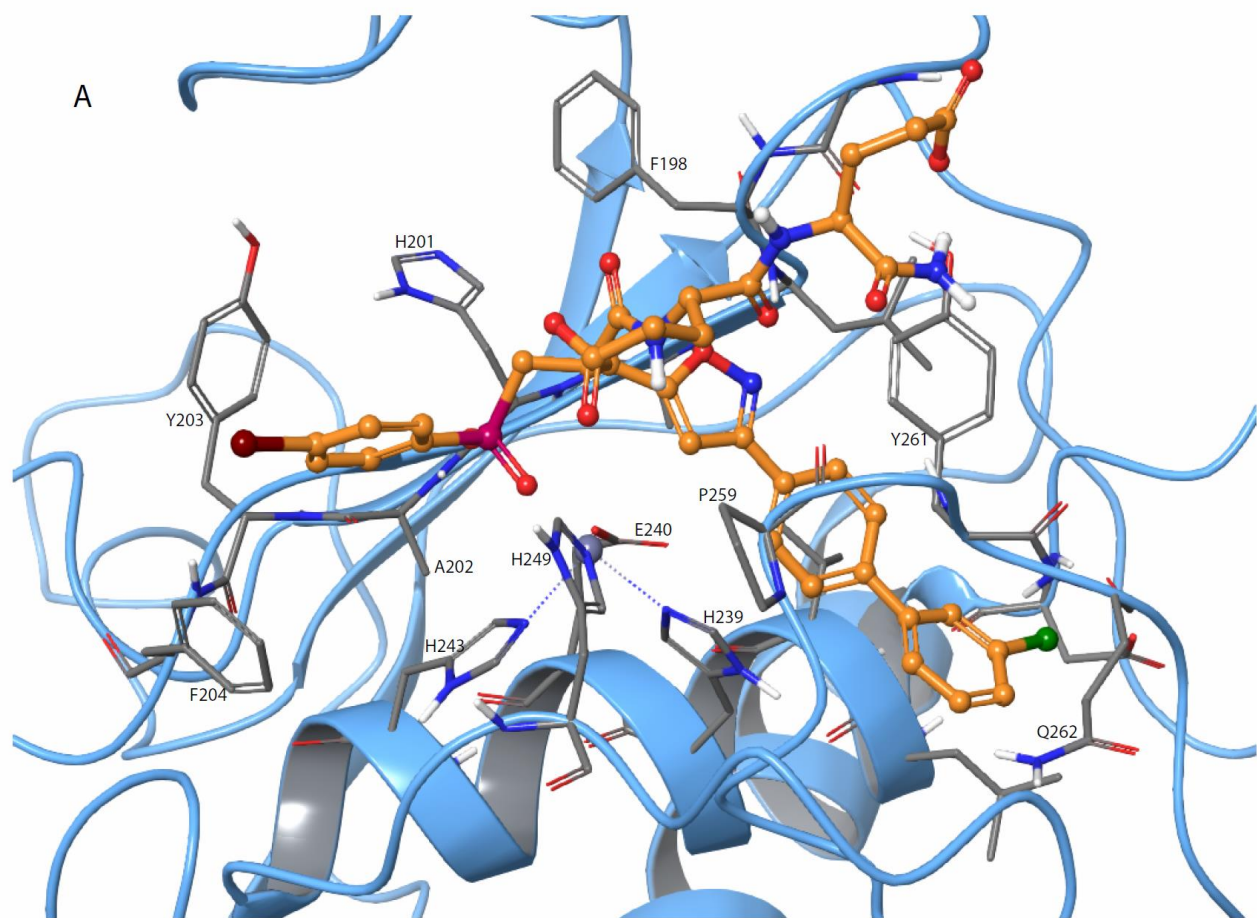


Figure 11. Induced fit docking of H-1 with MMP-14. A: The SSS enantiomer (gold-yellow) of H-1 docked into MMP-14. Colour coding of enzyme and ligand atoms is like in Figure 5. B: 2D illustrations of the interactions of the SSS-enantiomer of H-1 with amino acids in MMP-14. Amino acids within 4 Å of H-1 are included.

Supplementary Material

Interactions of substrates and phosphinyl containing inhibitors with human MMPs and bacterial virulence factors

Fatema Amatur Rahman¹, Imin Wushur¹, Bibek Chaulagain¹, Tra-Mi Nguyen¹, Olayiwola A. Adekoya², Nabin Malla¹, Jan-Olof Winberg¹, Ingebrigt Sylte^{1,3*}

¹ Molecular Pharmacology and Toxicology, Department of Medical Biology, Faculty of Health Sciences, UiT The Arctic University of Norway, NO-9037 Tromsø, Norway

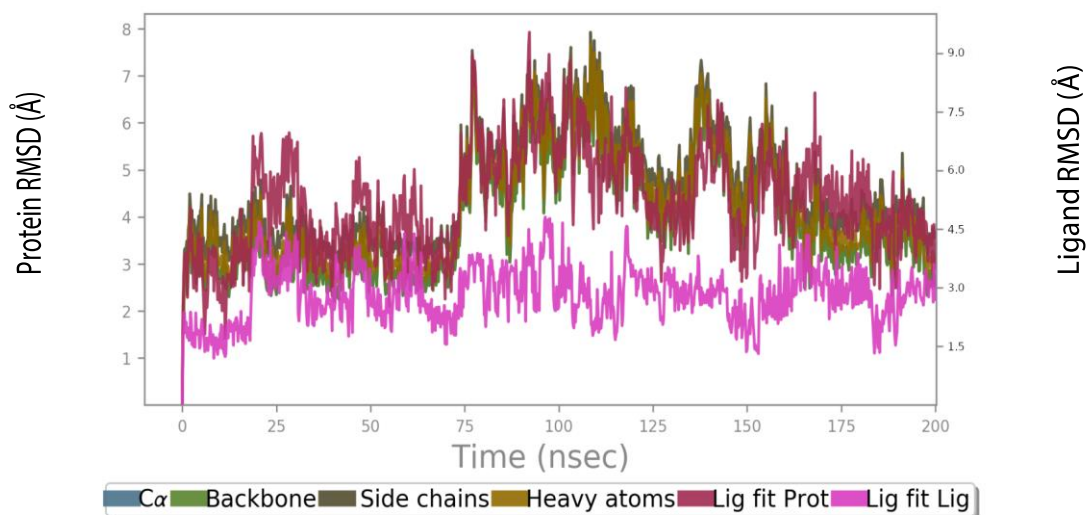
² Centre for Pharmacy, Department of Clinical Science, Faculty of Medicine, University of Bergen, Norway

³ Center for Research and Education, University Hospital of North Norway (UNN)

*Corresponding author: Ingebrigt Sylte, Molecular Pharmacology and Toxicology, Department of Medical Biology, Faculty of Health Sciences, UiT The Arctic University of Norway, NO-9037 Tromsø, Norway. Email: ingebrigt.sylte@uit.no

Supplementary Figure S1

MMP-9/ES001 complex



MMP-14/ES001 complex

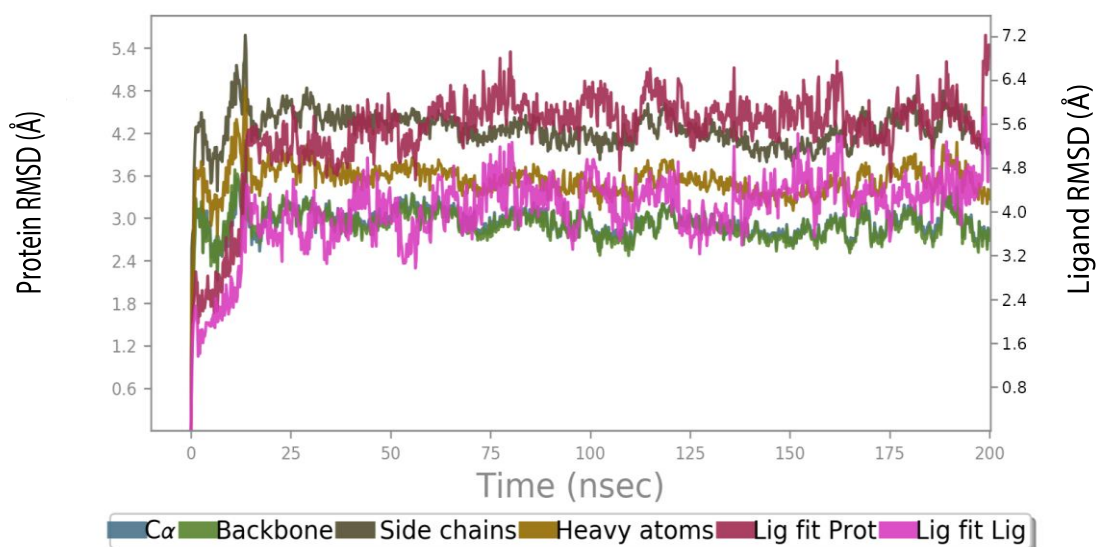


Figure S1. Root means square deviations (RMSDs) of enzyme and ligand (McaPLGL(Dpa)AR-NH₂, ES001) from the starting enzyme – ES001 complexes during 200 ns of molecular dynamics (MD) simulations. Above: ES001 with MMP-9. Below: ES001 with MMP-14.

Supplementary Figure S2

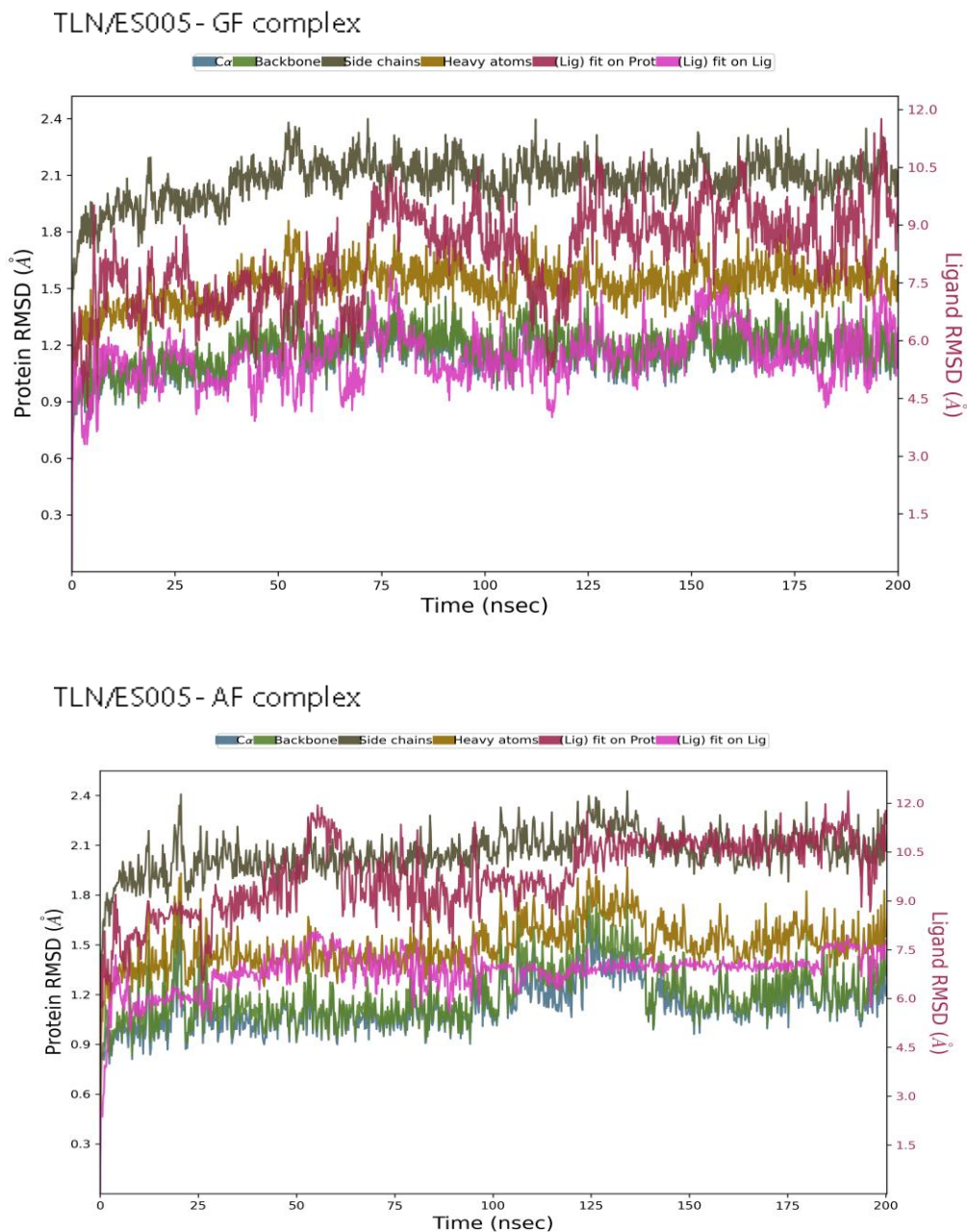


Figure S2. RMSDs of the thermolysin (TLN) and ligand (McaRPPGFSAF(Dnp)-OH, ES005) from starting TLN – ES005 complexes during 200 ns of MD simulations. Above: MD with Gly-Phe as P_1 and P_1' residues. Below: MD with Ala-Phe as P_1 and P_1' residues.

Supplementary Figure S3

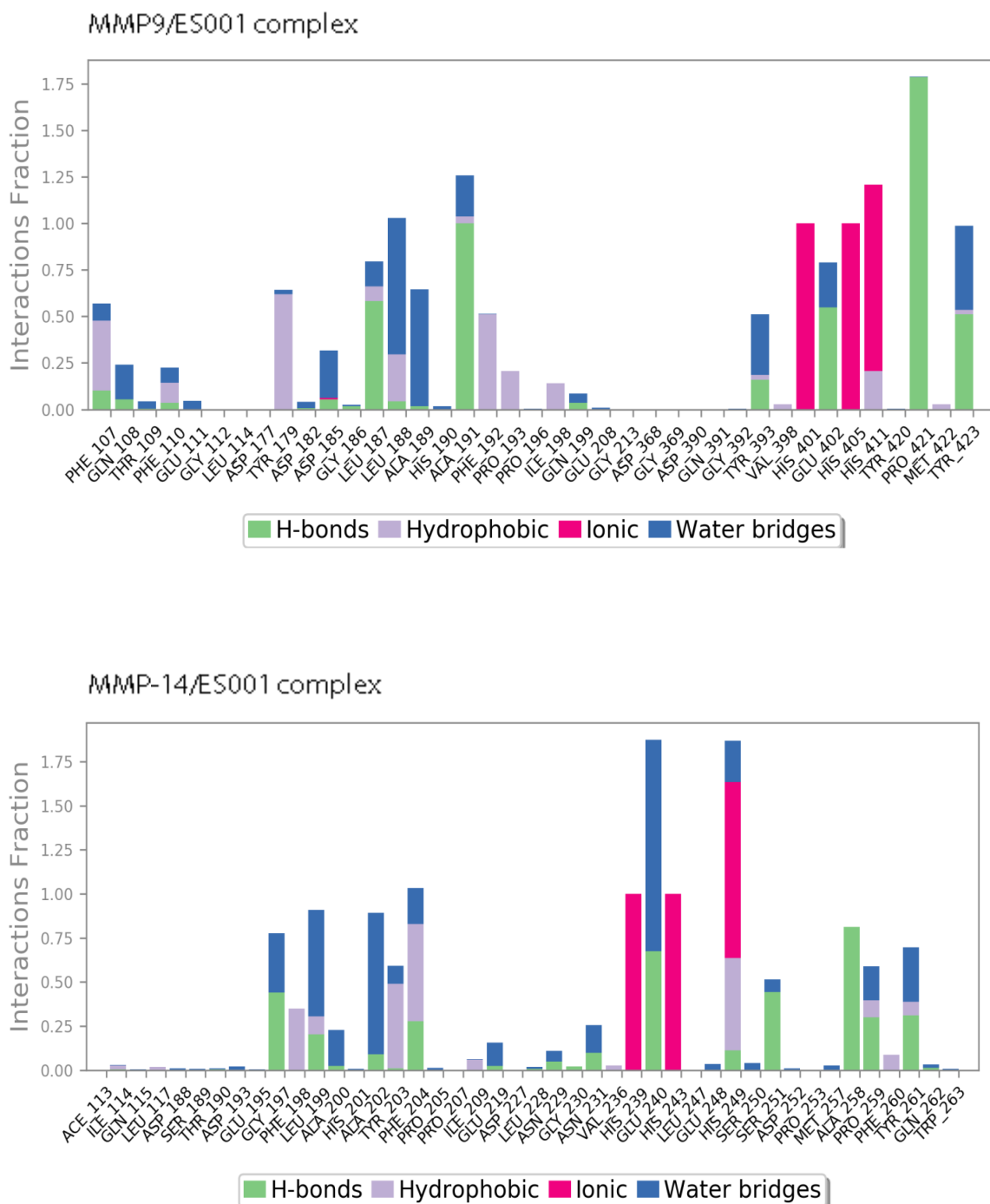


Figure S3. The Interactions of ES001 with amino acid side chains of MMP-9 (above) and MMP-14 (below) during 200 ns of MD simulation.

Supplementary Figure S4

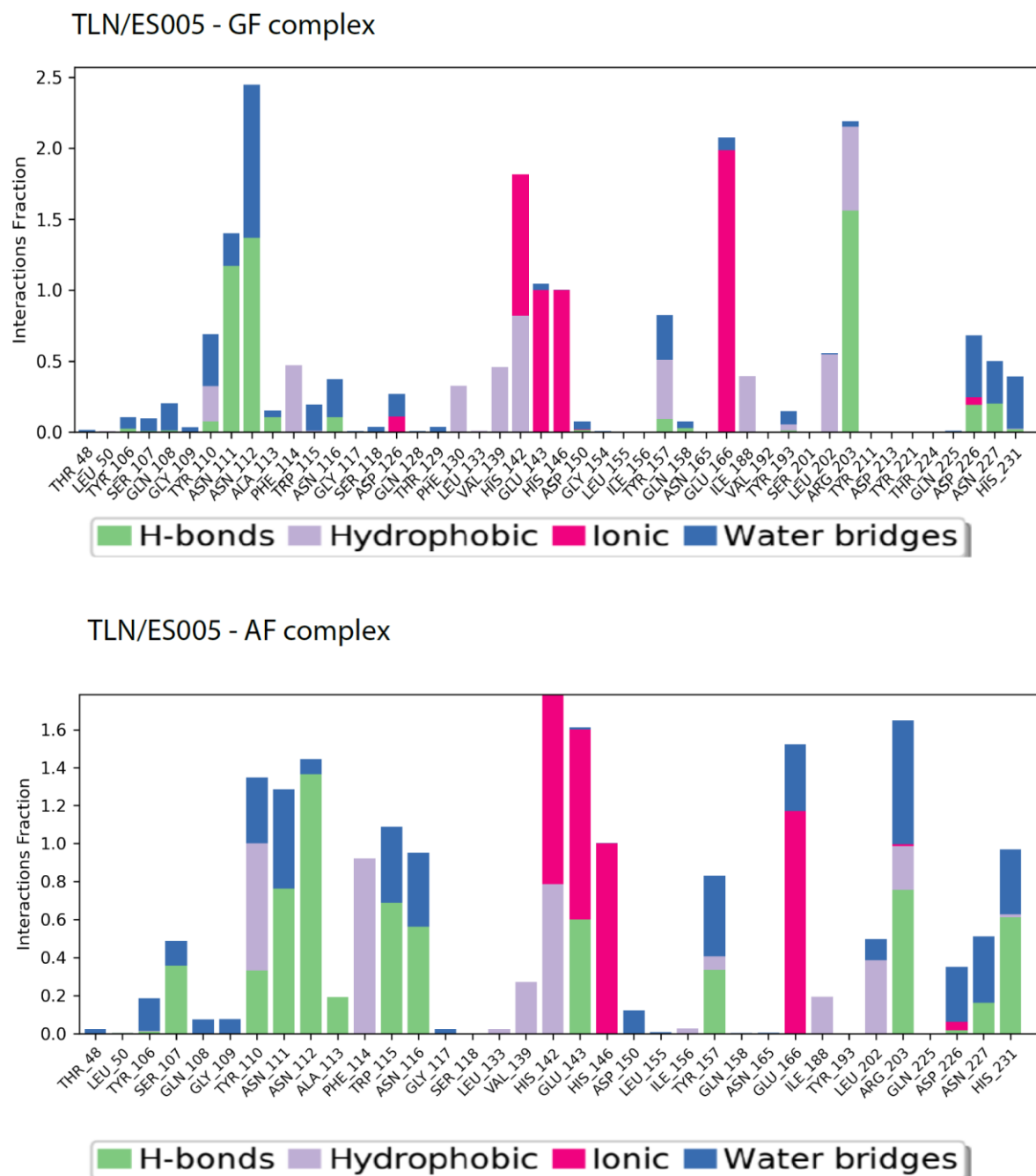


Figure S4. The interactions of the substrate McaRPPGFSAFK(Dnp)-OH (ES005) with side chains of TLN during 200 ns of MD simulations with Gly-Phe (above) and Ala-Phe as P_1 and P_1' residues. Putative P_1 and P_1' residues of ES005 are indicated in Figure 1.

Supplementary Figure S5

```

PLN   ---AEAG----GPGGNQKIGKYTYGSDYGPLIVNDRCEMDDGNVITVDMNSSTDDSKTTP 53
TLN   ITGTSTVGVGRGVLGDQKNINTTYS-TYY--YLQDN--TRGNIFTYDAK----- 45
ALN   --EAAATGTGKGVLDGTDKININSI-DGGF-SLEDL--THQKLSAYNFN----- 44
      : :      *  * : * : .      : : *      . : : : :

PLN   FRFACPTNT-----YKQVNGAYSPLNDAHFFGGVVFVKLYRDWFGTSPLTHK---LYMKVH 105
TLN   YRTTLPGLSLWADADNQFFASYDAPAVDAHYAGVTYDYKKNVHNRLSYDGNNAAIRSSVH 105
ALN   -DQTGQATLITNEDENFVKDDQRAGVDANYAKQTYDYKNTFGRESYDNHGSPIVSLTH 103
      : .      : . .      * : : : . . . * : : . .      : : . *

PLN   YG-----RSVENAYWDGTAMLFGDGATMFYP--LVSLDVAAHEVSHGFTEQNSGLIYRQ 158
TLN   YS-----QGYNNAFWNGSQMVYGDGDGQTFIPLSGGIDVVAHEALTHAVTDYTAGLIYQNE 160
ALN   VNHYGGQDNRNNAAWIGDKMIYGDGDGRTFTNLSGANDVVAHEALTHGVTQETANLEYKDQ 163
      .      . : * * * * * : : : : .      . * * . * * : : * * : : . * * : :

PLN   SGGMNEAFSDMAGEAAEFYMRGKNDFLIGYDIK--KSGALRYMDQPSRDGRSIDNASQ 215
TLN   SGAINEAISDIFGTLVEFYANKNPDWEIGEDVYTPGISGDSLRSMSDPAKYGDPDHYSKR 220
ALN   SGALNESFSDFVGYFV-----DDEDFLMGEDVYTPGKEGDALRSMSNPEQFGQPSHMKDY 218
      * * . : * : : * : * .      . * : : * * : : . . : * * * : * . .

PLN   YYN---GIDVHHSSGVYNRAFYLLANSP-----GWDTRKAFEVFDANRYWTATSN 264
TLN   YTGTQDNGGVHINSGIINKAAYLISQGGTHYGVSVVVGIGRDKLGKIFYRALTQYLTPTS 280
ALN   VYTEKDNGGVHTNSGIPNKAAYNVI-----QAIGKSKSEQIYYRALTEYLTSNSN 268
      . . * * . * : : * * * * : . . * * : : * * * * . * *

PLN   YNSGACGVIRSAQNR----NYSAADVTRAFSTVGVTCPAL 301
TLN   FSQLRAAAVQSATDLYGSTSQEVASVKQAFDAVGVK----- 316
ALN   FKDCKDALYQAAKDLYDEQTAE--QVYEAWNEVGVE----- 302
      : . . . : : * : . . . * . * : . * * *

```

Figure S5. Amino acid sequence alignments of the catalytic domain of pseudolysin (PLN), thermolysin (TLN) and aurolysin (ALN). SWISS-PROT accession codes; PLN: P14756, TLN: P00800, ALN P81177. The alignments were generated using Clustal Omega at the online services of EMBL-EBI (<http://www.ebi.ac.uk/services>). The zinc binding motif and the catalytic glutamic acid are highlighted in bold.

Supplementary Figure S6

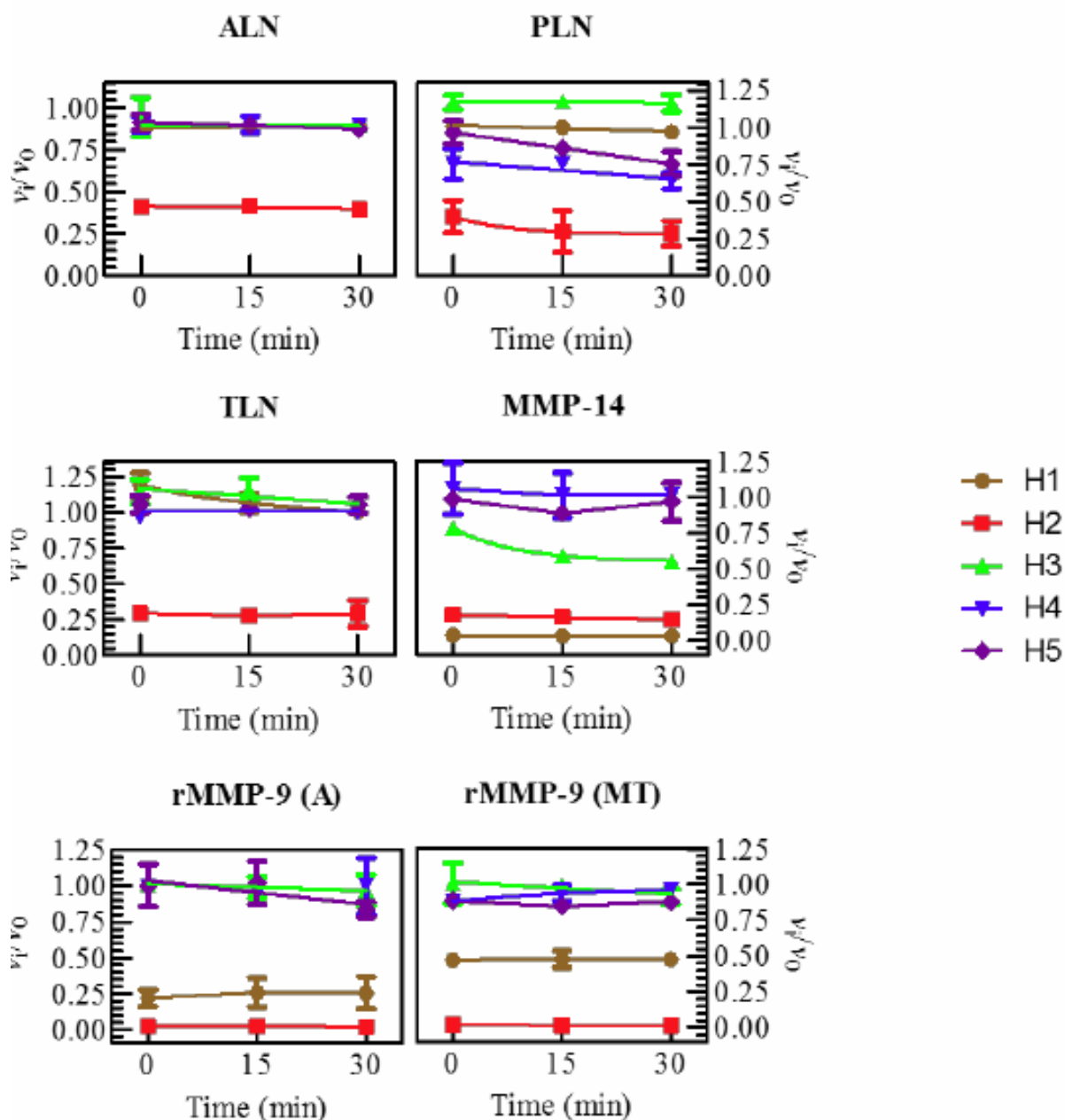


Figure S6. Time dependent inhibitory effects of 100 μM of the compounds (H1-H5) on the activity of aureolysin (ALN), pseudolysin (PLN), thermolysin (TLN), MMP-14, MMP-9 (A) and MMP-9 (MT). The experiments were performed as described in the material and methods section using a concentration of 4 μM of the substrate McaPLGL(Dpa)AR-NH₂ (ES001) for MMP-9 (A), MMP-9 (T) and MMP-14, and of the substrate McaRPPGFSAFK(Dnp)-OH (ES005) for TLN, ALN and PLN. Concentrations of the enzymes were as follows: 0.05 nM MMP-9(A), 0.05 nM MMP-9(MT), 1.0 nM MMP-14, 1.4 nM ALN, 0.5 nM PLN and 0.21 nM TLN. The v_t/v_0 (mean \pm s.d.) were based on 3-7 experiments.

